UNIVERSITÀ DEGLI STUDI DI MILANO
DIPARTIMENTO DI CHIMICA

CORSO DI DOTTORATO IN CHIMICA
XXXIII CICLO

DETECTION AND ISOLATION OF THE BACTERIAL SECOND MESSENGER (p)ppGpp

Dottorando: MARCO MINNECI

Tutor: Prof. Anna Bernardi

Co-tutor: Prof. Sara Sattin

A.A. 2019/2020

TABLE OF CONTENTS

List of Abbreviations

AA: acrylamide

AAS: atomic absorption spectroscopy

ADP: adenosine diphosphate

AIBN: azobisisobutyronitrile

AMP: adenosine monophosphate

ATP: adenosine triphosphate

ATR: attenuated total reflection

Boc: *tert*-butoxycarbonyl

CHEQ: chelation enhancement quenching

CF: cystic fibrosis

CFU: colony-forming unit

DCC: N,N'-Dicyclohexylcarbodiimide

DCU: N,N’-Dicyclohexylurea

DIEPA: N,N'-diisopropylethylamine

DMF: N,N’-dimethylformamide

DMA: N,N’-dimethylacrylamide

DMSO: dimethyl sulfoxide

DNA: deoxyribonucleic acid

DOSY: diffusion ordered spectroscopy

DPA: di-(2-picolyl)amine

ESI-MS: electrospray Ionization Mass Spectroscopy

EtOAc: ethyl acetate

GDP: guanosine diphosphate

GltX: Glutamate tRNA ligase

GMP: guanosine monophosphate

GTP: guanosine trisphosphate

GSH: glutathione

HATU: Hexafluorophosphate Azabenzotriazole Tetramethyl Uronium

HD: hydrolase domain

Hex: hexane

HPLC: high Performance Liquid Chromatography

IC_{50}: half maximal inhibitory concentration

J: coupling constant

MAPS: methacrylate propyl trimethoxysilyl

MIC: minimal inhibitory concentration

NAS: N-acryloxysuccinimide

NMR: nuclear magnetic resonance

PABA*: p*-aminobenzoic acid

PEI: polyethylenimine

pGpp: guanosine 3'-diphosphate-5'-phosphate

PMF: proton motive force

ppGpp: guanosine 3'-diphosphate-5'-diphosphate

pppGpp: guanosine 3'-diphosphate-5'-triphosphate

PPi: pyrophosphate

PPX: exopoly phosphatase

RNA: ribonucleic acid

RT: room temperature

Ser: Serine

SR: stringent response

SYNTH: synthetase domain

RSH: RelA-SpoT Homologous

TA: toxin-antitoxin

TB: tuberculosis

TFA: trifluoroacetic acid

TGA: thermo gravimetric analysis

THF: tetrahydrofuran

TLC: thin Layer Chromatography

TBDMSCl: Tert-Butyldimethylsilyl chloride

TMSCl: Trimethylsilyl chloride

TMEDA: tetramethyl ethylenediamine

tRNA: transfer RNA

Foreword

The present thesis focuses mainly on the production, isolation and quantitative detection of the second messenger nucleotide (p)ppGpp, a key intermediate in many regulatory processes in prokaryotic cells. This work was undertaken in the framework of a ERC funded project (ERC-StG, ERACHRON, grant number 758108) aimed at eradicating chronic infections by acting on the persister bacterial phenotype.

A small side project regarding the synthesis of a potential organocatalyst based on the alkaloid atropine is reported as Annex I.

Part One: Bacterial Persistence

Introduction

Antimicrobial resistance and tolerance

In the last decades, besides cancer and degenerative diseases, one of the main threats to global health has been antimicrobial resistance. Bacteria become 'resistant' when one or more genetic alterations confer them the ability to survive one or more antibiotics. The increasing prevalence of bacterial resistance is also due to the discovery void for antimicrobial compounds experienced in the last thirty years, as shown in Figure 1, which shows the approval of only two antimicrobial agents between 2008 and 2012. This shockingly low number is clearly insufficient for counteracting pathogens fast resistance mutation-rate.

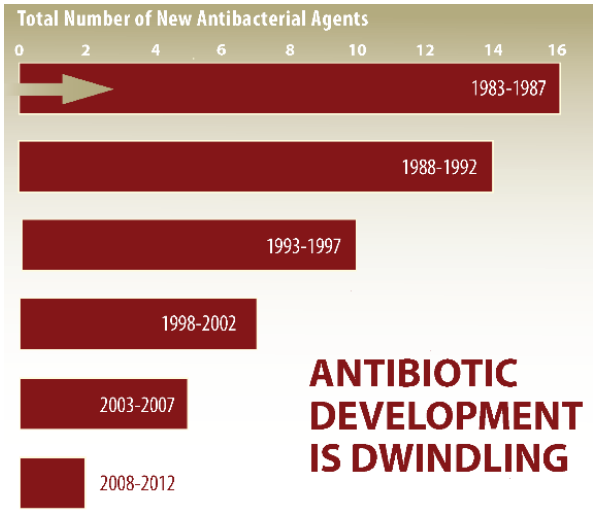

Figure 1: Number of new molecular entity (NME) systemic antibiotics approved by the US FDA per five-year period. (Taken from Spellberg et al., 2011[1])

In this post-antibiotic scenario, there is an urgent need for the development of new therapies to face bacterial infections and for the identification of new targets inside bacterial cells useful for their eradication from the host. Unfortunately, bacterial resistance is not the only mechanism through which bacterial cells can become drug-tolerant. Indeed, besides resistance, there is also a phenomenon known as bacterial persistence. The latter is a particular phenotype (not genetically acquired) that is activated stochastically as a background survival strategy but can also be triggered by stressful conditions, such as nutrient starvation and antibiotic treatment. Persistent cells are characterized by a temporary dormancy, which makes them insensitive towards antibiotics. If we consider an isogenic bacterial population in a planktonic state (living single-celled creatures floating

in their environment), we can always find, independently from the growth phase, a little fraction of bacteria (10^{-6} - 10^{-5} CFU) adopting this particular dormant/stationary transient state. Treating this population with an appropriate antibiotic dose[2] leads to a biphasic killing curve (Figure 2, grey), where the majority of the bacterial cells die within a few hours (red), while persisters awake stochastically over time. If they find a favorable environment (e.g., after the stress condition is absent from the system) they can give rise to a new bacterial population, identical to the initial one and still antibiotic-sensitive. For this reason, if they awake in the presence of the antibiotic, they die with a slower killing rate (green), equal to their resurgence rate. In a post-antibiotic scenario, bacterial persistence can be considered an important phenomenon since it can lead to chronic and recurrent infections.

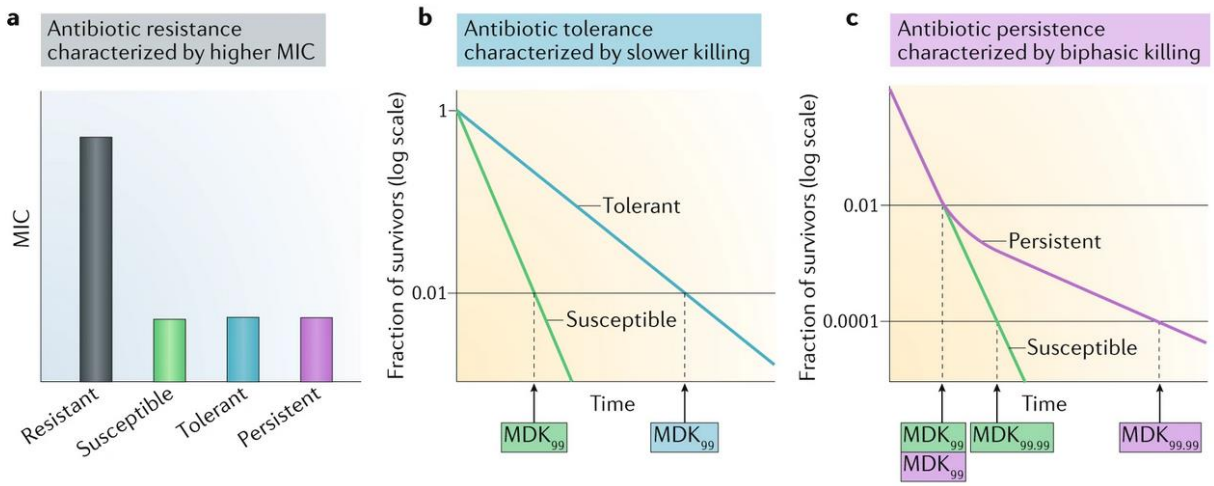

***Figure 2*: Resistance, tolerance and persistence are distinct responses to antibiotic treatment that lead to increased survival compared with susceptible cells. a)** To inhibit the growth of resistant bacteria, a substantially higher minimum inhibitory concentration (MIC) of the antibiotic is needed than for susceptible bacteria. **b**) Tolerance increases the minimum duration for killing (MDK), i.e. for 99% of bacterial cells in the population (MDK_{99}) compared with susceptible bacteria. **c)** Persistence leads to a similar MIC and a similar initial killing of the bacterial population compared with susceptible bacteria; however, the MDK for 99.99% of bacterial cells in the population ($MDK_{99.99}$) can be substantially higher owing to the survival of the persister cells. Pure exponential killing of the susceptible strain is rarely observed because most bacterial cultures have some level of persistence. (Taken from Balaban et al, 2019)[2]

The molecular mechanisms at the basis of persistence have not been univocally established and no specific treatment is currently available. One of the working hypotheses involves the upstream of the Stringent Response (SR), a survival biochemical pathway used by bacteria and many other organisms to face different stress conditions (e.g., nutrients starvation or antibiotic treatment)[3].
The present PhD thesis is part of a more complex research project that aims at hampering persisters formation by blocking SR at its early stage (ERC-StG ERACHRON, grant n. 758108).

Antimicrobial resistance

Since the discovery of Penicillin in 1929 by Fleming [4], antibiotics have been widely used as the most effective drugs to eradicate bacterial infections. Immediately after antibiotics market launch, scientists noted that some microbes could survive lethal doses[5], thus they coined the term 'drug-fast' (German: *-fets* = -proof) to refer to this property. Initially, this issue was faced by increasing the therapeutic dose, however some *in vitro* evidences showed that a gradual drug increase usually led to resistant microorganisms, while exposure to an initial high concertation did not[6]. Moreover, for each antibiotic a concentration threshold was determined, above which the drug was lethal.

In the following decades, many different chemical classes of antibiotics were discovered, such as sulfonamides, fluoroquinolones, β-lactams, aminoglycosides and macrolides in order to overcome acquired resistance (e.g., by increasing drug efflux or decreasing membrane permeability). Then, chemical modifications were introduced in each class in order to enlarge the scope of such antibiotics. All these drugs have in common the feature of targeting specific essential biochemical pathways univocally present in bacterial cells. Usually antibiotics interfere with essential processes, such as DNA replication, cell wall building and translation.

- *Inhibitors of DNA synthesis/replication*

Sulfonamides and fluoroquinolones interfere with the synthesis and the regulation/replication of bacterial DNA, respectively.

Sulfonamides do not directly target DNA, but they block the synthesis of tetrahydrofolic acid (Scheme 1), which is essential for thymidine synthesis. Lack of this nucleoside prevents DNA replication[7]. Usually, dihydropteroate synthase accumulates **dihydropteroic acid** by joining together *p*-aminobenzoic acid (**PABA**) and **dihydropteroate diphosphate** (grey pathway of Scheme 1). However, if sulfonamides are present, a competition in the active site of dihydropteroate synthase with **PABA** and sulfonamides takes place. As result, a '**false metabolite**' is yielded. Unlike the natural metabolite **dihydropteroic acid**, the false one cannot undergo D-glutamic acid conjugation, thus blocking thymidine biosynthesis.

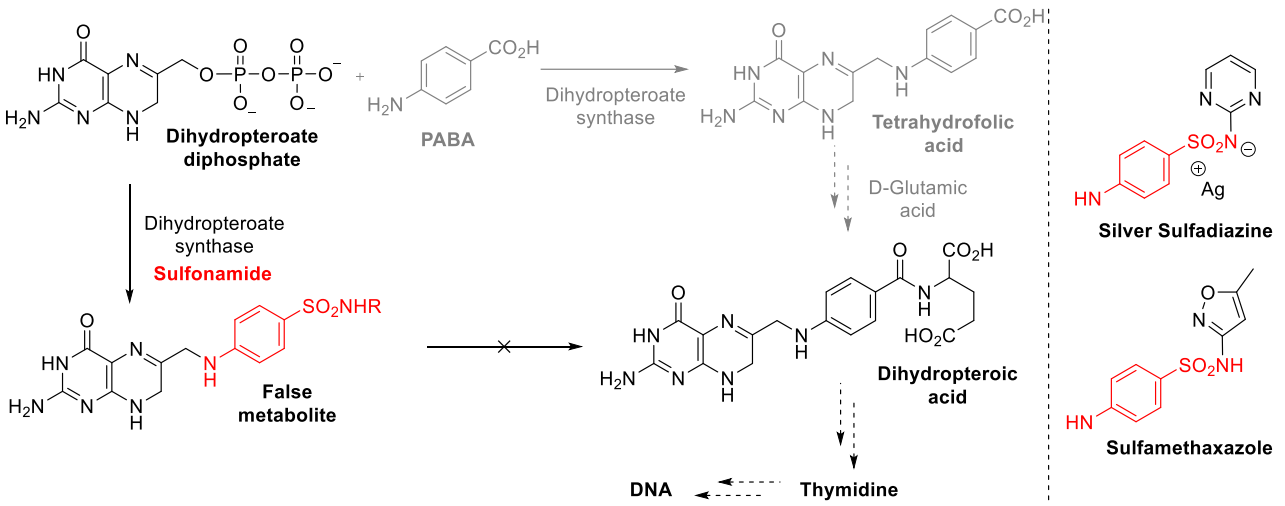

Scheme 1: **Synthesis of tetrahydrofolic acid** in absence of sulfonamides (grey) and the role of the antibiotic in DNA synthesis inhibition (black). On the right two examples of actual marketed sulfonamides with red-labelled pharmacophore moiety.

Bacteria have developed several strategies to survive in the presence of sulfonamides. The first bacterial response is a change in the drug influx/efflux equilibrium induced by either specific active membrane transporters overexpression or decrease of cell permeability that leads to a drop in antibiotic uptake.

Another survival strategy is the overproduction of PABA that displaces the sulfonamide from the enzymatic active site, thus allowing the synthesis of tetrahydrofolic acid (Scheme 1). Mutations at the enzyme active site level can lead to an improved selectivity for PABA over the sulfonamides. As additional survival strategy, in presence of sulfonamides, bacteria evolve the ability to bring exogenous folate inside the cell. When this resistant mechanism takes place, sulfonamide resistance could be overcome by addition of the dihydrofolate reductase inhibitor **Trimethoprim** (Scheme 2). In this way, exogenous folates cannot be converted into tetrahydrofolic acid. However, a single point mutation (Ile100Leu) in dihydrofolate reductase, or its over expression, leads to acquired trimethoprim resistance [8].

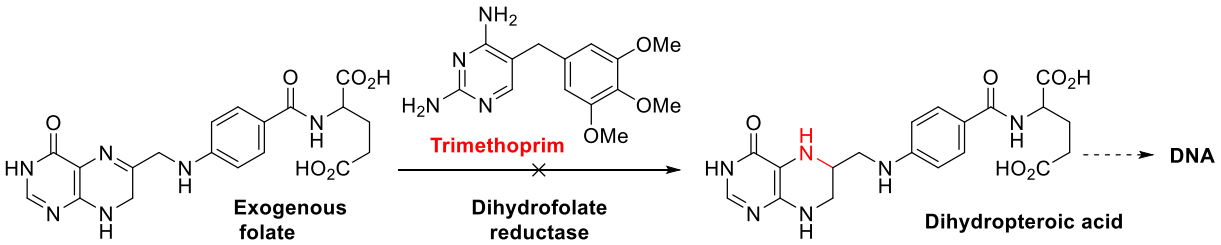

Scheme 2: **Structure and inhibition mechanism of the antibiotic trimethoprim**.

Fluoroquinolones, such as Besifloxacin and Levofloxacin (Figure 3), interact directly with DNA by targeting two fundamental DNA proteins: *DNA gyrase* (an ATP-dependent strain reducer) and *topoisomerase IV* (DNA metabolism regulator). Antibiotic binding to these enzymes causes DNA inaccessibility, leading to cell death. Cells became fluoroquinolone-resistant thanks to spontaneous alteration on DNA gyrase coding genes (*gyrA* and *gyrB*) and/or topoisomerase IV genes (*parC* and *parE*).

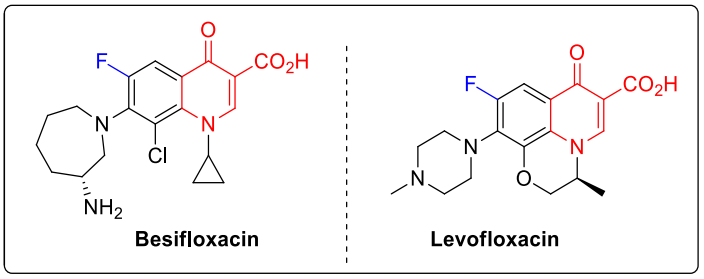

Figure 3: **Structure of two common fluoroquinolones,** pharmacophore moiety in red.

- *Inhibitors of bacterial cell wall biosynthesis*

The main representatives of this antibiotic class are penicillins, a class of antibiotics in which the pharmacophore moiety is a strained β-lactam. The mechanism of action of these antibiotics, shown in Scheme 3, relies on the irreversible ring-opening reaction of the **β-lactam** ring by the enzyme transpeptidase that, after covalent binding to penicillin, can no longer participate in cell wall construction due to the formation of adduct **A**.

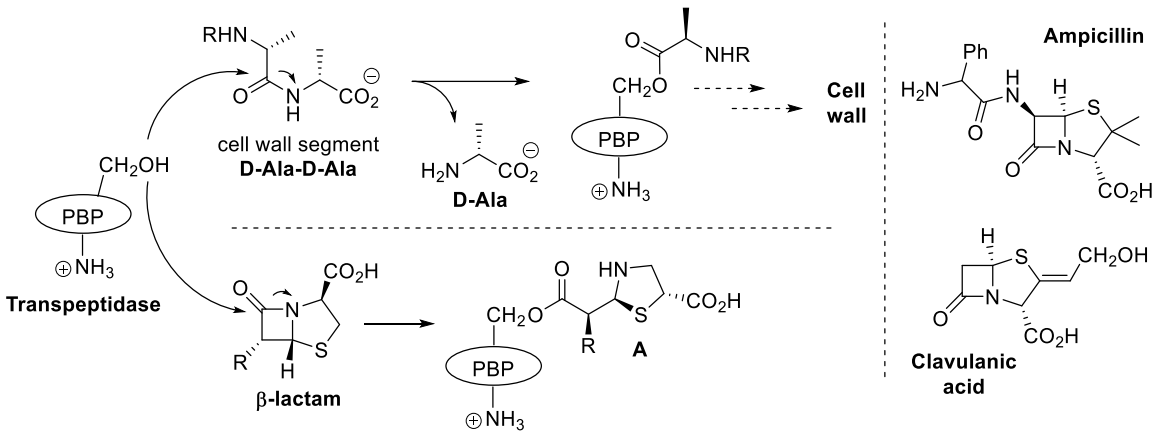

Scheme 3: **Inhibition of transpeptidase by β-lactam**. On the right, structures of **Ampicillin** and **Clavulanic acid**.

Penicillin resistance was first reported in 1940 [5] and ascribed to the presence of sophisticated serine-proteases, called β-lactamases, able to intercept and inactivate penicillins. Such acquired resistance can be sometimes overcome by adding β-lactamase suicide inhibitors, such as **clavulanic acid** Scheme 3), which undergoes irreversible reaction with β-lactamase, thus inactivating the enzyme.

- *Inhibitors of protein biosynthesis*

Aminoglycosides (e.g. Gentamicin) and macrolides (e.g. Erythromycin, Figure 4) bind to different regions of the prokaryotic ribosome and interfere with protein synthesis, leading to either mistranslation or aberrant proteins.

Interestingly, in the case of aminoglycosides, bacterial cells can also synthetize specific enzymes which selectively modify the drug. Indeed, aminoglycosides can be N-acetylated by aminoglycoside acetylase (AAC), O-adenylated by aminoglycoside nucleotide transferase (ANT) or O-phosphorylated by aminoglycoside phosphorylase (APH), as shown in Figure 4[9].

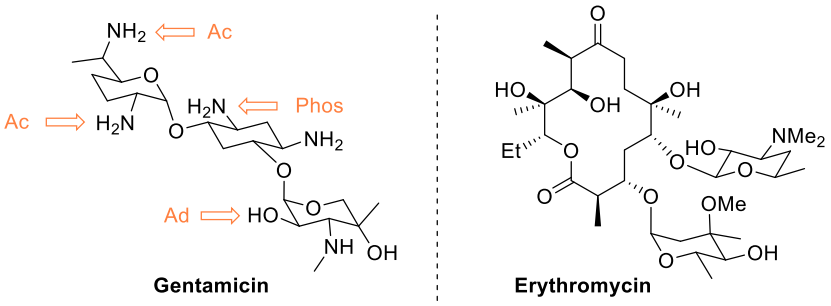

Figure 4: **Structures of the aminoglycoside Gentamicin and the macrolide Erythromycin.** Positions indicated by arrows can be inactivated by the corresponding specific enzyme: **Ac**: Acetylation (by AAC); **Ad**: Adenylation (by ANT); **Phos**: phosphorylation (by APH).

Through the years, different strategies have been employed against resistance, like some examples described above. However, it is not always possible to overcome resistance, hence the need for the discovery of new chemical classes of antibiotics is particularly urgent.

Bacterial persistence

Unlike resistant bacterial strains, a persister population does not expand in the presence of antibiotics, but rather shows very slow to no growth (Figure 5). The phenomenon, differently from resistance, is caused by a non-heritable phenotype alteration[10].

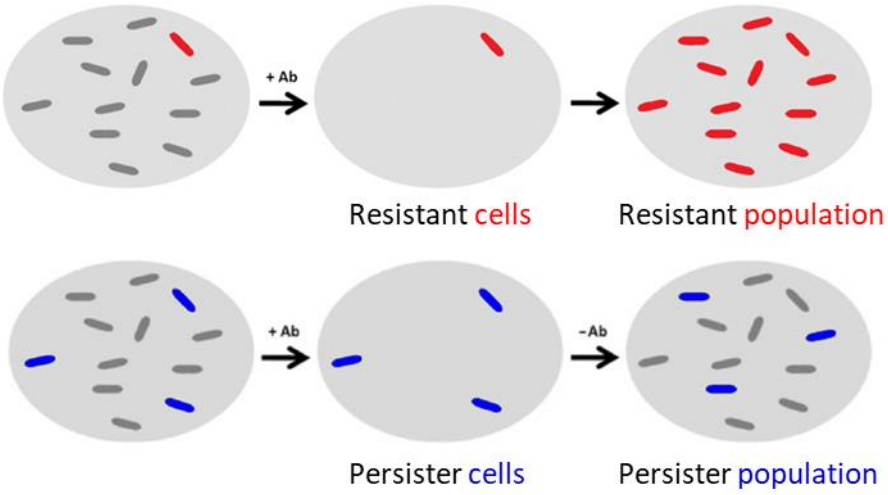

Figure 5: **Antibiotic resistance vs. persistence**. In the top panel, a microbial population containing resistant cells (red) is treated with antibiotics (+ Ab); as consequence, just the resistant cells survive. Upon regrowth, the entire colony is composed of resistant bacteria. In the bottom panel, a population containing persister cells (blue) undergoes antibiotic treatment and only persister cells remain. This time, the regrowth population exhibits the same susceptibility to antibiotics as the original one. (Adapted from Fauvart' et al., 2011[10])

The curious phenomenon was first reported by Bigger in 1944[11]. An army physician, Bigger described how antibiotics treatment often failed at sterilizing soldiers' wounds. When he investigated the phenomenon *in vitro*, he observed how penicillins were not able to sterilize *Staphylococcus aureus* cultures, with a little fraction of cells somehow surviving. Bigger called this singularity 'Persistence', meaning that cells "persisted" over antibiotics treatment. The brilliant physician understood that technological advancements were necessary for further investigation of the problem.

Unfortunately, persistence laid forgotten for many years, its existence obscured by the insurgence of the much more worrying genetic resistance, and its investigation hampered by the inadequate technological level at the time. This phenomenon has only recently been "rediscovered" and is currently under investigation by several groups worldwide. Although it is a non-inheritable trait, a gene characteristic of high-persister mutants in *E. coli* was identified in 1983[12]. Thanks to mutagenesis and phenotypic expression techniques, they isolated Hip (High persistence) mutants showing an increased persisters fraction (ca. 10^{-2} Colony-forming unit, CFU, in Hip *vs*. 10^{-5}/10^{-6} CFU

in wild-type), although maintaining antibiotic susceptibility upon resurgence. Twenty years later, researchers characterized the *hipA7* allele[13] as the one conferring high persistence.

Thanks to the availability of single cell analysis techniques, the Balaban's group[14] investigated the occurrence of persistence in single *E. coli* cells with the use of microfluidic devices. They followed the growth of individual bacterial cells under *i)* normal conditions, *ii)* antibiotic treatment and *iii)* restored permissive conditions (after ampicillin treatment, the few surviving cells were allowed to regrow in the absence of the drug). Surprisingly, persisters could be clearly identified already before ampicillin addition, thanks to a significantly reduced growth rate. Thanks to this pioneering work, it was possible to understand that persistence was linked to an inherent heterogeneity of growth rates in the bacterial population. Other techniques have been developed for the qualitative and quantitative analysis of persister cells, some of which will be discussed in the next chapters of this thesis.

Bacterial persistence is also believed to be strictly correlated with bacterial resistance. Even if the difference between the two phenomena is clear, persister bacteria, who already survived antibiotic treatment, might develop a genetic alteration to be permanently insensitive to the drug. In this scenario, persistence might be then seen as a 'helper' for cells resistance, since the impossibility to eradicate an infection is associated with the probability to generate new resistant strains. Moreover, mathematical modeling[15] has demonstrated that persistence leads to an extension of the duration of antibiotic treatments, often causing treatment failure and promoting resistance emergence.

A study made by De Groote and collaborators[16] found that fosfomycin resistance mechanisms affect persistence of *P. aeruginosa* upon treatment with the fluoroquinolone antibiotic ofloxacin. Fosfomycin [(1R,2S)-epoxypropylphosphonic acid, Scheme 4] is effective against both gram-positive and gram-negative bacteria. It is widely used for the treatment of lower urinary tract infections thanks to its excellent stability and broad activity spectrum. The bactericidal activity of the drug is exerted through inhibition of the enzyme UDP-(N-acetyl)glucosamine-3-enolpyruvyl transferase (MurA) which catalyzes the first step in prokaryotic cell wall biosynthesis (Scheme 4). Resistance to fosfomycin in *P. aeruginosa* [17] results from an altered activity of FosA[18], a glutathione (GSH) transferase that, when overexpressed, promotes GSH addition to fosfomycin, thus abolishing its antimicrobial activity (Scheme 4). Another resistance mechanism requires the inactivation of the fosfomycin transport protein GlpT[19].

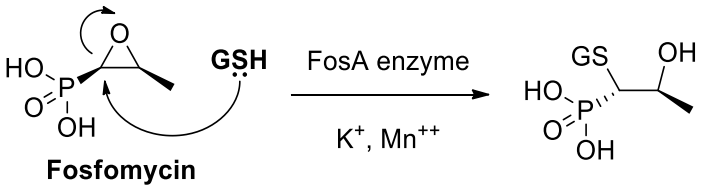

Scheme 4: **FosA is a Mn(II)-dependent metalloenzyme that catalyzes the conjugation of glutathione (GSH) to the epoxide ring of fosfomycin, inactivating the antibiotic.**

Overexpression of FosA or *glpT* knock out in *P. aeruginosa* resulted not only in a fosfomycin resistant strain, but also in a 50% drop in persisters fraction. For the first time, a direct molecular correlation between fosfomycin resistance and persistence was demonstrated[17].

The presence of persisters in cell cultures might induce some considerations about the intrinsic nature of this phenomenon. In fact, these data suggest that persistence has been developed under natural selective pressure to guarantee bacterial survival. With this in mind, persistence can be seen as a sort of '*insurance*' for bacterial populations, represented by a little subpopulation of latent/dormant cells. In other words, bacterial persistence is a defense mechanism implemented by some organisms against sudden environmental changes. Therefore, the clinical relevance of persistence is significant, especially considering the many uncertainties still surrounding their formation mechanism.

Clinical relevance

There are specific pathologies that are intrinsically related to persistence due to the nature of affected tissues in which bacteria can proliferate. Among these diseases, Cystic fibrosis, Candidiasis and Tuberculosis are the most relevant, either for their fatality or diffusion.

➢ Cystic Fibrosis

Cystic fibrosis (CF) is a hereditary fatal disease affecting Caucasian people and is characterized by an imbalance of chloride anion levels in epithelial tissues of lungs and intestines. Collins and coworkers[20] identified the portion of the anomalous CFTR gene responsible for CF disease on the long arm of chromosome 7 in the 1980s. Such gene codes for CFTR protein (Cystic fibrosis transmembrane conductance regulator) that conducts chloride ions across epithelial cell membranes. Mutations in *CFTR* affect the chloride ion channel functioning, thus leading to dysregulation of epithelial fluid. As a result, CF is characterized by secretion of thick mucus that obstructs respiratory tracts and creates a perfect environment for bacterial colonies proliferation. Indeed, most CF patients succumb as the consequence of a bacterial infection, usually by opportunistic pathogens like *P. aeruginosa* and members of the *Burkholderia* genus[21]. For a long time, the reason why these pathogens cells proliferating in CF patients were extremely tolerant to antibiotics remained unclear. Resistance was rejected as an explanation due to the fact that isolated *P. aeruginosa* cells from CF patients did not present mutations in their genome[22] . The analysis of 35 longitudinal clinical isolates of single CF patients, isolated between the age of 8 and 96 months, revealed a dramatic 100-fold increase in persistence of *P. aeruginosa* cells during treatment with several antibiotics [23]. The clinical study was then extended to a larger group of patients confirming the involvement of persistence.

➢ Candidiasis

Persistence is not limited to prokaryotes but can also be found in eukaryotic cells. One example is given by the pathogen *Candida albicans*, a fungus that represents a serious threat to human health especially in immunocompromised patients. Recently, an increasing incidence of candidiasis has been recorded in hospital environments. Probably, this effect is likely the result of *Candida* biofilms formed on medical indwelling devices such as catheters, heart valve replacements and prostheses. In 2006, LaFleur and coworkers analyzed *C. albicans* biofilms and reported the presence of antifungal-tolerant cells that were very similar to *E. coli* and *P. aeruginosa* persisters found in both

planktonic and biofilm populations[24]. However, *C. albicans* persister cells were not present in planktonic growths. LaFleur's group was also able to demonstrate that *in vivo* selection of *C. albicans hip* mutants occurs in patients with oral candidiasis.

- Tuberculosis

Human tuberculosis (TB) is one of the main examples of chronic infections, being listed among the top 10 causes of deaths worldwide by the World Health Organization[25]. It is also estimated that one out of three people carries *Mycobacterium tuberculosis*, TB etiological agent, in a latent form. The dormant bacterium awakes in 5-10% of patients leading to a chronic disease, which results in severe lung damage. Nowadays, TB can be cured with a 14-days antibiotic treatment, however complete eradication of *M. tuberculosis* is rarely achieved. Ojha and coworkers[26] demonstrated how *M. tuberculosis* cells can form complex biofilms containing drug-tolerant cells, which share important features with the already described persisters found in other bacterial species. Moreover, once in biofilms, *M. tuberculosis* cells are also insensitive to treatment with antibiotics targeting non-replicant bacteria at a concentration 100-fold higher than the usual MIC. In 2016, Torrey and coworkers[27] elucidated the mechanism of persisters formation in *M. tuberculosis*. In the study, they selected highly persistent (*hip*) mutants and were able to characterize them by whole genome sequencing and transcriptome analysis. *Ex vivo* tests showed that these mutants presented a higher than normal survival rate.

Mechanisms for persisters formation

At first glance, persistence might resemble a 'hibernation' state in which no biochemical activity occurs. However, the characteristic temporarily dormant state of a persister cell is more complicated. Indeed, many biochemical processes take place during cell lethargy and slowly replicating *Mycobacterium smegmatis* have been reported[28]. The mechanisms behind persisters formation are not completely clear and data suggest that different pathways might be involved.

- *Decreased energy levels*

Just like mitochondria in eukaryotes, each prokaryotic cell produces its own energy in form of ATP through the ATP synthase present in the inner cell membrane (Figure 6). This enzyme produces ATP from ADP and inorganic phosphate (Pi), coupling it to protons influx from the periplasmic space to the cytoplasm. Protons spontaneously flux into the cytoplasm due the presence of a constant membrane potential which causes both a chemical and electric potential difference. The resulting gradient is known as proton motive force (PMF). Alterations of this gradient seem to be correlated with persistence [29]. Indeed, the presence of PMF perturbing agents, in particular substances able to reduce it (e.g. salicylate [30]), enhance persisters formation.

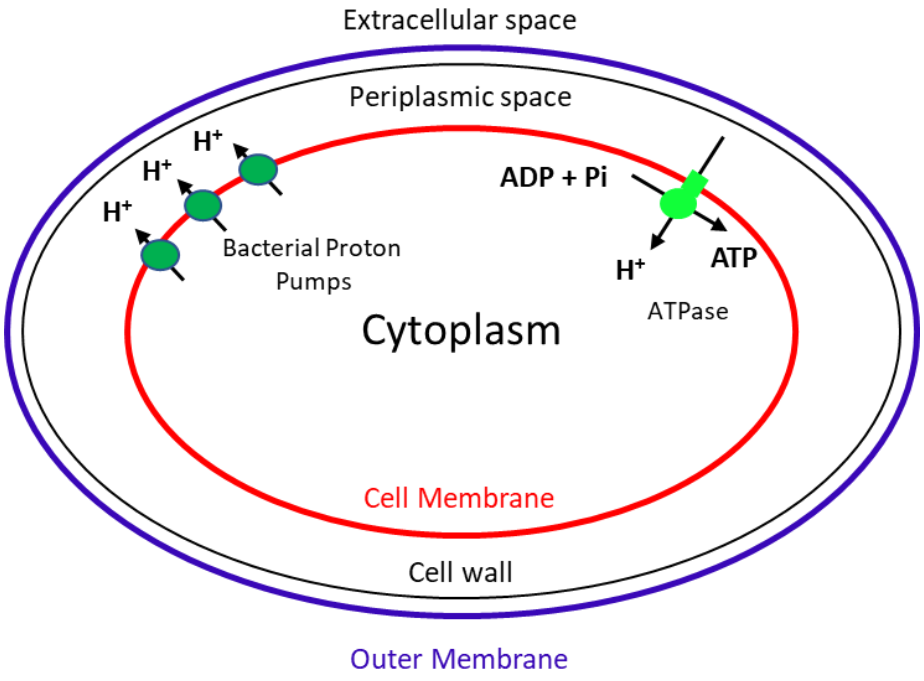

Figure 6: **Prokaryotic cell vignette depicting the mechanism behind energy production.**

In *E. coli*, PMF alterations by means of effectors, e.g. the fluoroquinolone **Ciprofloxacin**[31], has been correlated to enhanced persistence. Moreover, in planktonic *E. coli* cultures and *P. aeruginosa* biofilms, mannitol and glucose showed the ability to reduce the amount of persisters by increasing the PMF gradient[32].

Membrane potential and ATP levels affect persistence in several ways since reduced ATP levels lead to a slowdown in DNA, proteins and peptidoglycans synthesis. As a matter of fact, antibiotics targeting these biochemical processes, such as β-lactams, fluoroquinolones and amino glycosides, show a much lower efficacy, probably because their targets are less or even not active.

Some drugs, like **enopeptin A**, do not need active targets. Enopeptin A belongs to the acyldepsipeptide (ADEP) family (Figure 7). ADEP drugs deregulate ClpP protease (a universal prokaryotic protease), consequently leading to an uncontrolled detrimental proteolysis. If associated with another antimicrobial drug, ADEPs are able to eradicate persisters[33].

Besides its energetic involvement, ATP is also fundamental for the stability of many proteins, e.g. helping their solubility. Therefore, low ATP levels may cause the aggregation of essential proteins and be a trigger for the dormant state. This hypothesis was proven by Pu and coworkers[34], which observed that the DnaK-ClpB complex was essential for the efficient disaggregation of proteins present in dormant cells once they awake.

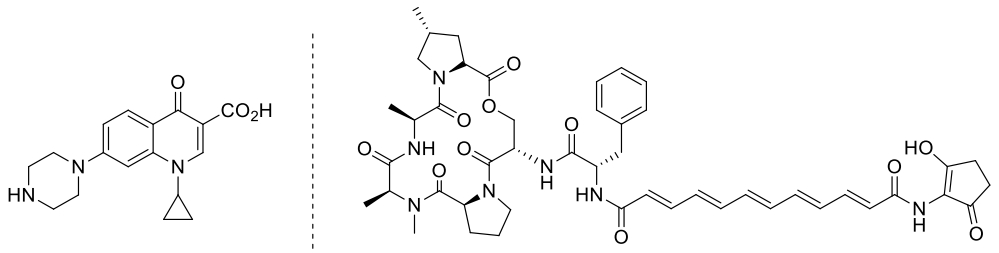

Figure 7: **Structures of the fluoroquinolone Ciprofloxacin** (left) **and the acyldepsipeptide (ADEP) enopeptin A** (right)**.**

- *Stress conditions*

The persisters fraction of a bacterial population is usually small and constant in wild-type strains under normal growth conditions but can be increased under stressful condition, such as i) starvation of fundamental nutrients, such as amino acids, fatty acids and/or metals; ii) oxidative and/or heat stress; iii) change (diauxic shift) of primary carbon sources; iv) antibiotic treatments[35].

Therefore, besides the basal level of persisters that naturally occur, such conditions induce the formation of new persisters, which add up to the preexistent ones (Figure 8), making pathogen eradication more difficult.

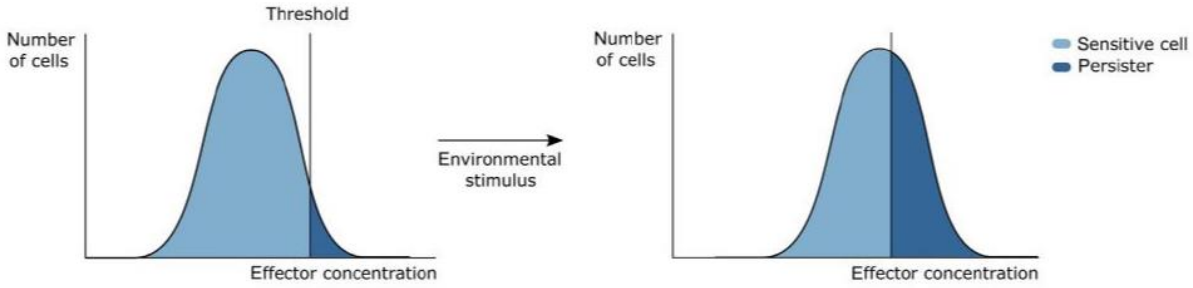

Figure 8: **Schematic illustration of basal persisters level *vs*. induced persistence**. (Taken from Wilmaerts et al., 2019[29])

Stressful conditions lead to the dormant state by a mechanism that involves *hipA* gene. Ectopic activation of *hipA* induces growth arrest and strongly inhibited replication, transcription and translation. Induction of the latter depends on intrinsic and/or extrinsic noise (e.g. external stimuli). HipA, the protein coded by *hipA*, is a eukaryotic-like serine-threonine kinase that specifically phosphorylates Ser239 on GltX (Glutamate tRNA ligase) when in complex with its substrate ($tRNA^{Glu}$). Once phosphorylated, the GltX: $tRNA^{Glu}$ complex is switched off. Even a very low expression of HipA usually leads to an enormous signal amplification due to the cascade of triggered reactions. This process has been proven by several experiments: LC-MS/MS analysis showed not only a molecular weight difference of 80 Da between regular GltX and GltX treated with HipA, corresponding to $H_2PO_4^-$ group, but also pointed out that the phosphorylation was just on Ser239. Moreover, by X-ray crystallography, it was possible to decipher the actual mechanism: on free GltX, Ser239 is part of a flexible loop that becomes approachable thanks to a conformational change induced by $tRNA^{Glu}$ binding. Uncharged $tRNA^{Glu}$ accumulates and enters in the ribosomal A site: such event triggers the release of RelA enzyme (Figure 9).

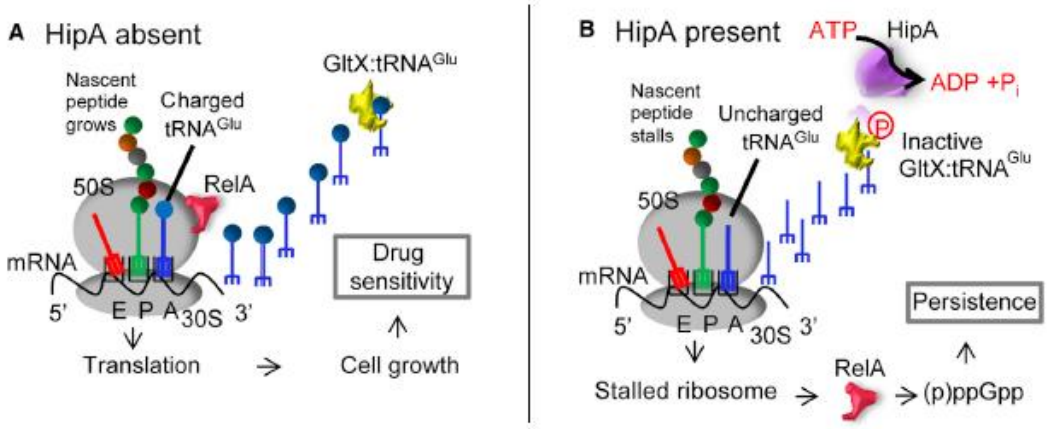

Figure 9: **A)** HipA absence allows regular function of the transcription process, while its presence **B)** HipA inactivate GltX leading to an uncharged tRNAGlu accumulation, RelA is then released and persistence is induced. (Taken from Germain et al., 2013[36])

RelA belongs to the RelA-SpoT Homologous (RSH) enzymes superfamily that play a key role in the shifting from regular growth to stasis by accumulating a specific modified nucleotide (guanosine tetra- or penta-phosphate). The latter event is the starting point for one of the main pathways involved in persisters formation, known as Stringent Response.

Stringent Response

One of the molecular mechanisms involved in persistence is the signaling *via* guanosine pentaphosphate/tetraphosphate (p)ppGpp, also known as "magic spot." (p)ppGpp is a very important stress second messenger which orchestrates the stringent response, a survival biochemical pathway used in stress conditions by many bacteria and other organisms[37]. (p)ppGpp is produced during amino acid or fatty acid starvation[38] by proteins belonging to the RelA/SpoT homologous family (RSH), as shown in scheme 5.

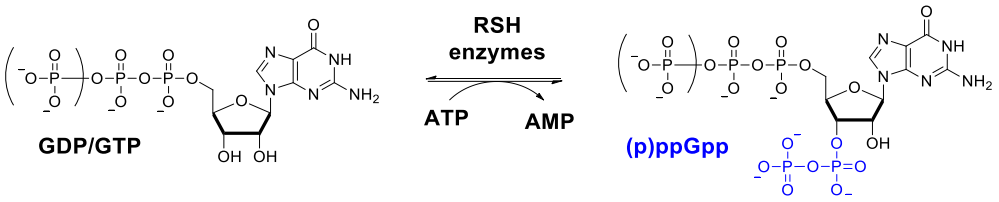

Scheme 5: **Synthesis of (p)ppGpp mediated by RSH enzymes.**

(p)ppGpp levels can also increase in response to a wide range of environmental signals, including oxygen variation[39], pH downshift[40], osmotic shock[41], temperature shift, or even exposure to darkness[42].

(p)ppGpp acts as an alarmone, playing pleiotropic effects on the cell, such as affecting DNA replication, protein synthesis, transcription inhibition and many others (Figure 10). In particular, in *E. coli*, the accumulation of (p)ppGpp causes the differential expression of approximately 500 genes, as it activates RpoS and RpoE (the sigma factors for the stationary phase and for periplasmic misfolded proteins[43], respectively). Moreover, (p)ppGpp directly inhibits DNA primase[44] and is thought to inhibit the synthesis of rRNA, which also affects translation globally, by regulating the transcription of the ribosomal modulation factor (Rmf)[45]. More specifically (p)ppGpp binds to the RNA polymerase, inducing an allosteric signal to the catalytic Mg^{2+} site, which severely decreases transcription and causes a global rewiring of the gene expression profile. Taken together, all these changes lead to dormancy or slow growth for most cells.

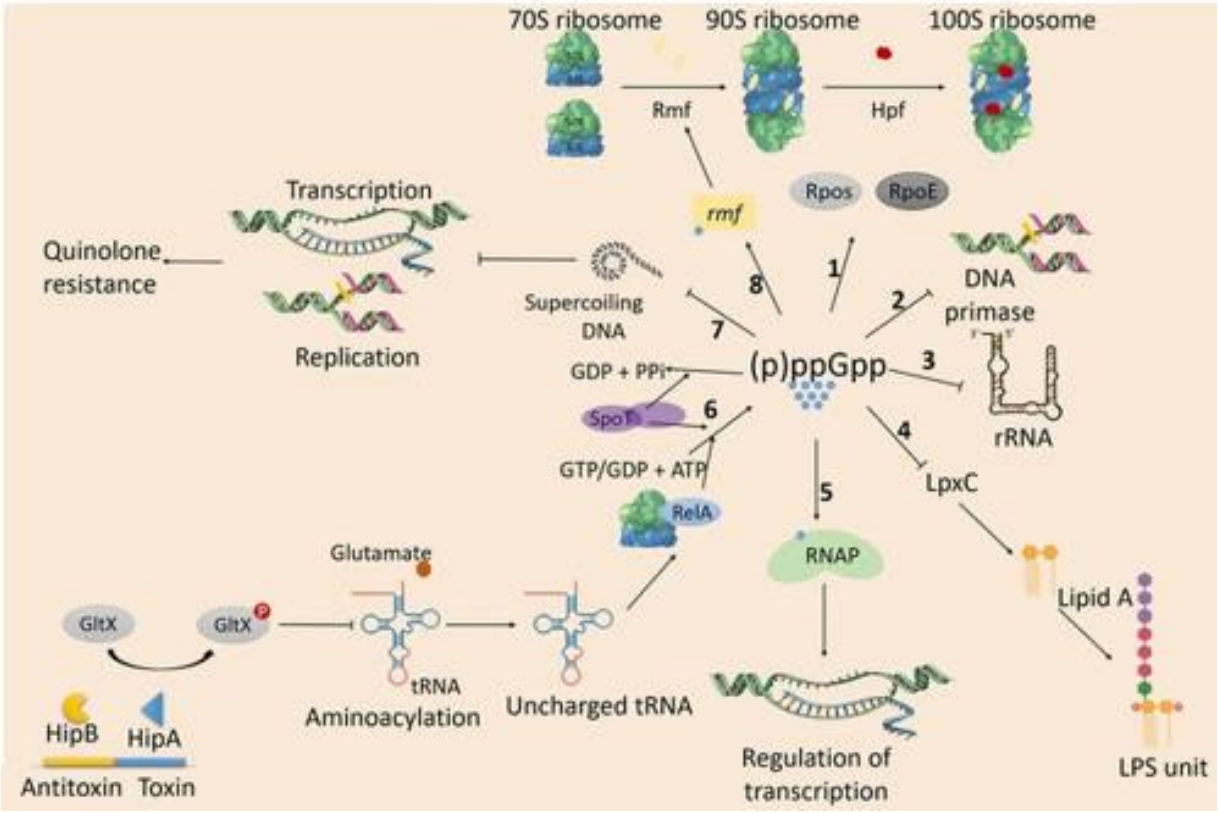

Figure 10: **Physiological pathways regulated by (p)ppGpp and the stringent response in *E. coli*. 1**, increased levels of (p)ppGpp induce transcription of RpoS and RpoE; **2**, (p)ppGpp inhibits DNA primase and thus replication; **3**, (p)ppGpp also inhibits transcription of rRNA, affecting the general translation; **4**, (p)ppGpp also deregulates LpxC, an enzyme catalyzing the first step of lipopolysaccharide (LPS) formation; **5**, (p)ppGpp binds to RNA polymerase (RNAP), regulating the transcription of many genes; **6**, according to certain models, HipA toxin would phosphorylate glutamyl-tRNA-synthetase (GltX), inactivating it and therefore impairing aminoacylation; **7**, (p)ppGpp can directly inhibit negative supercoiling of DNA in *E. coli*, associated with resistance to quinolones; **8**, (p)ppGpp induces the transcription of the ribosomal modulation factor (Rmf) and hibernation-promoting factor (Hpf), which play a role in ribosome dimerization, typical of persister cells. (p)ppGpp is also involved in immune evasion, virulence, and human pathogenesis. (Taken from Pacios et al., 2020[46])

We reasoned that blocking the activity of RSH enzymes, responsible for (p)ppGpp accumulation, could pave the way for new therapies against persistence and for the elucidation of its molecular details.

RSH superfamily

Superfamilies of enzymes usually comprise proteins that share sequence, function and/or structure similarities. In particular, the RSH superfamily comprises RelA and SpoT homologous enzymes, thus able to either synthetize or hydrolyze (p)ppGpp and taking part in SR. RSH members share some structural analogies especially in the local environment of the active site. These enzymes were first investigated in *E. coli*, where RelA and SpoT were discovered. RSH enzymes can be found in most bacterial genera, also in γ- and β- proteobacteria, meaning that they come from a common ancestor. From a functional and structural point of view, RSH enzymes can be divided in three classes: i) long RSHs, bifunctional enzymes that present both synthetase (SYNTH) and hydrolase (HYD) domains, generally also presenting a C-terminal regulatory region; ii) SAS: Small Alarmone Synthetases, able to only synthetize (p)ppGpp; iii) SAH: Small Alarmone Hydrolases, only able to hydrolyze (p)ppGpp. Both *E. coli*'s RelA and SpoT belong to the first class. However, RelA HYD domain is inactive and probably only useful for conformational reasons. These enzymes were first described in the context of SR. In fact, in amino acid starvation conditions, researchers observed that deacetylated tRNA accumulated and bound in the ribosomal A-site. This is the primary induction signal of SR: in fact, RelA can bind to stalled ribosomes, *via* its C-terminal region, and consumes ATP to produce (p)ppGpp from either GDP or GTP. Interestingly though, guanosine 3',5'-pentaphostate (pppGpp) is rapidly degraded to ppGpp in *E. coli* by pppGpp-phosphohydrolase (GPP) [47]. The actual significance of this mono-dephosphorylation is not completely clear. While RelA is the primary RSH enzyme for (p)ppGpp production in *E. coli*, SpoT main role is the hydrolysis of the alarmone. SpoT SYNTH domain is, in fact, significantly less active than the HYD one and responds to different stress stimuli with respect to RelA.

In our project, we decided to use as our main model a bifunctional RSH enzyme from *Streptococcus dysgalactiae subsp. equisimilis* (Rel_{Seq}) since its crystal structure was already available (Figure 11A). Rel_{Seq} needs bivalent metal cofactors for both its enzymatic activities, in particular Mg^{2+} and Mn^{2+} for (p)ppGpp synthesis and hydrolysis, respectively. An interesting feature in Rel_{Seq} is the inter-regulation of the two catalytic domains: indeed, the interaction of one domain with its substrate(s) (e.g. SYNTH with GDP and/or ATP) imposes conformational changes that are transmitted to the other domain (e.g. HYD) *via* a central three-helix bundle (Figure 11A, in grey), probably reducing its activity [48]. From a functional point of view, Rel_{Seq} presents a physiological imbalance between the basal activities of the two domains, shifted towards (p)ppGpp hydrolysis *in vivo*. Deletion of the C-

terminal region (Rel_{Seq}1-385) proved to revert the equilibrium in favor of (p)ppGpp synthesis *in vitro*[49].

In vitro data also suggest that, if both domains present the appropriate metal cofactor, Rel_{Seq} is able to perform both its activities, leading to a so-called futile cycle (Figure 11B), i.e. when two metabolic pathways run simultaneously in opposite directions. In this case, the SYNTH domain produces ppGpp consuming GDP and ATP, while the HYD one converts ppGpp back to GDP and pyrophosphate (PP_i). The overall result is ATP consumption and pyrophosphate accumulation, while concentrations of ppGpp and GDP remain constant[50].

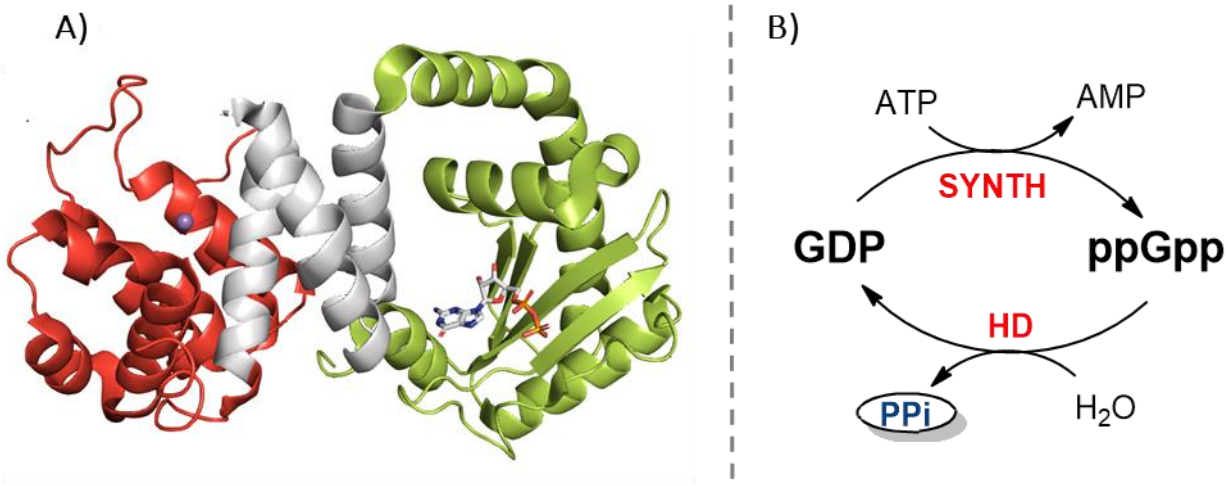

Figure 11: **A) Crystal structure of Rel_{Seq}** (PDB:1VJ7[51]): SYNTH domain in green cartoon with bound GDP in sticks representation; HYD domain in red cartoon; central three-helix bundle in gray cartoon. **B) Scheme of Rel_{Seq} futile cycle**.

Another RSH enzyme used in our project is a small alarmone synthetase from *Staphylococcus aureus* called RelP (Figure 12) that shares structural similarities with Rel_{Seq} SYNTH domain. As most SASs, RelP can transfer PPi moieties from ATP to GDP and GTP yielding pGpp, ppGpp and pppGpp, respectively.

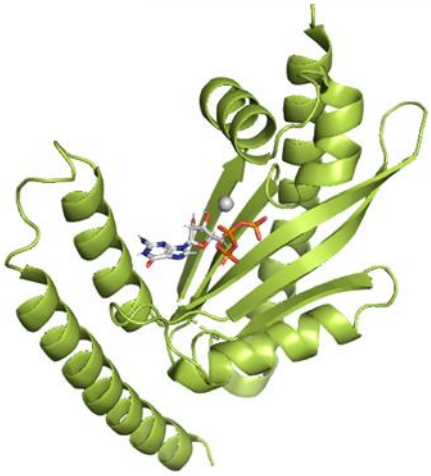

***Figure 12**:* **Crystal structure of RelP** (PDB: 6EWZ[52]) **with Mg^{2+} and GTP in its active site**.

Aim of the thesis

The goal of our research project, a part of which consists of the present PhD thesis, is the design and validation of RSH ligands that can inhibit (p)ppGpp synthesis.

The rationally designed ligands, once synthesized, need to be tested for Rel protein(s) affinity and for their ability to inhibit alarmone synthesis. My work consisted in the setup of a quantitative detection method of (p)ppGpp and in the optimization of its isolation and purification from its enzymatic preparation. In particular, herein I will describe the optimization of the synthesis of the (p)ppGpp specific chemosensor PyDPA (Chapter 1), the enzymatic synthesis and isolation on a preparative scale of ppGpp and the design of a ppGpp selective scavenging system (Chapter 2).

Chapter One

1.1 (p)ppGpp quantitative detection

The search of new enzyme inhibitors is a tough process that also relies on the reproducibility and accountability of biological assays used. The screening of dozens of compounds is challenging; therefore, relatively systematic high-throughput methods for biological analysis are valued. Likely, for most potential ligands, selected *in silico*, a preliminary *in vitro* screening, qualitative or semi-quantitative, is more than fine. However, for the most interesting candidates, an actual inhibition constant (e.g. IC_{50}) must be defined. To this aim, the ideal technique should be fast, feasible on large number of samples, cheap, suitable for all analyzed molecules and precise. For RSH enzymes, the most obvious biological assay is the detection of their enzymatic activity, hence of (p)ppGpp production. Through the years, researchers have used different methods for (p)ppGpp detection *in vitro*.

1.1.1 ^{32}P-labelled substrates

(p)ppGpp quantitative detection was first achieved using ^{32}P-labeled substrates, i.e. ^{32}P-ATP [53] or ^{32}P-GDP[54], that were measured by quantitative autoradiography of a TLC plate (Figure 1.1).

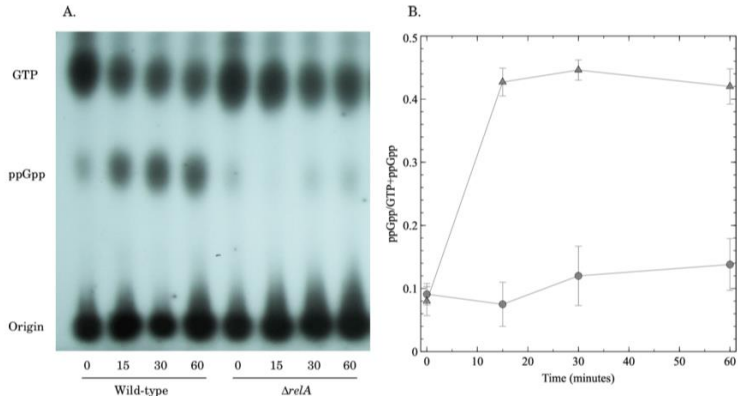

Figure 1.1: **A) An autoradiography TLC analysis used to study ppGpp accumulation**, between wild-type and ΔrelA *E. coli* strains at different time points. **B) ppGpp quantification over time**, with data derived from the TLC in panel A. (Taken from Cruvinel et al., 2019[55])

Radioactivity measurement is characterized by high sensitivity but is obviously less scalable and more problematic than traditional assays due to safety issues and protocols.

1.1.2 Fluorescence assays

Similar to radioactivity measurements, fluorescence spectroscopy is characterized by high sensitivity but does not have particular safety concerns. After absorbing light at a certain wavelength, fluorophores can emit in definite and specific regions of the spectrum. Emission detection at a 90° angle relative to the incident excitation radiation further improves sensitivity.

Phosphates are widespread in living cells and ubiquitously play significant roles in many biological processes. Examples are polyphosphate nucleotides, such as ATP, polynucleotides, like nucleic acids, and phosphorylated small molecules such as glucose-6-phosphate (G6P). Fluorescent detection of phosphate and pyrophosphate units has been achieved *via* coordination chemistry to Zn(II)-DPA binding motif(s) (Figure 1.2).

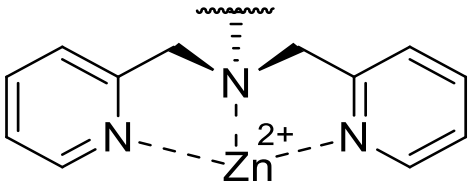

Figure 1.2: **Zn(II)-DPA motif.**

This strategy took inspiration from alkaline phosphatase (ALP) enzyme[56], which performs the hydrolysis of phospho-monoesters by means of two Zn(II) atoms carried in its active site (Figure 1.3).

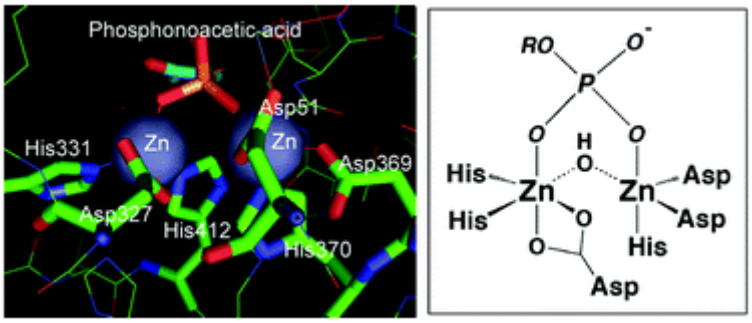

Figure 1.3: **Crystal structure of alkaline phosphatase active site**, in sticks (left) and lines (right). (Taken from Sakamoto et al., 2009[57])

Consequently, binuclear Zn(II)-DPA constructs efficiently bind pyrophosphate moieties[57].

A more sophisticated approach was required for the selective detection of ppGpp over other nucleotides such as ATP, GDP, etc. A specific ppGpp chemosensor would indeed require the assembly of the fluorophore only in the presence of such a "bidentate" ligand (i.e. bearing two pyrophosphate units). Rhee and coworkers designed such a system exploiting the ability of pyrene

to form excimers in solution even at low concentration[58]. An excimer (crasis of **Exci**ted Di**mer**) is a short-lived dimeric molecule formed by two species. Excimer formation occurs only between atoms or molecules in which at least one species has filled its valence shell, meaning that the molecule is in an electronic excited state.

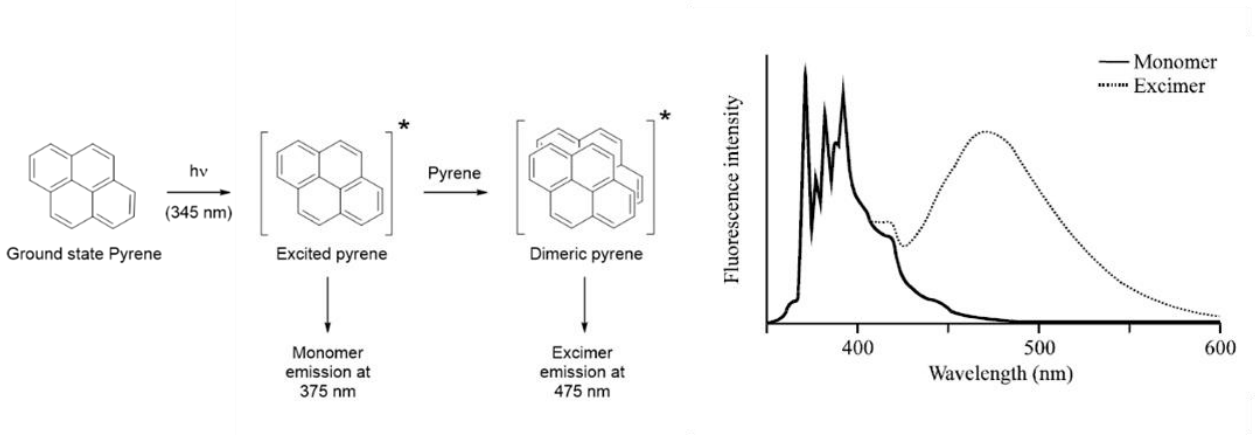

Scheme 1.1: **Different emissions spectra of the two possible fluorescent relaxation pathway of excited pyrene**. Bold line: spectrum of 'free' monomeric pyrene; dotted line: excimer spectrum (Adapted from Uddin et al., 2013[58])

Upon excitation at 345 nm, the pyrene moiety can emit either as monomeric species at 375 nm or as a dimer, i.e. the excimer, at 475 nm. The relaxation pathway undertaken depends on pyrene concentration, i.e. the possibility of dimers formation becomes higher increasing pyrene concentration. An important feature is the shape of the two emission spectra. The emission occurring from a single excited molecule provides a well-defined emission profile, due to a good separation between energy levels, while in the case of the excimer, the presence of several energetically close excited states leads to a broader emission signal. As shown in Figure 1.4, inorganic pyrophosphate (PPi) can promote excimer formation by coordinating two units of guanidinium pyrene[59].

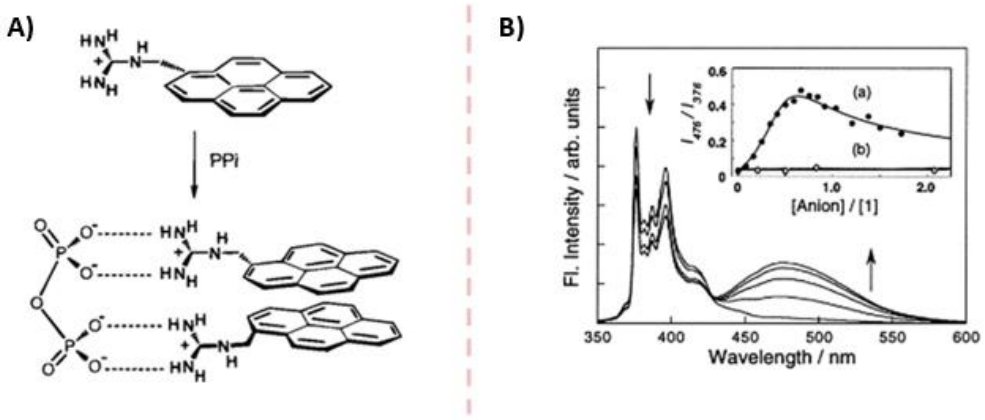

Figure 1.4: **A) Guanidinium pyrene alone or in complex with PPi; B) PPi effect on guanidinium pyrene fluorescence**. (Taken from Nishizawa et al. 1999[59])

Connecting a pyrene unit with the abovementioned Zn(II)-DPA moiety, allowed to obtain a fluorescent pyrophosphate sensor (Figure 1.5)[60] capable of 'ON-OFF' fluorescence sensing, since the excimer is formed only in the presence of pyrophosphate.

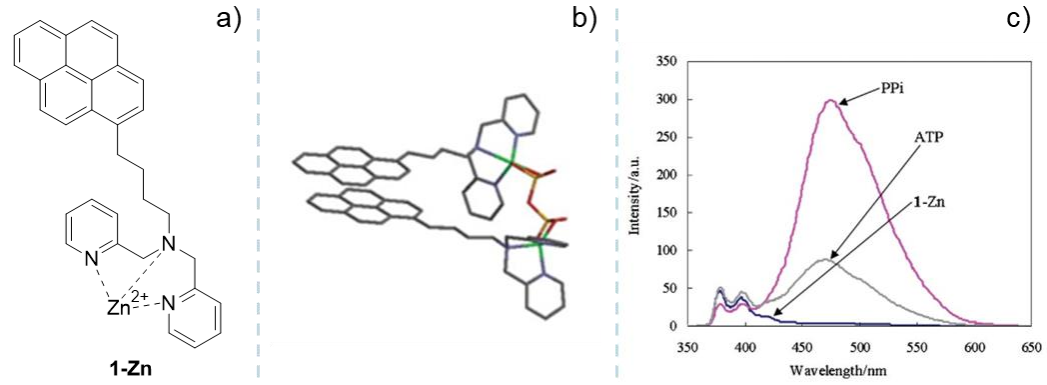

Figure 1.5: **A) Structure of the pyrophosphate chemosensor 1-Zn; B) Structure of PPi-chemosensor excimer**, with coloured bound pyrophosphate; **C) Fluorescence spectrum in presence of different ligands**, e.g. zinc, ATP and PPi. (Taken from Cho et al., [60])

1.1.3 PyDPA

Learning from all the considerations reported above, Rhee and coworkers designed a (p)ppGpp specific chemosensor, PyDPA[61] where the excimer-forming pyrene is connected through and aliphatic linker to a bis-Zn(II)-DPA moiety (Figure 1.6).

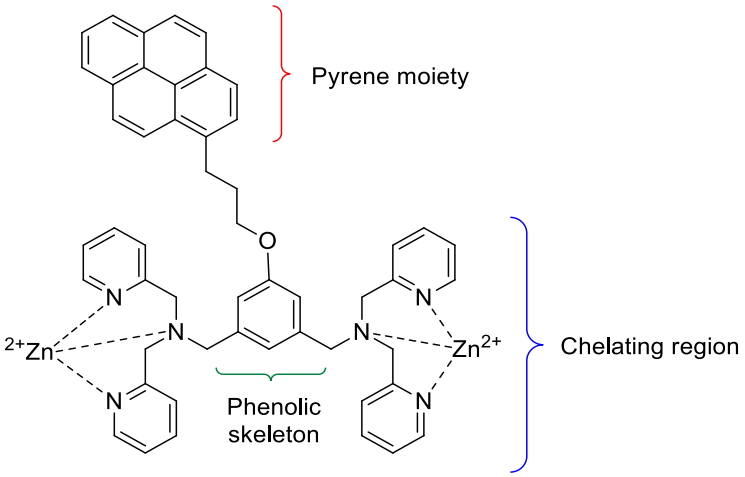

Figure 1.6: **PyDPA structure**.

In particular, when the two pyrophosphate units of (p)ppGpp are chelated by the bis-Zn(II)-DPA groups of two PyDPA molecules, the pyrene units can interact stack forming an excimer, as shown in Figure 1.7A.

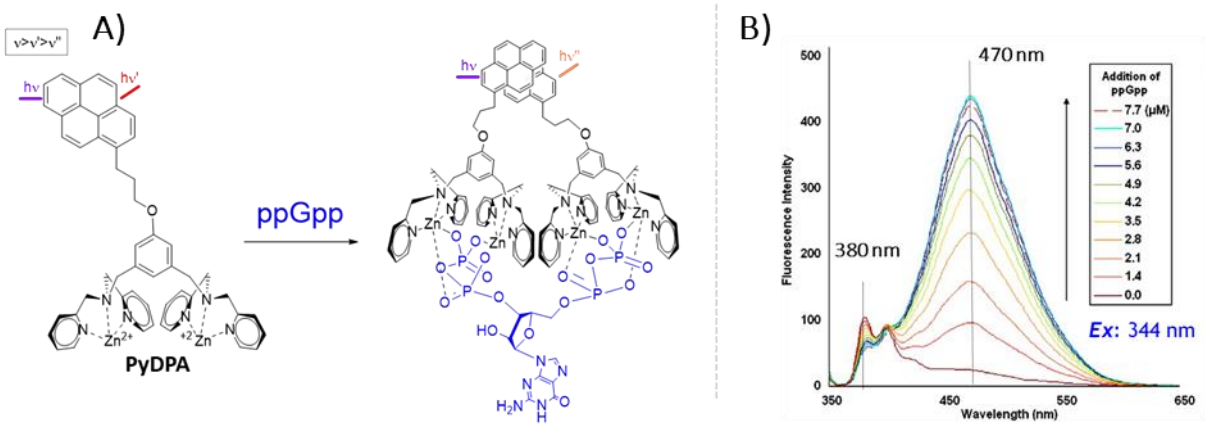

***Figure 1.7:* A) PyDPA excimer formation by interaction with ppGpp; B) 20 µM PyDPA fluorescence assay**, in presence of different ppGpp concentrations. Images (Taken from Rhee et al, 2008[61])

When excited at 344 nm, PyDPA (monomer) emits at 380 nm, while the dimer (excimer) emits at 470 nm. In the presence of molecules bearing only one pyrophosphate unit (e.g. ATP, GDP or PPi), PyDPA is able to form only 1:1 complexes with emission only at 380 nm.

If we subject PyDPA (20 µM) to increasing amounts of ppGpp, excimer emission intensity increases to a maximum up to 7 µM ppGpp. Higher concentrations (i.e. 7.7 µM, dashed line in Figure 1.7B) result in a lower signal, probably due to the inner filter effect, i.e. a quenching mechanism where some of the emitted light is reabsorbed by the system.

Furthermore, analysis of the fluorescence of PyDPA alone showed that its emission is lower if compared with that of pyrene. Experimental data suggested that quenching due to metal coordination is taking place, i.e. the so called CHEQ effect (CHelation Enhancement Quenching) [62]. Indeed, within a PyDPA molecule, a π-charge interaction between a Zn^{2+} ion and the pyrene moiety is forcing the structure into a folded conformation (Figure 1.8A). Addition of a pyrophosphate-bearing molecule (even the simple PPi) induces an open conformation with a higher fluorescence emission.

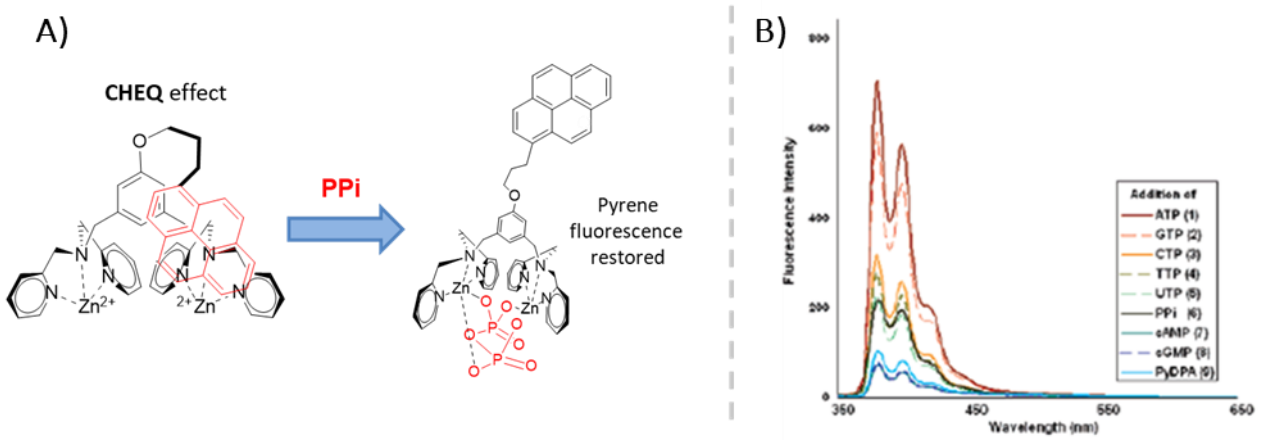

Figure 1.8: **A) PyDPA conformation in solution, alone and in complex with PPi; B) PyDPA emission spectra, alone and in presence of different phosphorylated compounds**. Image B) taken from Rhee et al.,[61])

Analysis of the 1:1 complexes of PyDPA with different nucleotides revealed a wide range of fluorescence emission intensities, with purines (i.e. GTP and ATP) showing stronger emissions than pyrimidines (i.e. CTP, UTP, TTP) and PPi (Figure 1.8B).

1.1.4 Effect of pyrophosphate

Experimental data pointed out how the presence of other nucleotides does not perturb (p)ppGpp spectrofluorometric assays, while PP_i does. In fact, while the (p)ppGpp-PyDPA complex is entropically favored, PPi is able to displace (p)ppGpp probably thanks to a much lower steric hindrance of the resulting complex. In a PPi-ppGpp competition assay, the effect of PPi was dramatically present already at very low concentration (Figure 1.9). Therefore, free inorganic pyrophosphate (PPi) is strongly detrimental for PyDPA fluorescence assay.

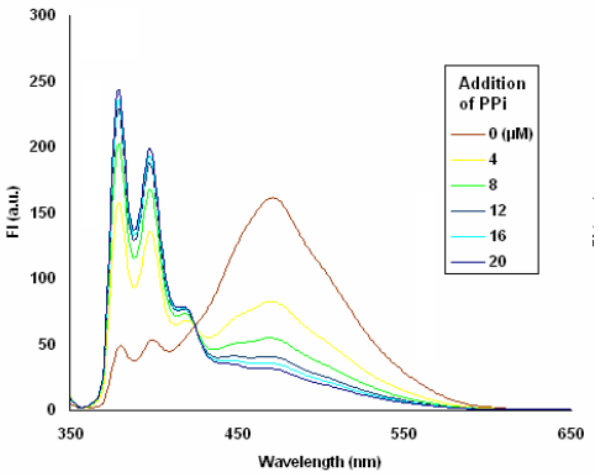

Figure 1.9: **Emission profile of a PyDPA (20 µM) and ppGpp (7 µM) solution upon the addition of different PPi concentrations**. It is possible to notice that 4 µM PPi almost leads to halving of excimer emission. Images (Taken from Rhee et al, 2008[61])

1.2 Optimized synthesis of PyDPA

Since PyDPA is not commercially available, we decided to synthesize it in our laboratories. Analyzing the synthetic approach reported in literature by Rhee and coworkers[61] (Scheme 1.2), we observed how the reported six steps sequence affords PyDPA in only 9 % overall yield.

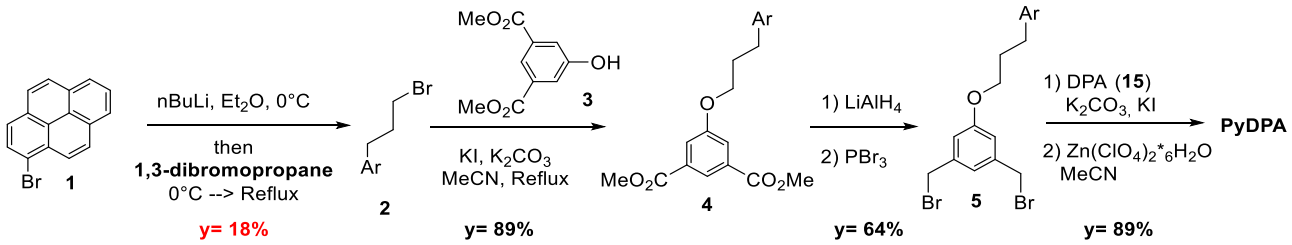

***Scheme 1.2*: PyDPA synthesis**, as reported in literature[61].

The first step, an 18% yield alkylation of lithiated 1-Bromopyrene, was the more problematic, and compromised the efficiency of the overall sequence. In order to overcome this issue, we explored different strategies to achieve common intermediate **4**, exploiting the reactivity of the Csp^2–Br bond in palladium-mediated reactions. In particular, in a Suzuki-type approach, allylation of phenol **3** afforded allyl-ether **6** (97% yield) but subsequent hydroboration with 9-BBN failed. Indeed, only degradation of the product was observed.

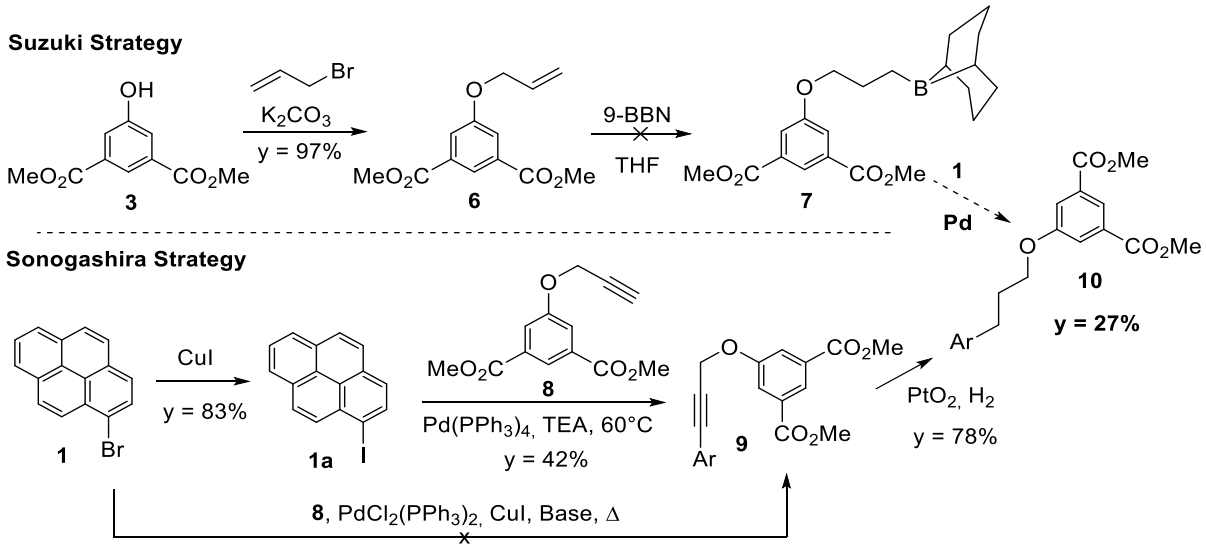

***Scheme 1.3:* New synthetic approaches**: *top panel,* Suzuki strategy; bottom panel, Sonogashira one.

Alternatively, we tried a Sonogashira coupling between **1** and alkyne **8,** but the low reactivity of the C-Br bond of **1** led us to its preliminary conversion to 1-Iodopyrene[63] **1a** (83% yield). In this case, product **9** was obtained in a still unsatisfactory 42 % yield. This may depend on the formation of the *Glaser adduct*[64] as side-product (Figure 1.11).

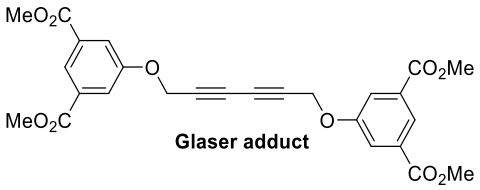

Figure 1.11: **Glaser adduct**

At this point, we decided to perform a copper-free Sonogashira coupling between 1-bromopyrene **1** and propargylic alcohol **11** as reported in literature[65], with yielded the desired compound **12** in 94% yield. Catalytic hydrogenation of **12** afforded in 96% yield alcohol **13** that was brominated in quantitative yield leading to compound **2** (Scheme 1.4).

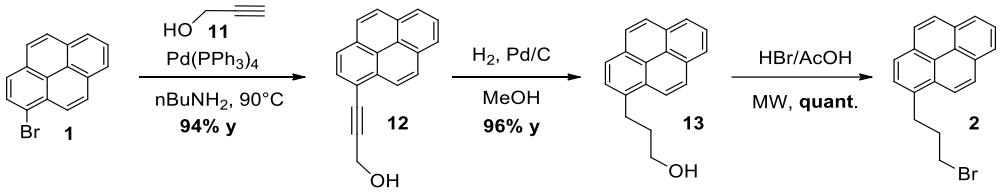

Scheme 1.4: **Alternative synthetic pathway of compound 2.**

The only other step of the original synthesis with a suboptimal yield was the reduction of diester **4**, performed in presence of $LiHAl_4$ (68% yield). We therefore decided to optimize it, making at the same time the synthesis more convergent, by performing the etherification reaction between compound **2** and triol **3a** instead of phenol **3**. **3a** can be obtained by quantitative reduction of **3** (Scheme 1.5) and the higher acidity of the phenol moiety allows its selective reaction under Williamson etherification conditions, affording compound **14** in 95 % yield, which undertook the same sequence as the original procedure[61]. In particular, bromination of **14** was followed by nucleophilic substitution with dipicolylamine (**15**), shorten as DPA, and formation of the zinc complex, i.e. the desired final compound PyDPA (80% yield over three steps, Scheme 1.5).

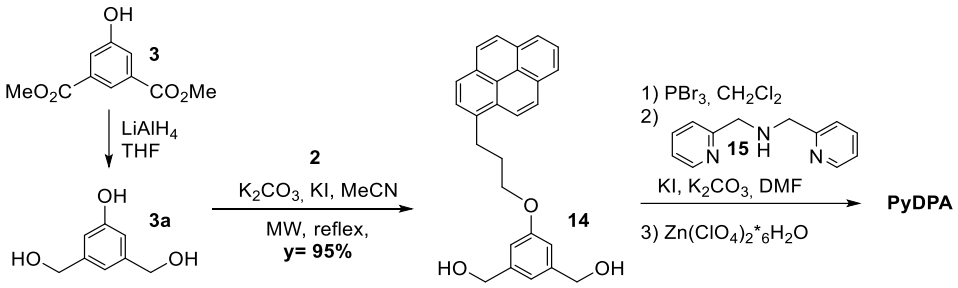

Scheme 1.5: **A more convergent strategy provides better yield.**

This optimized synthetic sequence comprises a total of seven steps instead of the six previously reported, but occurs with a much higher overall yield: 67 % *vs*. 9 %. A marginal improvement to the

overall yield was reported in 2013 by the another research group, starting from 1-pyrenecarboxaldehyde (19% over 8 steps)[66].

This work has been recently published [67] and raised the interest of several groups working in the field. We employed the synthesized PyDPA to quantify the alarmone (p)ppGpp as detailed in the following chapter. In order to do so, we also devised an efficient protocol for its enzymatic synthesis and isolation.

Chapter Two

2.1 Synthesis and isolation of ppGpp

ppGpp is commercialized (in very small amounts) as a 100 mM water solution of its lithium salt. Preliminary assays performed on such commercial batch produced puzzling results.

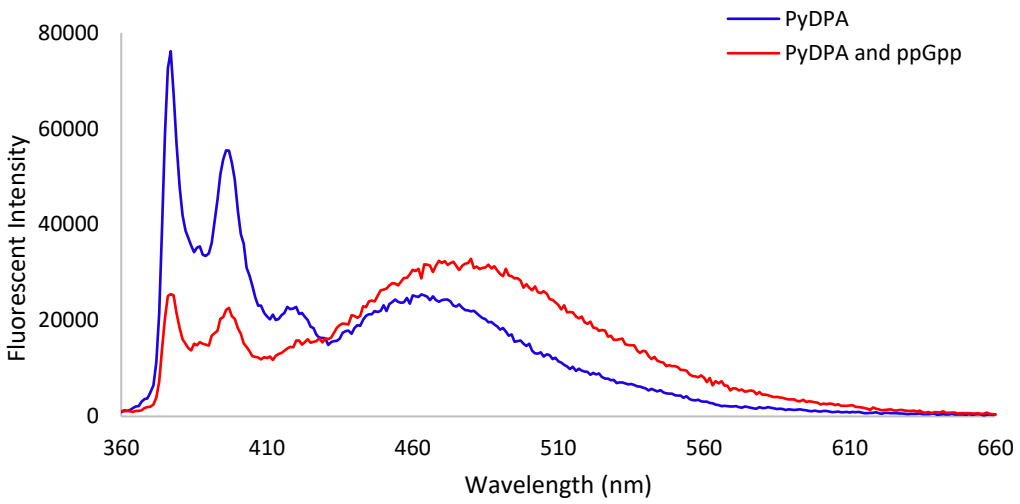

Figure 2.1: **Fluorescence spectra of a 20 µM PyDPA solution in 1 mM HEPES pH 7.4 in the absence** (blue) **and presence of 7 µM ppGpp** (red).

Indeed, while it was observed the expected decrease of pyrene monomer fluorescence at 370 nm, only a small enhancement was observed in the excimer region, at 480 nm. Upon further investigation with NMR spectroscopy, we found that the commercial ppGpp batch was partially hydrolyzed to GDP and PPi, but it was not possible to assess to what extent. As already discussed in paragraph 1.1.4, pyrophosphate is particularly detrimental in PyDPA fluorescence assays, since it interferes with the ternary complex formation. Given the cost and relatively low stability of commercial ppGpp, we decided to set up a protocol for its enzymatic production and subsequent isolation.

2.1.1 Enzymatic ppGpp synthesis

In the context of our project, we decided to carry out ppGpp synthesis through an enzymatic approach, exploiting Rel_{Seq}, a bifunctional RSH enzyme from *S. equisimilis*, which had been expressed and purified in our laboratories (Dr. Luca Sorrentino, PhD).

As already described in paragraph *RSH superfamily*, RSH enzymes are able to catalyze the transfer of a pyrophosphate group from ATP to the 3' position of either GDP or GTP, yielding ppGpp or pppGpp, respectively. We decided to focus our efforts on the more stable tetraphosphate form, ppGpp (Scheme 2.1).

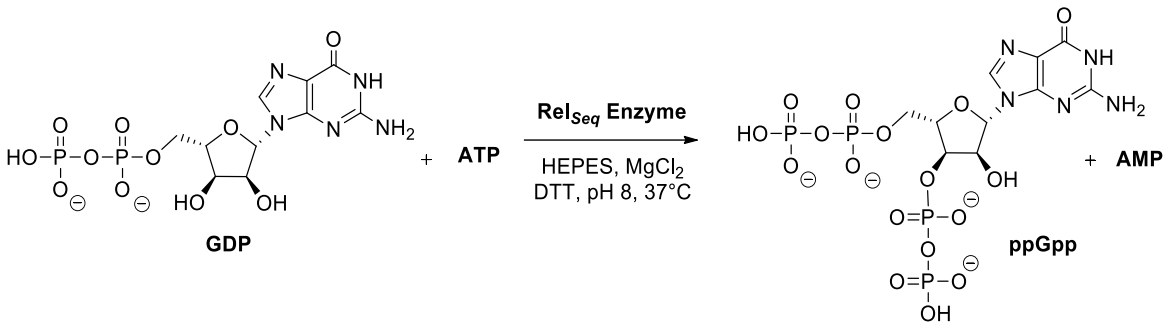

Scheme 2.1: **Phosphorylation reaction of GDP by the ATP-dependent Rel$_{Seq}$ enzyme.**

Reaction conditions adapted from Jain et al.[68], required the use of 50 mM HEPES as buffer at pH 8.0. The two substrates, ATP and GDP, were used in a 2:1 ratio at concentrations of 6 mM and 3 mM, respectively. In such conditions, GDP could be considered the limiting substrate. Given the fact that Rel$_{Seq}$ SYNTH domain requires Mg^{2+} for its functioning, the metal cofactor was added in the form of its chloride salt at a concentration of 10 mM, higher than the sum of the two nucleotide substrates. 1 mM DTT was also included to avoid the formation of unwanted disulfide bridges in/between Rel$_{Seq}$ molecules. The reaction was set up on 0.1 mg of protein (final concentration 0.2 mg/mL) and incubated at 37 °C for up to 5 h, to obtain complete conversion of GDP into ppGpp. The reaction was monitored by PEI-cellulose TLC that allows differentiating molecules with respect to the number of phosphate groups carried. Since the cellulose-based stationary phase does not withstand chemical developing reagents, UV-light absorption at 254 nm was used for spots detection. The detection is therefore only qualitative.

2.1.2 Analysis of ppGpp enzymatic production by ^{1}H-NMR

Quantification of ppGpp could potentially be achieved by HPLC or UPLC[69]. However, such techniques are difficult to implement on preparative scales and are time-consuming from an analytical point of view, when thinking about a medium-to high-throughput screening assay.

Inspired by a paper published by Guo and coworkers[70], we decided to investigate the use of nuclear magnetic resonance (NMR) to quantify either ATP consumption to AMP accumulation in ATP-dependent enzymatic reaction from ^{1}H-NMR signals. In such cases, the H_8 proton located on the adenine base (Figure 2.2) is particularly diagnostic, since it possesses an extremely high sensitivity to changes in its local environment. The H_2 protons of ATP and AMP are too close to each other for precise integration, while the anomeric protons $H_{1'}$ partially overlap, resulting in a pseudo-triplet signal.

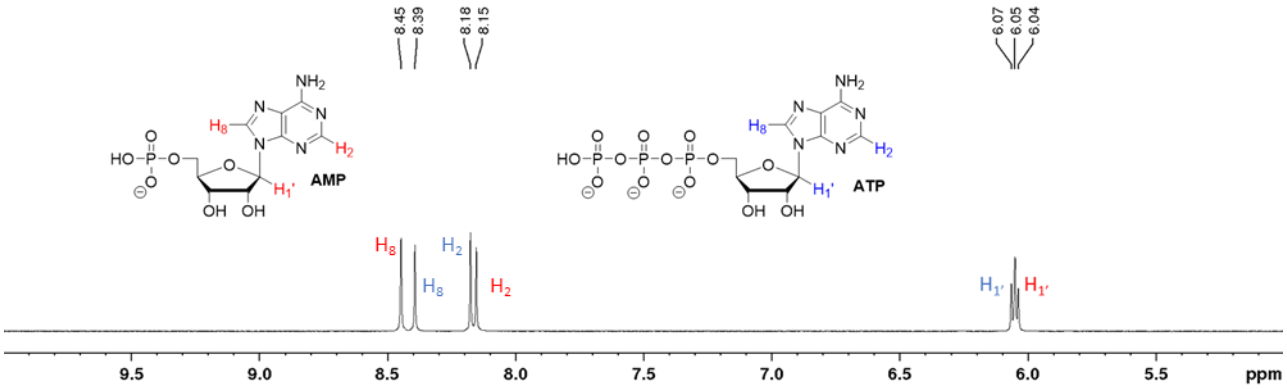

Figure 2.2: **Proton spectrum of AMP and ATP (1:1) mixture.** (400 MHz, D_2O)

Despite its many advantages, for this particular case, we still could not use NMR as a quantitative tool from a practical point of view. One of the main issues relies on the fact that protons belonging to the purine bases do not present neighboring active nuclei helping with their relaxation. Hence, long delay times (D1 up to 30 s) are required to obtain correct aromatic signals integral. Quantitative analyses would be therefore prohibitively long. Figure 2.3 shows the ^{1}H-NMR spectrum of the reaction mixture before addition of the enzyme, thus only the two substrates ATP and GDP can be detected. Being their ratio of 2:1 (ATP:GDP), after calibrating ATP H_8 integral (around 8.5 ppm) as 1, we expected all signals corresponding to ATP to have the same integral, while those corresponding to GDP to result 0.5. However, all integrals differed from the predicted value with the exception of GDP H_8 (around 8.1 ppm), due to the afore-mentioned quantification issues.

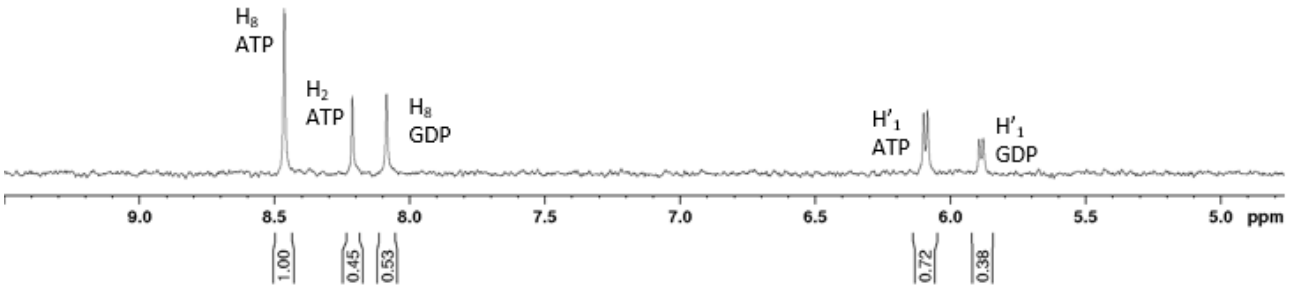

Figure 2.3: **Expansion of the ^{1}H-NMR spectrum of the reaction mixture at time zero.** ATP and GDP are present in a 2:1 ratio. (400 MHz, D_2O)

Anomeric signals cannot be accurately integrated either because the water suppression sequence applied (centered at 4.78 ppm) variably affects the integrals of signals around 6 ppm (Figure 2.3). Nonetheless, we extracted from proton NMR semi-quantitative information about the reaction progress.

Aliquots of the reaction mixture were diluted 10-fold with deuterium oxide and their ^{1}H-NMR spectra were recorded using a water suppression sequence. An example of enzymatic reaction checked by such technique is reported in figure 2.4.

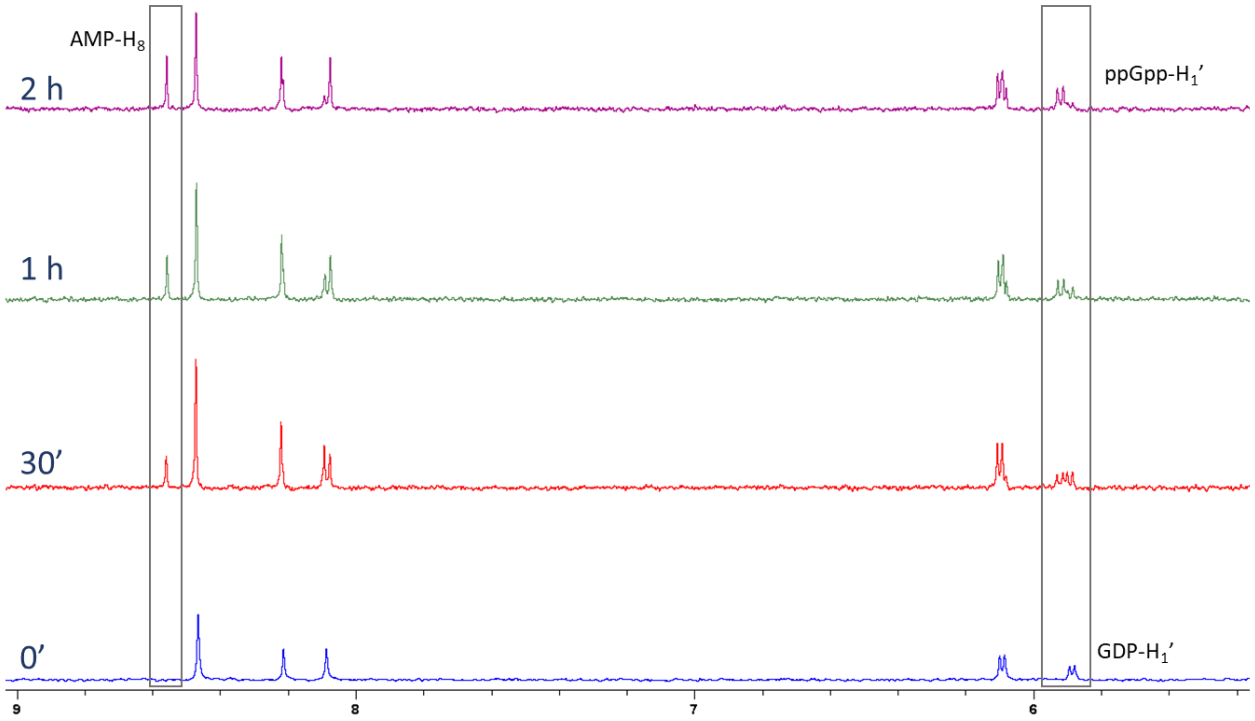

***Figure 2.4:* ^{1}H-NMR of ppGpp enzymatic synthesis over the time.** Diagnostic signals are boxed. (400 MHz, D_2O)

It can be noticed that, while absent at the beginning of the reaction (t= 0 h), AMP progressively accumulates over time, with concurrent ATP consumption. GDP and ppGpp $H_{1'}$ signals overlap, resulting in a sort of triplet when both nucleotides are present. The doublet corresponding to ppGpp $H_{1'}$ can be appreciated only after GDP consumption (t = 2 h). The use of a 600 MHz NMR instrument allows for a better signal separation (Figure 2.5), although precise integration remains elusive.

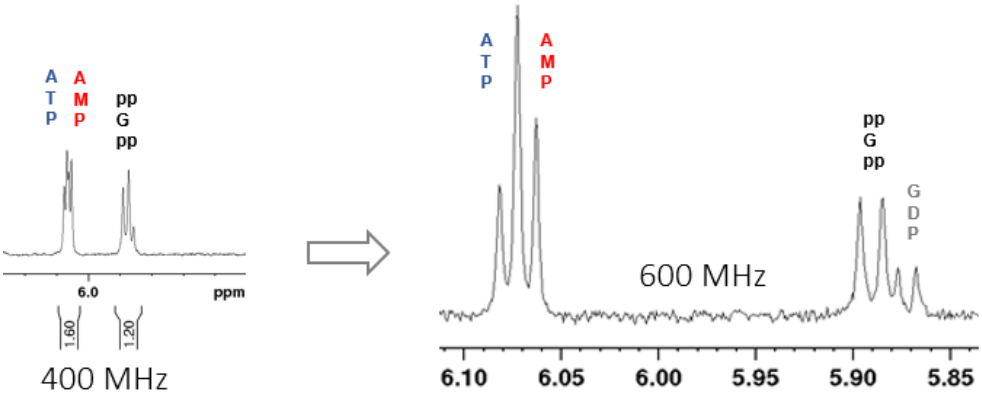

***Figure 2.5:* Expansion of the anomeric signals of the ribose moiety with a 400 MHz and 600 MHz instruments.**

With this tool in our hands, we investigated the effect of pH on the catalytic activity of Rel$_{Seq}$, estimating the reaction completion time at pH between 7.5 and 8.5, a narrow interval due to the limited buffering range of HEPES. As expected[50], the increase in pH correlated with faster reaction rates. Indeed, while up to 6 h were needed for reaction completion at pH 7.5, this time was lowered to 2 h and to 20 minutes at pH 8.0 and 8.5, respectively. We selected pH 8 as our preferred working pH.

In a following set of experiments, we also investigated Rel$_{Seq}$ substrate preference among GMP, GDP and GTP, thus assessing its ability to catalyze as well the synthesis of pppGpp (from GTP) and pGpp (from GMP), an additional modified nucleotide usually produced exclusively by monofunctional SAS (Figure 2.6).

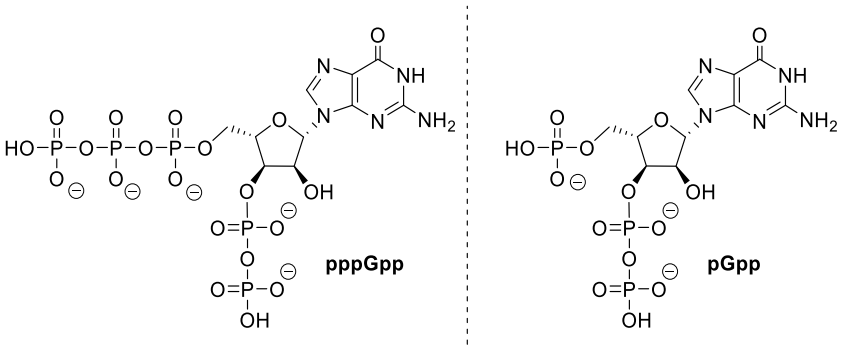

Figure 2.6: **Structures of pppGpp and pGpp.**

By using the same ^{1}H-NMR approach, no pGpp production could be observed, as expected. On the contrary, pppGpp synthesis was complete in less than 30 minutes at pH 8, suggesting a 4-fold faster reaction rate with respect to ppGpp. We can therefore assess that Rel$_{Seq}$ presents a better affinity for GTP than GDP. These results are in line with observation reported on RelA (Rel$_{Seq}$ homologous in *E. coli*)[47], where pppGpp is usually produced in higher levels than ppGpp, clearly indicating GTP as the preferred substrate.

2.1.3 ppGpp isolation

Different approaches are described in literature for ppGpp isolation from reaction mixtures. Most of them, however, are based on ion exchange with HPLC systems[69]. Such techniques are not particularly feasible for scale larger than few milligrams, thus we decided to set-up a new protocol. Our approach can be divided into two steps: nucleotide scavenging and ppGpp precipitation.

Scavenging of unwanted nucleotides

When GDP conversion into ppGpp is complete, the product is present in solution together with Rel_{Seq}, equimolar amounts of by-product AMP and unreacted ATP, HEPES buffer and salts. Removal of unwanted nucleotides (i.e. AMP and ATP) is the most challenging step due to structural similarity with the product. The only structural difference lies in the absence in the product of the 2'-3' vicinal diol present in AMP, ATP and in eventually unreacted GDP. The ability of boric acid under basic conditions (i.e. in the form of the tetrahedral anion $[B(OH)_4]^-$) to form cyclic borates with vicinal *cis*-diols of pentose sugars, such as ribose, is well known[71]. We therefore envisaged that a boronic acid resin, at the appropriate pH, could retain all the nucleotides present in our reaction mixture, except for ppGpp (Scheme 2.2). We decided to purchase from *Thermo Fisher Scientific* vendor the Pierce™ Boronic Acid Resin (supplied as 50%$_{w/v}$ aqueous slurry with 0.02 % sodium azide; Catalog number: 20244) because, although more expensive, it was the one with the higher nominal capacity, i.e. 110 µmol per milliliter of settled resin.

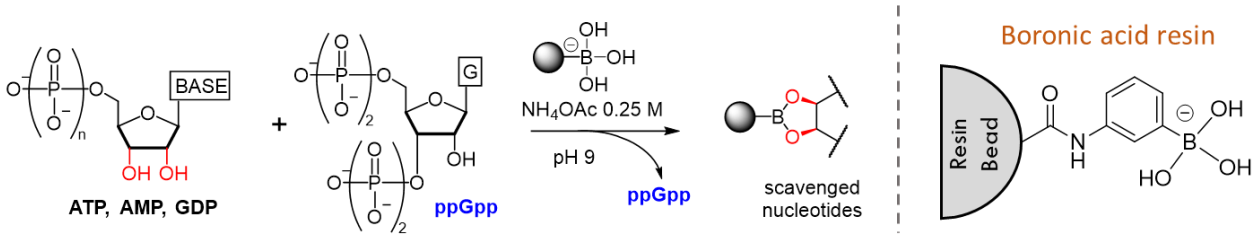

***Scheme 2.2*: Nucleotide scavenging with a boronic acid resin.**

Ideally, the product should not interact with the resin and should be retrieved in the flowthrough. Following the manufacturer's instructions, a solution of 0.25 M $AcONH_4$ pH 8.8 was used for resin equilibration and activation of the boron center. After sample adsorption, the flowthrough was collected. Subsequently, elution of bound nucleotides was performed with a 25 mM HCl solution. Collected fractions were analyzed by PEI cellulose TLC, with 0.75 M KH_2PO_4 as eluent.

During preliminary tests, we noticed a clear discrepancy between the claimed loading capacity of the resin (110 µmol/mL) and the experimental one that seemed to be much lower. We therefore investigated by ^{1}H-NMR, ^{13}C-NMR and ^{11}B-NMR the actual formation of the borate complex and whether some components of the reaction mixture could interfere with the binding event. Ribose and AMP were chosen to study the borate complex formation.

Ribose:

In water solutions, ribose is usually found as a 1:2 mixture of α and β anomers of the furanosidic form, that are characterized by specific ^{1}H-NMR anomeric signals (H_β: 4.9 ppm, H_α: 4.8 ppm). In principle, both anomers can form a complex with borate through their *cis* hydroxyl groups in positions 2 and 3. However, the presence of tetrahydroxyborate shifts the anomeric equilibrium towards the α anomer, due to the fact that the corresponding borate ester is preferentially formed thanks to higher acidity of its 2 -OH group. Moreover, two different species can be present in solution: LB^- and L_2B^-, where L represents a generic bound substrate (in this case ribose) and B the boron center (Scheme 2.3).

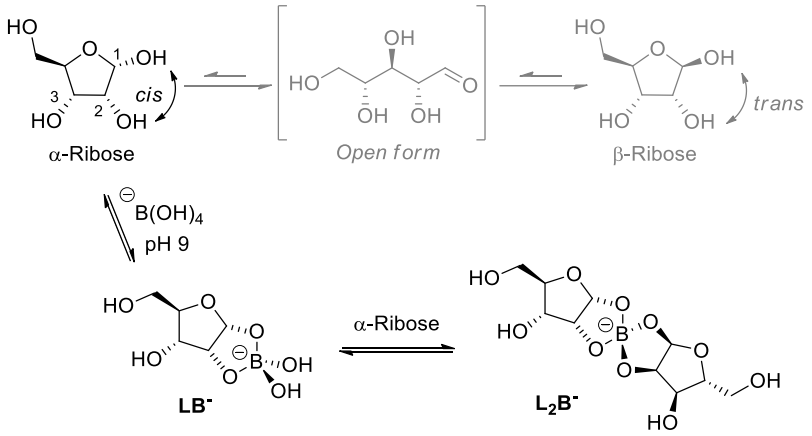

Scheme 2.3: **Equilibrium between α and β ribose anomers and complexes (LB^- and L_2B^-) formed by α-ribose with $^-B(OH)_4$.**

A sample containing ribose and $[B(OH)_4]^-$ in a 1:2 ratio was prepared. Proton NMR in H_20 was not particularly useful, since too many signals were present and water suppression sequence negatively affected the anomeric signals. On the contrary, ^{11}B-NMR provided clarifying data, as it is shown in figure 2.7. In fact, ^{11}B-NMR pointed out the presence of a major component at -12.9 ppm and a minor one at -7.9 ppm, corresponding to LB^- and L_2B^-, respectively. Since HEPES is the main component of the reaction mixture, it was added to the sample in order to understand if its presence negatively affected the complex. However, the presence of HEPES did not affect the chemical shifts of such signals. Therefore, we can conclude that the formation of both LB^- and L_2B^- is not influenced by HEPES.

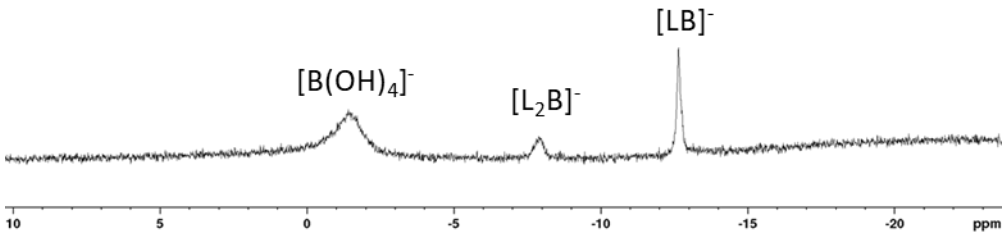

Figure 2.7: **^{11}B-NMR of a solution containing ribose and $^{-}B(OH)_4$ in a 1:2 ratio** (190 MHz, D_2O).

AMP:

AMP borate complex can be formed only with the two hydroxyl groups in position 2' and 3'. When AMP and $^{-}B(OH)_4$ are mixed respectively in a 1:2 ratio, only the LB^{-} species was found (-12.7 ppm). Therefore, a 1:2 AMP and $^{-}B(OH)_4$ mixture was used for ^{13}C-NMR analysis, where only carbon atoms in positions 2' and 3' showed a strong chemical shift from 70 ppm to 82 ppm and from 60 ppm to 62 ppm, respectively (Figure 2.8). The addition of HEPES did not perturb AMP-borate complex, as noticed by ^{13}C-NMR.

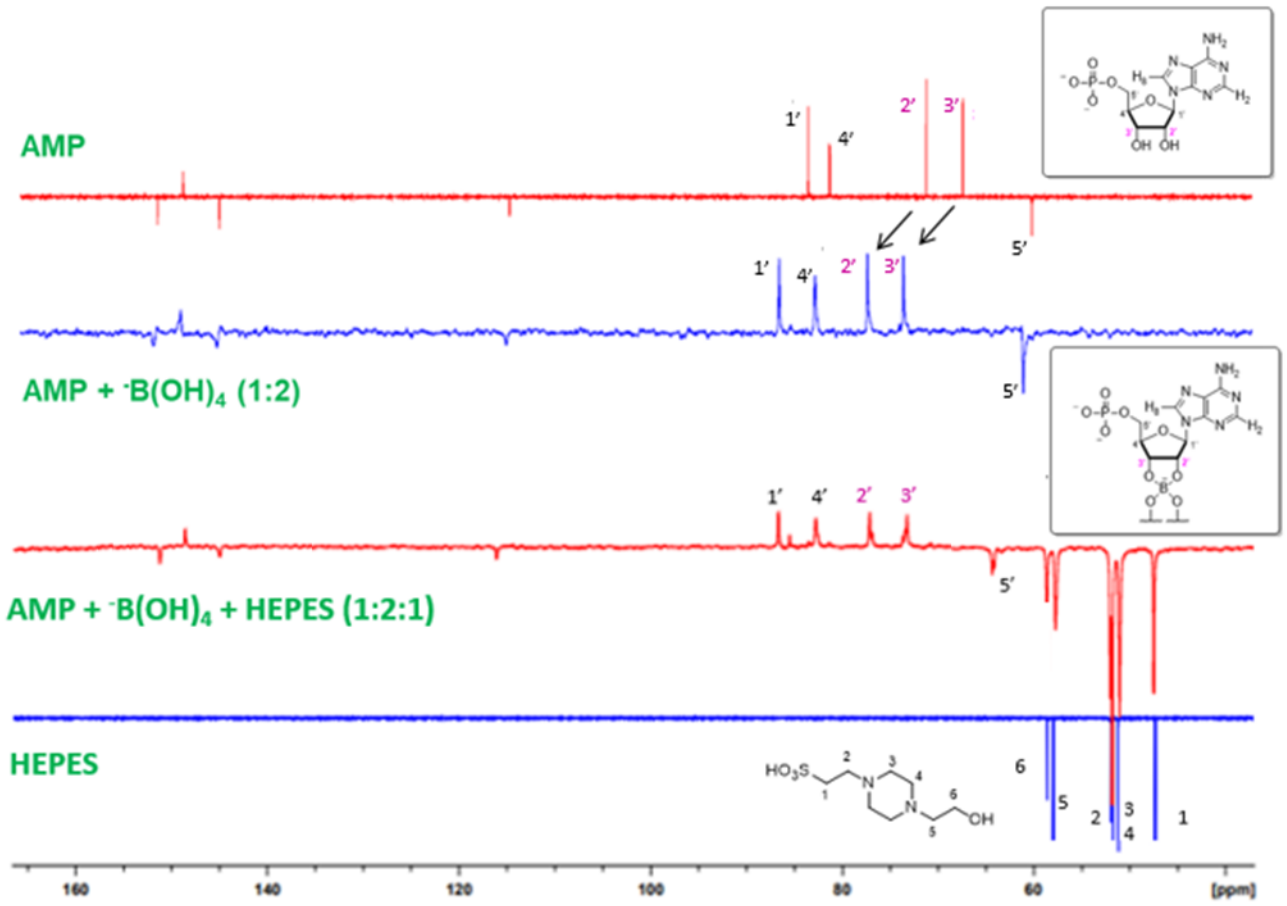

Figure 2.8: **^{13}C-NMR (APT) spectra overlap of AMP, AMP with $^{-}B(OH)_4$ ion and HEPES**. The stronger chemical shift changes are, as expected, on the $C_{2'}$ and $C_{3'}$ positions of AMP when $^{-}B(OH)_4$ is present. HEPES does not undergo variations in presence of $^{-}B(OH)_4$ and does not disturb the AMP/borate complex. (100 MHz, D_2O)

HEPES:

As a final check, we tested if HEPES could interact with $[B(OH)_4]^-$ by analyzing a 1:2 mixture with ^{1}H-NMR. The latter showed no changes in HEPES protons signals (Figure 2.9). We can therefore state that HEPES does not interfere with the purification procedure, since it is unable to interact with the boronic acid resin.

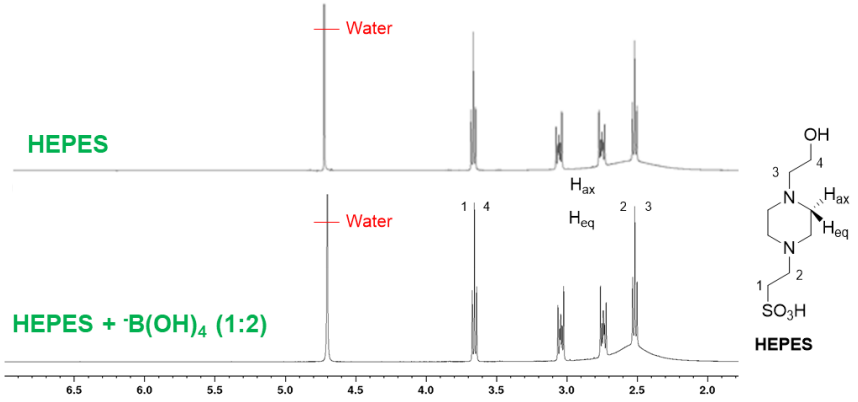

Figure 2.9: **^{1}H-NMR spectra overlap of HEPES and HEPES with tetrahydroxyborate ion** (400 MHz, D_2O).

We decided to perform some AMP loading tests to assess the actual loading capacity of the boronic acid resin. After several attempts with decreasing amount of nucleotide loaded compared to the nominal capacity, we found that the actual loading capacity of the boron acid scavenging resin was about 10 µmol/mL, ten times lower than the declared value (110 µmol/mL).

- *Resin scavenging general procedure:*

The protocol for the scavenging step was set up as follows: a defined amount of immobilized boronic acid gel (1 mL of settled resin per 0.5 mL of reaction mixture) were placed in a plastic column and packed by fluxing 5 column volumes (CV) of binding buffer, 0.25 M $AcONH_4$, pH 8.8. The final sample of ppGpp enzymatic synthesis was diluted 1:2 with binding buffer, and the resulting pH was adjusted to ca. 9. The solution was then loaded on the packed boronic acid gel and the flowthrough fraction was collected. Washing with 5 CV of binding buffer was performed and all fractions were analyzed by PEI cellulose TLC, to detect ppGpp presence and purity. Unfortunately, a faint ATP spot was detectable in all fractions. Therefore, fractions were pooled and fluxed again through the resin matrix, for a total of three times. This procedure guaranteed absence of ATP from fractions of interest.

We decided to investigate of the partial retention of ATP. Excluding any interference coming from HEPES, we reasoned that the Mg^{2+} ion might coordinate to ATP, somehow hampering the binding event. We addressed this hypothesis by ^{1}H-NMR on the following samples (500 µL):

1. AMP 3 mM, $^{-}B(OH)_4$ 6 mM, pH 7 and 9;
2. AMP 3 mM, $^{-}B(OH)_4$ 6 mM, $MgCl_2$ 10 mM, pH 7 and 9;
3. ATP 3 mM, $^{-}B(OH)_4$ 6 mM, pH 7 and 9;
4. ATP 3 mM, $^{-}B(OH)_4$ 6 mM, $MgCl_2$ 10 mM, pH 7 and 9;

Such samples were prepared replicating AMP, ATP and $MgCl_2$ concentration in the enzymatic reaction mixture, while borate was included in a 2:1 ratio with respect to the nucleotides to favour formation of the LB^{-} complex. Proton NMR of each sample were recorded (D_2O, 400 MHz). By means of the ratio of the H_8 signals of either ATP and AMP (occurring around 8.5 ppm), we estimated the amount of 'complex' and 'free nucleotide' in solution.

As shown in Figure 2.10, in absence of Mg^{2+}, the ratio of unbound/bound AMP was 3:1 already at pH 7 (panel B). Addition of the cation shifts the equilibrium towards the complex, resulting in a 1:1 ratio of unbound/bound AMP (panel A). At pH 9, no free AMP was detected, independently of Mg^{2+} presence. In the case of ATP, magnesium had a stronger effect. At pH 7, ATP was not able to form borate complexes, even in presence of magnesium. On the contrary, at pH 9, Mg^{2+} addition reverts the ratio of unbound/bound ATP from 2:1 (Panel D) to 1:2 (Panel C).

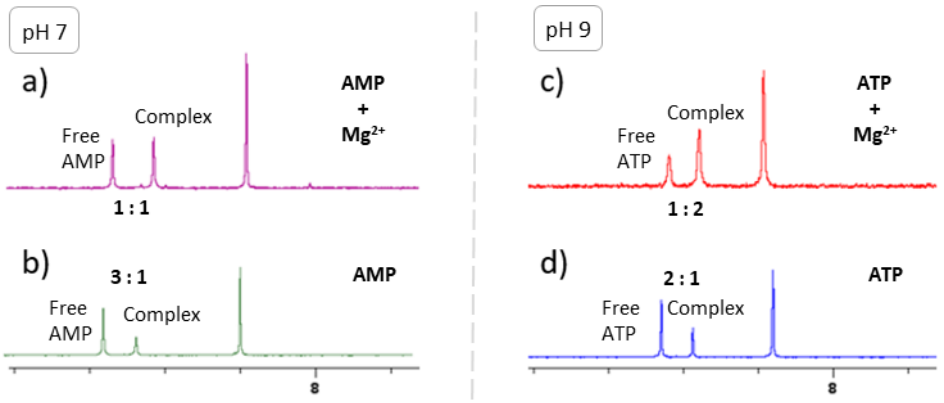

Figure 2.10: **Effect of magnesium on ATP and AMP borate complexes formation.**

We can therefore conclude that magnesium is actually helpful in borate complexes formation. On the other hand, pH seems to be the main player in the equilibrium. The boronic resin scavenger must be used at pH ca. 9, a value that does not ensure proper ATP binding. We also tried increasing the pH up to 11, but no improvement in ATP borate complexes formation was detected by NMR.

The only way to shift this equilibrium in our favor would be to use a larger excess of the resin. Therefore, in the case of ATP, the maximum loading capacity of the resin at pH 9 is even lower than 10 µmol/mL.

ppGpp precipitation

After scavenging the unreacted nucleotides, the flowthrough contained ppGpp along with HEPES, $MgCl_2$ and the binding buffer ammonium acetate. In particular, buffer and salts were present at a much higher concentration compared to the alarmone. After discarding both direct and reverse phase chromatography for lack of suitable separation conditions, we adopted the simple precipitation of the product as lithium salt, a technique generally applied for the isolation of RNAs[72]. Therefore, 10 M lithium chloride solution was added to the ppGpp solution (estimated concentration 0.2 mg/mL) at a final concentration of 1 M. The resulting solution was diluted 4-fold with cold ethanol. During 20 min incubation on ice, ppGpp precipitated out and the solution was centrifuged at 4500 rpm for 20 minutes at 4°C yielding a white pellet. After discarding the supernatant, the pellet was washed 3 times with cold ethanol and dried overnight under high vacuum. ppGpp was obtained with up to 80% yield, and ^{1}H-NMR revealed no detectable contaminants (Figure 2.11).

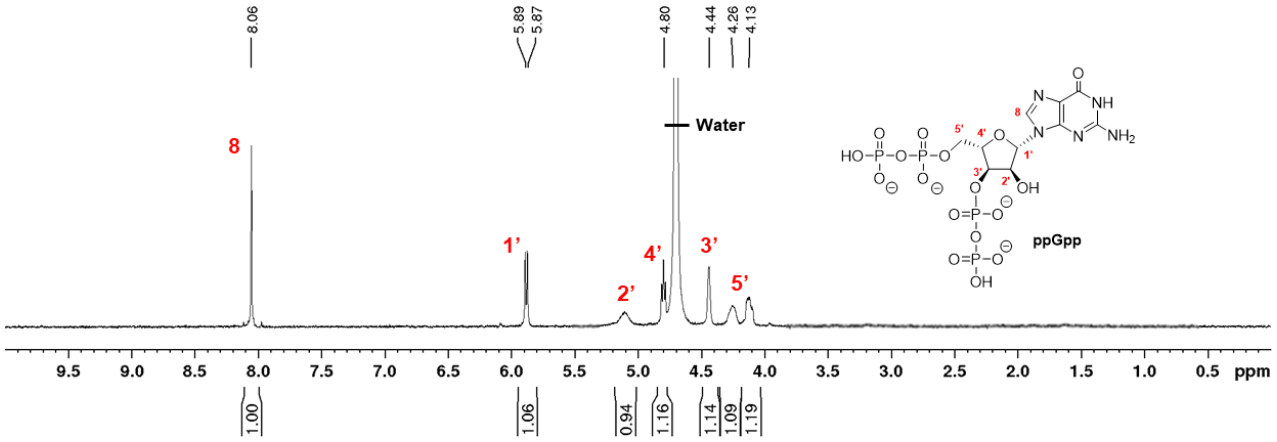

Figure 2.11: **^{1}H-NMR of purified ppGpp** (D_2O, 400 MHz).

PyDPA assay on newly purified ppGpp

The PyDPA assay was performed as already described in paragraph 2.1, using newly purified ppGpp. However, results were surprisingly worse. In fact, the ratio between the fluorescence intensity of pyrene excimer (470 nm) and of its monomer (380 nm), I_{470}/I_{380}, was already 0.7 with only PyDPA present in solution (Figure 2.12, blue line). Addition of 7 µM ppGpp led to an unexpected increase

of the monomer signal, instead of the excimer one, thus making the I_{470}/I_{380} ratio drop to 0.3 (Figure 2.12, red line).

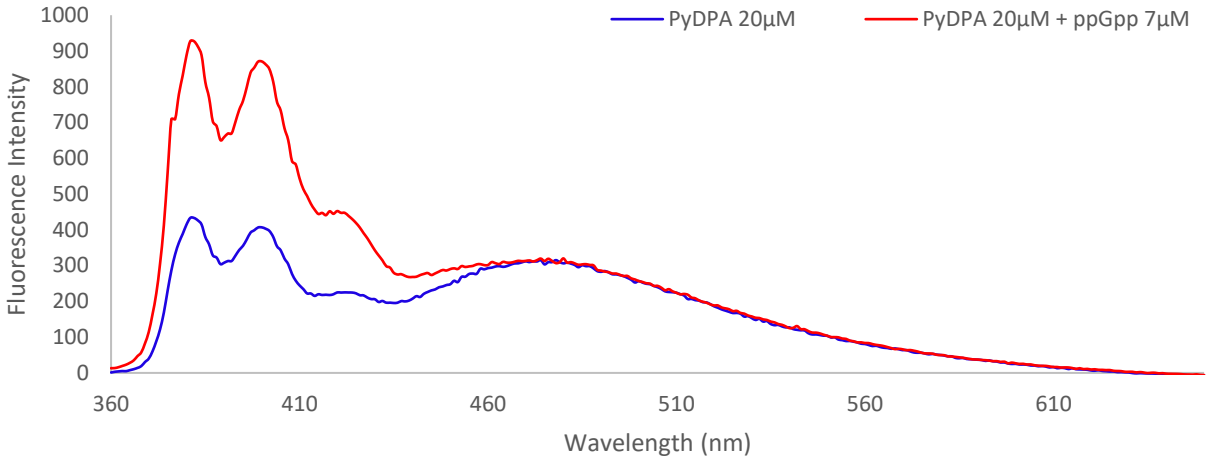

Figure 2.12: **PyDPA fluorescence alone and in presence of 7 µM ppGpp** (Ex: 344 nm).

To overcome the issue, we synthesized a new batch of PyDPA, but similar results were obtained. We reasoned that the very low solubility of PyDPA in water solutions could interfere with proper functioning of the assay. Therefore, we tried dissolving the chemosensor in different ways:

- A 2 mM stock solution of PyDPA in acetonitrile was prepared to ensure complete dissolution and absence of aggregates. After dilution in 1 mM HEPES, pH 7.4 to obtain a PyDPA concentration of 20 µM, the assay was repeated but results were identical.
- We dissolved PyDPA directly in water to obtain directly the working concentration of 20 µM with and without the HEPES buffer. However, no improvement was obtained.

We also checked whether PyDPA contained the right amount of zinc by ICP-MS. Such technique confirmed zinc presence at the expected concentration.

Since the increase in monomer emission is usually due to pyrophosphate presence, we reasoned that it could be present in purified ppGpp. Indeed, as explained in paragraph *RSH superfamily* (page 24), the Rel_{Seq} enzyme, used to carry out the enzymatic production of ppGpp, is bifunctional and can undergo a futile cycle in which both its SYNTH and HYD domains act simultaneously. Occurrence of this cycle usually results in pyrophosphate accumulation. However, Rel_{Seq} HYD domain needs Mn(II) for its functioning. While no manganese was added during the in-house production of both the enzyme and ppGpp, the ion might be naturally present in the purified protein, coming from *E. coli* cells. ICP-MS on Rel_{Seq} samples pointed out the presence of manganese, in excess with respect to the protein, thus activity of the HYD domain was surely present. Therefore, purified ppGpp could

contain pyrophosphate coming from Rel_{Seq} futile cycle. Such ion is not scavenged by the boronic acid resin and it also may precipitate as lithium salt. Moreover, it is not possible to detect its presence by ^{1}H-NMR and the quantity of ppGpp is too small to use ^{31}P-NMR either.

We therefore decided to estimate the amount of PPi present in ppGpp samples by looking at the discrepancy between the nominal concentration of an alarmone solution and the one measured by UV absorption at 256 nm. At this wavelength the guanine ring should absorbs light with approximately the same molar attenuation coefficient, regardless of the number of phosphates of the nucleotide. GDP molar attenuation coefficient was determined to be ε_{256} = 10300 M^{-1} cm^{-1} (Figure 2.13), a value that held true for GMP and GTP as well.

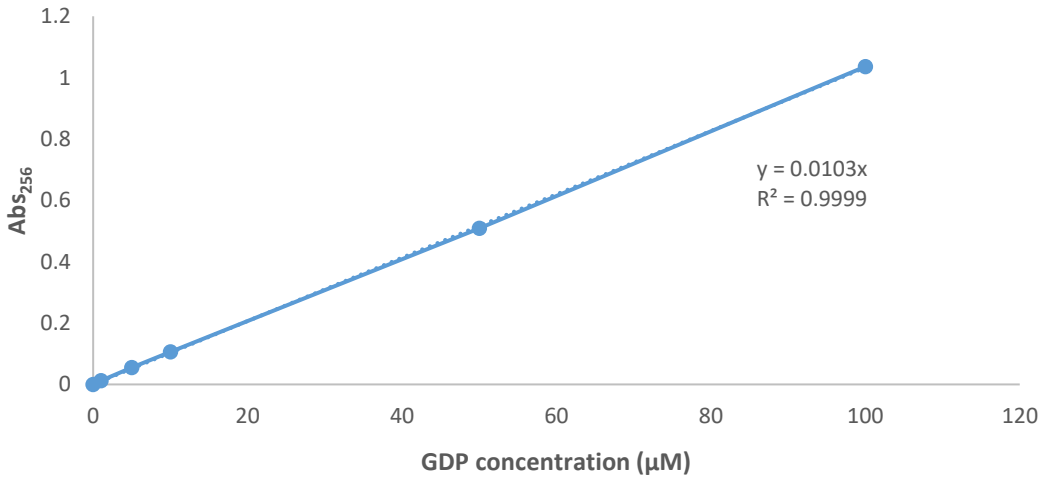

Figure 2.13: **GDP titration for calculation of its molar attenuation coefficient at 256 nm.**

When we measured the absorption of a nominal 7 µM ppGpp solution, we found a value corresponding to a 5.4 µM solution instead. Such difference in concentration was attributed to the presence of 23% of PPi (by assuming PPi as the only contaminant), thus justifying the negative outcome of PyDPA assays.

In order to precisely quantify the amount of PPi, we performed a commercially available pyrophosphate spectrophotometric assay[73] based on a series of enzymatic reactions that lead to NADH consumption (Scheme 2.4). In particular, two molecules of NADH are oxidized to NAD^{+} per each molecule of pyrophosphate present. Thus, PPi concentration can be derived from the disappearance of the NADH signal at 340 nm.

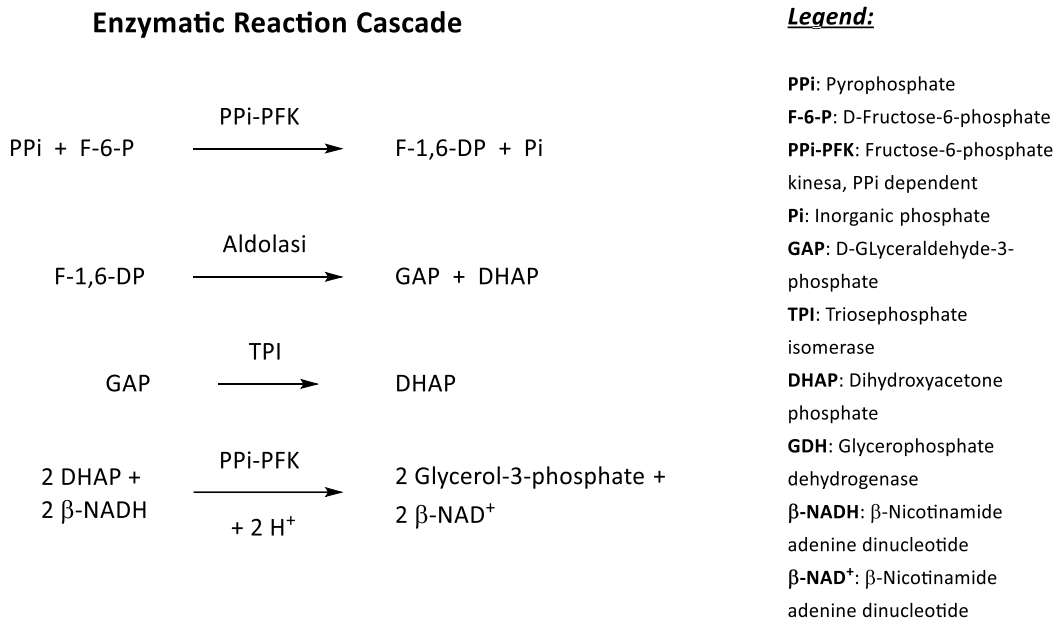

Scheme 2.4: **Enzymatic cascade occurring in PPi spectrophotometric assay**.

The spectrophotometric assay was performed according to the manufacturer's instructions. By data obtained, we could calculate that purified ppGpp contained 25% of PPi, with respect to moles. A value in line with the spectrophotometric data obtained above.

In order to avoid the risk of futile cycle occurrence in Rel_{Seq}, we decided to carry out in-house production of ppGpp by using RelP, a monofunctional synthetase from *S. aureus* (see paragraph *RSH superfamily*, page 24), already expressed and purified in our laboratories (Dr. Luca Sorrentino, PhD). The reaction carried out in similar conditions allowed to obtain a PPi-free ppGpp on a 30 mg scale, as demonstrated by a negative PPi assay.

This ppGpp sample was once again used to perform the PyDPA fluorescence detection assay but the results were still not fully reproducible.

.

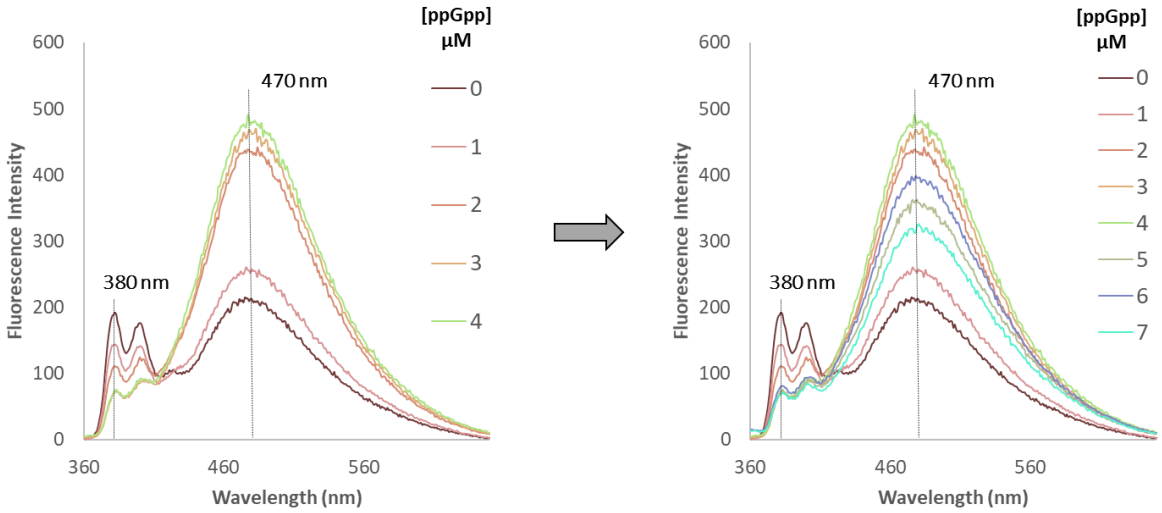

Figure 2.14: **Dose-response of a 20 µM PyDPA solution upon the addition of ppGpp**. On the left, the intensity of the excimer rises, while the monomer drops. At concentration of ppGpp higher than 4 µM (on the right), the excimer signal decreases.

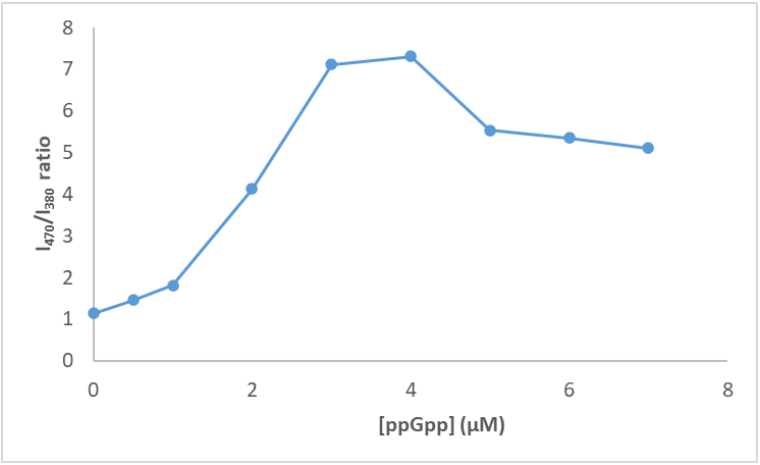

Figure 2.15: **Plot of I_{470}/I_{380} ratio *vs* ppGpp concentration**.

In particular, both I_{470} emission intensity and I_{470}/I_{380} ratio increased upon ppGpp addition up to 4 µM (7.3 ratio) but decreased at higher ppGpp concentrations.

This contrasted with literature data, where maximum I_{470}/I_{380} ratio was obtained at 7 µM ppGpp. These discrepancies and the lack of linearity of the response to ppGpp concentrations led us to discard, at least temporarily, this assay for the quantitative determination of (p)ppGpp.

Nonetheless, we drew inspiration from the PyDPA-(p)ppGpp complex formation for the design and construction of a ppGpp-selective scavenging system, as described in the following chapter.

2.2 Nucleotides scavenging beads

As mentioned above, the ppGpp-PyDPA complex structure inspired us for the design of a new ppGpp-selective scavenging resin (Figure 2.16). The idea is to replicate the chelation of the two terminal pyrophosphate unit by a solid-supported tetra-Zn/DPA system.

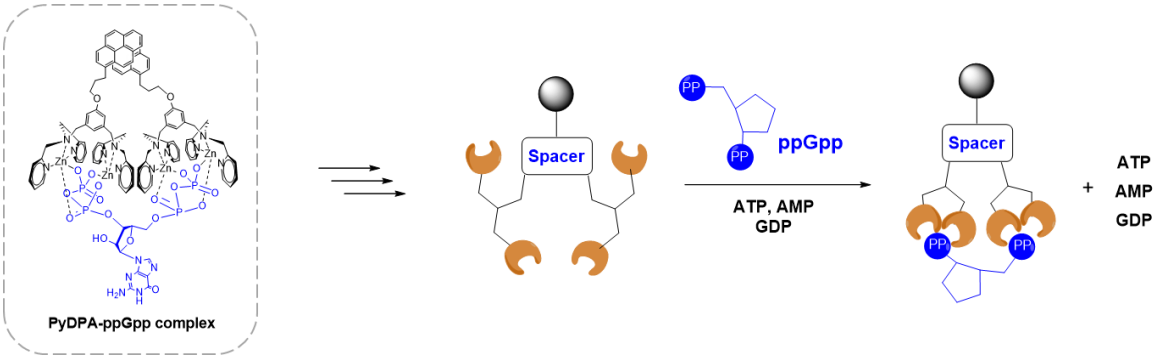

Figure 2.16: **Sketch of a new selective ppGpp scavenger**; it is based on the structure of PyDPA-ppGpp complex

The feasibility of the approach requires the assessment of several aspects, selectivity for ppGpp over other nucleotides being only one of them. Selectivity would depend on the distribution of the binding moiety on the solid support surface and on the correct spacing between the two bis-Zn/DPA units.

As a proof of concept, we therefore devised to build a simpler model, able to effectively bind nucleotides from a buffer solution (Figure 2.17), consisting in the display on a solid support of bis-Zn/DPA units, able to bind single pyrophosphate moieties.

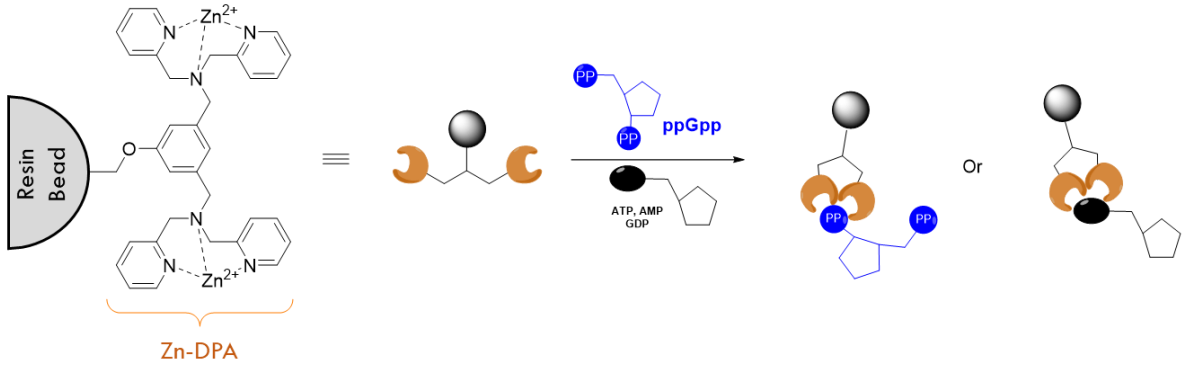

Figure 2.17: **Sketch of a resin able to recognise nucleotides.**

Scavenger resins are solid-supported entities able to interact with one or more components present in a reaction mixture, such as excess reagent that is removed from the solution. The nature of the interaction between the scavenger and its target molecule can be either covalent or electrostatic.

The attractiveness of this technique relies in its simplicity and in the significant time reduction compared to classical purification approaches.

Scavenger resins are generally constituted by cross-linked co-polymers, such as polystyrene (Merrifield Resin[74]) or polyacrylamide, bearing a small percentage of the reactive group, which has been introduced as a functionalized monomer. One example is the electrophile scavenger[75] reported below.

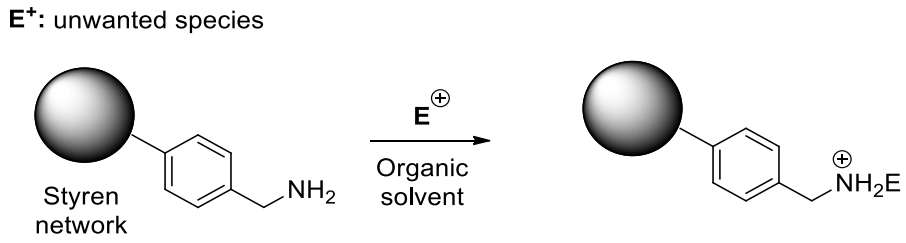

Figure 1.18: **Solid-supported electrophile scavenger resin.**

in principle, only small reactive group can be incorporated in a bulk co-polymerization approach. Nevertheless, we made few attempts as described below.

Bulk polymerization

Polyacrylamide (PAM) is a water-soluble white powder made of linear chains, obtained by the radical polymerization of acrylamide (AA) in the presence of initiators (R·) as shown in Scheme 2.5.

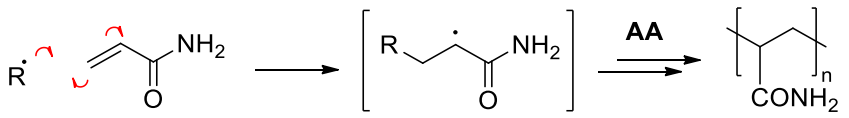

Scheme 2.5: Linear polyacrylamide radical chain polymerization

In order to maintain hydrophilicity but lower water solubility it is possible to introduce cross-links, forming a 3D network. Common cross-linking agents are bis-acrylamide (**16**) and divinyl benzene (**17**) (Figure 2.19). A tailor made cross-linker (**18**), was prepared from resorcinol and acryloyl chloride since it is better suited for reactions in apolar solvents than bis-acrylamide (Figure 2.19) .

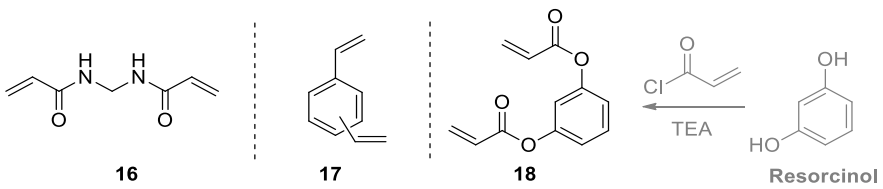

Figure 2.19: **Structures of bis-acrylamide (18), divinylbenzene (17) and bis-acryloyl resorcinol (18).**

The amount of cross-linker and the reaction kinetics strongly affect the properties of the final polymer. Therefore, monomers ratio and reaction conditions must be chosen appropriately.

We designed, as putative functional monomers for the co-polymerization with AA and a cross-linking agent, the synthetically simpler but less reactive Allyl-DPA (**19**) and the more reactive Acryl-DPA (**20**, Figure 2.20).

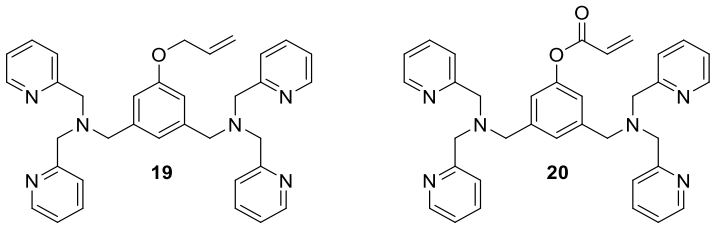

Figure 2.20: **Structures of the two possible monomers**. Both are bearing two DPA-like moieties, whereas they differ from each other for the reactive group, indeed one present an allylic pendant (**allyl-DPA**) and the other an acrylic one (**Acryl-DPA**).

Allyl-DPA synthesis

As depicted in scheme 2.6 (Approach 1), phenol **3** and allyl bromide undergo Williamson etherification, followed by reduction with lithium aluminum hydride. The diol **21** is obtained with 94% yield and without purification it reacts with PBr_3. The obtained bis-bromine undergoes nucleophilic substitution with DPA (Dipicolylamine) and **Allyl-DPA** is obtained through 4 steps with a 70% overall yield. Performing the etherification after the reduction step did not improve the overall yield.

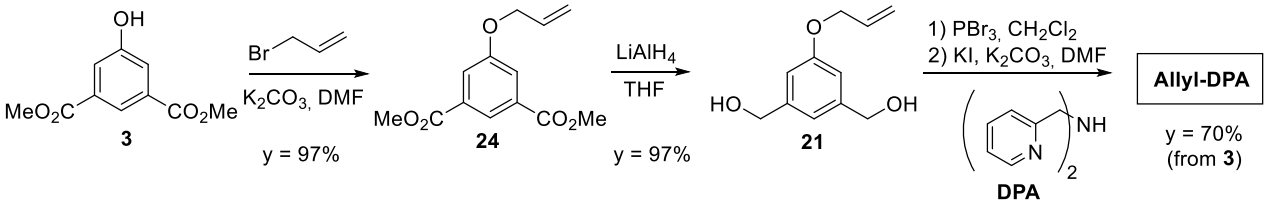

Scheme 2.6: **Synthesis of Ally-DPA (19).**

Acryl-DPA synthesis

The synthetic route applied for Acryl-DPA (**20**) is shown in Scheme 2.7. Compound **3a** was brominated and the phenol protected as TBDMS ether in high yield (92%). The resulting compound **26** is subjected to nucleophilic substitution with DPA and the silyl ether removed with TBAF. Esterification with acryloyl chloride has not been performed yet, since the resulting product would be only partially stable.

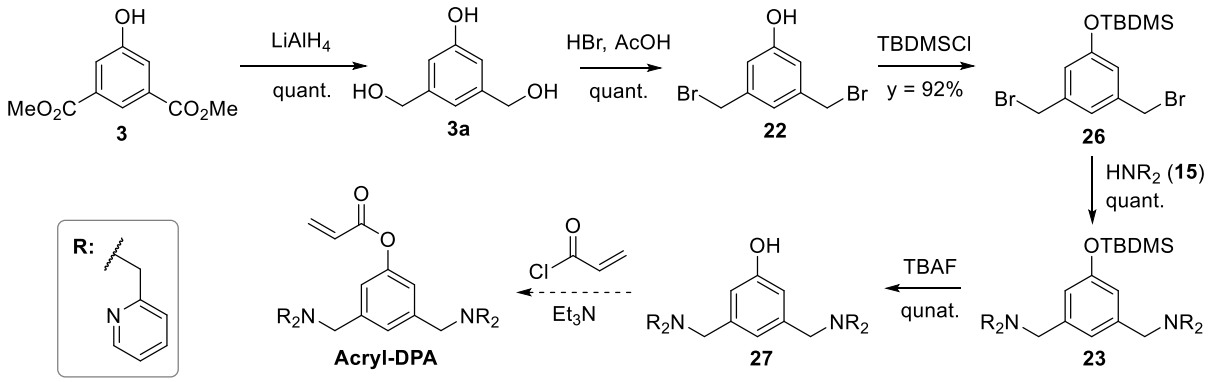

Scheme 2.7: **Planned synthesis of Acryl-DPA (20).** The actual synthesis stopped at phenol **27**.

Radical Polymerization

Firstly, we attempted acrylamide (**AA**) polymerization, following the procedure reported by Cappelletti and coworkers[76]. Therefore, acrylamide was dissolved in degassed toluene at 80°C for 24 h in presence of 1% of AIBN as initiator. After precipitation with MeOH, polyacrylamide (**PAM**) was collected as a white powder in 90% yields.

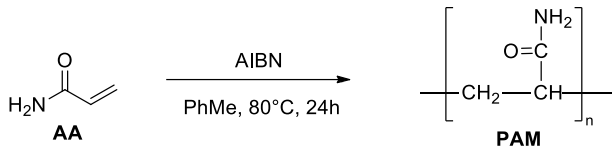

Figure 2.21: **Synthesis of linear polyacrylamide chians (PAM).**

In the same conditions, we attempted the copolymerization of acrylamide (**AA**) with 5% of Allyl-DPA (**19**). As before, after methanol precipitation, the polymer **PAM_19** was obtained in high yield (80%). ^{1}H-NMR revealed that only a tiny amount of **19** was incorporated in the linear polyacrylamide chains. Since the degree of functionalization seemed quite low, probably due to both reactivity and solubility, we reasoned to apply a different approach to the manufacturing. Since, no cross-linking agents were used the resulting polymers are meant to be linear. Indeed, they easily dissolve in water, indicating that the degree of cross-linking is very low. The molecular weight of the polymers were not investigated, because it was beyond the scope of the thesis.

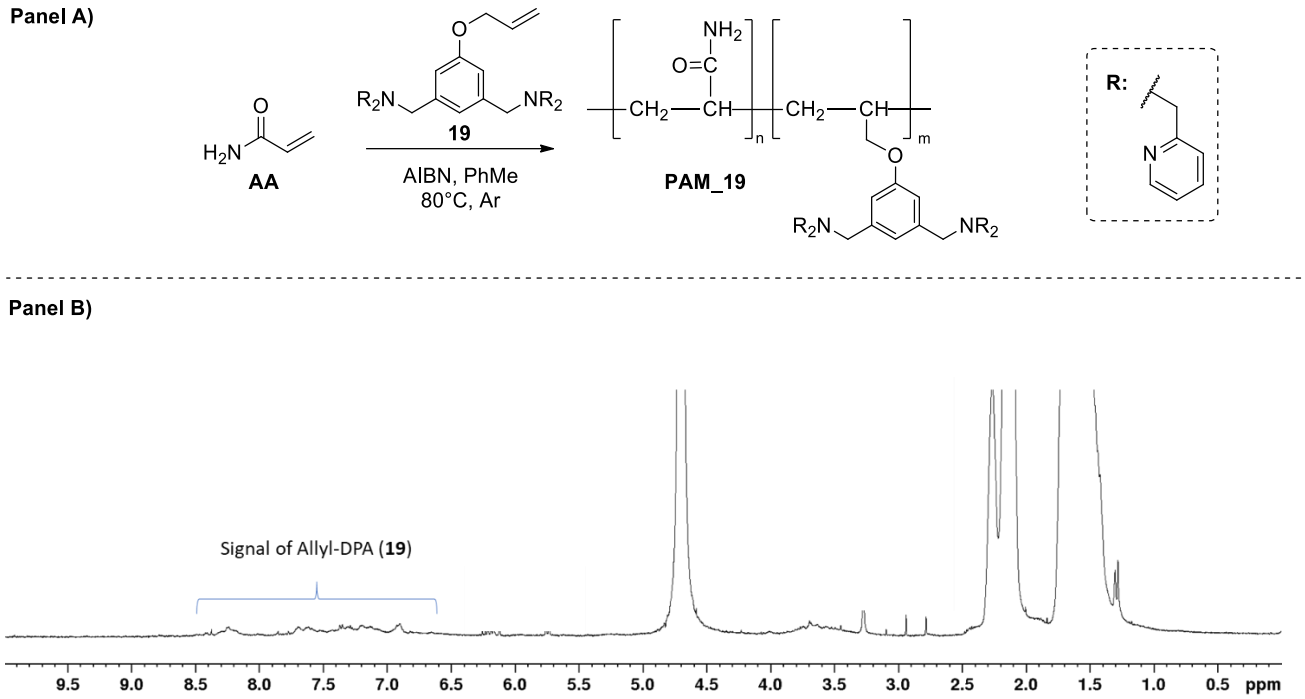

Figure 2.22: **Panel A) Copolymerization of AA and (allyl-DPA) 19 to afford a linear polyacrylamide (PAM_19) containing some Ally-DPA moieties. Panel B) Proton NMR of PAM_19.** D_2O, 400 MHz

Functional polymer coating of an inert solid support

Thanks to a collaboration with prof. Marcella Chiari at the SCITEC-CNR Institute in Milan, we changed our strategy towards the functionalization of a linear polymer with the binding moiety to be used for the coating of spherical particles serving as inert support. This approach would require the assessment of different aspects, as shown in Figure 2.23. An inert solid support of choice (a) undergoes surface activation (b); a suitable linear polymer (c) is functionalized with DPA units (d); The activated support is coated with the functionalized polymer (e) and the DPA unit are complexed with Zn(II) (f). The loading capacity of the resin is tested (g) and the bound nucleotides released (h). In principle, the binding capacity should be restored and the resin reused.

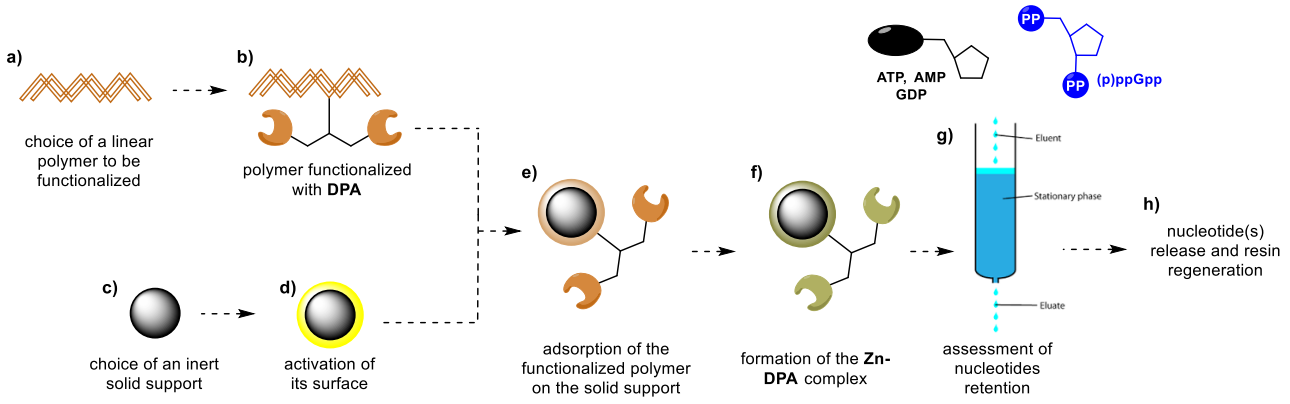

Figure 2.23: **The 'assembling approach' depicted from stage a) to stage h).**

a) Choice of a suitable linear polymer

Capitalizing on the experience of the Chiari's group on the functionalization of glass surfaces, we decided to explore the possibility of anchoring a linear N,N-dimethylacrylamide-based polymer to a siliceous bead surface through MAPS (γ-methacryloxypropyltrimethoxysilane) functional groups (Figure 2.24). NAS (N-acryloxysuccinimide) was introduced as the functional group reactive to nucleophiles (i.e. amines) that will allow the anchoring of a suitable DPA moiety. Copolymer DMA-NAS-MAPS (known as MCP-4) was therefore prepared by radical copolymerization of DMA, MAPS and NAS in 89:1:10 molar ratio[77]. Interestingly, N,N-dimethyl acrylamide (DMA) is soluble in both water and organic solvents, greatly simplifying its handling and maintaining the hydrophilicity required for its use in aqueous solutions.

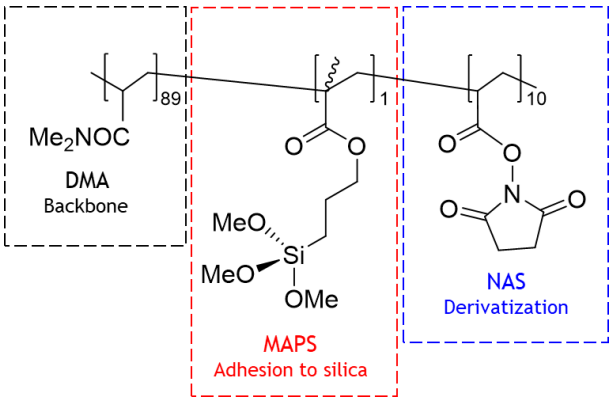

Figure 2.24: **Structure of copolymer DMA-NAS-MAPS (MCP-4)**

Even if for our purposes the actual average molecular weight of the polymer is not particularly relevant, we attempted MCP-4 characterization by MALDI-TOF MS analysis following technical details found for acrylamides MALDI analysis[78]. HCCA (α-cyano-4-hydroxycinnamic acid), DHB (2,5-dihydroxybenzoic acid), IAA (trans-indole acrylic acid), dithranol and sinapinic acid matrixes have been used to ensure proper laser ionisation. Sinapinic acid provided the best results, where a Gaussian distribution of the polymer centred at 2800 Da was observed. Each peak was spaced by 99.1 Da, corresponding to the molecular weight dimethylacrylamide (DMA).

b) Polymer functionalization:

The reactivity of NAS towards nucleophiles led us to modify allyl- and acryl- portions of **19** and **20** into a longer linker, terminated with a primary non-hindered amine, as in compound **28** (Figure 2.25).

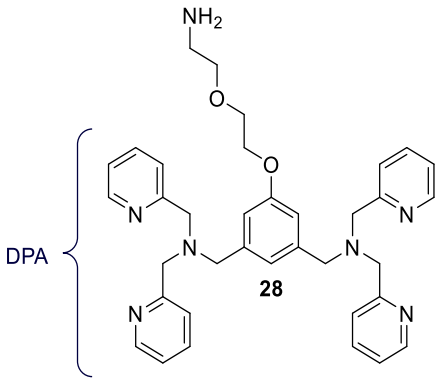

Figure 2.25: **Structure of compound 28.**

Amine **28** was prepared by the etherification reaction between phenol **27** and linker **29**[79] (Scheme 2.9). Compound **29** can be easily obtained in two steps in 80% yield starting from the commercially available 2-(2-Aminoethoxy)ethanol (**30**).

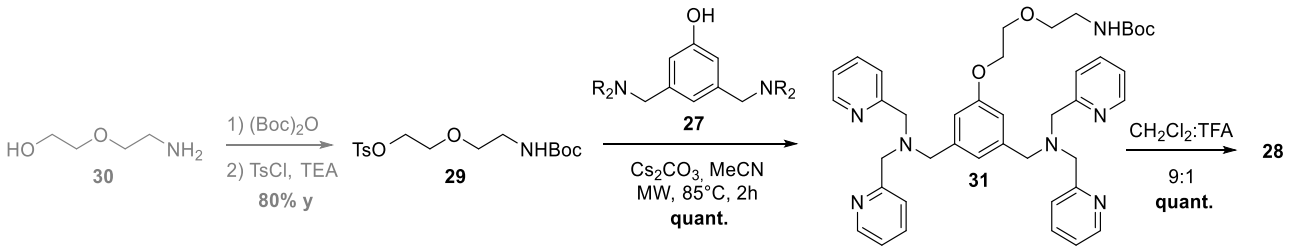

Scheme 2.8: **Synthesis of compound 28**

Phenol **27** (prepared as shown in Scheme 2.8) reacts with **29** leading to the formation of the corresponding ether (**31**) in quantitative yield. Finally, Boc protective group removal was achieved in acidic conditions in quantitative yield. Starting from compound (**3**) the synthetic sequence comprises 7 steps with a 92% overall yield on a scale up to 800mg. MCP-4 is then reacted with 0.6 mol equivalents of **28** (refereed to NAS) in dry THF and disappearance of the amine is monitored by TLC (Scheme 2.9). We exploited only 60% of the NAS groups in order to obtain a functionalized polymer still water soluble, essential feature in the coating step. Indeed, higher degrees of functionalization might lead to insoluble polymers.

Functionalized polymer **32** was isolated by precipitation as a pale orange powder with either Et_2O or hexane.

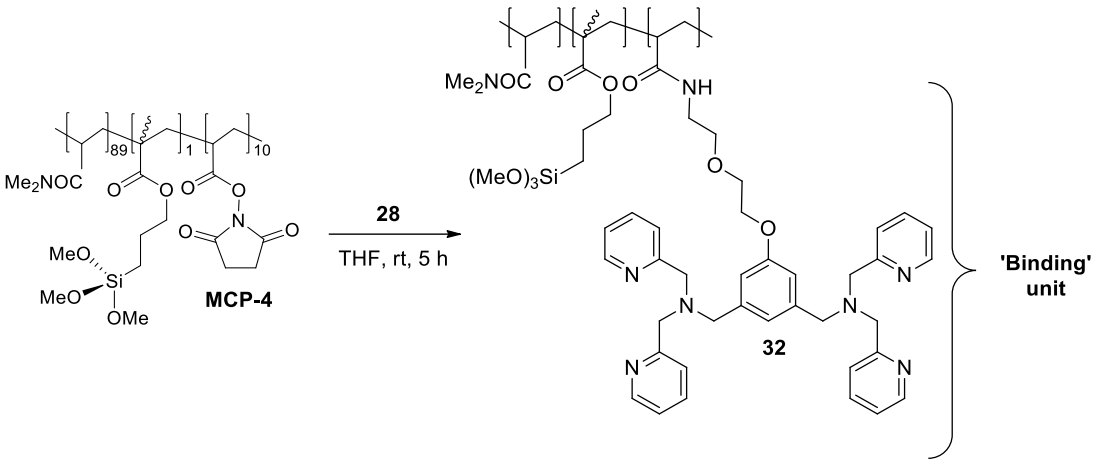

Scheme 2.9: **Functionalization of MCP-4 polymer with amine 28.**

Characterization of the functionalized polymer

The functionalized polymer needs to be characterized in terms of amount of binding unit attached (degree of functionalization), covalent nature of the bond, presence of residual reactive groups and possible impurities or by-products. These aspects were evaluated by means of different techniques, reported as follows.

NMR techniques

^{1}H-NMR in D_2O allowed verifying the maintained hydrophilicity of the polymer and the presence of the aromatic signals of the binding unit (Figure 2.26).

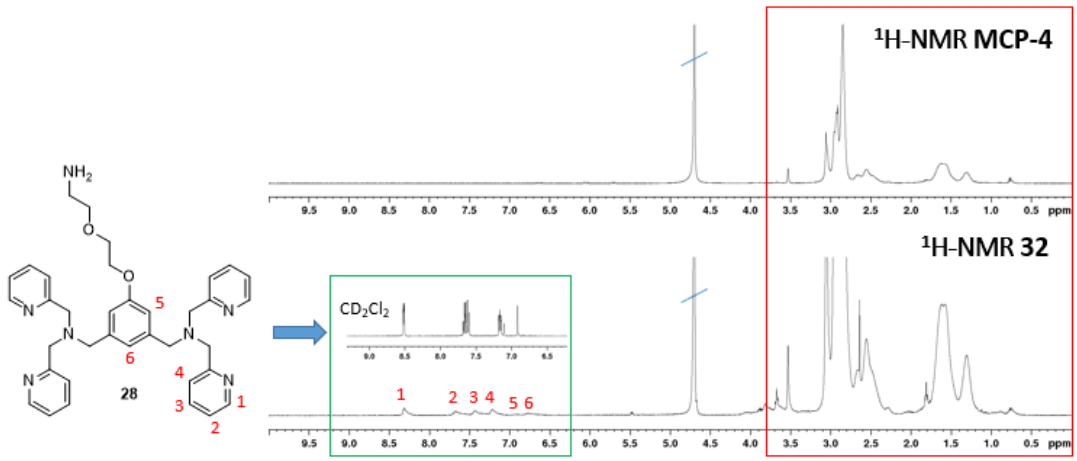

Figure 2.26: ^{1}H-NMR of compound **32** recorded (D_2O, 400 MHz) compared with MCP-4 and the aromatic region of compound 28 (green square). **32** spectrum scale is magnified compared to MCP-4 spectrum in order to put emphasis on the aromatics rings signals. The two spectra are recorded at the same concentration, i.e. 10 mg/mL.

Due to the macromolecular nature of **32** and to the small amount of binding unit attached, the aforementioned aromatic signals were recognizable although broad and difficult to integrate. The broadness of the aromatic portion was already an indication of a higher correlation time, confirmed also in a more concentrated DMSO-d6 sample (Figure 2.27).

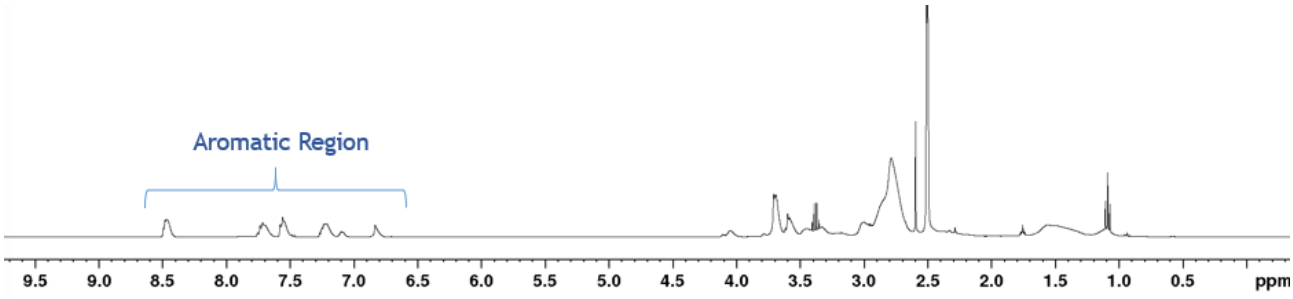

Figure 2.27: **proton NMR of compound 32** (DMSO-d6, 400 MHz).

Definitive proof of the covalent nature of the bond came from a 2D-NMR Diffusion Ordered Spectroscopy (DOSY) experiment, where the diffusion coefficient is plotted against the chemical shift. Diffusion coefficient (D) of the molecules in solution is derived from its correlation time, which is in turn linked to its molecular weight. Small molecules will diffuse more rapidly than macromolecules, showing higher D values. In particular, the aromatic signals of **32** showed the same diffusion coefficient of the aliphatic polymer signals between 0 and 5 ppm ($logD_1$ = -10.5, Figure 2.28).

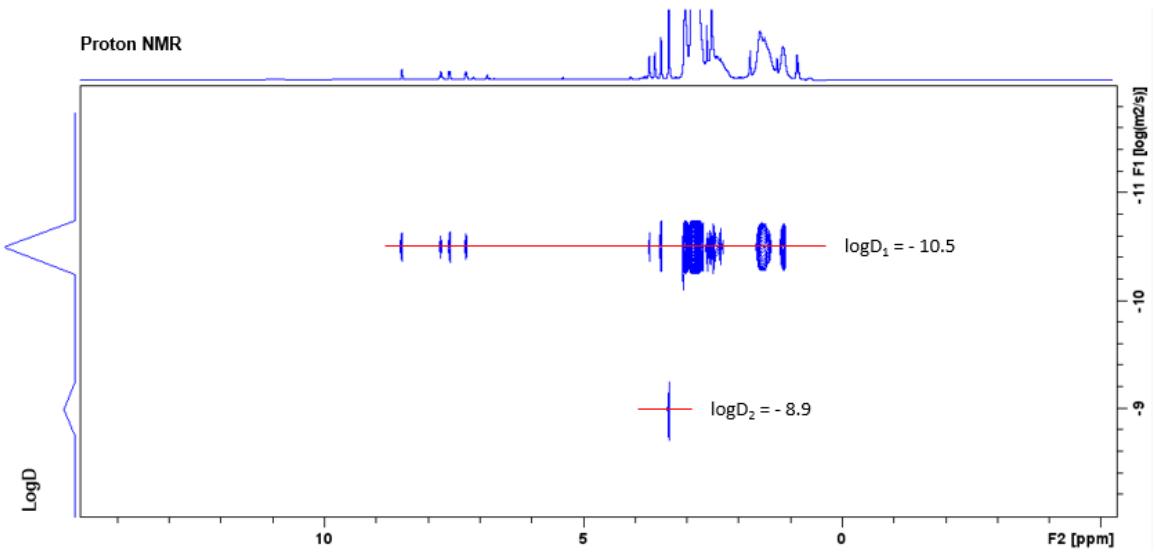

Figure 2.28: **DOSY analysis of functionalized polymer 32;** DMSO-d6, 400 MHz

Had the association of **28** been of non-covalent nature, we would have observed two sets of signals with the aromatic signals diffusing at a D value closer to that of the residual water observed at 3.33 ppm ($logD_2$ = -8.9). Indeed, compound **28** alone diffuses at a logD = -9.7 (Figure 2.29)

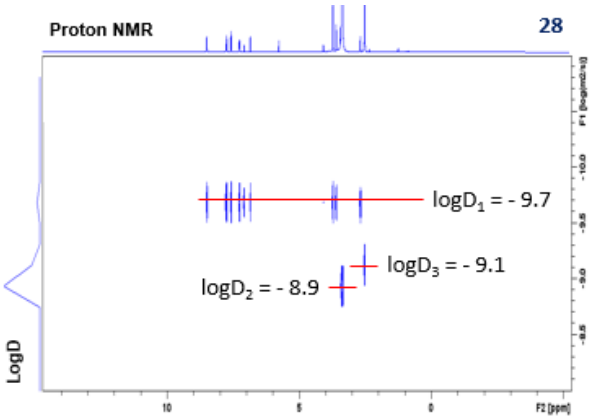

Figure 2.29: **DOSY spectrum of compound 28**; DMSO-d6, 400 MHz.

IR spectroscopy

ATR-IR (attenuated total reflection - infrared spectroscopy) analysis was performed directly on the solid polymer. Unfortunately, the strong signal attributed in MCP-4 to the C=O stretching of the dimethylacrylamide backbone amide group (peak 9 at 1621.84 cm^{-1}; Figure 2.30, left) prevented the detection of the amide bond formed upon polymer functionalization. We monitored instead the peak intensity reduction of the NAS activated ester C=O stretching (peak 8 at 1737.55 cm^{-1}; Figure 2.30, left). Indeed, the ATR-IR spectrum of **32** showed a much weaker peak at 1737.55 cm^{-1} (peak 3; Figure 2.30, right). Thus, we concluded that most of the NAS reactive groups had reacted with amine **28**.

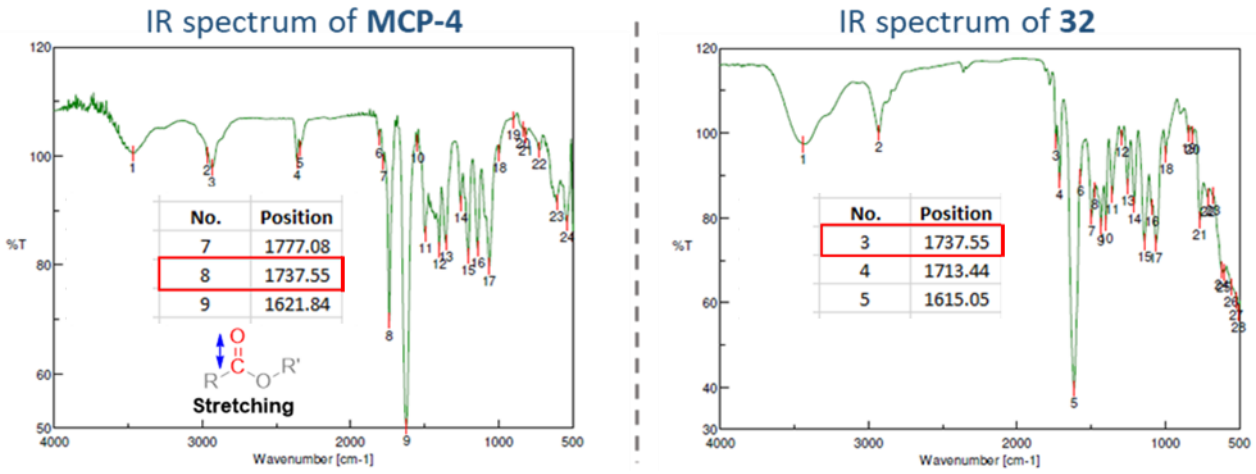

Figure 2.30: **IR spectra of MCP-4 and compound 32.**

UV-visible spectroscopy

Quantification of the binder units displayed by the polymer was achieved by UV-vis spectrophotometry. We first measured the molar attenuation coefficient of compound **28** at 261

nm in water, since it is the maximum absorption wavelength for this compound (Figure 2.31, left). The ε_{261} value was found to be 13200 M^{-1} cm^{-1} (in water) with a linearity range up to at least 80 µM (Figure 2.31, right).

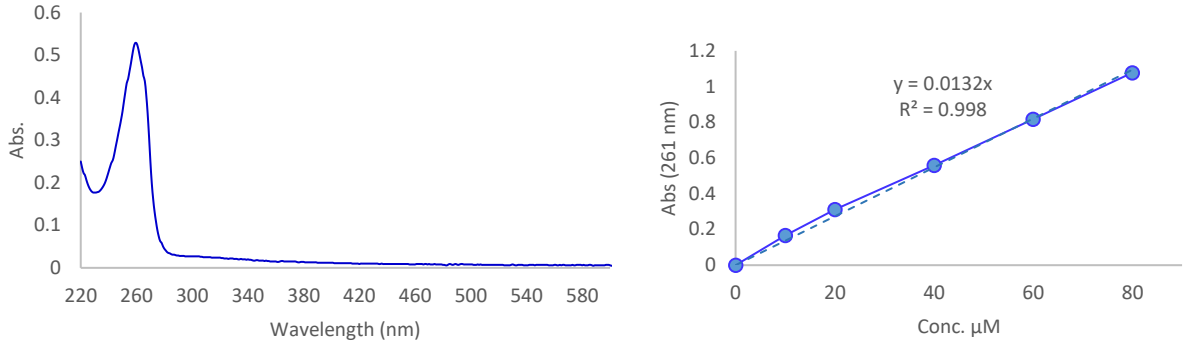

Figure 2.31: UV-vis Absorption profile of compound 28 (left); Plot of the concentration and the absorption values of samples contenting different amount of amine 28 (right).

We then verified that the UV absorption properties of the binding unit when attached to the polymer did not change significantly. In particular, the UV absorption spectrum of polymer **32** in water showed still a relative absorption maximum peak at 261 nm (Figure 2.32). Assuming that the molar attenuation coefficient of the binding unit was not altered significantly by its incorporation into the polymer backbone,[80] we estimated a loading of 0.5 µmol of binding units per mg of functionalized polymer, corresponding to a 6% molar. This finding was fully satisfying when compared to the sub-stoichiometric amount of **28** used in the functionalization step (6 moles of **28** per 10 moles of reactive NAS groups).

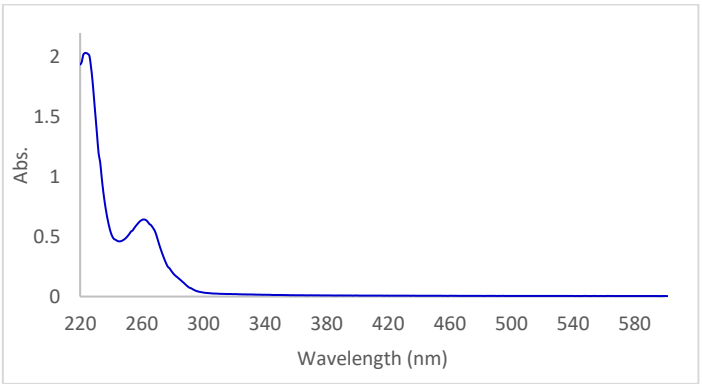

Figure 2.32: Absorption profile of polymer 32; the maximum is found at 261 nm.

c) Choice of the inert solid support

As mentioned above, our first inert solid-support choice were small siliceous particles. In particular, we first tried to use sand with an average particle diameter of 300 µm. Sand is constituted by tiny quartz grains, one of the allotropic forms of silicon dioxide (SiO_2), and their surface is mostly inert. Stable polymer adhesion would therefore require a preliminary surface activation treatment to expose reactive silanols groups. While glass surfaces are generally activated with plasma[81], spherical particles like sand would require a chemical activation[82].

The total surface area per gram of sand was calculated to be $A_{tot} = 2.9 \cdot 10^3$ mm^2/g (see experimental section).

d) Sand surface activation

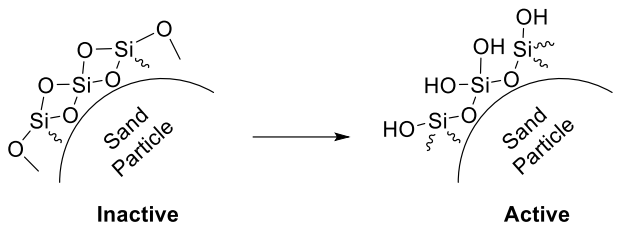

Figure 2.33: **Activation of sand particles surface**

Following the procedure used in the Chiari's group, we treated the sand first with 1 M HCl and then with 1 M NaOH. Hydrochloric acid destroys the outer shell Si-O-Si bridges and generates free Si-OH groups. Sodium hydroxide neutralizes the remaining acid and deprotonates to some extent silanols in order to have stronger nucleophiles. Finally, the sand was washed with water and recovered by filtration. A polymer adhesion trial on this material revealed that no organic material was present on its surface. Harsher activation conditions such as 2 M HNO_3 or a 5:1:1 mixture of water: 30% NH_4OH : 30% H_2O_2 at 70°C were not effective either. We therefore decided to switch to the more reactive silica.

Silica

Silica surface is inherently rich in silanols. The type we chose has smaller particles (100 µm diameter). The total surface area per gram of silica was 175 m^2/g, as reported in its data sheet.

e) Polymer adsorption on the solid support

Adhesion of the functionalized polymer **32** onto the silica particles surface was achieved by shaking the silica particles in a 1% w/V solution of **32** in water (Scheme 2.10). The final polymer/silica weight ratio 1:15. The reaction was considered complete when no polymer could be detected in the supernatant (by ^{1}H-NMR).

The crude product was isolated by filtration and then subjected to *curing*, a thermal treatment at 80°C that promotes covalent bond formation between surface silanols and the -Si(OH)$_3$ groups of

the polymer. This treatment ensured the stability of **33** that was verified by suspending a sample in D_2O for 45 minutes. ^{1}H-NMR of the supernatant confirmed that no leakage occurred over time.

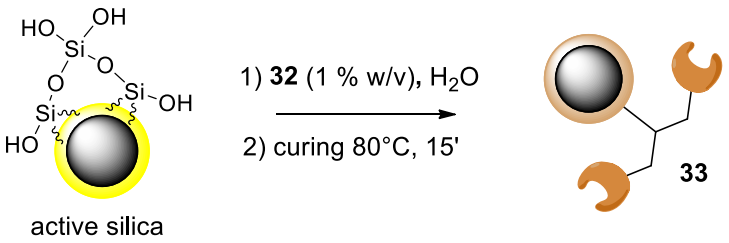

Scheme 2.10: **Silica coating with polymer 32.**

In order to confirm the quantitative adhesion of the polymer onto the silica surface we performed thermogravimetric analysis (TGA)[83]. The TGA instrument is essentially a very precise scale and a crucible where the sample is placed (Figure 2.34). The crucible is heated over time up to 1000°C at a certain rate. Weight loss due to solvents/water evaporation first, and organic material decomposition second, is monitored and recorded. The analysis can be performed under inert atmosphere (i.e. Ar, N_2) or under oxidizing conditions (air or O_2).

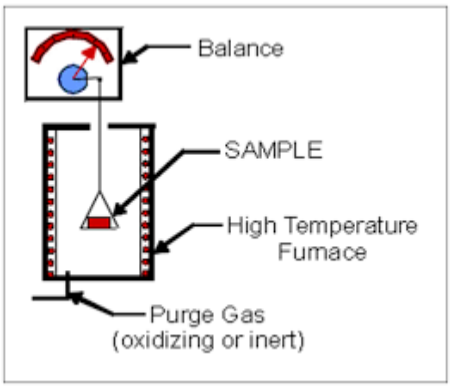

Figure 2.34: **TGA apparatus**

The resulting thermogram provides a plot of the weight loss versus temperature. We performed a TGA analysis on different batches of coated silica prepared as described above. In all cases, a puzzling three times higher weight loss than expected was observed.

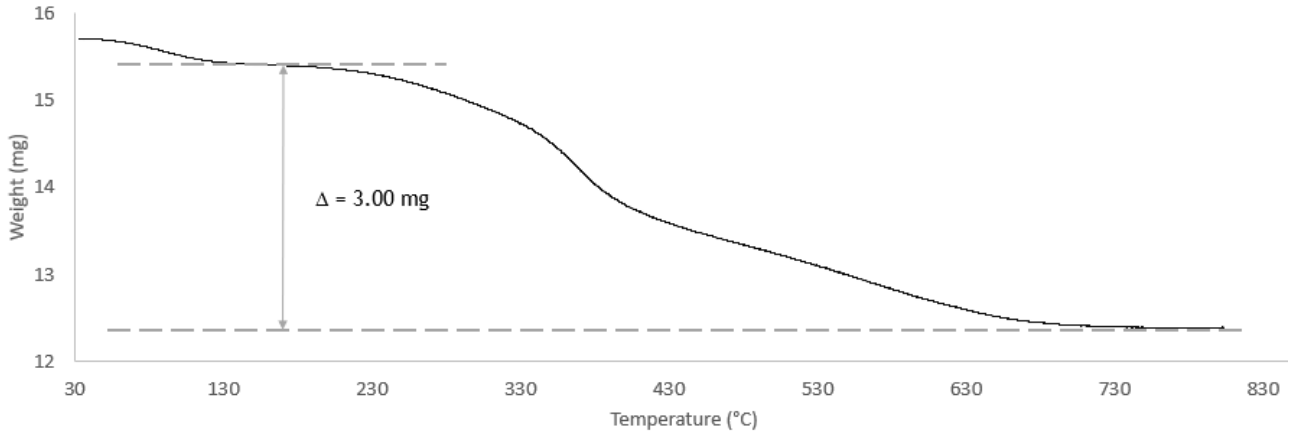

Figure 2.35: **TGA profile of a 15.7 mg sample of coated silica 33.**

As shown for example in Figure 2.35, up to 150°C we observed a small weight loss due to solvent evaporation. About half of the total weight loss was observed between 150 and 400°C, when the aliphatic portion of the organic molecules are decomposed. The *tail* observed between 400 and 650°C should be ascribed to aromatic moieties combustion. Afterwards, the curve reaches a plateau and only inorganic material remains in the crucible. The 3 mg weight loss shown in Figure 2.35 therefore corresponds to 20% of the total sample mass, a number in contrast with the ca. 6% w/w of organic material we would expect for quantitative adhesion of the polymer used for coating.

TGA performed on silica alone showed no weigh loss upon thermic treatment (Figure 2.36, left), while TGA on a sample of functionalized polymer showed complete decomposition and no overestimate of the sample loaded (Figure 2.36, right).

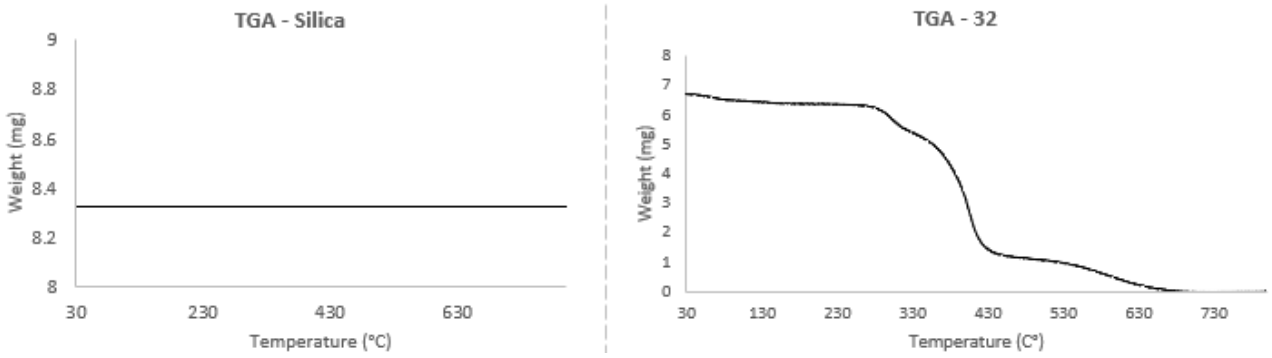

Figure 2.36*:* **TGA profiles of silica (*left*) and functionalized polymer 32 (*right*).**

After these control experiments, we could only conclude that, most likely, the coating process leads to the incorporation within the polymeric matrix of some water that is released only during polymer decomposition. This would certainly be an interesting feature, useful for our applications, which

would be worthwhile investigating in the future. In the meanwhile, we assumed the coating step to be quantitative. Therefore, since the degree of functionalization was found to be 0.5 µmol of binding unit per milligram of functionalized polymer **32,** and coated silica **33** is supposedly bearing 60 mg of **32** per gram of resin, we estimated 30 µmol of binding units per gram of coated silica **33**.

f) Formation of the Zn-DPA complex

After packing the coated silica **33**, Zinc/DPA complex formation was achieved by fluxing a zinc perchlorate water solution through the coated silica (Scheme 2.11). Excess of the zinc salt was removed fluxing water. The functional resin is ready to use or can be stored can be dried in vacuum.

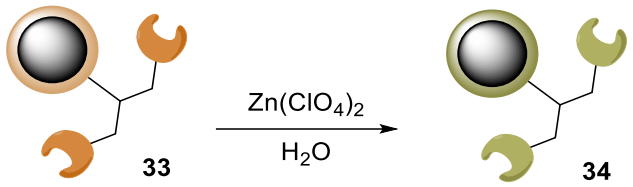

Scheme 2.11: Sketch of Zinc incorporation.

We first estimated the amount of Zinc loaded onto the resin as the 1:1 molar ratio with the dipicolylamine units calculated previously for the adhesion step (i.e. 60 µmol of Zn^{++} per gram of resin). In principle, measurement of the zinc amount directly on the solid sample could be performed by X-ray fluorescence (XRF) spectroscopy, but this technique requires gram-scale samples that were outside of our capabilities. We opted instead to treat a sample of resin with 2M HCl in order to release the zinc ion from the DPA complex. The Zinc-enriched solution obtained was subjected to atomic absorption spectroscopy (AAS) analysis, revealing a content of Zn^{++} equal to 42 µmol per gram of resin, corresponding to a 70% zinc loading. It also implies that the maximum nucleotide loading capacity expected is 21 µmol per gram of resin **34**, since two zinc ions are required for the recognition of a single nucleotide. Nevertheless, additional experiments will be performed on new batches of resin **34** to demonstrate the reproducibility of the zinc incorporation procedure.

g) Assessment of the nucleotides retention capacity

Analogously to the determination of the amount of Zinc loaded onto the resin, the assessment of nucleotide loading capacity was performed in a catch and release fashion. In particular, the amount of unbound nucleotide present in the flowthrough was determined by UV-VIS spectroscopy.

The required molar attenuation coefficients for GMP, GDP and ppGpp were experimentally measured as $\varepsilon_{256} = 10300\ M^{-1} \cdot cm^{-1}$ as previously described (*see section* PyDPA fluorescence assay). We determined the ε values for Adenosine-based nucleotides, i.e. AMP, ADP and ATP, as well, finding a value of $\varepsilon_{260} = 12500\ M^{-1} \cdot cm^{-1}$ (see experimental section).

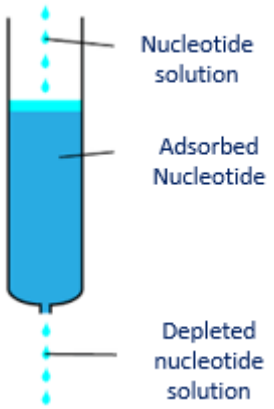

Figure 2.37: **Schematization of the nucleotide loading capacity test.**

After packing a small syringe, equipped with a frit septum, with the functional resin (indicatively 200 mg in a 2 mL syringe), 1 mL aliquots of 1 mM water solutions of ADP (the nucleotide chosen to run all preliminary loading tests) were added to the resin and eluted with water. The flow-through 1 mL fractions was analysed for UV-absorption at 260nm that would indicate the presence of unbound ADP. We observed a loading capacity between 2.8 µmol, corresponding to 14 µmol /g of resin **34**. The loading test was performed for other nucleotides as well (i.e. AMP, ATP, GMP and GDP) and we observed that monophosphate nucleotides, i.e. AMP and GMP, have a lower affinity to the resin, since no more than 10 µmoles per gram have been found. On the other hand, ATP, ADP and GDP showed a greater affinity to the resin as shown in the table below.

Table 2.1: **Experimental loading capacity determined for all the tested nucleotides.**

Nucleotide	**Loading capacity (µmol/g)**
ATP	13.5
ADP	14
AMP	9
GDP	11
GMP	8

In order to verify the effect of pH on the loading capacity, the tests were repeated using nucleotide solutions in HEPES buffer (10 mM, pH 8.5). The results were consistent with those previously obtained. These values are compatible with the maximum loading capacity of ca. 21 µmol nucleotide/g of resin calculated on the basis of the resin zinc content. At this point, only the last steps remained to be evaluated, i.e. the release of bound nucleotides and resin regeneration.
We tested ppGpp affinity towards the resin **34** loading only 5 µmol per gram of resin. In fact, higher ppGpp amounts are prohibitive, therefore we preferred to save ppGpp for further assays.

h) Nucleotides release

The Zn/DPA-pyrophosphate group association event takes place under neutral to slightly basic conditions. Therefore, the complex can be disrupted by lowering the pH. When eluting with 1 M HCl, nucleotides recovery was quantitative for all the tested nucleotides, as determined spectrophotometrically. In the case of ADP, nucleotide-containing fractions were also collected and lyophilized, yielding a weight consistent with the amount of ADP used. The recovered nucleotide was analyzed by ^{1}H-NMR (both in D_2O and DMSO-d6, 400 MHz). Interestingly, traces of coating polymer **32** were detected in the proton spectrum, indicating that the releasing condition might be too harsh. Using 0.1-0.2 M HCl allowed quantitative recovery without polymer release in the flowthrough. Additional analyses will be performed in order to verify if such acid solutions also lead to Zinc release from the resin. We thus moved to milder conditions, such as 50 mM ammonium formate (pH 4.56), that proved to be effective although up to 3-fold greater volumes of releasing solution were needed for complete nucleotide recovery.
In order to mime the composition of the enzymatic reaction mixture from which we would like to extract ppGpp, we performed similar loading tests with an equimolar solution of nucleotides, i.e. ATP, AMP and ppGpp. Since UV absorption does not allow distinguishing between different nucleotides in solution, we analysed the flowthrough fractions by PEI-cellulose TLC and ^{1}H-NMR. Loading 4.5 µmol of the ternary mixture on the same amount of resin used before, we observed only AMP in the flow-through, confirming the preference of the system for pyrophosphates over monophosphates. Both ATP and ppGpp were quantitatively recovered after release.

Resin regeneration

After nucleotide release, the acidity of the releasing solution was neutralized by eluting 5 mL 10 mM HEPES buffer at pH 8.5 and, as a precaution, a 0.21 M zinc perchlorate solution was fluxed as well.

A nucleotide loading test performed on this regenerated resin showed a loading capacity 30% lower than the initial one. Further optimizations will be required to improve this performance.

2.3 Specific ppGpp chelating group synthesis

The resin shown in the previous chapter certainly has a considerable practical utility, although in our case it has been used mainly as 'proof of concept'. A system bearing ppGpp-selective moieties, as established in the model study, should be manufactured by coating the silica using a properly functionalised polymer followed by zinc incorporation. As earlier, we have the possibility to modify a single step in the approach without interfering with the whole process. The design of a ppGpp-selective binding element is the only step missing for the creation of the ppGpp resin scavenger. Such selective group will be inserted in MCP-4 polymer (Scheme 2.13), while all other steps remain the same previously used.

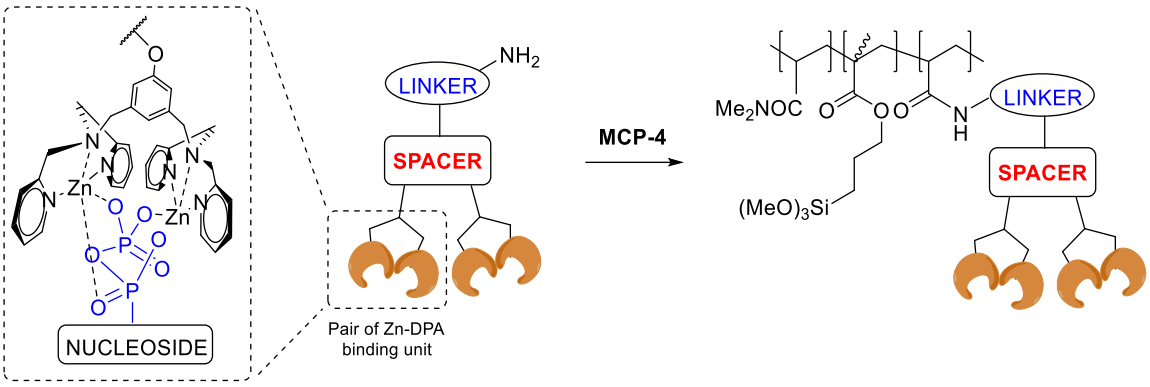

Scheme 2.13: **Generic structure of a binder specific to ppGpp.**

To generate a ppGpp selective binder, we need a moiety bearing two pairs of Zn-DPA binding units that must be properly spaced in order to 'fit' around ppGpp. The '*spacer*' must also present a linear chain (*linker*) ending with a primary non-hindered amine in order to react easily with MCP-4. ppGpp recognition will occur by interaction of Zn-DPA moieties and ppGpp pyrophosphates units

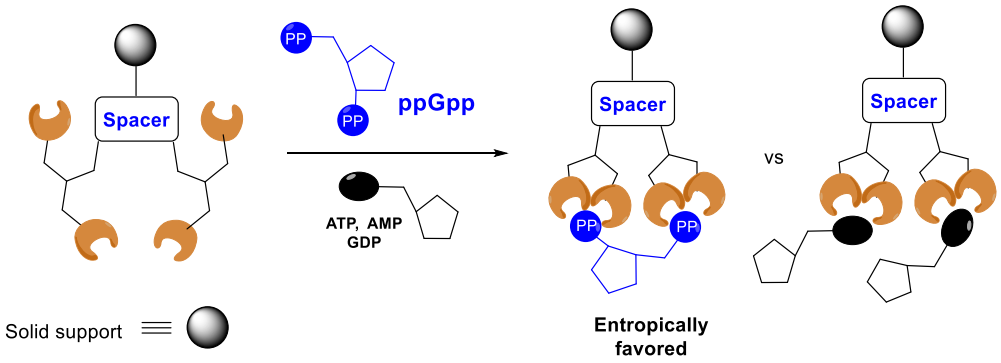

Figure 2.38: **Recognition mode of the supported ppGpp selective scavenger.** ppGpp binding is entropically favoured

The ppGpp-selectivity will be provided by the chelating event, which should lead to the formation of a more favoured adduct than would be formed if the bond were to take place with two regular nucleotides (Figure 2.38).

By merging all the structural requirements, i.e. *Binding units*, *spacer* and *linker*, we designed compound **35** (Scheme 2.14). The '*binding unit*' can be prepared as previously reported for phenol **27** (from 5-hydroxyisophthalate dimethyl ester **3** and **DPA**, Scheme 2.8, paragraph 2.2).

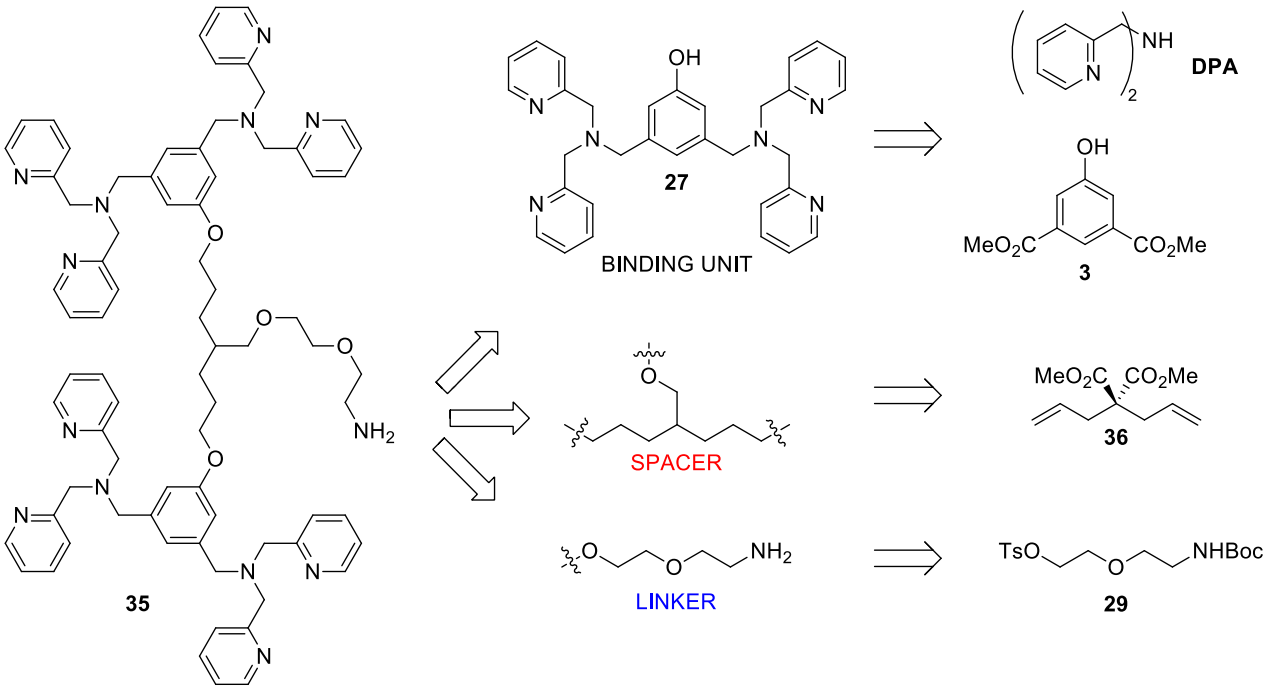

Scheme 2.14: **Design and retro-synthetic approach for the specific ppGpp chelating moiety.**

As *spacer,* we came up with an aliphatic chain, branched in its center. The ramification acts as a handle for the *linker* anchoring. Such spacing structure can be obtained from commercially available malonate **36**. Similarly, the precursor for the *linker* moiety could be the bifunctional molecule **29**[79], previously synthesized (paragraph 2.2, Scheme 2.9)

The synthesis of **35** started from elaboration of **36**, as shown in scheme 2.14. As reported in scheme 2.15, compound **36** underwent hydrolysis under basic conditions and decarboxylation to afford **38** in quantitative fashion. To install the required leaving group, acid **38** was treated with a saturated solution of HBr in acetic acid (ca. 33% w/w) in 0.22 M hexane as reported in literature[84]. The outcome of the hydrobromic acid addition is 100% anti-Markovnikov and afforded dibromide **39** in 78% yields. Borane dimethylsulfide ($H_3B{\cdot}SMe_2$) THF solution was used to reduce the acid moiety of dibromide **39** affording compound **40** in quantitative yield (78% overall yields from the four steps).

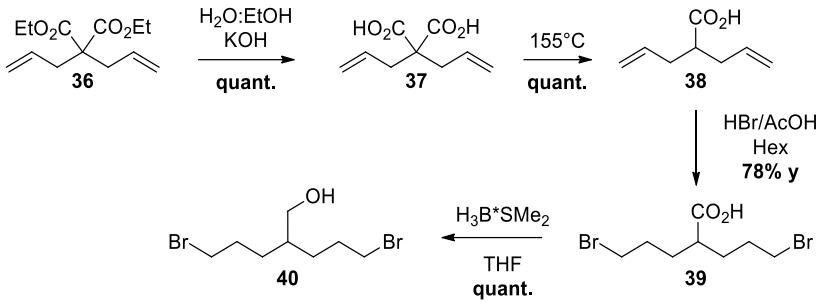

Scheme 2.15: **Synthesis of the *'spacer core'* 38.**

Phenol **41** was used as a model to optimize the reaction conditions for the bis-arylether formation from **39**. The substitution reaction between dibromide **40** and phenol proceeds with only 32% yield using Cs_2CO_3 as base and KI as a promoter in DMF at 85°C under microwaves irradiation for 1h. Besides unreacted phenol, which was recovered, a side-product was also found, most likely the intramolecular cyclization product of **40**.

On the contrary, reaction of **42** with linker **29** occurred smoothly. The latter reaction was performed by dissolving **42** in dry DMF and adding sodium hydride, followed by addition of **29** in excess (1.15 eq.). The conversion this time appeared to be quantitative.

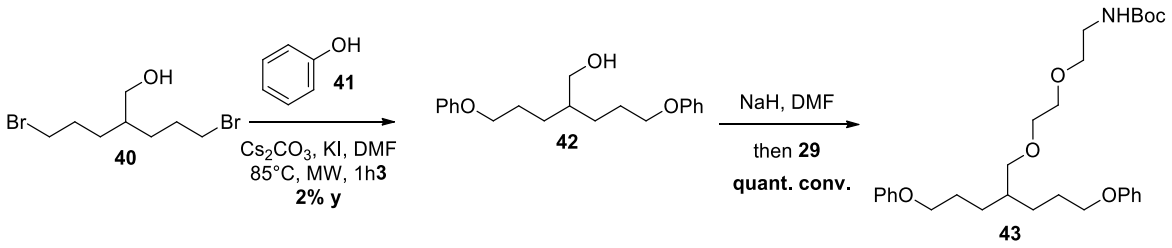

Scheme 2.16: **Study on the feasibility of compound 35 synthesis.**

Despite the low yield occurring in the reaction between phenol and compound **40**, we moved on the actual synthesis (Scheme 2.17). Therefore, dibromide **40** and phenol **27** were placed together using the condition just reported in the case of phenol in scheme 2.16. The reaction was stirred for 1h at 85°C and the solvent evaporated. The proton NMR of the crude was not diagnostic except for the disappearance of the -C$\underline{H}_2$Br moiety triplet signal occurring at 3.44 ppm ($CDCl_3$). ESI-MS revealed the presence of starting phenol **27** and of product **43** (m/z 1159.17), but the highest peak was found at m/z 643.23, corresponding to pyran **44**, while the desired product **43** was only 40% of the peak intensity.

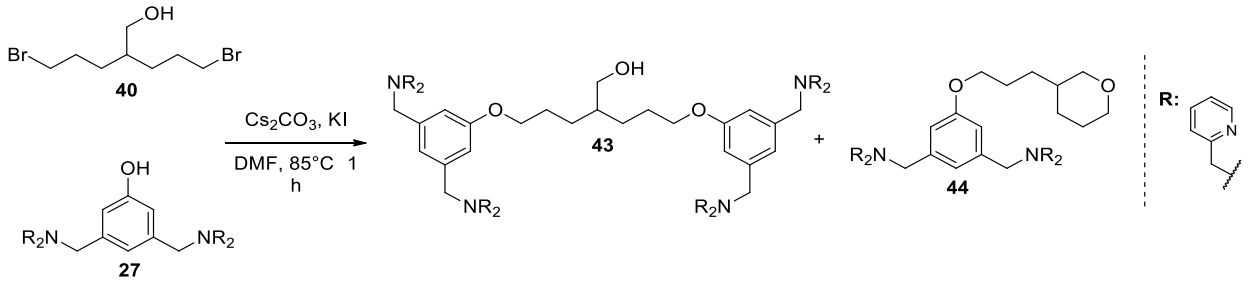

Scheme 2.17: **reaction of the dibromide 40 with the phenol 27. Side product 44 is the main component of the crude.**

Attempts to chromatography (CH_2Cl_2:MeOH) yielded no product **43**. We also tried chromatography with ammonia-doped solvents, but the situation remained the same. The low conversion/yield problem seems related to the intramolecular cyclization reaction taking place between the alcohol and the bromide in **40**, which leads to compound **44**. We attempted to avoid this unwanted event by protecting the alcohol with silylether protective groups. Neither protection with TBDMSCl nor with TMSCl resulted in the desired protected product.

The cyclization to **44** is most likely due to a combination between the basic reaction conditions and the bulkiness of phenol **27**. Perhaps, by removing basic agent (i.e. carbonate) and using a better nucleophile the problem could be overcome. Hence, we opted to use the primary amine **28** (synthesised by coupling between phenol **27** and linker **29** as described in detail in paragraph 2.2). Amine **28** is less hindered than phenol **27** and carbonate is not required. As matter of fact, the molecule obtained by coupling of amine **28** with dibromide **40** is a slightly longer than initially designed (molecule **45**) as shown in the *panel A* of scheme 2.18. However, the latter seems still suitable for the selective binging of ppGpp.

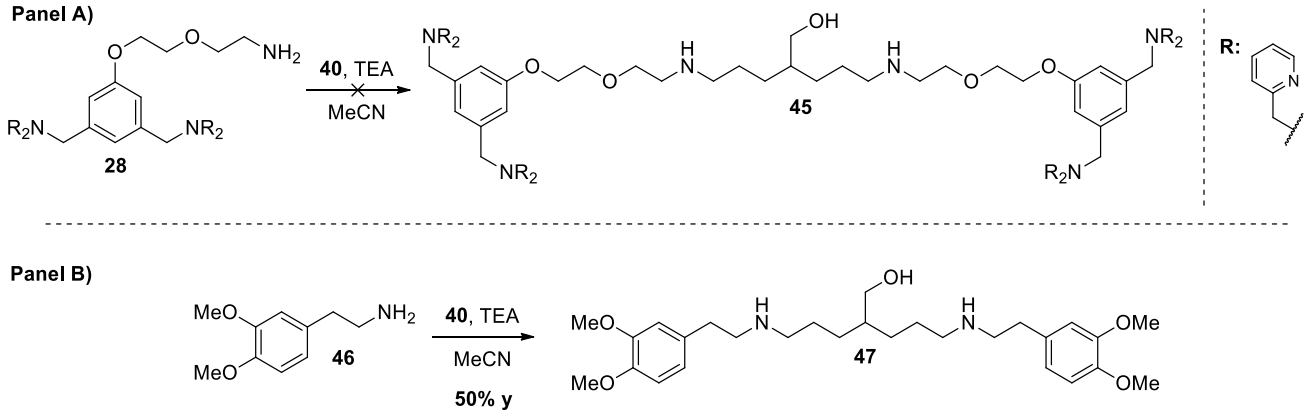

Scheme 2.18: **Panel A) Structure and synthesis of the new spacer 45; Panel B) Test on the reaction feasibility.**

We first tested the reaction feasibility using amine **46** with dibromide **40** (scheme 2.18, *panel B*). The reaction was stirred at rt for 2 h in 0.1 M CH_3CN solution and afforded compound **47** with an acceptable 50% yield after chromatographic purification (CH_2Cl_2:MeOH 95:5 doped with ammonia). We therefore used the same conditions to carry out the coupling between amine **28** and dibromide **40**. This time though the reaction did not work, indeed by ESI-MS we found the signal of product **45** (m/z: 1334.62) as ca. 10% of the base peak (m/z: 626.43). Nonetheless, we attempted to purify **45** by chromatography (CH_2Cl_2:MeOH 95:5 doped with ammonia) but we could not isolate the product. Due to all the problems encountered, we decided to move to a completely different structure of the *spacer* element. The structure we need, as already mentioned, must be bifunctional to connect the *binding units* on one site and the *linker* on the other one. As shown in scheme 2.19, we reasoned to use glutamic acid (**49**) as *spacer* for the selective ppGpp binder.

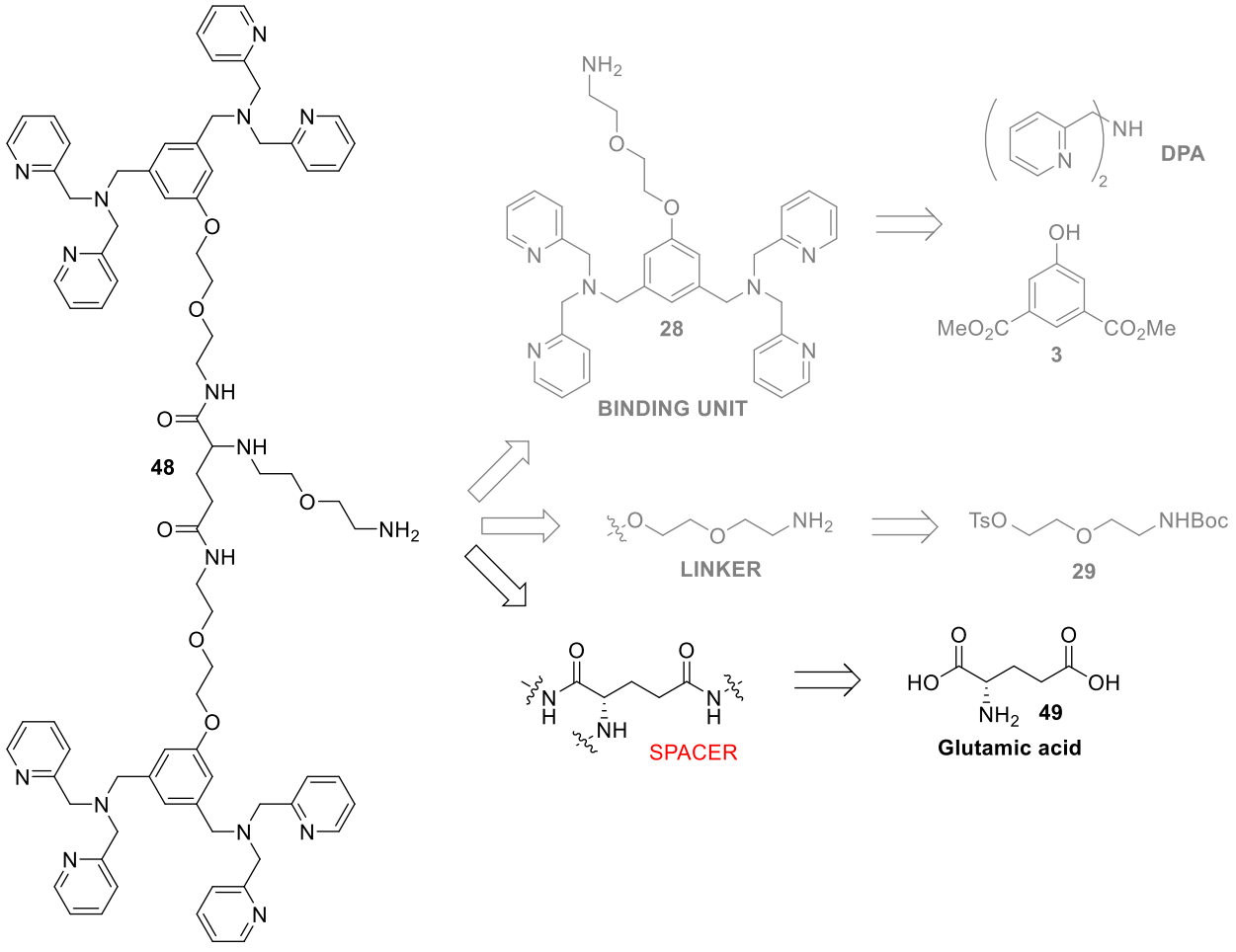

Scheme 2.19: **Design and retro-synthetic approach for alternative specific ppGpp chelating moiety (48).**

We actually used the natural occurring enantiomer of glutamic acid, i.e. L- series, since it is cheaper and already available in our laboratories, even though our application should not require a specific stereochemical configuration.

The idea is to form amide bonds between amine **28** and glutamic acid (**49**). The α-amino group of the aminoacid will be exploited to anchor the *linker*, as shown in Scheme 2.20.

As reported in scheme 2.20, glutamic acid was protected with $(Boc)_2O$ in an acetone/water 1:1 mixture to afford compound **50** (91% yield). Activated diester **52** was obtained through condensation between **50** and hydroxysuccinimide **51** in presence of DCC as condensing agent. At the end of the reaction, DCU was filtered off and the product was precipitated in Et_2O. The crude was directly used in the next step.

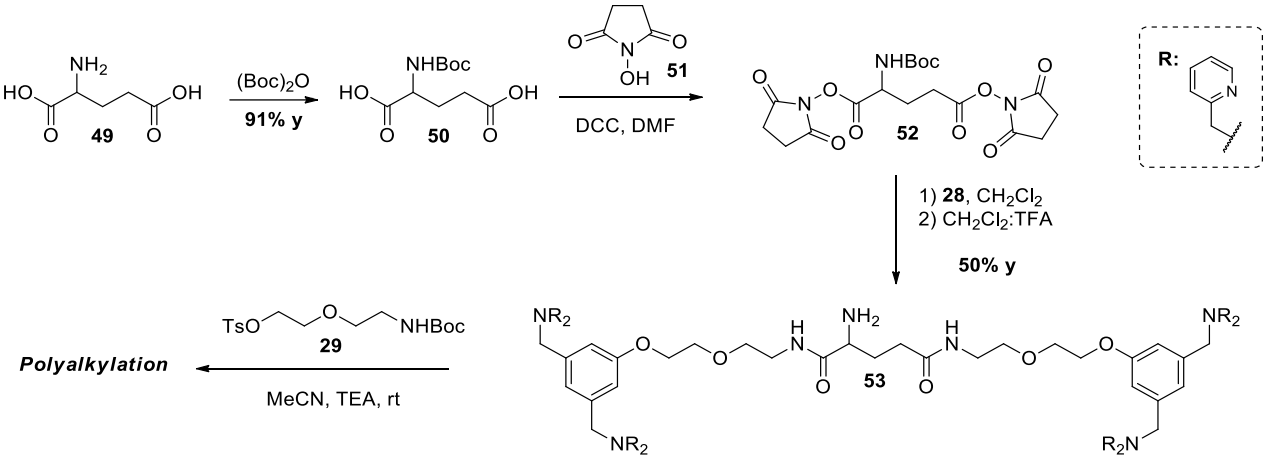

Scheme 2.20: **Synthetic pathway to compound 48.**

The activated diester **52** was stirred with two equivalents of amine **28** in CH_2Cl_2. The resulting product was treated with a CH_2Cl_2/TFA 9:1 mixture to remove the Boc and afford compound **53** with 50% yield over the two steps. Finally, we attempted the connection of linker **29** by alkylation of the α-amino group of **53**. Unfortunately, we mainly obtained poly-alkylated adducts.

Thus, we decided to switch linker in order to use an acylation of 'glutamate core' instead of the previous alkylation. Since we had run out of **53** in the alkylation trials, we also decided to make the process more convergent by acylating the glutamic acid unit, followed by bis-DPA binding units insertion (Scheme 2.21). For the acylation, we chose a longer *linker*, i.e. N-Boc-ω-aminoundecanoic acid (**54**), to achieve better spacing from the solid support. Dimethyl glutamate **55** and acid **54** were treated with **HATU** as condensing agent affording **56** in 83% yield. Hydrolysis with LiOH provided diacid **57** in 95% yields. The two carboxylic groups of **57** were activated as N-hydroxysuccinimidate

by DCC and N-hydroxysuccinimide (**51**) in DMF. As before, DCU was filtered off and the product **58** was collected after Et_2O precipitation.

The activated diester **58** was mixed with two equivalents of amine **28** in CH_2Cl_2 to afford **59** in quantitative fashion. To conclude, the Boc was removed with TFA to afford the final target molecule **60** in 90% yield.

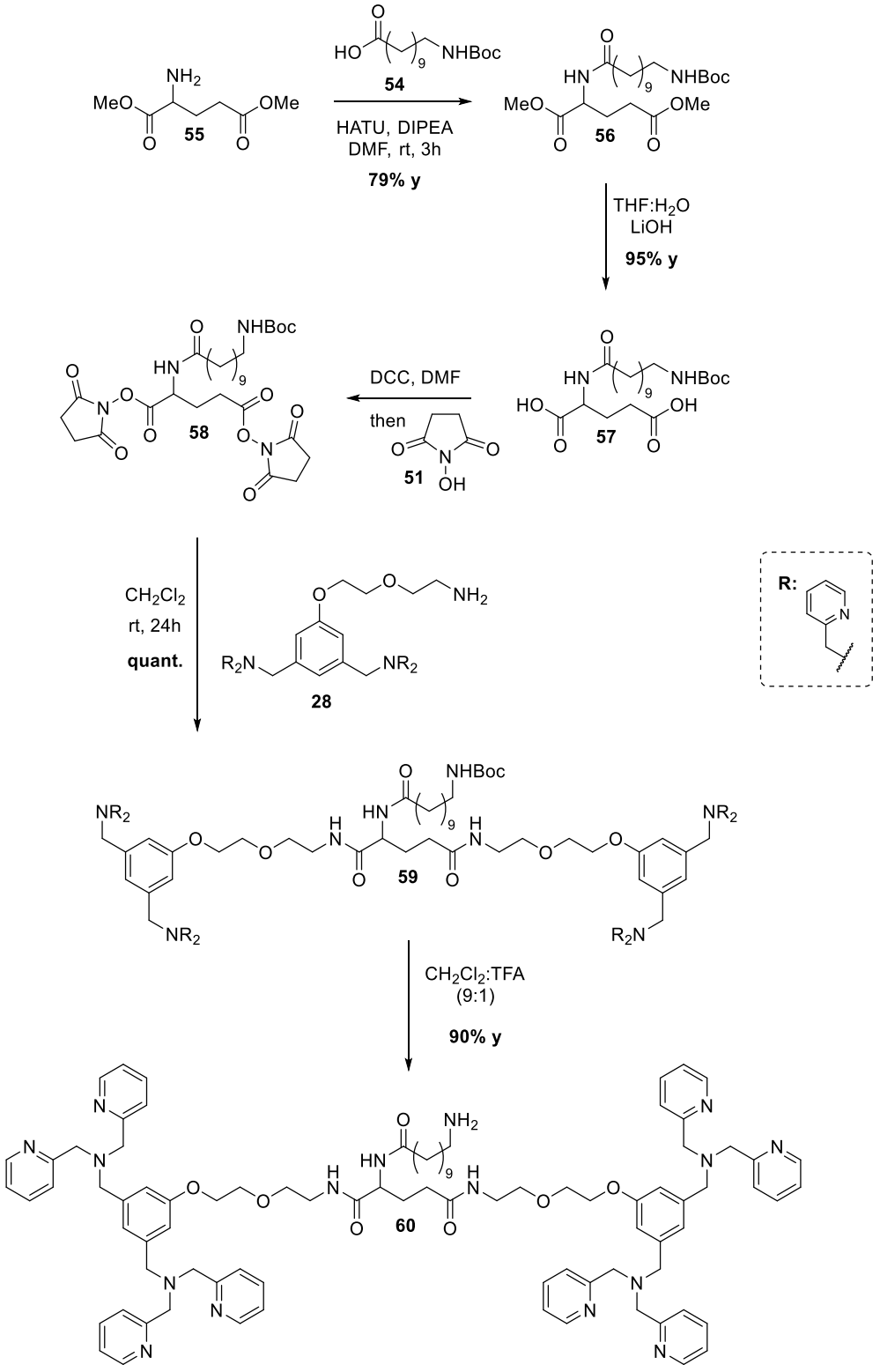

Scheme 2.21: **Synthesis of the designed ppGpp binder 60.**

To sum up, the synthesis of the designed ppGpp selective ligand **60** was optimized to obtain the target molecule in five steps with a 71% overall yield with respect to compound **54** or in two steps with a 90% overall yield with respect to compound **28** (Scheme 2.21).

Preliminary NMR investigations have been performed in order to prove ppGpp-binding to compound **60**. In particular, saturation-transfer difference[85] (STD, a bioaffinity technique used for the analysis of small ligand-macromolecule (i.e. receptor) interaction) experiments were used. STD is based on the possibility of selectively saturating the protons of the receptor (in this case compound **60**) by irradiating a frequency (in this case the aliphatic tail) at which only the protons of the macromolecule can resonate and not the protons of the small molecule. Due to effective spin diffusion, saturation quickly propagates across the entire macromolecule. If the ligand binds to the receptor, saturation will be transferred through space to the ligand. As result, the STD spectrum will reveal selectively the protons in proximity to the receptor, their signal intensity inversely proportional to the proton-receptor distance

The experiments were performed by preparing a solution containing 15 µM of binder **60** (i.e. the receptor) and 1.5 mM of ppGpp and 1.5 mM of ADP in deuterium oxide (ligand : receptor ratio 100:1[86]). 30 µM of zinc perchlorate was added to form *in situ* the chelating units (shorten as **60*Zn**).

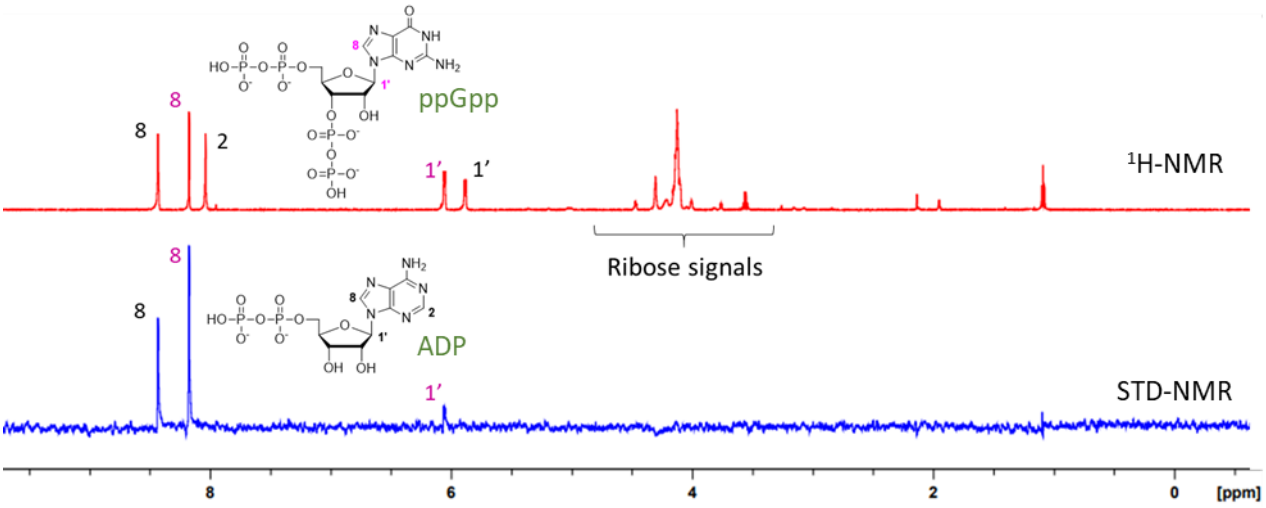

Figure 2.39: Red) ^{1}H-NMR of ADP and GDP 1:1 mixture; Blue) STD-NMR of a 100:100:1 mixture of ADP, ppGpp and **60*Zn**. (D_2O, 600 MHz, sample irradiation at -0.05 ppm)

As shown in figure 2.39, the STD spectrum shows that both ppGpp and ADP can bind to the receptor **60*Zn,** and in particular the interaction involves the nucleobase ring, as evidenced by the strong signal of both H8 protons. In addition, it is possible to appreciate that, in the case of ppGpp, of the ligand-receptor interaction extends to the ribose ring (see H_1' signal)

Thanks to such encouraging data, compound **60** will be used for the functionalization of polymer **MCP-4**. After the anchoring of the functionalized polymer on silica, we will test the actual ppGpp-selective scavenging ability.

Conclusion and future perspectives

During my PhD, I worked on the detection of the unusual nucleotide (p)ppGpp by means of the selective chemosensor PyPDA. Even though the fluorescence-based PyDPA assay did not result in a quantitative and robust method for ppGpp detection, it allowed us to optimize the synthesis of PyDPA increasing the overall yield from 9% to 67% (*ChemBioChem* **2019**, *20*, 1717-1721).

The alarmone ppGpp was synthesised using both Rel_{Seq} and RelP and isolated as a pure compound on a scale up to 30 mg.

Inspired by the working of the chemosensor, we developed a nucleotide specific scavenging system that is potentially recyclable upon further optimization.

Selectivity of the system towards ppGpp compared to other nucleotides has been addressed with the design and synthesis of ligand **60**. Further optimizations are needed to achieve the final product but the binding studies carried out in solution showed promising results.

Experimental Section

General procedures and materials

All commercial reagents (Abcr, Acros, Alfa Aesar, Biosynth, Fluka, Merck, VWR and Zentek) were used without further purification. Dichloromethane was distilled using calcium hydride as drying agent. Ethanol, THF, Toluene and DMF were bought dry from Merck in closed ampoules. All solvents were of reagent grade or HPLC grade.

^{1}H-NMR and ^{13}C APT NMR were recorded on a Bruker Advance 400 MHz instrument at 298 K; the chemical shifts are expressed in ppm and are referred to TMS. The δ (ppm) axis was calibrated on the solvent residual signal for which every spectrum was recorded: $CDCl_3$ (7.26 for ^{1}H and 77.16 for ^{13}C), CD_3OD (3.34 for ^{1}H and 49.86 for ^{13}C), CD_2Cl_2 (5.32 for ^{1}H and 54.00 for ^{13}C), DMSO-d6 (2.50 for ^{1}H and 39.50 for ^{13}C), CD_3CN (1.94 for ^{1}H and 118.3 for ^{13}C). The signal shapes (^{1}H-NMR) are abbreviated as s (singlet), d (doublet), t (triplet), q (quartet), qui (quintet), sex (sextet), m (multiplet), dd (doublet doublets), td (triplet doublets). COSY and HSQC experiments were used to assist the ^{1}H and ^{13}C resonance assignments. Mass spectra were obtained with the help of a ThermoFisherLCQ (ESI).

Thin layer chromatography (TLC) was performed with pre-coated Silica Gel 60 F254 plates or PEI-cellulose TLC F254 (Sigma-Aldrich or Merck Millipore) subsequently stained with:

- UV-light (254 and 366 nm);
- Molibdic reagent (Pancaldi): 21 g $(NH_4)_6Mo_7O_{24}$ $4H_2O$ (ammonium heptamolibdate tetrahydrate), 1 g $Ce(SO_4)_2$ and 31 mL H_2SO_4 in 470 mL H_2O;
- Potassium permanganate: 3 g $KMnO_4$, 20 g K_2CO_3, 5 mL NaOH (5% sol. in H_2O) in 300 mL H_2O;
- Ninhydrin: 300 mg ninhydrin, 3 mL glacial AcOH in 100 mL abs. EtOH;
- Dragendorff's reagent: 1.7 g $Bi(NO_3)_3 \bullet 5H_2O$, 20 mL glacial AcOH, 80 mL H_2O and 100 mL KI (50% sol. In H_2O)

Automated chromatography was carried out using Biotage Isolera Prime with double UV detection; Biotage SNAP KP-Sil cartridges were employed.

Microwave-assisted organic synthesis was achieved using Biotage Initiator^{+} synthesizer.

For infrared (IR) spectroscopy an FT/IT-4000TypeA_ATR-PRO-ONE was used.

Synthesis of 3-(pyren-1-yl)prop-2-yn-1-ol (12)[1]

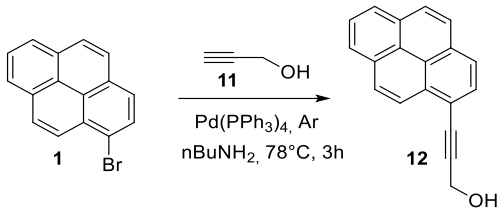

1-bromopyrene (**1**) (100 mg, 0.356 mmol, 1 eq.) and $Pd(PPh_3)_4$ (13 mg, 0.011 mmol, 0.03 eq.) were dissolved in degassed $nBuNH_2$ (12 mL, [1] = 0.03 M). Propargylic alcohol **11** (102 μL, 1.78 mmol, 5 eq.) was added to the mixture and the reaction was stirred under reflux conditions for 3 h (TLC Hex:EtOAc 2:1, R_f(**12**) = 0.39; staining: Molibdic reagent). Upon completion, the reaction was quenched with 4 mL of HCl 6 M and product **12** was extracted with ethyl acetate (3 x 20 mL). The reunited organic phases were then dried over Na_2SO_4 and concentrated in vacuum. The crude was purified by automated chromatography (Hex with a gradient of EtOAc from 10% to 67%). The solvent was evaporated at reduced pressure to obtain **12** as a yellow solid.

Yield: 85.1 mg, 95%.

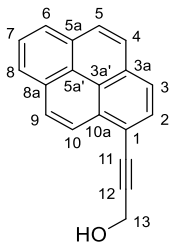

^{1}H-NMR (400MHz, $CDCl_3$): δ(ppm)= 8.55 (d, 1H, H_3, $J_{2\text{-}3}$ = 9.2 Hz), 8.25 - 8.01 (m, 8H, H_2, H_4, H_5, H_6, H_7, H_8, H_9, H_{10}), 4.72 (d, 2H, H_{13}, $J_{13\text{-}OH}$ = 6.1 Hz), 1.82 ppm (t, 1H; -OH); **^{13}C NMR (100 MHz, CDCl3):** δ(ppm)= 132.2 (C_1), 131.5 (C_{5a}), 131.3 (C_{8a}), 131.1 (C_{3a}), 129.9 (C_{10a}), 128.5 (C_2), 128.4 (C_9), 127.3 (C_5), 126.9 ($C_{5a'}$), 126.7 ($C_{3a'}$), 126.4 (C_4), 126.2 (C_7), 125.7 (C_6), 125.5 (C_8), 124.5 (C_{10}), 124.4 (C_3), 92.9 (C_{11}), 84.9 (C_{12}), 52.2 (C_{13}).

ESI-MS: calculated for $[C_{19}H_{12}ONa]^+$: 279.08; found: 279.28.

[1]P.S. Addy *et al.,Chem. Comm.*, **2013**, *49*, 1930-1932

Synthesis of 3-(pyren-1-yl)propan-1-ol (13)[2]

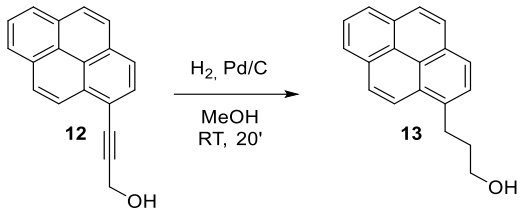

Compound **12**(184 mg, 0.718 mmol, 1 eq.) was dissolved in freshly distilled MeOH (24 mL, [**12**] = 0.03 M). 10%-Pd/C (38 mg, 0.041 mmol, 0.05 eq.) was added and the reaction was placed under hydrogen atmosphere (TLC Hex:EtOAc 6:4, R_f(**13**) = 0.43; staining: Molibdic reagent). Upon completion, the catalyst was filtered over a celite pad and the solvent evaporated at reduced pressure to obtain **13** with high purity.

Yield: 179 mg, 96%.

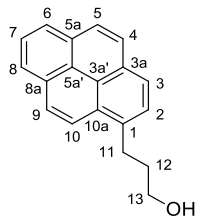

^{1}H-NMR (400MHz, $CDCl_3$): δ(ppm)= 8.32 (d, 1H, H_3, $J_{2\text{-}3}$ = 9.4 Hz), 8.19 - 8.15 (dd, 2H, H_6, H_8, $J_{6\text{-}7} = J_{7\text{-}8}$ = 7.5 Hz), 8.14 - 8.09 (m, 2H, H_2, H_9), 8.06 - 8.01 (m, 2H, H_4, H_5), 7.99 (t, 1H, H_7), 7.90 (d, 1H, H_{10}), 3.80 (t, 2H, H_{13}, $J_{12\text{-}13}$ = 6.1 Hz), 3.50 - 3.43 (m, 2H, H_{11}), 2.18 – 2.10 (m, 2H, H_{12});

^{13}C NMR (100 MHz, CDCl3): δ(ppm)= 136.3 (C_1), 131.6 (C_{5a}), 131.0 (C_{8a}), 131.1 (C_{3a}), 128.8 (C_{10a}), 127.7 (C_2), 127.6 (C_9), 127.5 (C_5), 127.4 (C_4), 126.2 (C_7), 125.3 ($C_{3a'}$), 125.2 ($C_{5a'}$), 125.1 (C_6), 125.0 (C_8), 124.9 (C_{10}), 123.4 (C_3), 62.6 (C_{13}), 34.7 (C_{11}), 29.8 (C_{12});

ESI-MS: calculated for $[C_{19}H_{16}ONa]^+$: 283.10; found: 282.96.

[2] L. S. Gossett *et al.*, *Bioorg And Med. Chem. Letters,* **1996**, *6 (4)*, 473-476

Synthesis of 1-(3-bromopropyl)pyrene (2)[3]

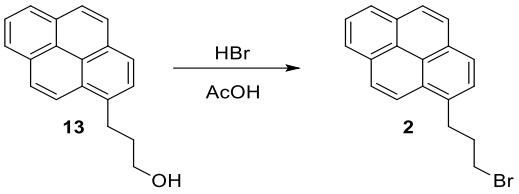

Compound **13** (179 mg, 0.68 mmol, 1 eq.) was dissolved in 1.4 mL of an acetic acid solution of **HBr** (33%$_{w/w}$) (2 mL per mmol **13**). The reaction was stirred under microwave irradiation at 100°C for 40 minutes (TLC Hex:EtOAc 7:3, R_f(**2**) = 0.77; staining: Molibdic reagent). Upon completion, the mixture was diluted with 10 mL EtOAc and washed with $NaHCO_3$ 50%$_{w/v}$ (3 x 10 mL) and water (1 x 10 mL). The organic phase was dried over Na_2SO_4 and the solvent evaporated to obtain **2** as a brown viscous oil.

Yield: 218 mg, quantitative.

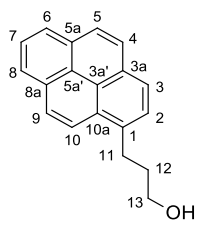

^{1}H-NMR (400MHz, $CDCl_3$): δ(ppm)= 8.29 (d, 1H, H_3, J_{2-3} = 9.2 Hz), 8.20 - 8.15 (dd, 2H, H_6, H_8, $J_{6-7} = J_{7-8}$ = 7.6 Hz), 8.15 - 8.10 (m, 2H, H_2, H_9), 8.03 (s, 2H, H_4, H_5), 7.99 (t, 1H, H_7), 7.90 (d, 1H, H_{10}), 3.56 - 3.47 (m, 4H, H_{11}, H_{13}), 2.41 (quint., 2H, H_{12}, J_{12-13} = 6.9 Hz);

^{13}C NMR (100 MHz, CDCl3): δ(ppm)= 134.9 (C_1), 131.6 (C_{5a}), 131.3 (C_{3a}), 131.0 (C_{8a}), 128.8 (C_{10a}), 127.7 (C_2), 127.6 (C_9), 127.0 (C_5), 126.0 (C_4), 125.2 (C_7), 125.1 (C_6), 125.0 (C_8, $C_{5a'}$), 124.9 (C_{10}), 123.4 (C_3), 123.3 ($C_{3a'}$), 37.4 (C_{12}), 33.6 (C_{13}), 31.8 (C_{11});

ESI-MS: calculated for $[C_{19}H_{16}Br]^+$: 323.04; found: 323.03.

[3]O. K. Rasheed *et al.*, *Synlett*, **2016**, *27*, 905-911

Synthesis of (5-hydroxy-1,3-phenylene)dimethanol (3a)[4]

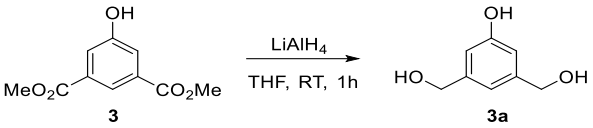

Dimethyl-5-dicarboxylic acid **3** (5.040 g, 24 mmol, 1 eq.) was dissolved in 60 mL of dry THF. 36 mL of a 2 M solution of $LiAlH_4$ (72 mmol, 3 eq.) in THF were slowly added (**Warning**: H_2 release) keeping the flask in a water bath to avoid temperature increase. The reaction was stirred at RT for 1h (TLC CH_2Cl_2:MeOH 9:1, R_f(**3a**) = 0.20; staining: $KMnO_4$). Since only the desired product **3a** was detected by TLC, the reaction was quenched with 20 mL of 10 $\%_{v/v}$ H_2SO_4 and the product was extracted with a large amount (150 mL) of EtOAc. The organic phase was dried over Na_2SO_4 and the solvent evaporated to obtain **3a** with high purity.

Yield: 3.7 g, quantitative.

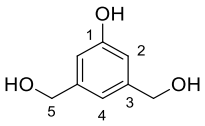

^{1}H-NMR (400MHz, CD_3OD): δ (ppm)= 6.77 (s, 1H, H_4), 6.67 (s, 2H, H_5), 4.49 (s, 4H, H_2).

[4]O. K. Rasheed *et al.*, *Synlett*, **2016**, *27*, 905-911

Synthesis of (5-(3-(pyren-1-yl)propoxy)-1,3-phenylene) dimethanol (14)

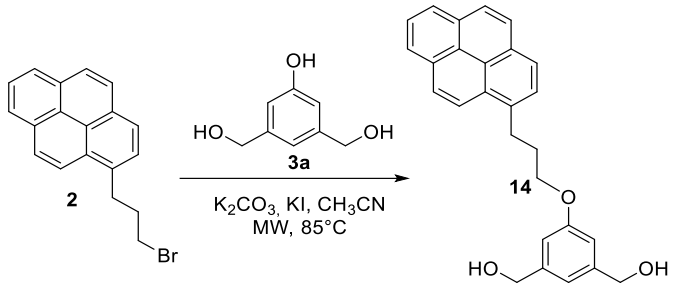

Compound **2** (100 mg, 0.31 mmol, 1 eq.), compound **3a** (57.2 mg, 0.37 mmol, 1.2 eq.), oven-dried K_2CO_3 (128 mg, 0.93 mmol, 3 eq.) and KI (56 mg, 0.34 mmol, 1.1 eq.) were dissolved in 2 mL of dry CH_3CN ([**2**] = 0.15 M). The reaction was stirred under microwave irradiation at 85°C for 17 h (TLC CH_2Cl_2:MeOH 95:5, R_f (**14**) = 0.26). Acetonitrile was evaporated and the resulting brown solid was dissolved in 15 mL of EtOAc and washed with water (3 x 5 mL) and brine (1 x 5 mL). The organic phase was dried over $MgSO_4$ and the solvent evaporated at reduced pressure. The crude was purified via automated flash chromatography (CH_2Cl_2: MeOH 95:5).

Yield: 116.3 mg, 95%.

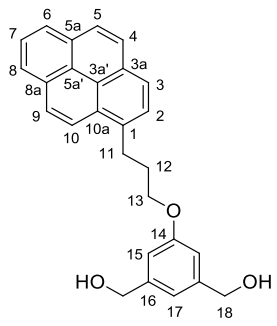

^{1}H-NMR (400MHz, $CDCl_3$): δ(ppm)= 8.32 (d, 1H, H_3, $J_{2\text{-}3}$ = 9.6 Hz), 8.17 (d, 1H, H_6, H_8, $J_{6\text{-}7} = J_{7\text{-}8}$ = 7.6 Hz), 8.13 - 8.07 (m, 2H, H_2, H_9), 8.03 (s, 2H, H_4, H_5), 7.99 (t, 1H, H_7), 7.90 (d, 1H, H_{10}), 6.95 (s, 1H, H_{17}), 6.87 (s, 2H, H_{15}), 4.67 (s, 4H, H_{18}), 4.07 (t, 2H, H_{13}, $J_{12\text{-}13}$ = 6.1 Hz), 3.56 (t, 2H, H_{11}, $J_{11\text{-}12}$ = 7.4 Hz), 2.35 (quint., 2H, H_{12});

^{13}C NMR (100 MHz, CDCl3): δ(ppm)= 159.6 (C_{14}), 139.8 (C_{16}), 135.7 (C_1), 131.6 (C_{5a}), 131.0 (C_{8a}), 130.1 (C_{3a}), 128.9 (C_{10a}), 127.6 (C_2, C_9, C_5), 126.9 (C_4), 126.0 (C_7), 125.3 ($C_{5a'}$), 125.1 ($C_{3a'}$, C_6), 125.0 (C_8, C_{10}), 123.4 (C_3), 122.0 (C_{17}), 115.4 (C_{15}), 67.3 (C_{13}), 33.1 (C_{18}), 31.2 (C_{12}), 29.8 (C_{11}).

ESI-MS: calculated for $[C_{27}H_{24}O_3Na]^+$: 419.16; found: 419.25.

Synthesis of 1-(3-(3,5-bis(bromomethyl)phenoxy)propyl) pyrene (5)[5]

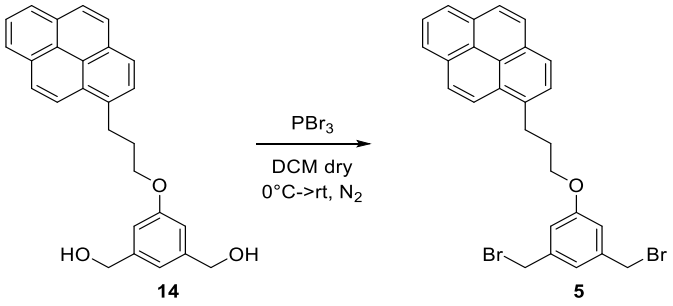

Compound **14** (25 mg, 0.07 mmol, 1 eq.) was dissolved in 280 µl of dry CH_2Cl_2 and cooled at 0 °C. **PBr_3** (15 µL, 0.16 mmol, 2.3 eq.) was added and the reaction was stirred at RT for 1 h 20 minutes (TLC Hex: EtOAc 9:1, R_f(**5**) = 0.40; staining: Molibdic reagent). Upon completion, the reaction was quenched with 100 µL of MeOH at 0°C and then the solvent was removed under reduced pressure. The crude was dissolved in 10 mL of CH_2Cl_2 and washed using a 25%$_{w/v}$ solution of $NaHCO_3$ (1 x 10 mL) at a pH of about 8. After washing with water (2 x 10 mL) and brine (1 x 5 mL), the organic phase was dried over $MgSO_4$ and concentrated under vacuum to obtain pure product **5**.

Yield: 32.4 mg, 89%.

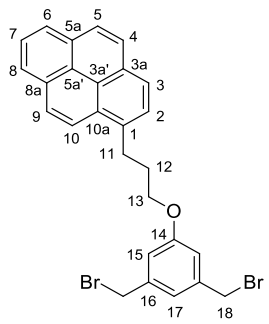

^{1}H-NMR (400MHz, $CDCl_3$): δ(ppm)= 8.32 (d, 1H, H_3, $J_{2\text{-}3}$ = 9.4 Hz), 8.17 (d, 1H, H_6, H_8, $J_{6\text{-}7} = J_{7\text{-}8}$ = 7.8 Hz), 8.13 - 8.07 (m, 2H, H_2, H_9), 8.03 (s, 2H, H_4, H_5), 7.99 (t, 1H, H_7), 7.90 (d, 1H, H_{10}), 7.00 (s, 1H, H_{17}), 6.88 (s, 2H, H_{15}), 4.42 (s, 4H, H_{18}), 4.06 (t, 2H, H_{13}, $J_{12\text{-}13}$ = 6.0 Hz), 3.56 (t, 2H, H_{11}, $J_{11\text{-}12}$ = 7.3 Hz), 2.35 (quint., 2H, H_{12});

^{13}C NMR (100 MHz, CDCl3): δ(ppm)= 159.7 (C_{14}), 142.9 (C_{16}), 135.9 (C_1), 131.6 (C_{5a}), 131.0 (C_{8a}), 130.1 (C_{3a}), 128.9 (C_{10a}), 127.6 (C_2), 127.6 (C_9), 127.5 (C_5), 126.85 (C_4), 126.0 (C_7), 125.3 ($C_{5a'}$), 125.1 ($C_{3a'}$), 125.1 (C_6), 125.0 (C_8), 124.9 (C_{10}), 123.5 (C_3), 117.6 (C_{17}), 112.6 (C_{15}), 67.1 (C_{13}), 65.3 (C_{18}), 31.3 (C_{12}), 29.9 (C_{11}).

ESI-MS: calculated for $[C_{27}H_{22}OBr_2]^+$: 522.00; found: 522.12.

[5]H. W. Rhee *et al., JACS*, **2008**, *130*, 784-785

Synthesis of N,N'-((5-(3-(pyren-1-yl)propoxy)-1,3-phenylene)bis (methyl ene))bis(1-(pyridin-2-yl)-N-(pyridine-2-ylmethyl)methanamine) (5a)[6]

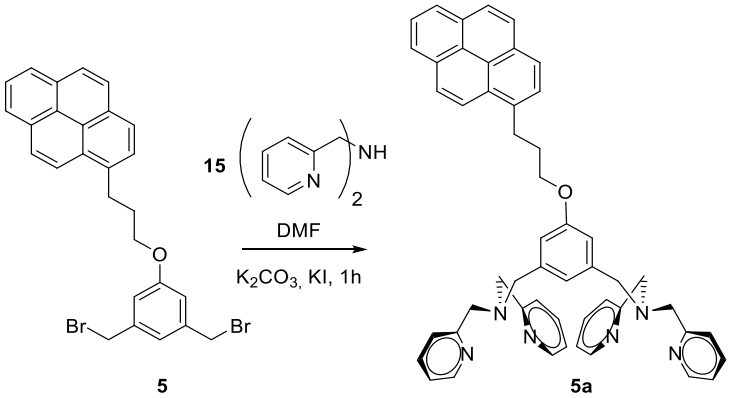

Compound **5** (27 mg, 0.051 mmol, 1 eq.) was dissolved in 350 µL of dry DMF, together with oven-dried KI (18 mg, 0.107 mmol, 2.1 eq.) and K_2CO_3 (21.1mg, 0.153 mmol, 2.2 eq.). Under Ar atmosphere, bis(2-picolyl)amine **15** (20 µL, 0.107 mmol, 2.1 eq.) was added to the stirring mixture. The reaction was stirred at RT for 1 h (TLC CH_2Cl_2:MeOH 95:5, R_f(**5a**)= 0.34; staining: Dragendorff). Upon completion, the solvent was evaporated and the resulting crude was dissolved in 15 mL of EtOAc. After washing with water (2 x 10 mL) and brine (1 x 10 mL), the organic phase was dried over Na_2SO_4 and the solvent evaporated at reduced pressure to obtain product **5a** with high purity.

Yield: 34 mg, 88%.

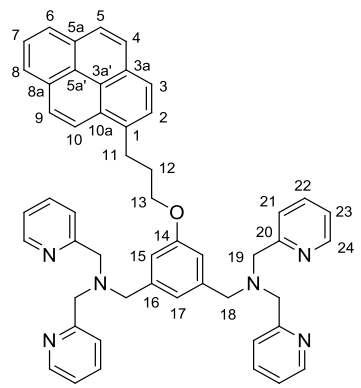

^{1}H-NMR (400MHz, $CDCl_3$): δ(ppm)= 8.48 (d, 4H, H_{24}, $J_{23\text{-}24}$ = 5.1 Hz), 8.30 (d, 1H, H_3, $J_{2\text{-}3}$ = 9.3 Hz), 8.15 (d, 1H, H_6, H_8, $J_{6\text{-}7} = J_{7\text{-}8}$ = 7.8 Hz), 8.12 - 8.04 (m, 2H, H_2, H_9), 8.03 (s, 2H, H_4, H_5), 7.99 (t, 1H, H_7), 7.90 (d, 1H, H_{10}), 7.60 - 7.49 (m, 8H, H_{21}, H_{22}), 7.12 - 7.04 (m, 5H, H_{17}, H_{23}), 6.92 (s, 2H, H_{15}), 4.06 (t, 2H, H_{13}, $J_{12\text{-}13}$ = 6.0 Hz), 3.80 (s, 8H, H_{19}), 3.65 (s, 4H, H_{18}), 3.56 (t, 2H, H_{11}, $J_{11\text{-}12}$ = 7.3 Hz), 2.35 (quint., 2H, H_{12});

^{13}C-NMR (100MHz, $CDCl_3$): δ(ppm)= 159.8 (C_{20}), 159.3 (C_{14}), 149.0 (C_{24}), 140.7 (C_{16}), 136.5 (C_{21}), 135.9 (C_1), 131.5 (C_{5a}), 130.9 (C_{8a}), 130.0 (C_{3a}), 128.9 (C_{10a}), 127.6 (C_2), 127.5 (C_9), 127.4 (C_5), 126.8 (C_4), 125.9 (C_7), 125.2 ($C_{5a'}$), 125.0 ($C_{3a'}$), 125.0 (C_6), 124.9 (C_8), 124.9 (C_{10}), 123.4 (C_3), 122.8 (C_{22}), 122.0 (C_{17}), 121.6 (C_{23}), 113.7 (C_{15}), 66.9 (C_{13}), 60.1 (C_{19}), 58.7 (C_{18}), 31.3 (C_{12}), 29.8 (C_{11}).

[6]H. W. Rhee *et al., JACS*, **2008**, *130*, 784-785

ESI-MS: calculated for $[C_{51}H_{46}N_6O]^+$: 758.37; found: 758.71.

Synthesis of PyDPA[7]

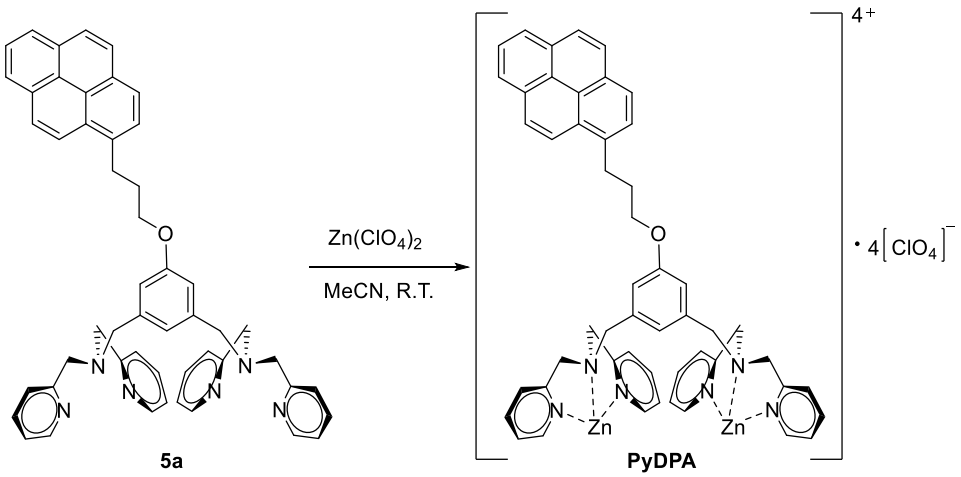

Compound **5a** (17 mg, 0.021 mmol, 1 eq.) was dissolved in 210 µL of dry CH_3CN. $Zn(ClO_4)_2 \cdot 6H_2O$ (17 mg, 0.044 mmol, 2.05 eq.) was added to the stirring mixture and the reaction stirred at RT for 1 h. The reaction progress was checked by TLC (CH_2Cl_2: MeOH 9:1, R_f (**5a**)= 0.57, R_f (**PyDPA**) = 0.07, Staining: Molibdic reagent) and RP-TLC (MeCN:H_2O 1:1, R_f (Zn perchlorate) 0.84, R_f (**PyDPA**)= 0.15, Staining: ninhydrin). Upon completion, the solvent was evaporated at reduced pressure to obtain pure **PyDPA**. **Yield**: 34 mg, quantitative**.**

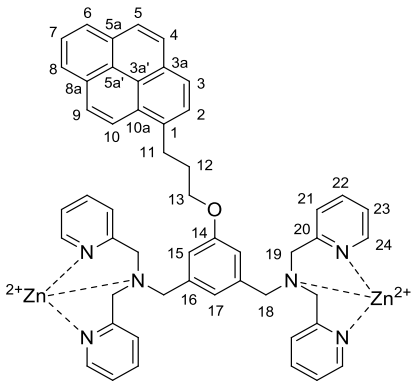

^{1}H-NMR (400MHz, CD_3CN): δ(ppm)= 8.74 (d, 4H, H_{24}, $J_{23\text{-}24}$ = 5.3 Hz), 8.37 (d, 1H, H_3, $J_{2\text{-}3}$ = 9.2 Hz), 8.21 - 8.09 (m, 3H, H_6, H_8, H_9), 8.07 - 7.90 (m, 9H, H_2, H_4, H_5, H_7, H_{10}, H_{23}), 7.67 (t, 4H, H_{21}, $J_{21\text{-}22}$ = 6.3 Hz), 7.33 (t, 4H, H_{21}, $J_{21\text{-}22}$ = 7.8 Hz), 6.73 (m, 2H, H_{17}), 6.71 (s, 2H, H_{15}), 4.16 (d, 4H, H_{19}, J_{gem} = 16.0 Hz), 4.02 (t, 2H, H_{13}, $J_{12\text{-}13}$ = 5.5 Hz), 3.82 (s, 4H, H_{18}), 3.64 (d, 4H, H_{19}), 3.61 (t, 2H, H_{11}, $J_{11\text{-}12}$ = 7.3 Hz), 2.36 (quint., 2H, H_{12});

^{13}C-NMR (100MHz, CD_3CN): δ(ppm)= 160.4 (C_{14}), 155.4 (C_{20}), 149.1 (C_{24}), 143.0 (C_{22}), 137.3 (C_{16}), 134.3 (C_1), 132.3 (C_{5a}), 131.8 (C_{8a}), 130.9 (C_{3a}), 129.8 (C_{10a}), 128.9 (C_2), 128.5 (C_9), 128.2 (C_5), 127.7 (C_4), 127.4 (C_{15}), 127.2 (C_7), 126.4 (C_{23}), 126.1 (C_{10}), 126.0 (C_{21}), 126.0 (C_6), 125.8 (C_8), 125.7 ($C_{5a'}$), 125.5 ($C_{3a'}$), 124.6 (C_3), 119.0 (C_{17}), 67.9 (C_{13}), 56.9 (C_{18}), 55.8 (C_{19}), 31.9 (C_{12}), 29.6 (C_{11}).

ESI-MS: calculated for $[C_{51}H_{46}N_6O_{13}Zn_2Cl_3]^+$: 1187.07; found: 1187.28.

[7]H. W. Rhee *et al., JACS*, **2008**, *130*, 784-785

Synthesis of Polyacrylamide (PAM)

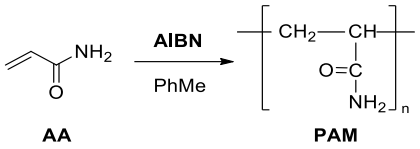

Acrylamide (**AA**) (2 g, 28.1 mmol, 1 eq.) was dissolved in degassed toluene (80 mL, [**AA**] = 0.35 M), then **AIBN** (18 mg, 0.107 mmol, 2.1 eq.) was added. The reaction was left at 80 °C in a condenser-equipped system. After 24 h, the reaction was cooled down at RT. The polymer was precipitated by pouring the reaction mixture in 500 mL MeOH. The resulting mixture was stirred for 15 minutes and filtered on a Büchner funnel. The white solid was washed several times with MeOH and left under high vacuum for 48 h.

Yield: 1.8 g, 90%.

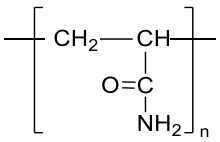

^{1}H-NMR (400 MHz, D_2O): δ (ppm)= 2.45 - 2.02 (brd, 1H, CH), 1.82 – 1.32 (brd, 2H, CH_2).

Synthesis of 1,3-phenylene diacrylate (18)

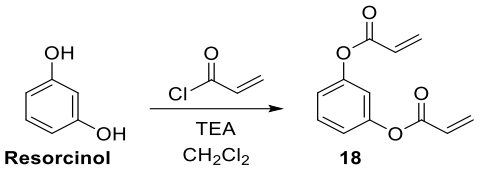

Resorcinol (500 mg, 4.5 mmol, 1 eq.) was dissolved in 15 mL of dry CH_2Cl_2 ([**Resorcinol**] = 0.3 M). The solution was cooled at 0°C and **TEA** (1.4 mL, 10 mmol, 2.2 eq.) was added dropwise. **Acryloyl chloride** (940 µL, 11.6 mmol, 2.4 eq.) was slowly added to the resulting solution. The reaction was stirred for 1.5 h (TLC Hex: EtOAc 8:2, R_f(**Monoester**) = 0.18; R_f(**18**) = 0.4, staining: $KMnO_4$) and, even though some monoester was still present, the solvent was removed and automated flash chromatography (Eluent: Hex with a gradient of EtOAc from 10% to 40%) was performed.

Yield: 350 mg, 36%.

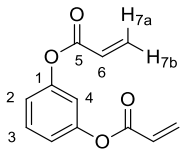

^{1}H-NMR (400 MHz, $CDCl_3$): δ (ppm)= 7.43 (t, 1H, H_3, $J_{3\text{-}2}$ 8.2 Hz), 7.11 – 7.01 (m, 3H, H_2, H_4), 6.65 (dd, 2H, H_{7a}, $J_{7a\text{-}6}$ = 16 Hz, $J_{7a\text{-}7b}$ = 2 Hz), 6.33 (dd, 2H, H_6, $J_{6\text{-}7b}$ = 10 Hz), 6.15 (dd, 2H, H_{7b}).

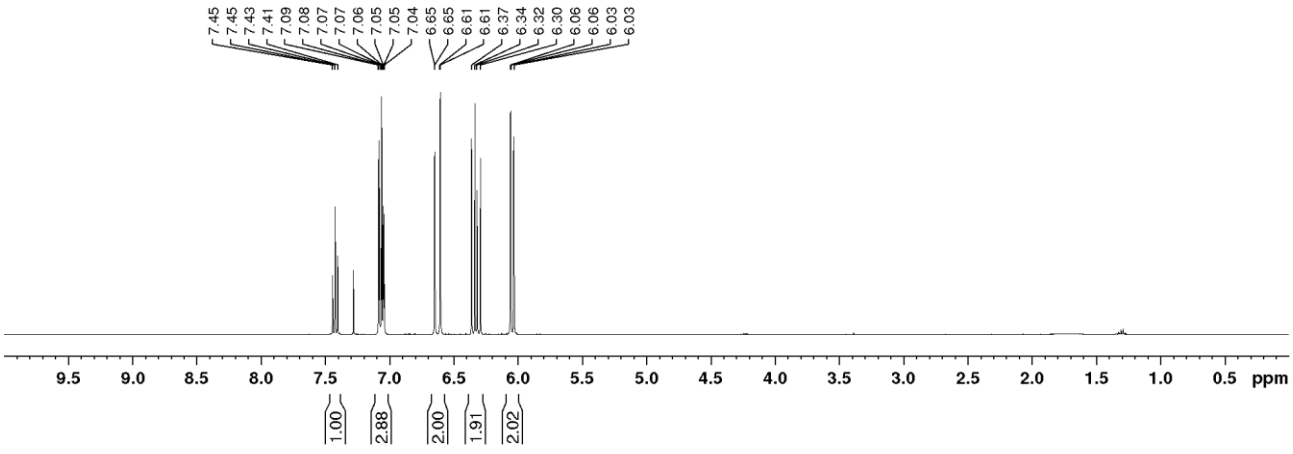

^{13}C-NMR (100MHz, $CDCl_3$): δ (ppm)= 164.1 (C_5), 151.0 (C_1), 132.9 (C_7), 129.8 (C_3), 127.7 (C_6), 119.0 (C_2), 115.4 (C_4).

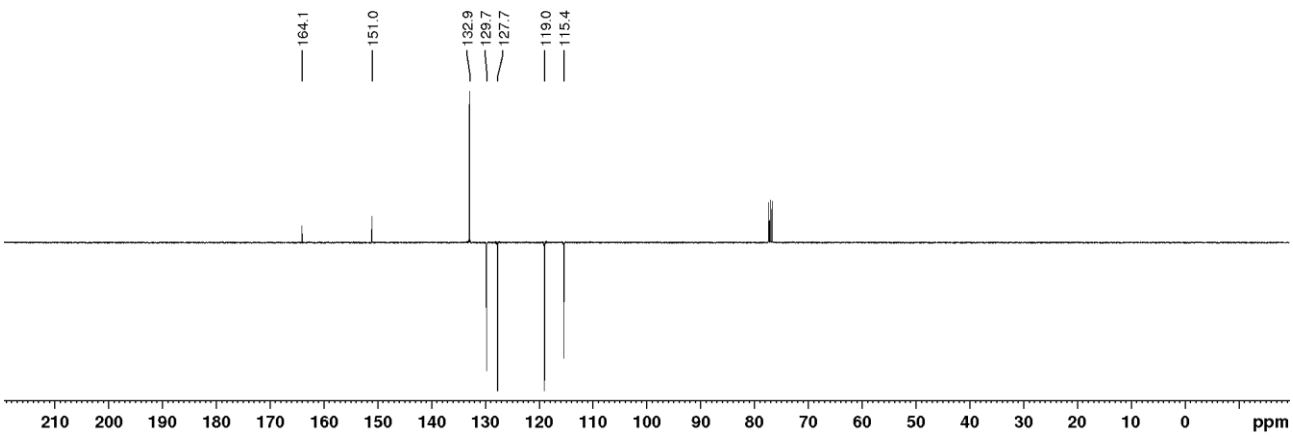

ESI-MS: calculated for $[C_{12}H_{11}O_4]^+$: 219.06; found: 219.17.

Synthesis of dimethyl 5-(allyloxy)isophthalate (24)

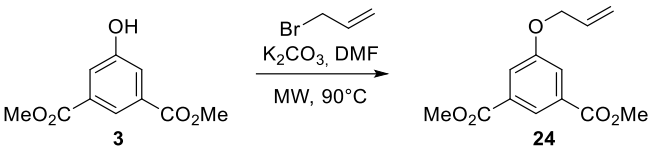

Dimethyl 5-hydroxyisophthalate **3** (1.5 g, 7.1 mmol, 1 eq.) was dissolved in dry DMF (14.3 mL, [**3**] = 0.5 M) together with K_2CO_3 (1.58 g, 11.6 mmol, 1.6 eq.) and Allyl-Br (1.02 mL, 11.6 mmol, 1.6 eq.). The reaction was stirred under microwave irradiation at 90°C for 1.5 h (TLC Hex:EtOAc 8:2, R_f(**24**)= 0.44; Staining: Molibdic reagent). Upon completion, most DMF was removed at reduced pressure. The resulting crude was then dissolved in CH_2Cl_2 (100 mL) and washed with water (2 x 75 mL). The organic phase was dried over Na_2SO_4 and evaporated at reduced pressure to obtain pure product **24**.

Yield: 1.73 g, 97 %.

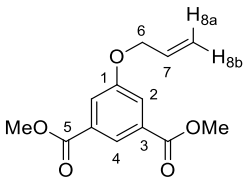

^{1}H-NMR (400MHz, $CDCl_3$): δ (ppm)= 8.30 (t, 1H, H_4, $J_{2\text{-}4}$ = 1.4 Hz), 7.78 (d, 2H, H_2), 6.16 - 6.01 (m, 1H, H_7), 5.50 (dq, 1H, H_{8a}, $J_{8a\text{-}8b}$ = $J_{8a\text{-}6}$ = 1.5 Hz, $J_{8a\text{-}7}$ = 16 Hz), 5.40 (dt, 1H, H_{8b}, $J_{8b\text{-}7}$ = 8 Hz), 4.65 (dt, 2H, H_6, $J_{6\text{-}7}$ = 16 Hz), 3.96 (s, 6H, CO_2Me).

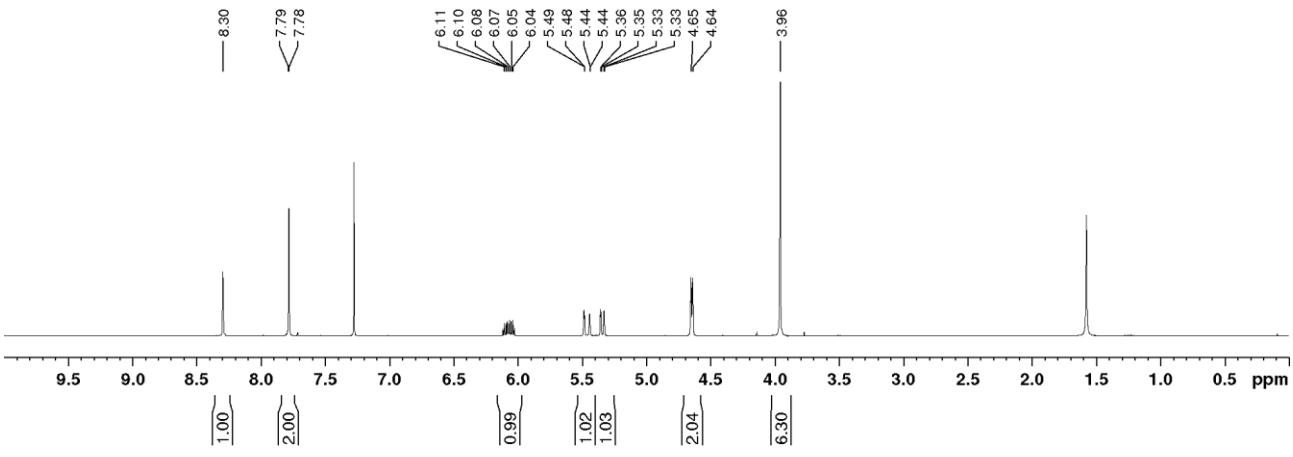

^{13}C-NMR (100MHz, $CDCl_3$): δ (ppm)= 166.1 (C_5),158.6 (C_1), 132.4 (C_7), 131.8 (C_3), 123.1 (C_4), 120.1 (C_2), 118.2 (C_8), 69.2 (C_6), 52.4 (O<u>Me</u>).

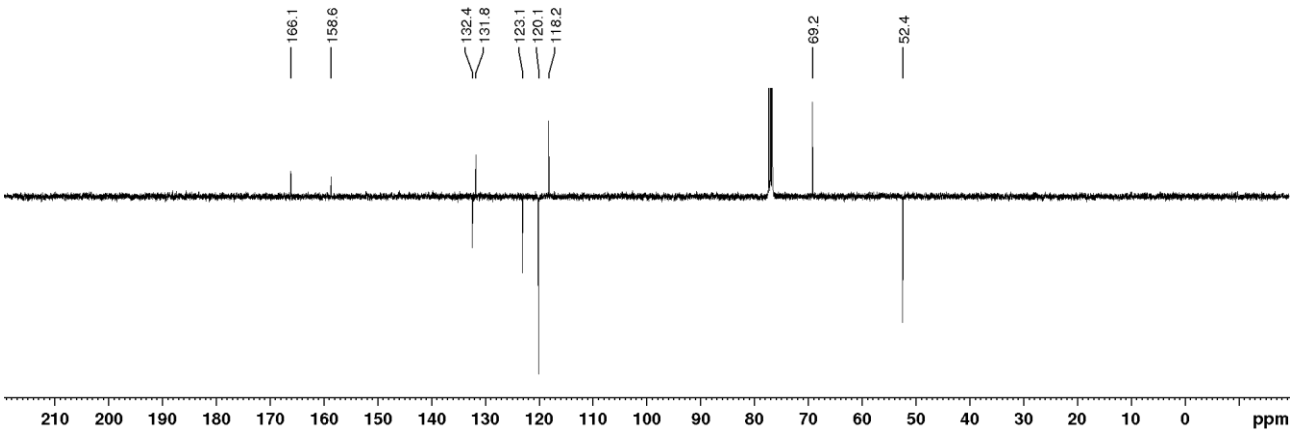

ESI-MS: calculated for $[C_{13}H_{14}O_5Na]^+$: 273.06; found: 273.25.

Synthesis of (5-(allyloxy)-1,3-phenylene)dimethanol (21)

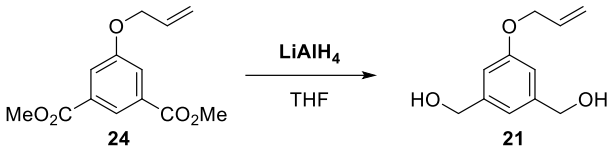

Compound **24** (500 g, 2 mmol, 1 eq.) was dissolved in 8 mL of dry THF ([**24**] = 0.25 M). $LiAlH_4$ (228 mg, 6 mmol, 3 eq.) was carefully added keeping the flask in a water bath to avoid temperature increase. The reaction was stirred at RT for 2 h (TLC CH_2Cl_2:MeOH 9:1, R_f(**21**) = 0.14; staining: $KMnO_4$). Upon completion, the reaction was quenched with 3 mL of 10 $\%_{v/v}$ H_2SO_4 and the pure product was extracted with a large amount (2 x 40 mL) of EtOAc.

Yield: 378 mg, 97%.

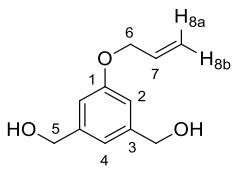

^{1}H-NMR (400MHz, CD_3OH): δ (ppm)= 6.81 (s, 1H, H_4), 6.74 (s, 2H, H_2), 6.02 - 5.90 (m, 1H, H_7), 5.30 (dq, 1H, H_{8a}, $J_{8a\text{-}8b} = J_{8a\text{-}6} = 1.5$ Hz, $J_{8a\text{-}7} = 16$ Hz), 5.15 (dt, 1H, H_{8b}, $J_{8b\text{-}7} = 8$ Hz), 4.48 - 4.42 (m, 6H, H_5, H_6).

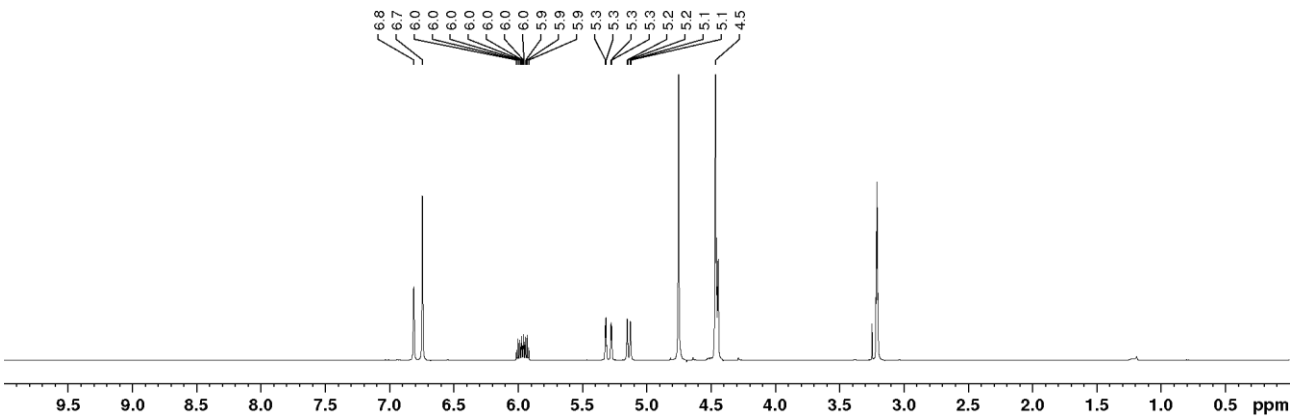

^{13}C-NMR (100MHz, CD_3OH): δ(ppm)= 159.0 (C_1),143.0 (C_3), 133.6 (C_7), 117.3 (C_4), 115.9 (C_8), 111.6 (C_2), 68.3 (C_6), 63.7 (C_5).

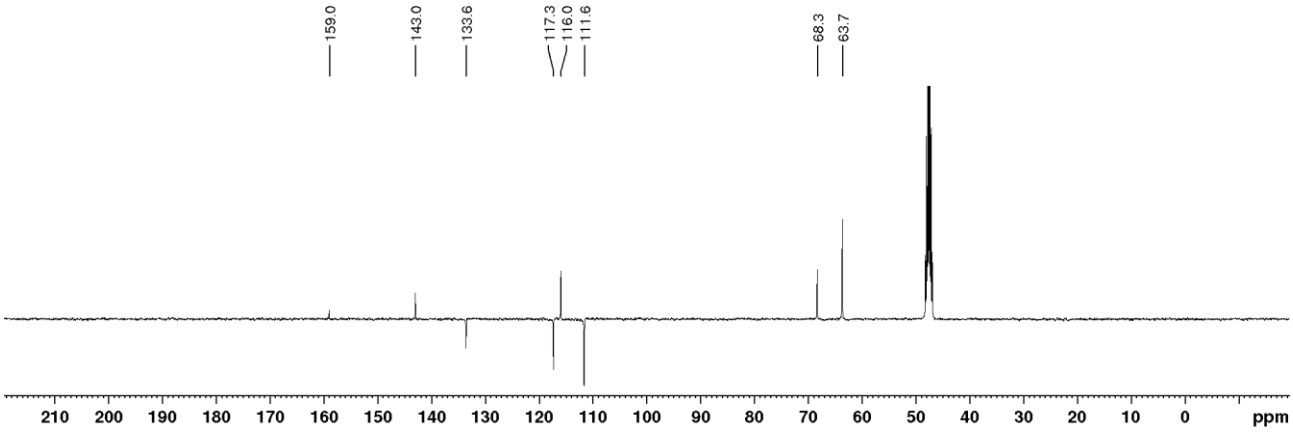

ESI-MS: calculated for $[C_{11}H_{15}O_3]^+$: 195.09; found: 195.01.

Synthesis of (5-(allyloxy)-1,3-phenylene)dimethanol (21)

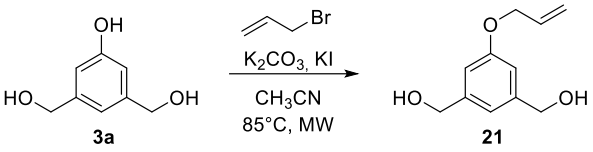

Compound **3a** (100 mg, 0.64 mmol, 1 eq.), K_2CO_3 (265 mg, 1.92 mmol, 3 eq.) and KI (120 mg, 0.72 mmol, 1.1 eq.) were dissolved in 4.2 mL of dry CH_3CN ([**3a**] = 0.15 M). Allyl bromide (64 µL, 0.72 mmol, 1.1 eq.) was carefully added. The reaction was stirred under microwave irradiation at 85°C for 1 h (TLC CH_2Cl_2:MeOH 9:1, R_f(**21**) = 0.43; staining: Molibdic reagent). CH_3CN was removed and the crude was purified by automated chromatography (Eluent: CH_2Cl_2 with a gradient of MeOH from 0% to 10%).

Yield: 99 mg, 80%.

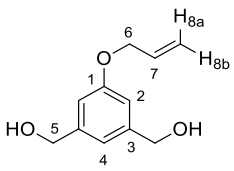

^{1}H-NMR (400MHz, CD_3OH): δ (ppm)= 6.81 (s, 1H, H_4), 6.74 (s, 2H, H_2), 6.02 - 5.90 (m, 1H, H_7), 5.30 (dq, 1H, H_{8a}, $J_{8a\text{-}8b} = J_{8a\text{-}6} = 1.5$ Hz, $J_{8a\text{-}7} = 16$ Hz), 5.15 (dt, 1H, H_{8b}, $J_{8b\text{-}7} = 8$ Hz), 4.48 - 4.42 (m, 6H, H_5, H_6).

^{13}C-NMR (100MHz, CD_3OH): δ(ppm)= 159.0 (C_1),143.0 (C_3), 133.6 (C_7), 117.3 (C_4), 115.9 (C_8), 111.6 (C_2), 68.3 (C_6), 63.7 (C_5).

Synthesis of 1-(allyloxy)-3,5-bis(bromomethyl)benzene (21a)

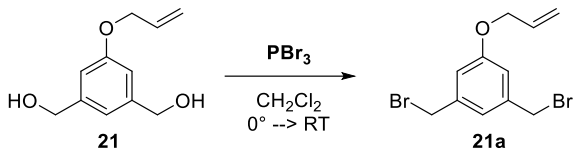

Compound **21** (100 mg, 0.51 mmol, 1 eq.) was dissolved in 790 µL of dry CH_2Cl_2. Separately, a solution made of PBr_3 (110 µL, 1.18 mmol, 2.3 eq.) in 1.21 mL of dry CH_2Cl_2 was prepared and slowly added to the first one at 0 °C. The reaction was stirred at RT for 1 h 20 minutes (TLC Hex:EtOAc 9:1, R_f(**21a**) = 0.6; staining: $KMnO_4$ and CH_2Cl_2:MeOH 9:1, R_f(**21**) = 0.4; staining: Molibdic reagent). Upon completion, the reaction was quenched by adding 800 µL of MeOH dropwise. After solvent evaporation, the crude was dissolved in 5 mL of CH_2Cl_2 and washed with a 25%$_{w/v}$ solution of $NaHCO_3$ (1 x 5 mL) at a pH of about 8. After washing with water (2 x 5 mL) and brine (1 x 5 mL), the organic phase was dried over $MgSO_4$ and concentrated under vacuum to obtain **21a** with high purity.

Yield: 138 mg, 85%.

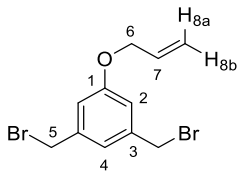

^{1}H-NMR (400MHz, $CDCl_3$): δ (ppm)= 7.02 (s, 1H, H_4), 6.90 (s, 2H, H_2), 6.12 - 6.00 (m, 1H, H_7), 5.44 (dq, 1H, H_{8a}, J_{8a-8b} = J_{8a-6} = 1.5 Hz, J_{8a-7} = 16 Hz), 5.32 (dt, 1H, H_{8b}, J_{8b-7} = 8 Hz), 4.57 (dt, 2H, H_6, J_{6-7} = 5.3 Hz), 4.45 (s, 4H, H_5).

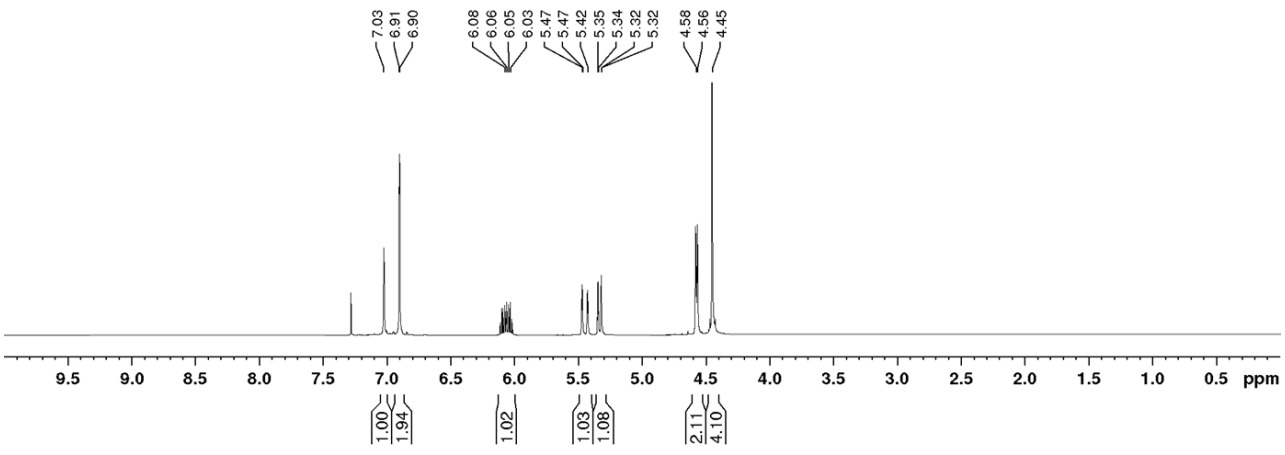

^{13}C-NMR (100MHz, $CDCl_3$): δ(ppm)= 159.0 (C_1),139.6 (C_3), 132.6 (C_7), 122.0 (C_4), 118.0 (C_8), 115.5 (C_2), 69.0 (C_6), 32.8 (C_5).

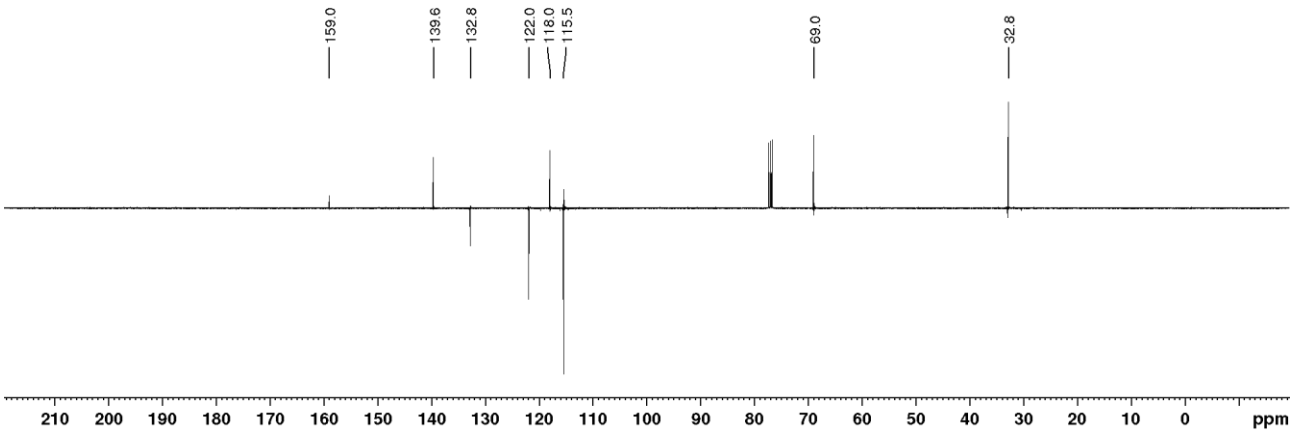

ESI-MS: calculated for $[C_{11}H_{12}Br_2ONa]^+$: 342.92; found: 343.08.

Synthesis of N,N'-((5-(allyloxy)-1,3-phenylene)bis(methyl ene))bis(1-(pyridin-2-yl)-N-(pyridin-2-ylmethyl) methanamine) (19)

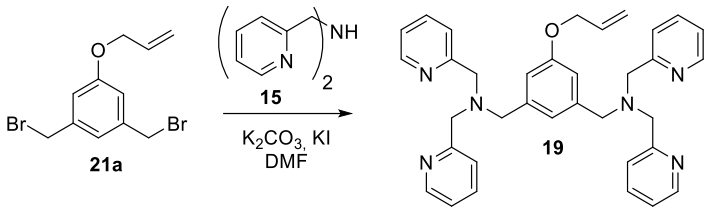

Compound **21a** (1.500 g, 4.7 mmol, 1 eq.), oven-dried KI (1.630 g, 9.8 mmol, 2.1 eq.) and K_2CO_3 (1.420 mg, 10.3 mmol, 2.2 eq.) were dissolved in 31 mL of dry DMF ([**21a**] = 0.15 M). Bis(2-picolyl)amine **15** (850 µL, 9.8 mmol, 2.1 eq.) was added to the stirring mixture. The reaction was stirred at RT for 1h 30 minutes (TLC Hex:EtOAc 8:2, R_f(**21a**) = 0.88; staining: $KMnO_4$/Molibdic reagent and CH_2Cl_2:MeOH 9:1, R_f(**19**) = 0.1; staining: Dragendorff). Most DMF was removed at reduced pressure. The resulting crude was dissolved in 50 mL EtOAc and washed with water (2 x 50 mL). The organic phase was dried over Na_2SO_4 and the solvent evaporated. The crude was purified by automated flash chromatography (Eluent: Hex with a gradient of EtOAc from 12% to 60%).

Yield: 2.6 g, quantitative.

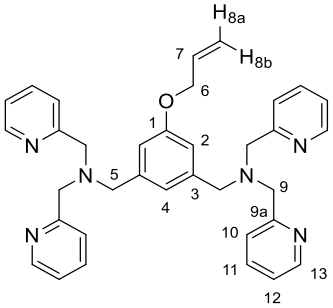

^{1}H-NMR (400MHz, CD_2Cl_2): δ (ppm)= 8.53 - 8.49 (m, 4H, H_{13}), 7.69 - 7.58 (m, 8H, H_{12}, H_{11}), 7.19 - 7.09 (m, 5H, H_{10}, H_4), 6.93 (s, 2H, H_2), 6.16 - 6.03 (m, 1H, H_7), 5.44 (dq, 1H, H_{8a}, $J_{8a\text{-}8b}$ = $J_{8a\text{-}6}$ = 1.5 Hz, $J_{8a\text{-}7}$ = 16 Hz), 5.30 (dt, 1H, H_{8b}, $J_{8b\text{-}7}$ = 8 Hz), 4.57 (dt, 2H, H_6, $J_{6\text{-}7}$ = 5.3 Hz), 3.90 (s, 8H, H_9), 3.66 (s, 4H, H_5).

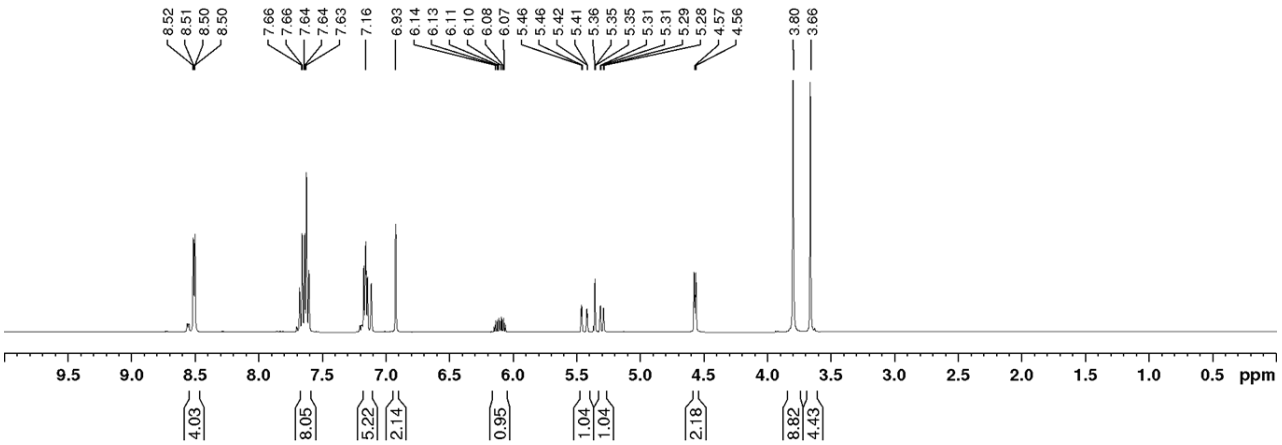

^{13}C-NMR (100MHz, CD_2Cl_2): δ(ppm)= 159.9 (C_1), 158.8 (C_{9a}), 148.9 (C_{13}), 140.8 (C_3), 136.2 (C_{11}), 133.7 (C_7), 122.6 (C_{12}), 121.8 (C_{10}), 121.6 (C_4), 117.1 (C_8), 113.6 (C_2), 68.7 (C_6), 60.0 (C_9), 58.4 (C_5).

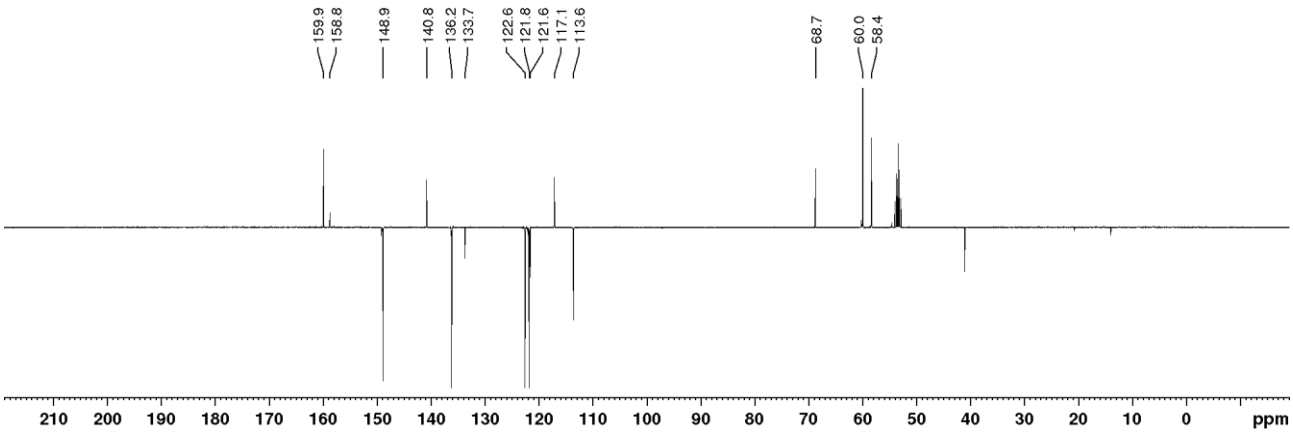

ESI-MS: calculated for $[C_{35}H_{37}N_6O]^+$: 557.30; found: 557.45.

Synthesis 3,5-bis(bromomethyl)phenol (22)

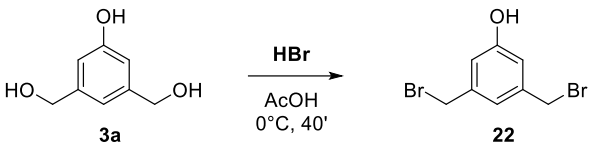

Compound **3a** (3.7 g, 24 mmol, 1 eq.) was dissolved in 48 mL of an acetic acid solution of **HBr** (33%$_{w/w}$) (2 mL per mmol **3a**). The reaction was stirred at 0 °C for 40 minutes (TLC Hex:EtOAc 8:2, R_f(**22**) = 0.26; staining: Molibdic reagent). Excess HBr was removed at reduced pressure and the mixture was diluted with a 50%$_{w/v}$ $NaHCO_3$ solution till pH 5 was reached. The product was then extracted with CH_2Cl_2 (2 x 100 mL). The organic phase was washed with water (2 x 70 mL) and brine (1 x 50 mL) and then dried over Na_2SO_4. After solvent evaporation, automated flash chromatography was performed (Eluent: Hex with a gradient of EtOAc from 0% to 40%).

Yield: 6.6 g, quantitative.

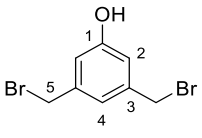

H-NMR (400MHz, $CDCl_3$): δ (ppm) = 7.01 (s, 1H, H_4), 6.83 (d, 2H, H_2, $J_{2\text{-}4}$ = 1.2 Hz), 5.07 (brd, 1H, O<u>H</u>), 4.43 (s, 4H, H_5).

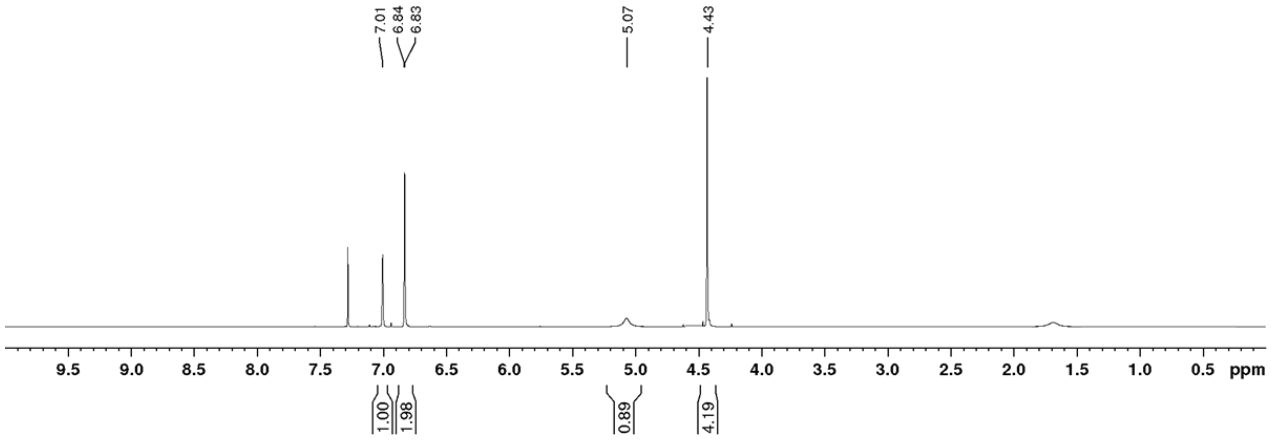

^{13}C-NMR (100MHz, $CDCl_3$): δ (ppm) = 122.0 (C_4), 116.1 (C_2), 32.5 (C_5).

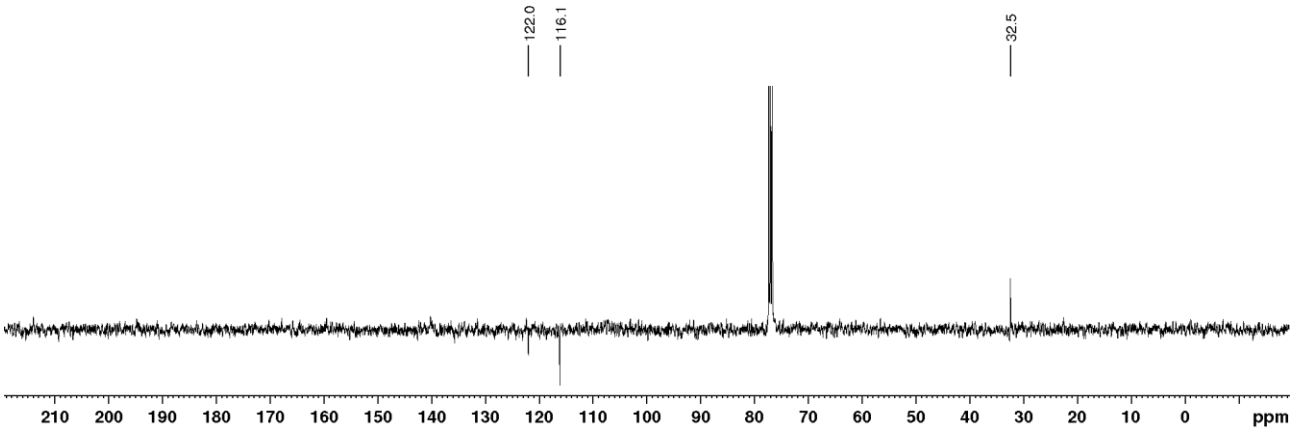

ESI-MS: calculated for $[C_8H_7Br_2O]^-$: 278.89; found: 278.61.

Synthesis (3,5-bis(bromomethyl)phenoxy)(tert-butyl)dimethylsilane (26)

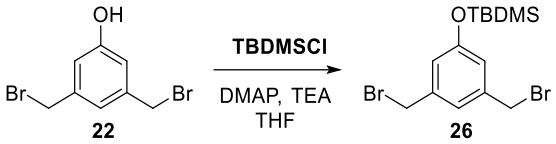

Compound **22** (280 mg, 1 mmol, 1 eq.) was dissolved in dry THF (5 mL, [**22**] = 0.2 M) at 0°C in an ice bath. Dry TEA (210 µL, 1.5 mmol, 1.5 eq.) and DMAP (13 mg, 0.1 mmol, 0.1 eq.) were then added. Lastly, TBDMSCl (166 mg, 1.2 mmol, 1.2 eq.) was added to the mixture. The reaction was stirred at RT for 1 h (TLC Hex:EtOAc 8:2, R_f(**26**)= 0.82; Staining: Molibdic reagent). Upon completion, the reaction mixture was diluted with CH_2Cl_2 (30 mL) and washed with a 50%$_{w/v}$ $NaHCO_3$ solution (1 x 20 mL) and with brine (1 x 20 mL). The organic phase was dried over Na_2SO_4 and the solvent evaporated to obtain pure product **26**.

Yield: 377 mg; 96%.

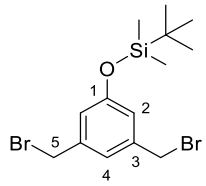

^{1}H-NMR (400MHz, $CDCl_3$): δ (ppm)= 7.03 (s, 1H, H_4), 6.82 (s, 2H, H_2, $J_{2\text{-}4}$ = 1.2 Hz), 4.43 (s, 4H, H_5), 1.01 (s, 9H, SiC<u>Me</u>$_3$), 0.24 (s, 6H, Si<u>Me</u>$_2$).

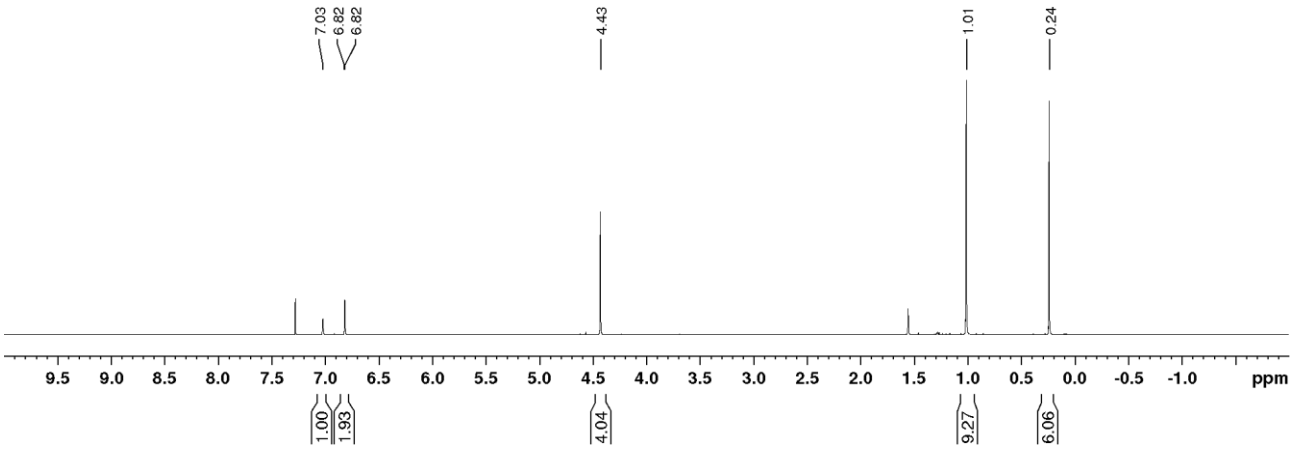

^{13}C-NMR (100MHz, $CDCl_3$): δ(ppm)= 156.1 (C_1), 139.6 (C_3), 122.4 (C_4), 120.8 (C_2), 32.8 (C_5), 25.6 (SiC($\underline{C}H_3)_3$), 4.4 (Si$\underline{C}H_3$).

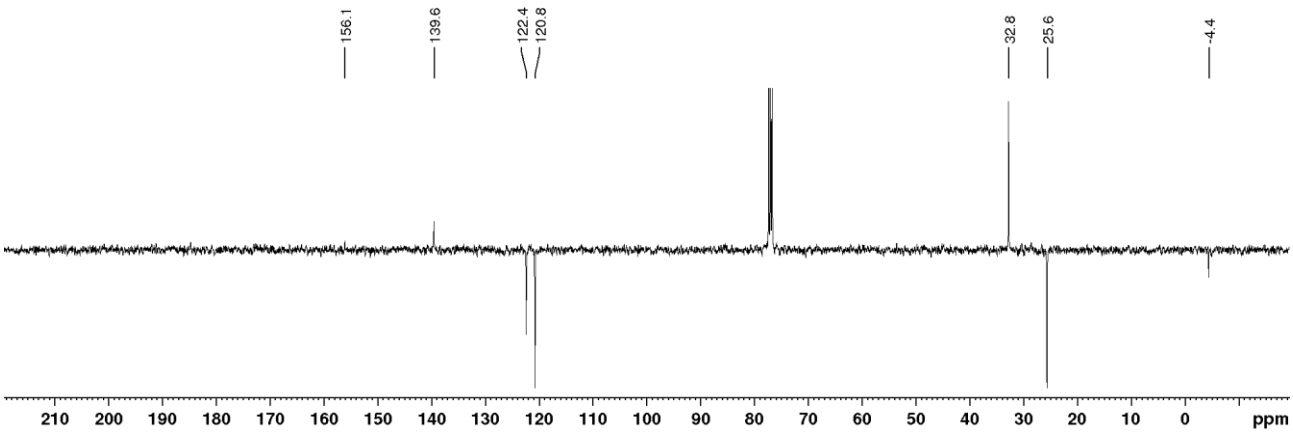

ESI-MS: calculated for $[C_{16}H_{25}Br_2O_5Si]^+$: 395.11; found: 395.27.

Synthesis of N,N'-((5-((tert-butyldimethylsilyl)oxy)-1,3-phenylene)bis (methylene)) bis(1-(pyridin-2-yl)-N-(pyridin-2-ylmethyl)methanamine) (23)

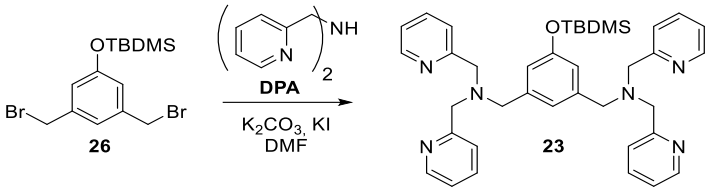

Compound **26** (1 g, 2.5 mmol, 1 eq.) was dissolved in 16 mL of dry DMF. Oven-dried KI (870 mg, 5.25 mmol, 2.1 eq.) and K_2CO_3 (720 mg, 5.25 mmol, 2.1 eq.) were added. Under Ar atmosphere, Bis(2-picolyl)amine (**DPA**, 930 µL, 5.2 mmol, 2.05 eq.) was added to the stirring mixture. The reaction was stirred at RT for 1 h (TLC Hex:EtOAc 8:2, R_f (**26**) = 0.78; staining: $KMnO_4$ and CH_2Cl_2: MeOH 95:5, R_f (**23**) = 0.4; staining: Dragendorff). Upon completion, DMF was evaporated. The resulting crude was dissolved in 30 mL of CH_2Cl_2 and washed with water (2 x 20 mL) and brine (1 x 20 mL). The organic phase was dried over Na_2SO_4 and the solvent evaporated to obtain pure product **23**.

Yield: 1.6 g, quantitative.

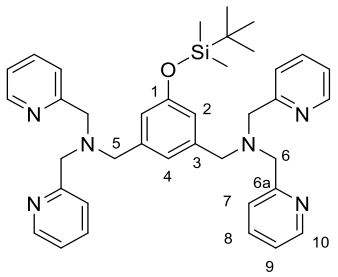

^{1}H-NMR (400MHz, $CDCl_3$): δ (ppm) = 8.53 - 8.49 (m, 4H, H_{10}), 7.66 - 7.55 (m, 8H, H_9, H_8), 7.16 - 7.11 (m, 4H, H_7), 7.07 (s, 1H, H_2), 6.82 (d, 2H, H_1, $J_{4\text{-}2}$ = 1.0 Hz), 3.83 (s, 8H, C_6), 3.65 (s, 4H, C_5), 0.98 (s, 9H, $C(C\underline{H}_3)_3$), 0.18 (s, 6H, $Si(C\underline{H}_3)_2$).

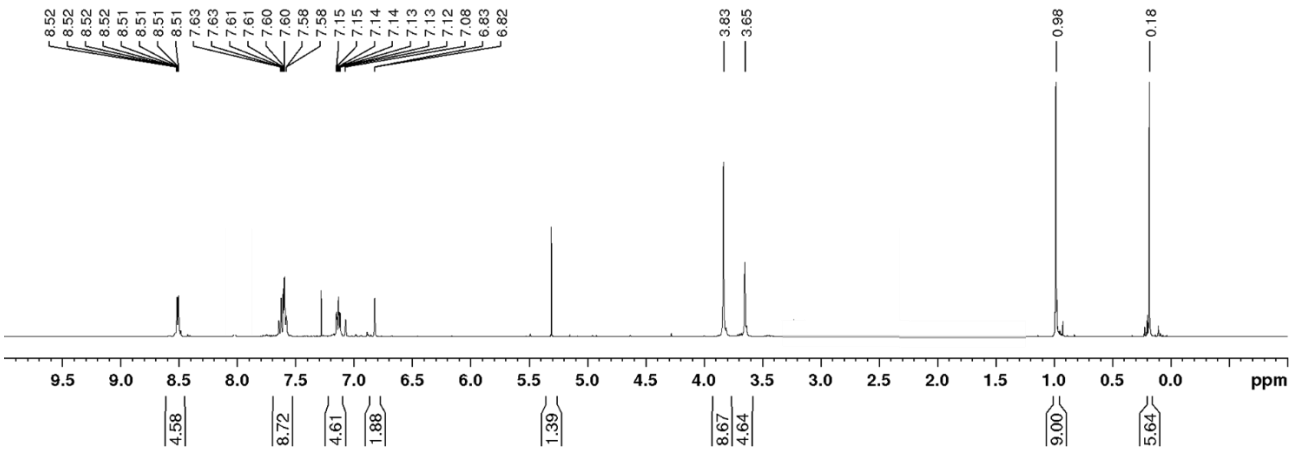

^{13}C-NMR (100MHz, $CDCl_3$): δ (ppm) = 159.4 (C_{5a}), 156.8 (C_1), 148.7 (C_5), 140.6 (C_3), 136.4 (C_6), 122.8 (C_7), 121.9 (C_8), 120.4 (C_4), 114.5 (C_2), 59.8 (C_6), 58.3 (C_5), 25.6 ($SiC(\underline{C}H_3)_3$), 4.4 ($Si\underline{C}H_3$).

Synthesis of 3,5-bis((bis(pyridin-2-ylmethyl)amino)methyl)phenol (27)

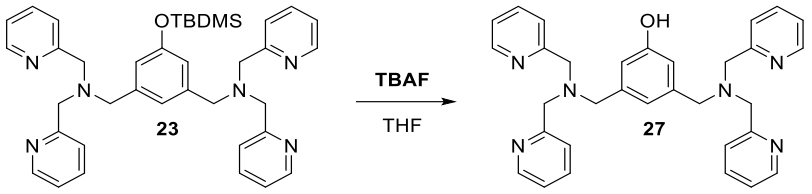

Compound **23** (1.29 g, 2 mmol, 1 eq.) was dissolved in dry THF (8 mL) under N_2 atmosphere, then a 1 M solution of **TBAF** in THF (2 mL, 2 mmol, 1 eq.) was slowly added. The reaction was stirred at RT for 30 minutes (TLC CH_2Cl_2: MeOH 85:15, R_f (**27**) = 0.48; Staining: Dragendorff). Upon completion, the solvent was removed at reduced pressure. The resulting crude was dissolved in 10 mL EtOAc and washed with acid water (pH 5, 2 x 10 mL).The organic phase was dried over Na_2SO_4 and the solvent removed at reduced pressure to obtain product **27** with satisfying purity.

Yield: 930 mg, 90%.

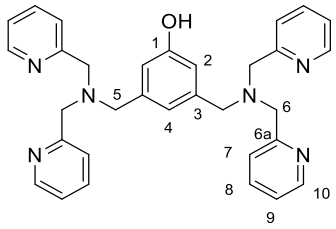

^{1}H-NMR (400MHz, CD_2Cl_2): δ (ppm) = 8.54 – 8.50 (m, 4H, H_{10}), 7.68 – 7.60 (m, 8H, H_9, H_8), 7.19 – 7.14 (m, 4H, H_7), 6.98 (s, 1H, H_4), 6.91 (s, 2H, H_2), 3.89 (s, 8H, NC<u>H</u>$_2$Py), 3.66 (s, 4H, ArC<u>H</u>$_2$N).

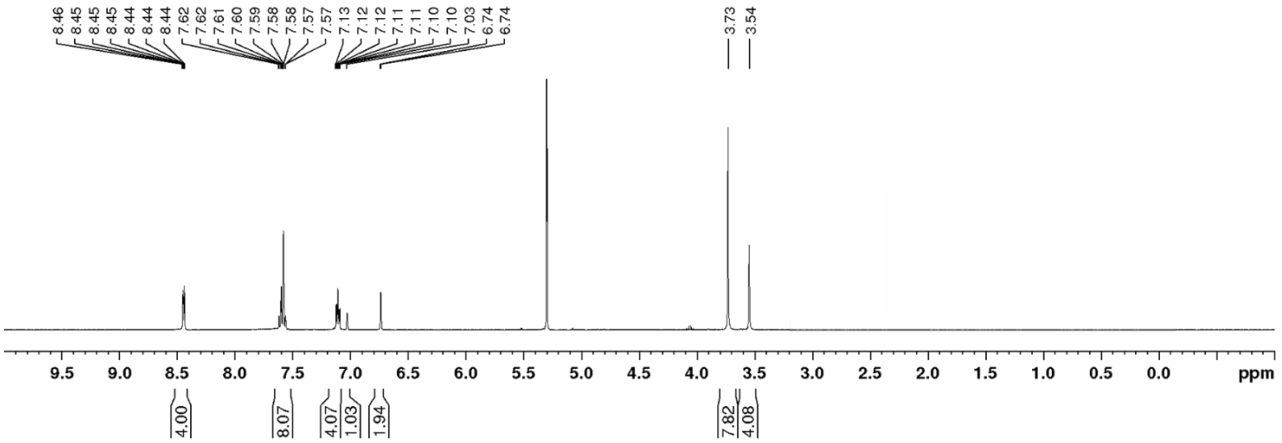

^{13}C-NMR (100MHz, CD_2Cl_2): δ (ppm) = 159.4 (C_{5a}), 156.8 (C_1), 148.7 (C_5), 140.6 (C_3), 136.4 (C_6), 122.8 (C_7), 121.9 (C_8), 120.4 (C_4), 114.5 (C_2), 59.8 (C_6), 58.3 (C_5).

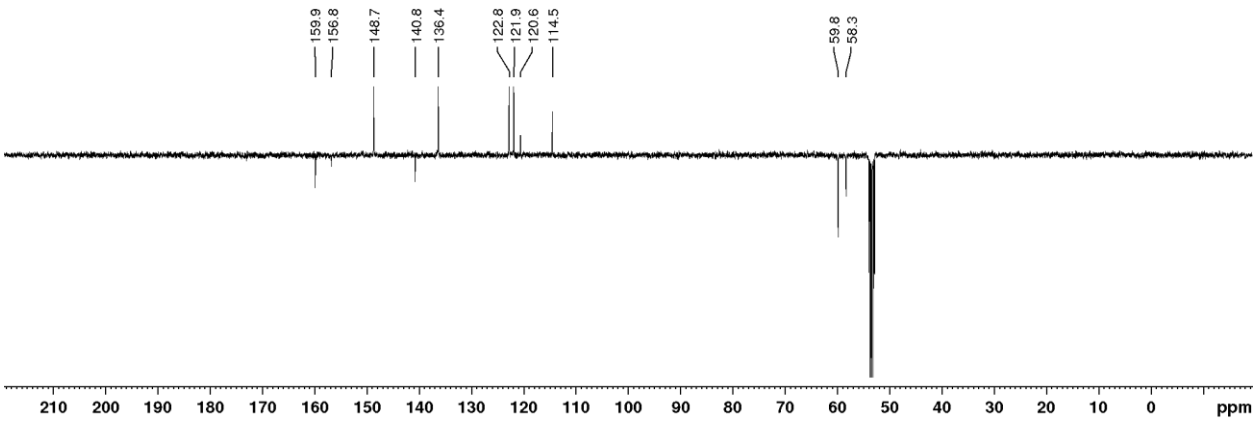

EI-MS: calculated for $[C_{32}H_{32}N_6O]^+$: 517.26; found: 516.98.

Synthesis of tert-butyl (2-(2-hydroxyethoxy)ethyl) carbamate (30a)[79]

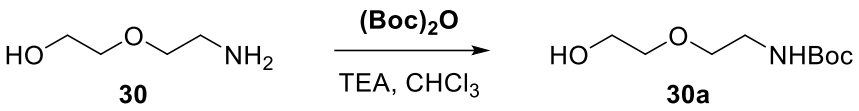

2-(2-aminoethoxy)ethanol (**30**) (4.8 mL, 47.8 mmol, 1 eq.) was dissolved in $CHCl_3$ (220 mL, [**30**]= 0.2) M). Separately, **Boc_2O** (10.45 g, 47.8 mmol, 1 eq.) was dissolved in 20 mL of $CHCl_3$. The latter solution was slowly added to the first one and the reaction stirred at RT for 3 h (TLC CH_2Cl_2: MeOH 9:1, R_f (**30a**) = 0.47; Staining: Ninhydrin). Upon completion, the solvent was removed at reduced pressure. The resulting crude was purified by automated chromatography (Eluent: CH_2Cl_2 with a gradient of MeOH from 0% to 20%).

Yield: 9 g, 92%.

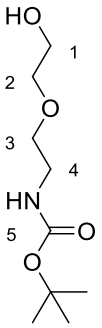

^{1}H-NMR (400MHz, $CDCl_3$): δ (ppm) = 3.71 (t, 2H, H_1, J_{1-2} = 4.80 Hz), 3.57-3.50 (m, 4H, H_2, H_3), 3.29 (t, 2H, H_4), 1.42 (s, 9H, $C(C\underline{H}_3)_3$).

^{13}C-NMR (100MHz, $CDCl_3$): δ (ppm) = 156.2 (C_5), 79.4 ($O\underline{C}(CH_3)_3$), 72.2 (C_2), 70.2 (C_3), 61.5 (C_1), 40.4 (C_4), 28.4 ($OC(\underline{C}H_3)_3$).

ESI-MS: calculated for $[C_9H_{19}NO_4Na]^+$: 228.13; found: 228.17.

Synthesis of 2-(2-((tert-butoxycarbonyl)amino)ethoxy)ethyl 4-methylbenzenesulfonate (29)

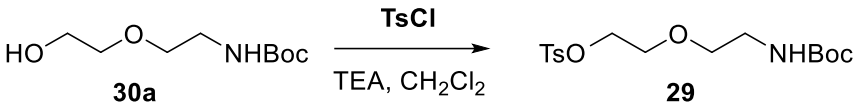

Compound **30a** (9 g, 43.8 mmol, 1 eq.) was dissolved in dry CH_2Cl_2 (110 mL, [5]=0.4 M) under N_2 atmosphere. The mixture is cooled at 0°C, then **TEA** (15 mL, 109.6 mmol, 2.5 eq.) was added dropwise. Lastly, **TsCl** (10 g, 52.6 mmol, 1.2 eq.) was added to the stirring mixture. The reaction was stirred at room temperature for 3 h (TLC Hex: EtOAc 6:4, R_f (**29**) = 0.35; Staining: Ninhydrin). Upon completion, the resulting crude was washed with water (1x100 mL). The organic phase was dried over Na_2SO_4 and the solvent removed at reduced pressure. The crude was purified by automated flash chromatography (Eluent: Hex with a gradient of EtOAc from 10% to 80%).

Yield: 13.7 mg, 90%

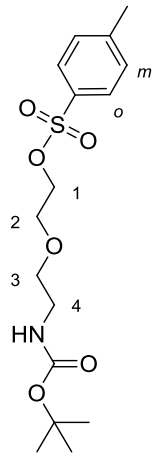

^{1}H-NMR (400MHz, $CDCl_3$): δ (ppm) = 7.83 (d, 2H, H_o, $J_{o\text{-}m}$ = 8.14 Hz), 7.38 (d, 2H, H_m), 4.81 (brd, 1H, N<u>H</u>), 4.19 (t, 2H, H_1, $J_{1\text{-}2}$ = 4.7 Hz), 3.66 (t, 2H, H_3, $J_{3\text{-}4}$ = 5.1 Hz), 3.47 (t, 2H, H_2), 3.25 (q, 2H, H_4), 2.48 (s, 3H, ArC<u>H</u>$_3$), 1.47 (s, 9H, C(C<u>H</u>$_3$)$_3$).

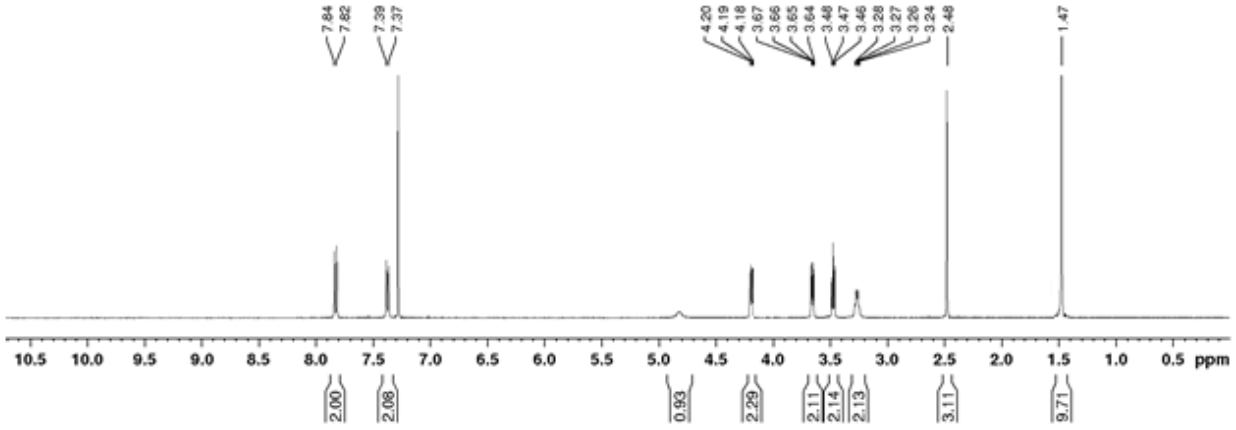

^{13}C-NMR (100MHz, $CDCl_3$): δ (ppm) = 144.9 (O_3S-C), 129.8 (C_m), 128.0 (C_o), 70.4 (C_3), 69.0 (C_2), 68.4 (C_1), 40.2 (C_4), 28.4 ($OC(CH_3)_3$), 21.6 ($ArCH_3$).

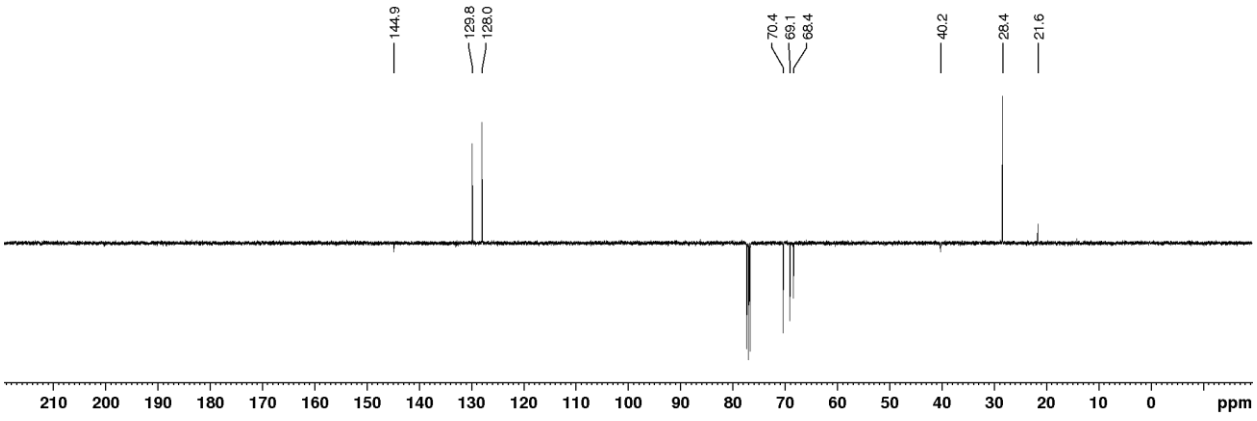

ESI-MS: calculated for $[C_{16}H_{25}NO_6SNa]^+$: 382.14; found: 382.01.

Synthesis of tert-butyl (2-(2-(3,5-bis((bis(pyridin-2-ylmethyl) amino)methyl) phenoxy)ethoxy)ethyl)carbamate (31)

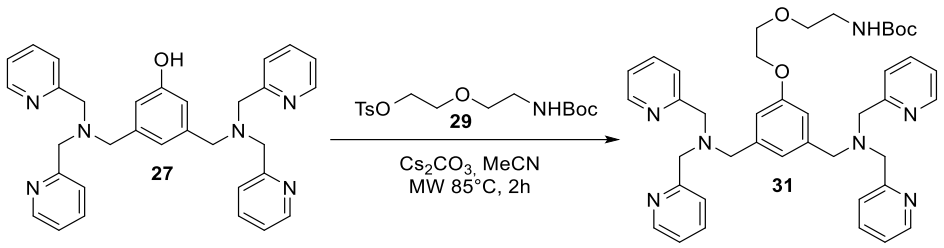

Compound **27** (910 mg, 1.76 mmol, 1 eq.), compound **29** (633 mg, 1.76 mmol, 1 eq.) and **Cs_2CO_3** (631 mg, 1.94 mmol, 1.1 eq.) were dissolved in 12 mL of dry CH_3CN, ([**27**] **=** 0.15 M). The reaction was stirred under microwave irradiation at 85°C for 2 h (TLC CH_2Cl_2: MeOH 9:1, R_f (**27**) = 0.44, R_f (**29**) = 0.94, R_f (**31**) = 0.5; staining: Ninhydrin). Upon completion, the solvent was evaporated and the resulting crude was dissolved in 10 mL EtOAc. The organic phase was washed with acid water (pH 5, 2 x 15 mL) and saturated $NaHCO_3$ solution (1 x 10 mL). The organic phase was dried over Na_2SO_4 and the solvent evaporated to obtain pure product **31**.

Yield: 1.21 mg, quantitative

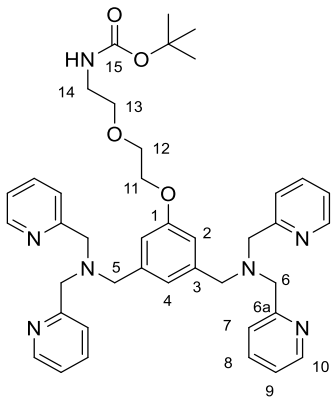

^{1}H-NMR (400MHz, CD_2Cl_2): δ (ppm) = 8.53 - 8.50 (m, 4H, H_{10}), 7.69 - 7.59 (m, 8H, H_9, H_8), 7.20 - 7.13 (m, 5H, H_7, H_4), 6.92 (s, 2H, H_2), 5.04 (brd, 1H, N<u>H</u>), 4.14 (t, 2H, H_{11}, $J_{11\text{-}12}$= 5.1 Hz), 3.85 - 3.76 (m, 10H, C_6, H_{12}), 3.66 (s, 4H, C_5), 3.61 (t, 2H, H_{13}, $J_{13\text{-}14}$ = 5.7 Hz), 3.34 (q, 2H, H_{14}), 1.43 (s, 9H, C(C<u>H</u>$_3$)$_3$).

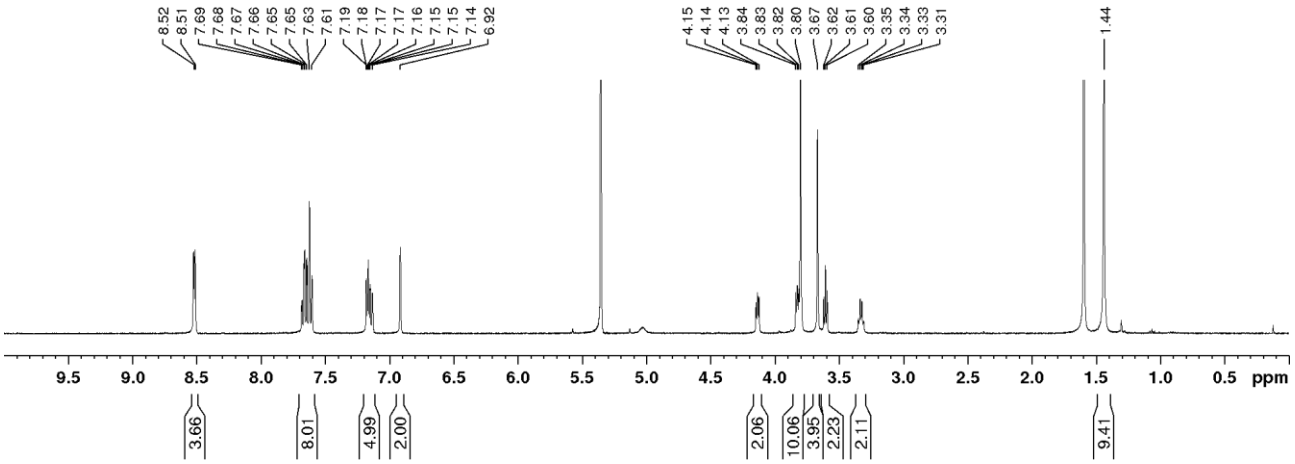

^{13}C-NMR (100MHz, CD_2Cl_2): δ (ppm) = 159.9 (C_6), 158.9 (C_1), 148.9 (C_{10}), 140.8 (C_3), 136.2 (C_9), 122.7 (C_8), 121.8 (C_2, C_7), 113.5 (C_4), 70.4 (C_{13}), 69.5 (C_{12}), 67.3 (C_{11}), 59.9 (C_6), 58.4 (C_5), 40.4 (C_{14}), 28.1 ($C(\underline{C}H_3)_3$).

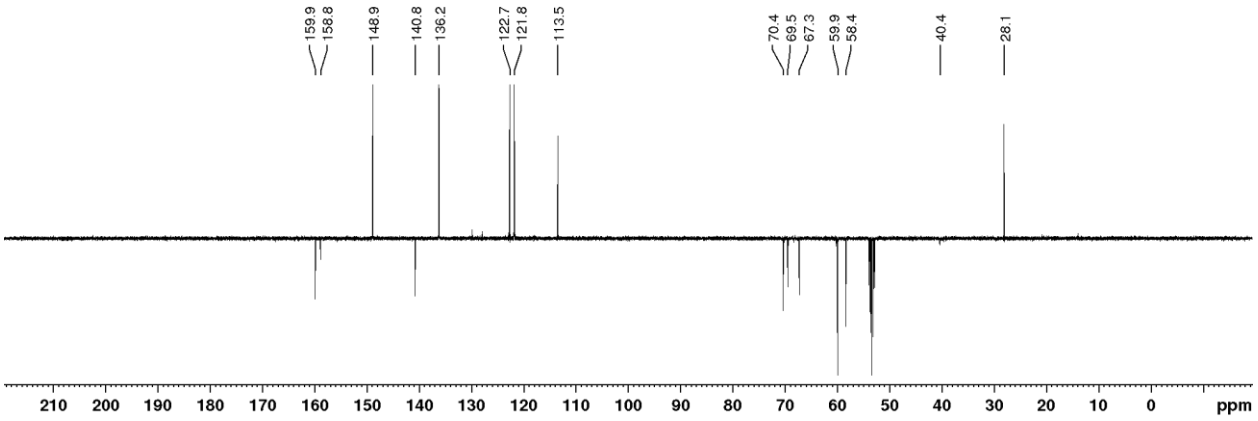

ESI-MS: calculated for $[C_{41}H_{49}N_7O_4Na]^+$: 726.38; found: 726.56.

Synthesis of N,N'-((5-(2-(2-aminoethoxy)ethoxy)-1,3-phenylene)bis (methylene)) bis(1-(pyridin-2-yl)-N-(pyridin-2-ylmethyl)methanamine) (28)

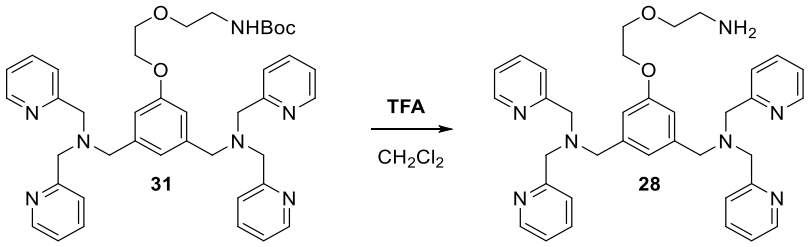

Compound **31** (328 mg, 0.46 mmol, 1 eq.) was dissolved in 10 mL of a 9:1 mixture of CH_2Cl_2: TFA and the reaction stirred at RT for 30 minutes (TLC CH_2Cl_2: MeOH 8:2, R_f (**28**) = 0.10; staining: Dragendorff or Ninhydrin). Upon completion, TFA was stripped with toluene (3 x 5 mL). The product was dissolved in 30 mL CH_2Cl_2 and washed with a saturated $NaHCO_3$ solution (2 x 20 mL). The organic phase was dried over Na_2SO_4 and the solvent evaporated to obtain pure product **28**.

Yield: 280 mg, quantitative.

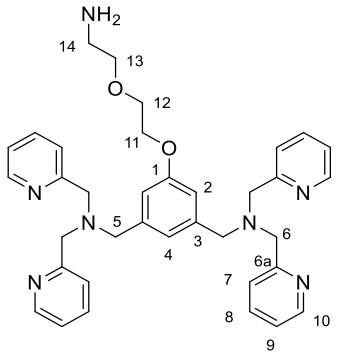

^{1}H-NMR (400MHz, CD_2Cl_2): δ (ppm)= 8.53 - 8.49 (m, 4H, H_{10}), 7.71 - 7.58 (m, 8H, H_9, H_8), 7.21 - 7.13 (m, 4H, H_7), 7.10 (s, 1H, H_4), 6.96 (s, 2H, H_2), 4.14 (t, 2H, H_{11}, $J_{11\text{-}1}$= 5.1 Hz), 3.85 - 3.77 (m, 10H, H_6, H_{12}), 3.65 (s, 4H, H_5), 3.57 (t, 2H, H_{13}, $J_{13\text{-}14}$ = 5.7 Hz), 2.88 (q, 2H, H_{14}).

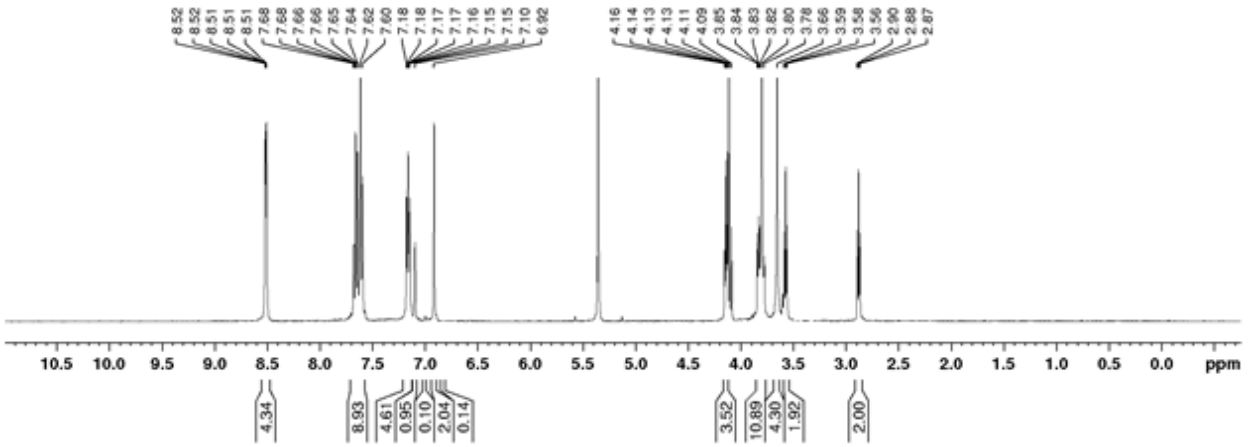

^{13}C-NMR (100MHz, CD_2Cl_2): δ (ppm) = 159.9 (C_6), 158.9 (C_1), 148.9 (C_{10}), 140.8 (C_3), 136.2 (C_9), 122.7 (C_8), 121.8 (C_2, C_7), 113.5 (C_4), 73.4 (C_{13}), 69.6 (C_{12}), 67.5 (C_{11}), 60.0 (C_6), 58.4 (C_5), 41.7 (C_{14}).

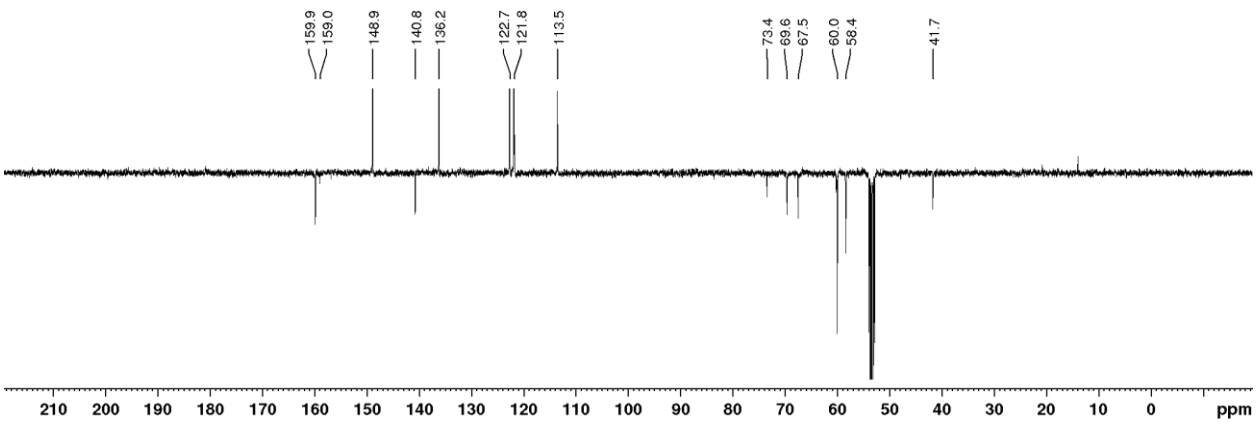

ESI-MS: calculated for $[C_{41}H_{49}N_7O_4Na]^+$: 626.33; found: 626.49.

Synthesis of 2,2-diallylmalonic acid (37)

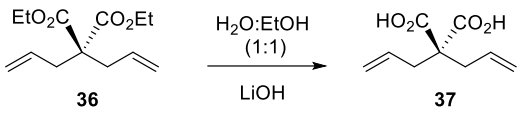

Diallyl ethyl malonate **36** (500 mg, 2.08 mmol, 1 eq.) was dissolved in a 2:1 EtOH:H_2O mixture (3 mL, [**36**]= 0.75 M), then KOH (290 mg, 5.2 mmol, 2.5 eq.) was added. The reaction was stirred under microwave irradiation at 85° for 1 h. The reaction was check by proton NMR of the reaction mixture (DMSO-d^6). Upon completion, EtOH was removed at reduced pressure. The remaining solution was acidified with a 1 M HCl solution till pH 1 was reached. Subsequently, extraction with Et_2O (3 x 10 mL) was performed. The organic phase was dried over Na_2SO_4 and the solvent evaporated to obtain product **37** as a white powder.

Yield: 1.9 g, quantitative.

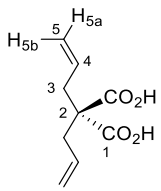

^{1}H-NMR (400MHz, DMSO-d^6): δ (ppm)= 12.83 (s, 2H, $CO_2\underline{H}$), 5.72 - 5.57 (m, 2H, H_3), 5.17 - 5.04 (m, 4H, H_{5a}, H_{5b}), 2.47 (d, 4H, H_3).

^{13}C-NMR (100MHz, DMSO-d^6): δ(ppm)= 172.4 (C_1), 133.5 (C_5), 119.3 (C_4), 56.8 (C_2), 36.5 (C_3).

ESI-MS: calculated for $[C_8H_{11}O_2]^-$: 183.07; found: 183.17.

Synthesis of 2-allylpent-4-enoic acid (38)

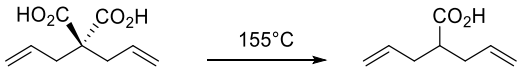

37 **38**

Compound **37** (500 mg, 2.7 mmol, 1 eq.) was heated up to 155°C for 45 minutes to obtain product **38** as a brownish liquid. Reaction progress was checked by ^{1}H-NMR (Me_2CO-d6).

Yield: 380 mg, quantitative.

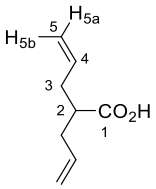

^{1}H-NMR (400MHz, $CDCl_3$): δ (ppm)= 10.81 (brd, 2H, $CO_2\underline{H}$), 5.72 - 5.57 (m, 2H, H_3), 5.17 - 5.04 (m, 4H, H_{5a}, H_{5b}), 2.47 (d, 4H, H_3).

^{13}C-NMR (100MHz, $CDCl_3$): δ(ppm)= 181.4 (C_1), 134.8 (C_5), 117.3 (C_4), 44.8 (C_2), 35.4 (C_3).

ESI-MS: calculated for $[C_8H_{11}O_2]^-$: 139.08; found: 139.19.

Synthesis of 5-bromo-2-(3-bromopropyl)pentanoic acid (39)

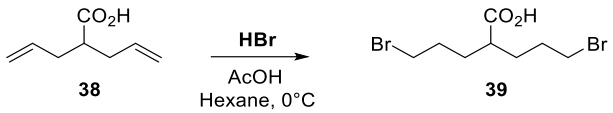

38 39

Compound **38** (605 mg, 4.3 mmol, 1 eq.) was dissolved in dry Hex (20 mL, [**38**] = 0.22 M) and cooled at 0° C, then and a saturated solution of **HBr** (33%$_{w/w}$) in acetic acid (3.2 mL, 17.2 mmol, 4 eq.) was slowly added. The solution was stirred at RT for 1 h. The hexane layer was decanted and washed with water (2 x 10 mL). The organic phase was dried over Na_2SO_4 and the solvent removed at pressure to obtain pure product **39** as a colorless liquid.

Yield: 1.12 mg, 86 %.

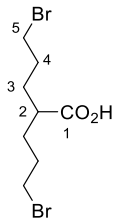

^{1}H-NMR (400MHz, $CDCl_3$): δ (ppm)= 3.44 (t, 4H, H_5, J_{5-4} = 6.6 Hz), 2.51 - 2.41 (m, 1H, H_2), 2.03 - 1.73 (m, 8H, H_4, H_3).

^{13}C-NMR (100MHz, $CDCl_3$): δ(ppm)= 181.2 (C_1), 43.7 (C_2), 33.0 (C_5), 30.5 (C_4), 30.2 (C_3).

ESI-MS: calculated for $[C_8H_{15}Br_2O_2]^+$: 302.93; found: 302.61.

Synthesis of 5-bromo-2-(3-bromopropyl)pentan-1-ol (40)

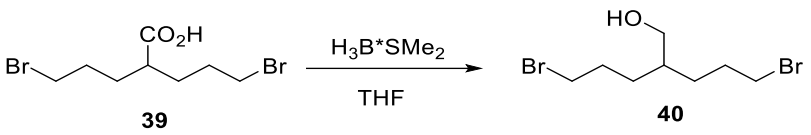

39 **40**

Compound **39** (500 mg, 1.65 mmol, 1 eq.) was dissolved in dry THF (3.1 mL, [**39**] = 0.4 M) and cooled at 0 °C, then a 1 M solution of $H_3B{\cdot}SMe_2$ (1 mL, 2 mmol, 1.2 eq.) was slowly added. The solution was stirred at rt. After 3h, the reaction was quenched with 5 mL MeOH. The solvent was then removed at reduced pressure to obtain pure product **40**.

Yield: 475 mg, quantitative.

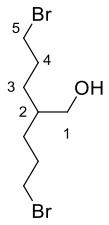

^{1}H-NMR (400MHz, $CDCl_3$): δ (ppm)= 3.60 (d, 2H, H_1, $J_{1\text{-}2}$ = 5.1 Hz), 3.43 (t, 4H, H_5, $J_{5\text{-}4}$ = 1 Hz), 2.00 - 1.41 (m, 9H, H_5, H_4, H_3, H_2).

^{13}C-NMR (100MHz, $CDCl_3$): δ(ppm)= 65.1 (C_1), 33.9 (C_2), 33.0 (C_5), 30.5 (C_4), 30.2 (C_3).

ESI-MS: calculated for $[C_8H_{17}Br_2ONa]^+$: 310.95; found: 311.15.

Synthesis of 2-((tert-butoxycarbonyl)amino)pentanedioic acid (49)

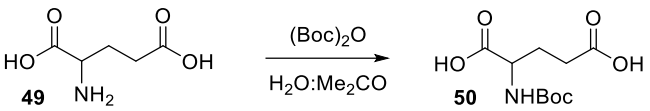

L-glutamic acid (**49**) (500 mg, 3.4 mmol, 1 eq.) was dissolved in 17 mL of water. **$(Boc)_2O$** (650 mg, 4.1 mmol, 1.2 eq.) was dissolved in 17 mL of acetone. The latter solution was slowly added to the first one and the reaction stirred at rt overnight. The following morning, acetone was evaporated and the remaining aqueous solution was acidified with HCl 1 M until product (**50**) precipitates out of the solution (pH 2). The product was then extracted with Et_2O (2 x 30 mL). The organic phase was dried over Na_2SO_4 and the evaporated at reduced pressure to obtain pure product **50**.

Yield: 770 mg, 92%.

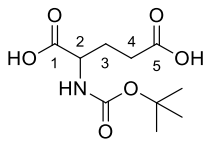

^{1}H-NMR (400MHz, DMSO-d^6): δ (ppm)= 12.30 (s, , 2H, COO<u>H</u>), 7.08 (d, 1H, 1H, N<u>H</u>Boc), 3.95 - 3.86 (m, 1H, H_2), 2.36 - 2.22 (m, 2H, H_4), 1.95 - 1.85 (m, 1H, H_{3a}), 1.80 - 1.65 (m, 1H, H_{3b}), 1.33 (s, 9H, OC(C<u>H</u>$_3$)$_3$).

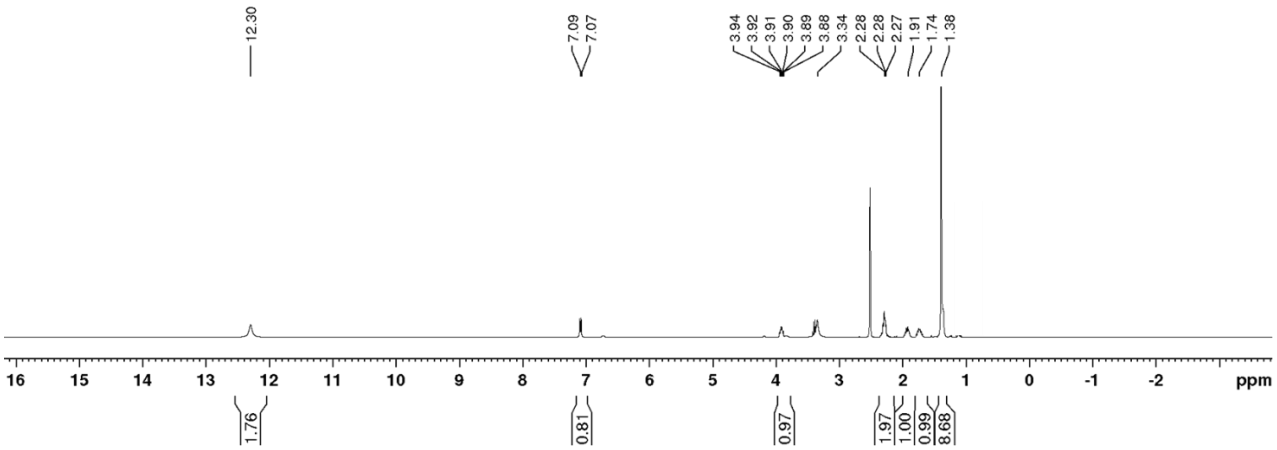

^{13}C-NMR (100MHz, DMSO-d^{6}): δ (ppm) = 174.3 (C_5), 174.2 (C_1), 156.0 (N-C=O), 78.5 (OCMe$_3$), 53.1 (C_2), 30.6 (C_4), 28.7 (OC(CH$_3$)$_3$), 26.5 (C_3).

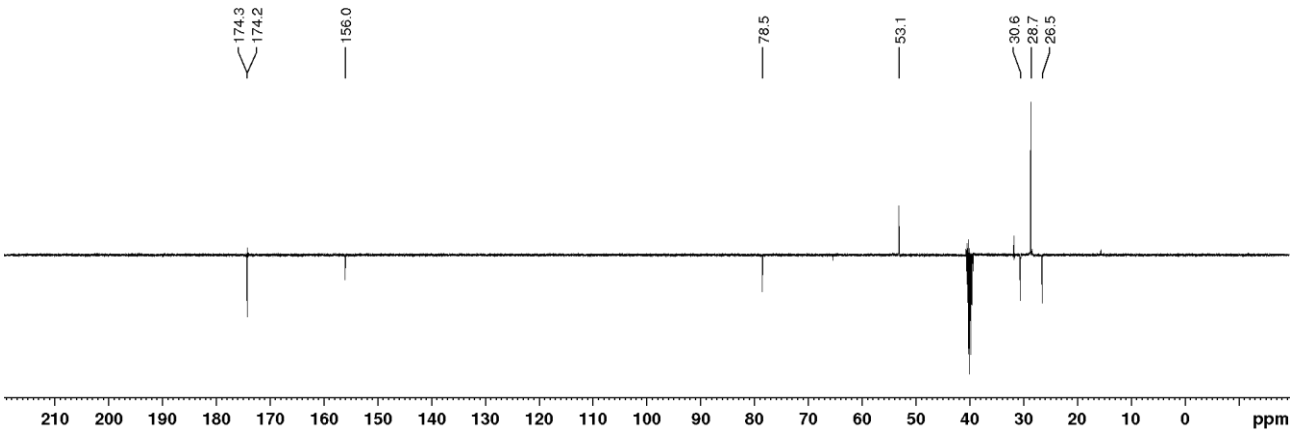

ESI-MS: calculated for $[C_{10}H_{17}NO_6Na]^+$: 270.11; found: 270.50.

Synthesis of bis(2,5-dioxopyrrolidin-1-yl) 2-(11-((tert-butoxycarbonyl) amino) undecanamido)pentanedioate (52)

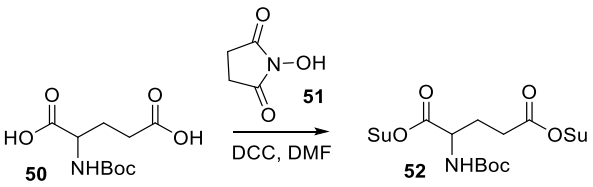

Compound **50** (247 mg, 1 mmol, 1 eq.) and DCC (454 mg, 2.2 mmol, 2.2 eq.) were dissolved in 5 mL of dry DMF ([**50**] = 0.2 M). The reaction was left stirring at rt for 5 h, then N-hydroxysuccinimide (**51**) (254 mg, 2.2 mmol, 2.2 eq.) was added and the reaction stirred at rt overnight. The following morning, the suspension was filtered on a Büchner funnel and the filtrate concentrated *in vacuo*. The resulting crude was suspended in 3 mL CH_2Cl_2 and filtered on a Büchner funnel. The product was isolated after precipitation with 10 mL Et_2O and subsequent vacuum filtration. The obtained white powder was left under high one night and directly used in the next step.

Yield: 650 mg

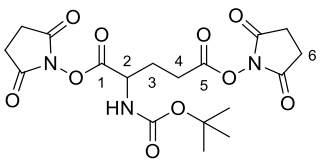

^{1}H-NMR (400MHz, $CDCl_3$): δ (ppm)= 5.29 (brd, 1H, H_2), 4.79 (brd, 1H, 1H, N<u>H</u>Boc), 2.89 - 2.76 (m, 10H, H_6, H_4), 2.48 - 2.34 (m, 2H, H_{3a}), 2.33 - 2.22 (m, 1H, H_{3b}), 1.45 (s, 9H, OC($C\underline{H}_3$)$_3$).

Synthesis of tert-butyl (11-((1,17-bis(3,5-bis((bis(pyridin-2-ylmethyl)amino) methyl)phenoxy)-7,11-dioxo-3,15-dioxa-6,12-diazaheptadecan-8-yl)amino)-11-oxoundecyl) carbamate (52a)

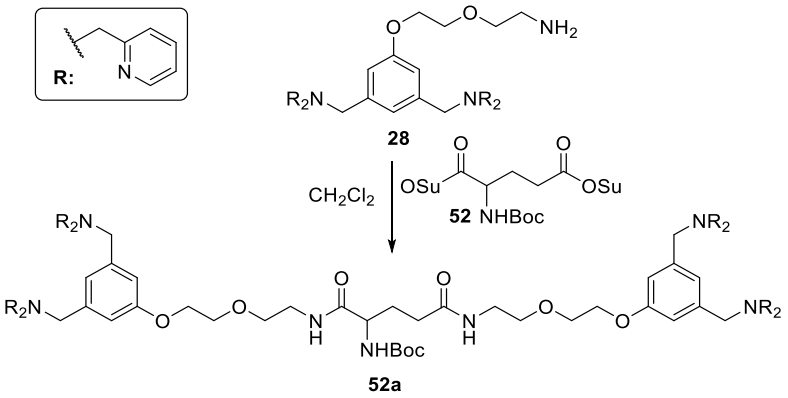

Activated ester **52** (24 mg, 0.055 mmol, 1 eq.) and amine **28** (70 mg, 0.11 mmol, 2 eq.) were dissolved in 5 mL of dry CH_2Cl_2 ([**52**] = 0.1 M) and the reaction stirred at rt overnight. The following, the reaction was washed with a non-saturated solution of $NaHCO_3$ (2 x 5 mL). The organic phase was dried over Na_2SO_4 and the solvent removed at reduced pressure. The crude was purified via automated chromatography (Eluent: CH_2Cl_2, doped with ammonia, with 5% of MeOH).

Yield: 50 mg, 65 %

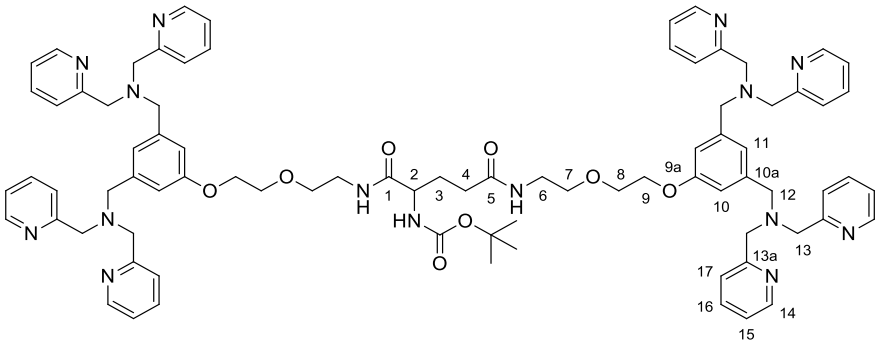

^{1}H-NMR (400MHz, CD_2Cl_2): δ (ppm)= 8.39 (d, 8H, H_{14}, $J_{14\text{-}15}$ = 4.2 Hz), 7.57 - 7.45 (m, 16H, H_{15}, H_{16}), 7.10 - 6.96 (m, 10H, H_4, H_{17}), 6.77 (s, 4H, H_{10}), 4.07 - 3.90 (m, 5H, H_2, H_9), 3.75 - 3.60 (m, 20H, H_8, H_{12}), 3.59 - 3.43 (m, 12H, H_7, H_{13}), 3.42 - 3.19 (m, 4H, H_6), 2.24 - 2.05 (m, 2H, H_4), 1.91 - 1.75 (m, 2H, H_3), 1.27 (s, 9H, $OC(C\underline{H}_3)_3$).

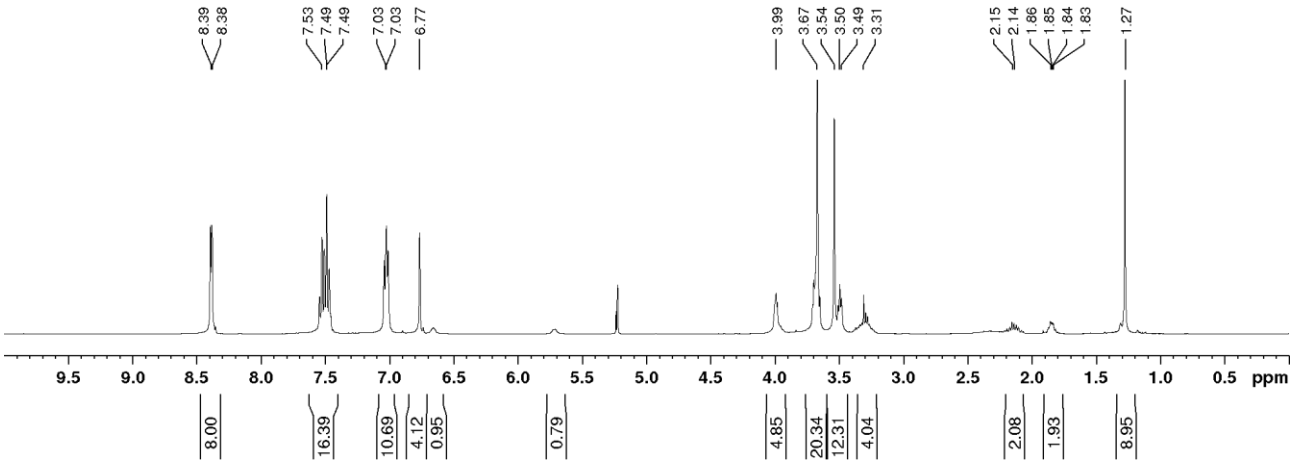

^{13}C-NMR (100MHz, CD_2Cl_2): δ (ppm) = 172.6 (C_1), 171.7 (C_5), 159.8 (C_{13a}), 158.8 (C_{9a}), 148.9, (C_{14}), 140.8 (C_{10a}), 136.2 (C_{15}), 122.7 (C_{16}), 121.9 (C_{17}), 113.5 (C_4), 79.4 (O<u>C</u>(CH_3)$_3$), 69.7 (C_7), 69.5 (C_8), 67.2 (C_9), 59.9 (C_{13}), 58.3 (C_{12}), 54.0 (C_2), 39.3 (C_6), 39.2 (C_{6a}), 32.4 (C_4), 28.8 (C_3), 28.1 (OC(C<u>H</u>$_3$)$_3$).

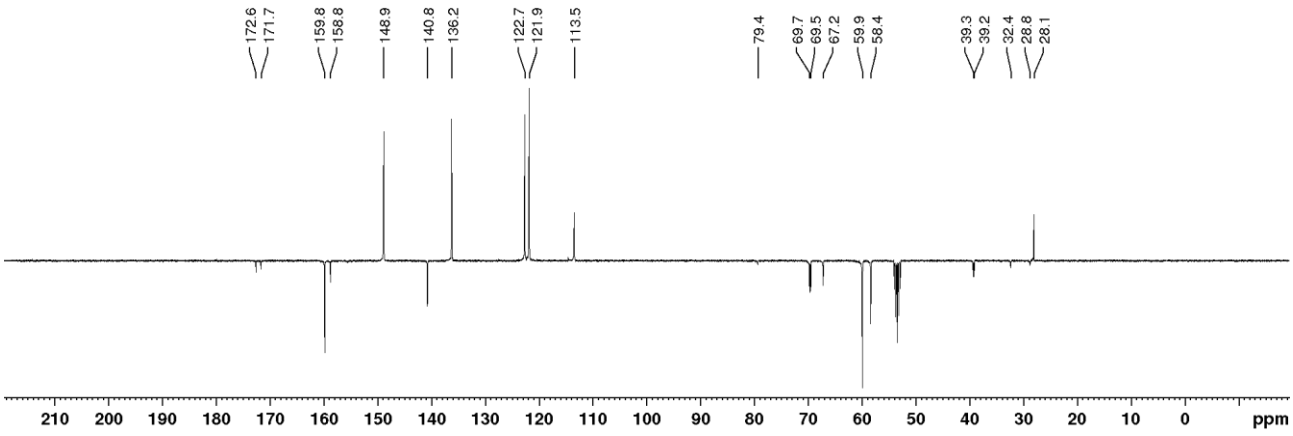

ESI-MS: calculated for $[C_{82}H_{95}N_{15}O_8Na]^+$: 1440.75; found: 1440.55.

Synthesis of 2-(11-aminoundecanamido)-N1,N5-bis(2-(2-(3,5-bis((bis(pyridin-2-ylmethyl)amino)methyl)phenoxy) ethoxy)ethyl)pentanediamide (53)

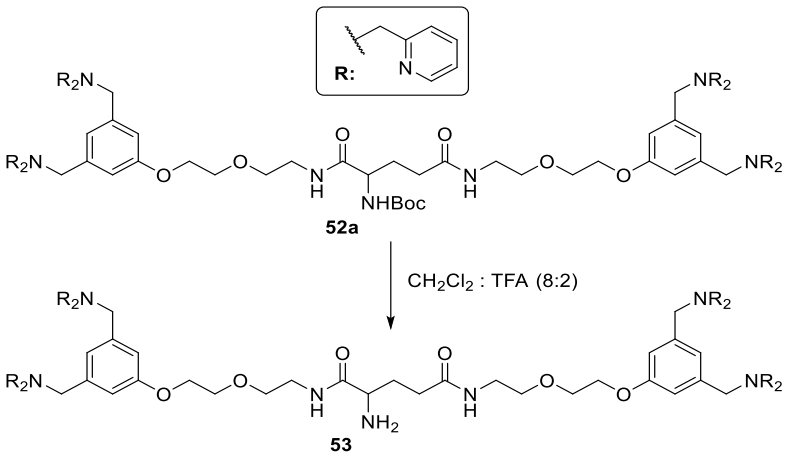

Compound **52a** (50 mg, 0.035 mmol, 1 eq.) was dissolved in 8:2 solution of CH_2Cl_2:TFA (1 mL, [**52a**] = M) and the reaction was stirred at rt for 40 minutes. The solvent was removed at reduced pressure and TFA stripped with toluene. The resulting crude was dissolved in 10 mLCH_2Cl_2 and washed with a non-saturated solution of $NaHCO_3$ (2 x 5 mL). The organic phase was dried over Na_2SO_4 and the solvent removed at reduced pressure.

Yield: 44 mg, 96%.

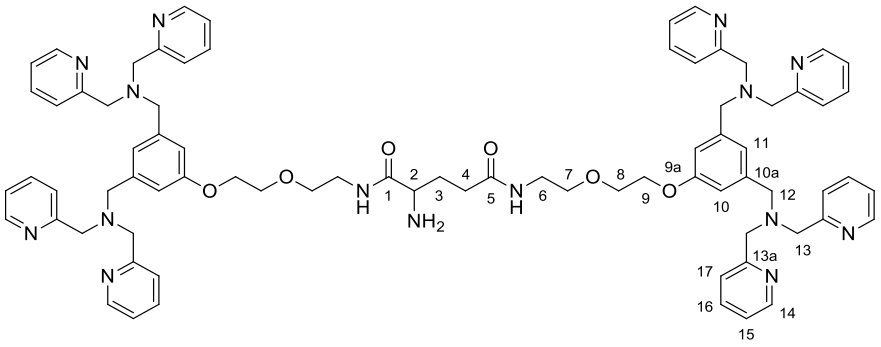

^{1}H-NMR (400MHz, CD_2Cl_2): δ (ppm)= 8.39 (d, 8H, H_{14}, $J_{14\text{-}15}$ = 4.2 Hz), 7.57 - 7.45 (m, 16H, H_{15}, H_{16}), 7.10 - 6.96 (m, 10H, H_4, H_{17}), 6.77 (s, 4H, H_{10}), 4.07 - 3.90 (m, 5H, H_2, H_9), 3.75 - 3.60 (m, 20H, H_8, H_{12}), 3.59 - 3.43 (m, 12H, H_7, H_{13}), 3.42 - 3.19 (m, 4H, H_6), 2.24 - 2.05 (m, 2H, H_4), 1.91 - 1.75 (m, 2H, H_3), 1.27 (s, 9H, $OC(C\underline{H}_3)_3$).

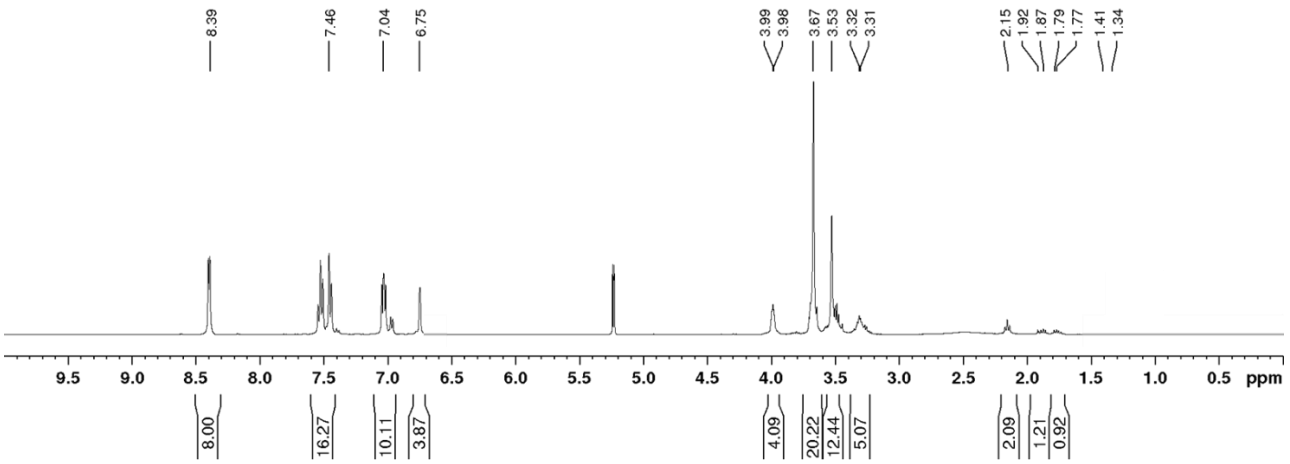

^{13}C-NMR (100MHz, CD_2Cl_2): δ (ppm) = 172.6 (C_1, C_5), 159.7 (C_{13a}), 158.8 (C_{9a}), 149.0, (C_{14}), 140.6 (C_{10a}), 136.3 (C_{15}), 122.7 (C_{16}), 121.9 (C_{17}), 113.6 (C_4), 69.8 (C_7), 69.4 (C_8), 67.3 (C_9), 60.0 (C_{13}), 58.5 (C_{12}), 54.3 (C_2), 39.1 (C_6), 38.9 (C_{6a}), 32.7 (C_4), 30.9 (C_3).

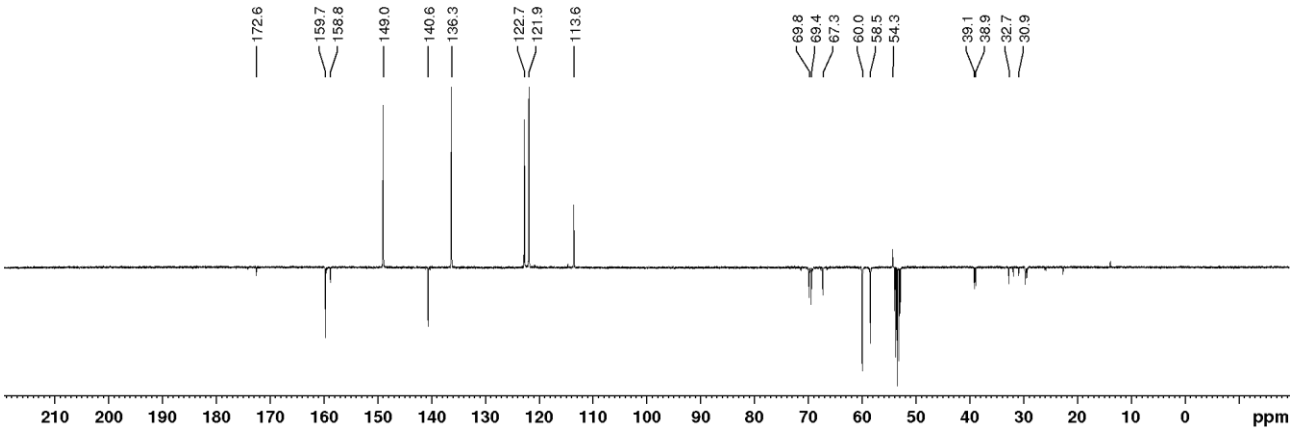

ESI-MS: calculated for $[C_{77}H_{87}N_{15}O_6Na]^+$: 1340.70; found: 1340.48.

Synthesis of dimethyl 2-(11-((tert-butoxycarbonyl)amino) undecanamido) pentanedioate (56)

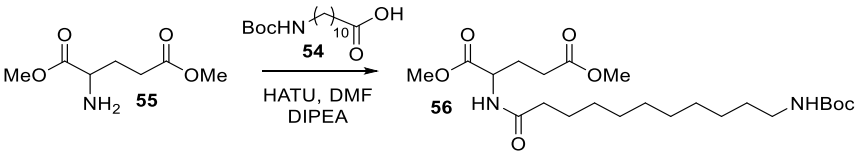

Dimethyl glutamate **55** (302 mg, 1 mmol, 1 eq.) and **HATU** (420 mg, 1.1 mmol, 1.1 eq.) were dissolved in 5 mL of dry DMF, then **DIPEA** (350 µL, 2.2 mmol, 2.2 eq.) was slowly added. The reaction was stirred at rt for 30 minutes. Separately, diester **55** was dissolved in 5 mL of dry DMF and added dropwise to the reaction mixture. The solution was stirred at RT for 1h (TLC CH_2Cl_2: MeOH 96:4, R_f (**55**) = 0.5; staining: Ninhydrin; Hex EtOAc 1:1, R_f (**56**) = 0.5; staining: Ninhydrin). Upon completion, DMF was removed under vacuum. The resulting crude was dissolved in 50 mL CH_2Cl_2 and washed with a 0.5 M HCl solution (1 x 50 mL) and a saturated solution of $NaHCO_3$ (1 x 30 mL). The organic phase was dried over Na_2SO_4 and the solvent evaporated. The crude was purified via automated flash chromatography (Eluent: Hex with a gradient of EtOAc from 0% to 100%).

Yield: 381 mg, 83%.

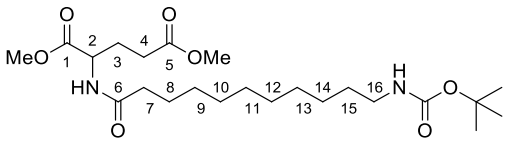

^{1}H-NMR (400MHz, $CDCl_3$): δ (ppm)= 6.16 (d, 1H, N<u>H</u>, $J_{NH\text{-}2}$ = 7.2), 4.69 - 4.61 (m, 1H, H_2), 4.52 (brd, 1H, N<u>H</u>), 3.77 (s, 3H, OMe), 3.70 (s, 3H, OMe), 3.12 (d, 2H, H_{16}, $J_{NH\text{-}\mathbf{16}\text{-}15}$ = 6.4), 2.51 - 2.33 (m, 2H, H_4), 2.28 - 2.17 (m, 3H, $H_{7,}$ H_{3a}), 2.07 - 1.96 (m, 1H, H_{3b}), 1.64 (qui, 2H, H_8, $J_{8\text{-}7}$ = 7.2), 1.46 (s, 11H, H_{15}, OC($C\underline{H}_3$)$_3$), 1.29 (brd, 12H, $H_{9,}$ $H_{10,}$ $H_{11,}$ $H_{12,}$ $H_{13,}$ H_{14}).

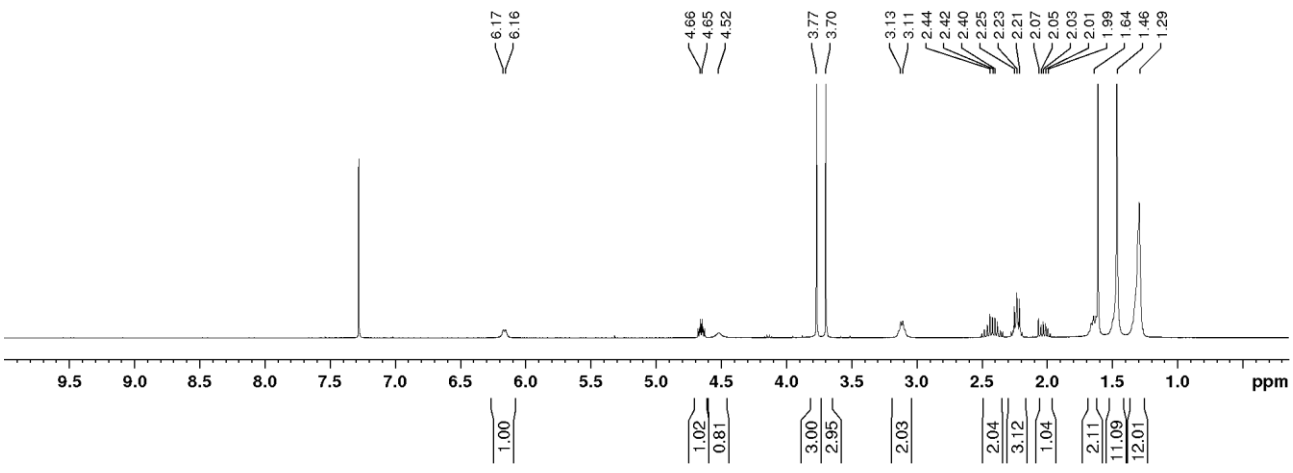

^{13}C-NMR (100MHz, $CDCl_3$): δ (ppm) = 173.3 (C_1), 173.1 (C_5), 172.5 (C_6), 52.5 (OMe), 51.9 (OMe), 51.5 (C_2), 40.6 (C_{16}), 36.5 (C_7), 30.1 (C_4, C_{15}), 29.4 - 29.2 (C_9, C_{10}, C_{11}, C_{12}, C_{13}, C_{14}), 28.4 (OC($C\underline{H}_3$)$_3$), 27.4 (C_3), 25.5 (C_8).

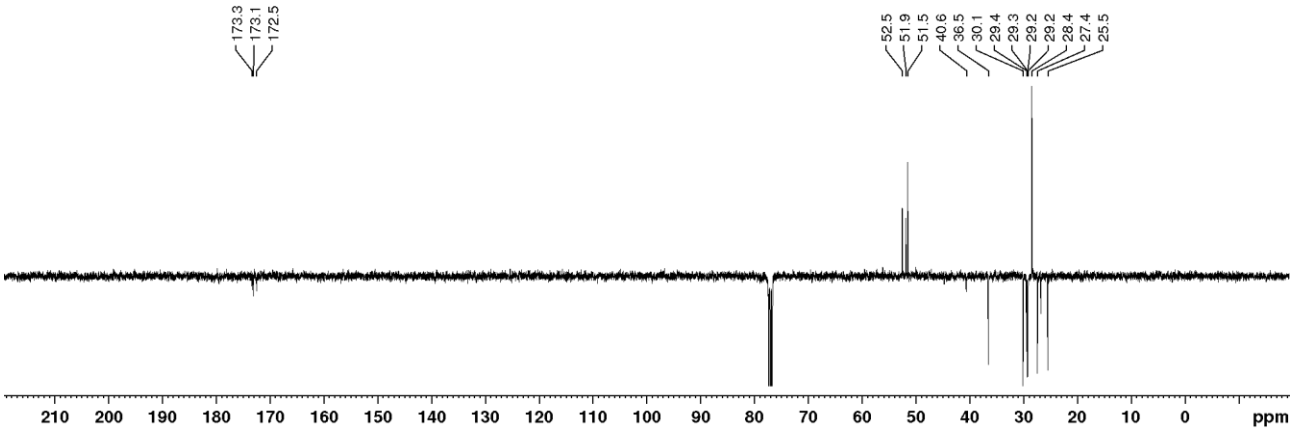

ESI-MS: calculated for $[C_{23}H_{42}N_2O_7Na]^+$: 481.30; found: 481.41.

Synthesis of dimethyl 2-(11-((tert-butoxycarbonyl)amino) undecanamido) pentanedioate (57)

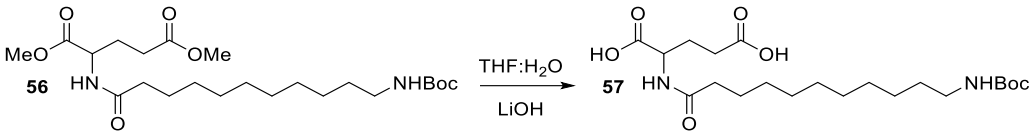

Compound **56** (380 mg, 0.82 mmol, 1 eq.) was dissolved in 10 mL of THF. Separately, $LiOH \cdot H_2O$ (137 mg, 3.3 mmol, 4 eq.) was dissolved in 10 mL of water and added to the first solution. The reaction was stirred at rt for 6 h. Upon completion, as determined by ^{1}H-NMR, THF was removed at reduced pressure and the remaining water solution was acidified till pH 2 with HCl 1 M. The product is then extracted with EtOAc (2 x 10 mL). The organic phase was dried over Na_2SO_4 and the solvent evaporated to obtain pure product **57**.

Yield: 335 mg 95%.

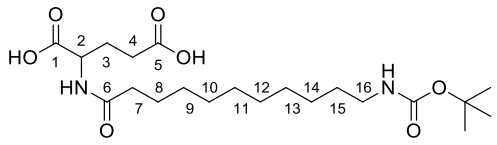

^{1}H-NMR (400MHz, MeOD-d^4): δ (ppm)= 4.44 (dd, 1H, H_2, $J_{2\text{-}3a}$ = 5, $J_{2\text{-}3b}$ = 5), 3.03 (t, 2H, H_{16}, $J_{16\text{-}15}$ = 6.7), 2.41 (t, 2H, H_4, $J_{4\text{-}3}$ = 7.6), 2.26 (t, 3H, H_7, $J_{7\text{-}8}$ = 7.6), 2.23 - 2.14 (m, 1H, H_{3a}), 2.01 - 1.88 (m, 1H, H_{3b}), 1.62 (qui, 2H, H_8, $J_{8\text{-}7}$ = 7.1), 1.45 (s, 11H, H_{15}, $OC(C\underline{H}_3)_3$), 1.33 (brd, 12H, H_9, H_{10}, H_{11}, H_{12}, H_{13}, H_{14}).

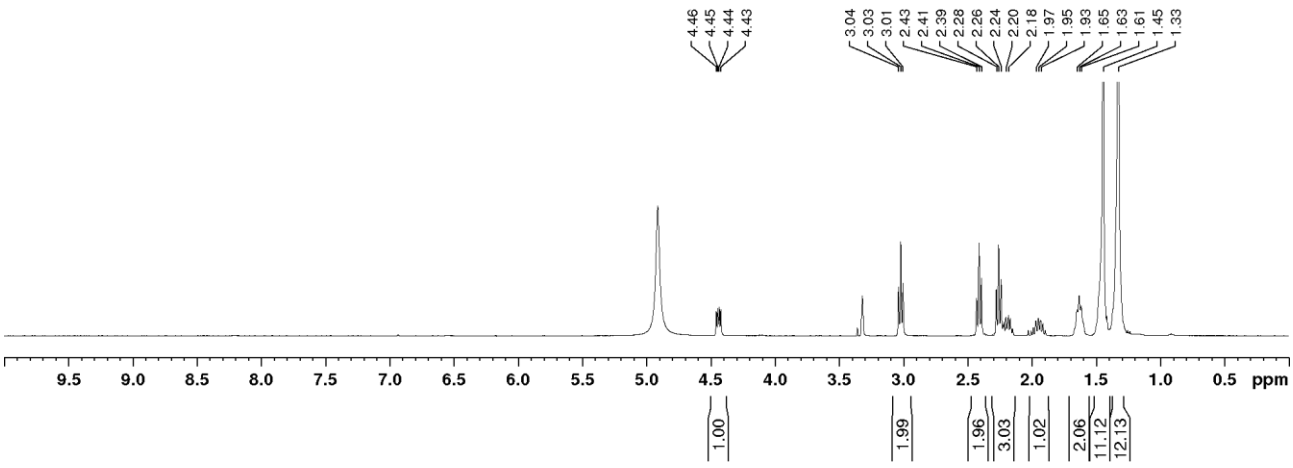

^{13}C-NMR (100MHz, MeOD-d^4): δ (ppm) = 175.1 (C_1), 174.9 (C_5), 173.6 (C_6), 157.2 (N-C=O), 78.4 ($OC(CH_3)_3$), 51.5 (C_2), 40.0 (C_{16}), 35.4 (C_4), 29.8 (C_4), 29.6 - 28.8 (C_9, C_{10}, C_{11}, C_{12}, C_{13}, C_{14}), 27.4 ($OC(CH_3)_3$), 26.4 (C_3), 25.5 (C_8).

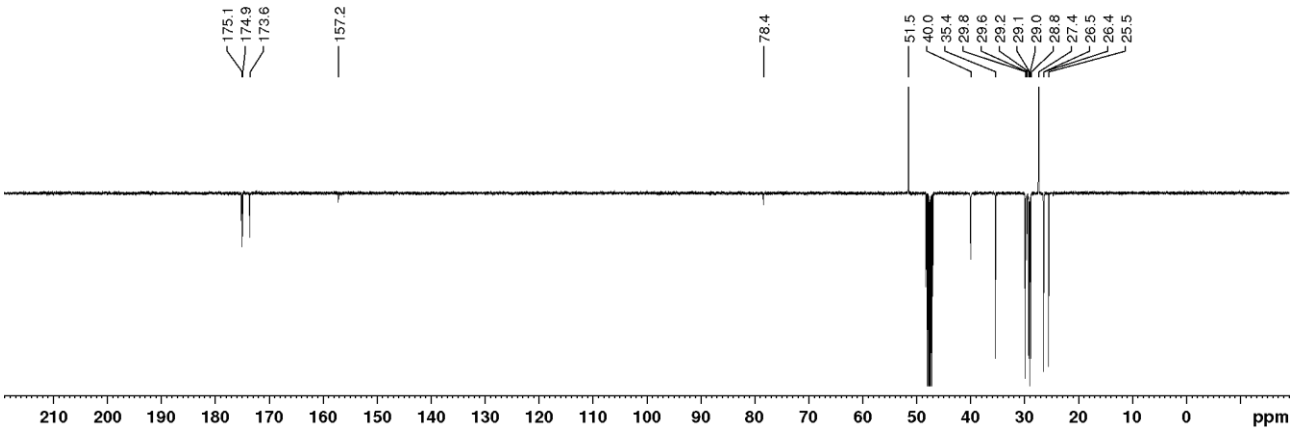

ESI-MS: calculated for $[C_{21}H_{38}N_2O_6Na]^+$: 453.27; found: 453.52.

Synthesis of bis(2,5-dioxopyrrolidin-1-yl) 2-(11-((tert-butoxycarbonyl)amino) undecanamido)pentanedioate (58)

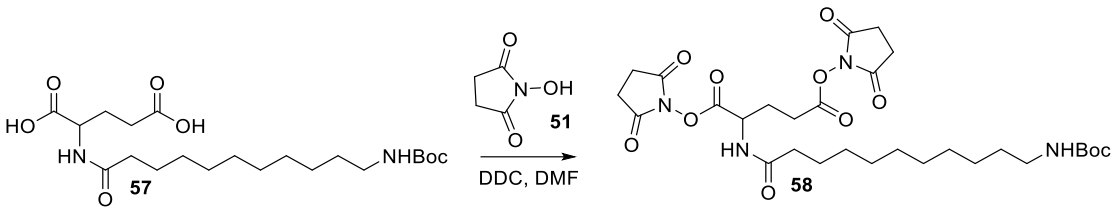

Diacid **57** (300 mg, 0.7 mmol, 1 eq.) was dissolved in 4 mL of dry DMF ([**57**] = 0.2 M), then **DCC** (316 mg, 1.53 mmol, 2.2 eq.) was added. The reaction was left stirring at RT for 5 h, then N-hydroxysuccinimide (**51**) (176 mg, 1.53 mmol, 2.2 eq.) was added. The reaction was stirred at rt overnight. The following morning, the suspension was filtered on a Büchner funnel and the filtrate concentrated *in vacuo*. The resulting crude was suspended in 3 mL CH_2Cl_2 and filtered on a Büchner funnel. The product was isolated after precipitation with 10 mL Et_2O and subsequent vacuum filtration. The obtained white powder was left under high one night and directly used in the next step.

Yield: 650 mg.

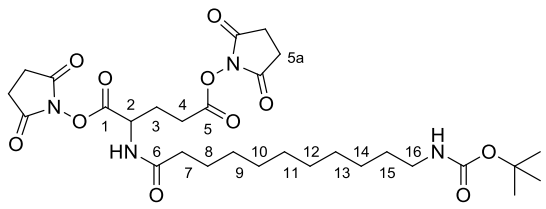

^{1}H-NMR (400MHz, $CDCl_3$): δ (ppm)= 6.52 (d, 1H, N<u>H</u>, $J_{NH\text{-}2}$ = 8.1), 5.22 – 5.13 (m, 1H, H_2), 4.55 (brd, 1H, N<u>H</u>), 3.12 (d, 2H, H_{16}, $J_{NH\text{-}\mathbf{16}\text{-}15}$ = 6.7), 2.87 (brd, 10H, H_4, H_{5a}), 2.55 - 2.46 (m, 1H, H_{3a}), 2.44 - 2.35 (m, 1H, H_{3b}), 2.25 (m, 2H, H_7, $J_{8\text{-}7}$ = 7.2), 1.64 (qui, 2H, H_8), 1.46 (s, 11H, H_{15}, OC($C\underline{H}_3$)$_3$), 1.28 (brd, 12H, H_9, H_{10}, H_{11}, H_{12}, H_{13}, H_{14}).

Synthesis of tert-butyl (11-((1,17-bis(3,5-bis((bis(pyridin-2-ylmethyl)amino) methyl)phenoxy)-7,11-dioxo-3,15-dioxa-6,12-diazaheptadecan-8-yl)amino)-11-oxoundecyl)carbamate (59)

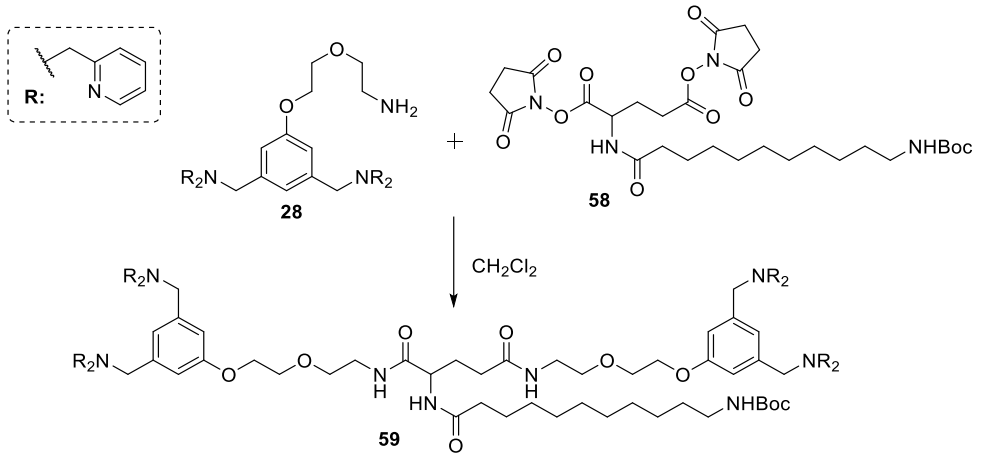

Activated ester **58** (40 mg, 0.065 mmol, 1 eq.) and amine **28** (80 mg, 0.13 mmols, 2 eq.) were dissolved in 5 mL of dry CH_2Cl_2 ([**58**] = 0.013 M) and the reaction stirred at RT overnightThe following morning, the reaction was washed with a non-saturated solution of $NaHCO_3$ (2 x 5 mL). The organic phase was dried over Na_2SO_4 and the solvent removed at reduced pressure to obtain product **59** in sufficient purity.

Yield: 102 mg, quantitative.

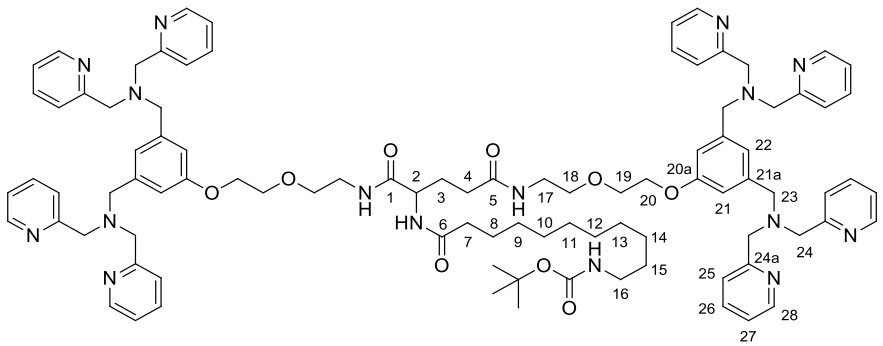

^{1}H-NMR (400MHz, CD_2Cl_2): δ (ppm)= 8.45 - 8.32 (m, 8H, H_{28}), 7.60 - 7.43 (m, 16H, H_{26}, H_{27}), 7.11 – 6.99 (m, 10H, H_{25}, H_{22}), 6.77 (s, 4H, H_{21}), 4.22 (q, 1H, H_2, $J_{1\text{-}2}$ = 7.0 Hz), 4.07 - 3.94 (m, 4H, H_{20}), 3.75 - 3.61 (m, 20H, H_{19}, H_{24}), 3.58 - 3.44 (m, 12H, H_{23}, H_{18}), 3.40 - 3.19 (m, 4H, H_{17}), 2.95 (q, 2H, H_{16}, $J_{16\text{-}15}$ = 6.5 Hz), 2.27 - 2.17 (m, 1H, H_{3a}), 2.15 - 2.06 (m, 1H, H_{3b}), 2.03 (t, 2H, H_7, $J_{7\text{-}8}$ = 7.5 Hz), 1.90 - 1.80 (m, 2H, H_4), 1.45 (m, 2H, H_8), 1.32 (s, 11H, H_9, $OC(C\underline{H}_3)_3$), 1.14 (brd, 12H, H_9, H_{10}, H_{11}, H_{12}, H_{13}, H_{14}).

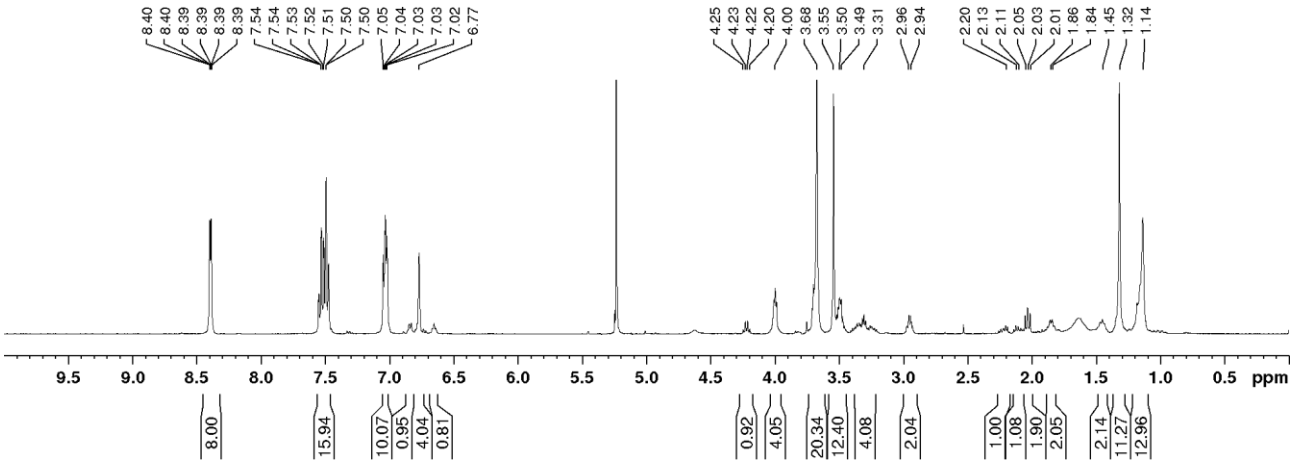

^{13}C-NMR (100MHz, CD_2Cl_2): δ (ppm) = 173.1 (C_5), 172.8 (C_1), 171.4 (C_6), 159.8 (C_{24a}), 158.8 (C_{20a}), 148.9 (C_{28}), 140.7 (C_{21a}), 136.2 (C_{27}), 122.7 (C_{26}), 121.8 (C_{22}, C_{25}), 113.5 (C_{21}), 69.7 (C_{18}), 69.5 (C_{19}), 67.2 (C_{20}), 59.9 (C_{24}), 58.4 (C_{23}), 52.7 (C_2), 40.5 (C_{16}), 39.3 (C_{17}), 36.4 (C_7), 32.5 (C_3), 30.0 - 28.6 (C_4, C_9, C_{10}, C_{11}, C_{12}, C_{13}, C_{14}, C_{15}), 28.4 ($OC(C\underline{H}_3)_3$), 27.4 (C_3), 25.5 (C_8).

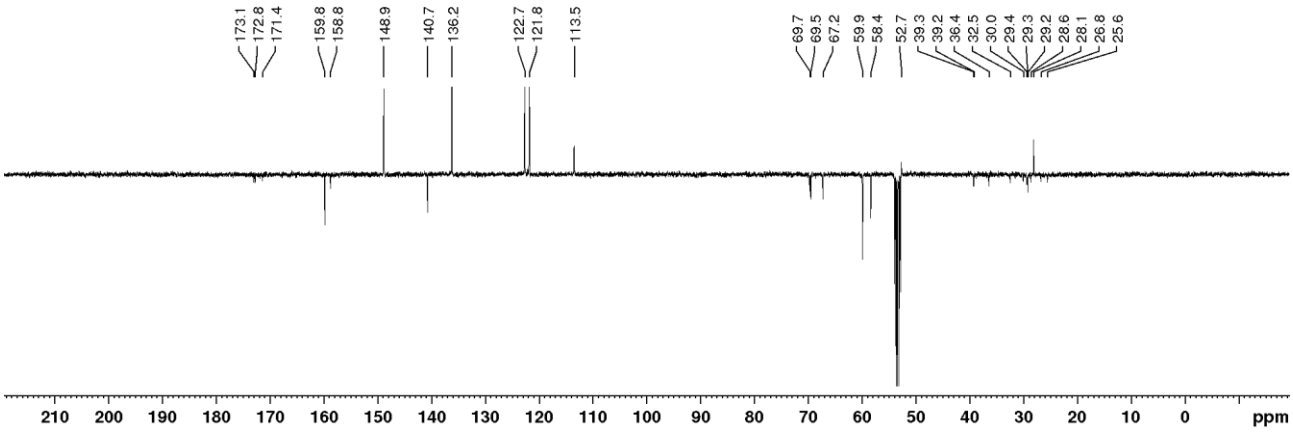

ESI-MS: calculated for $[C_{93}H_{116}N_{16}O_9Na]^+$: 1624.91; found: 1624.17.

Synthesis of 2-(11-aminoundecanamido)-N1,N5-bis(2-(2-(3,5-bis((bis(pyridin-2-ylmethyl)amino)methyl)phenoxy) ethoxy)ethyl)pentanediamide (60)

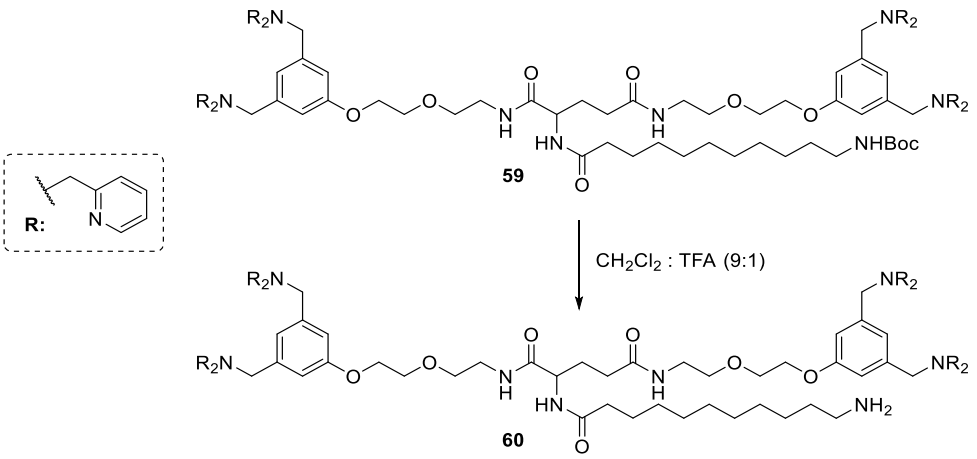

Compound **59** (102 mg, 0.065 mmol, 1 eq.) was dissolved in a 9:1 CH_2Cl_2:TFA solution (1 mL, [**60**] = 0.065 M) and the reaction stirred at rt for 40 minutes. The reaction mixture was washed with a non-saturated solution of $NaHCO_3$ (2 x 5 mL). The organic phase was dried over Na_2SO_4 and the solvent removed at reduced pressure to obtain pure product **60**.

Yield: 80 mg, 90 %

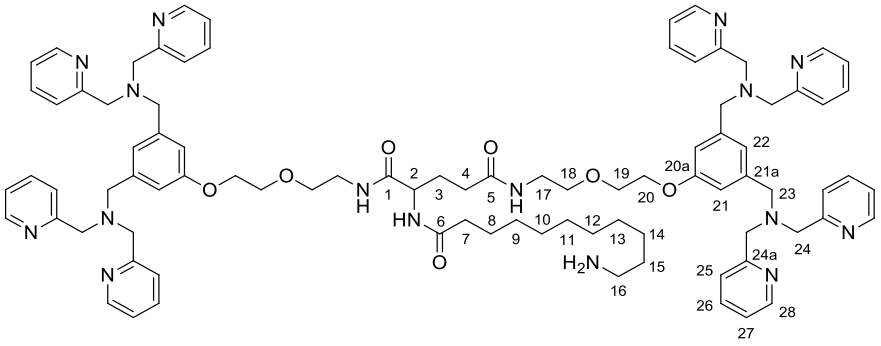

^{1}H-NMR (400MHz, CD_2Cl_2): δ (ppm)= 8.45 - 8.32 (m, 8H, H_{28}), 7.60 - 7.43 (m, 16H, H_{26}, H_{27}), 7.10 – 7.00 (m, 8H, H_{25}), 6.98 (s, 2H, H22), 6.75 (s, 4H, H_{21}), 4.24 (q, 1H, H_2, $J_{1\text{-}2}$ = 7.0 Hz), 4.07 - 3.94 (m, 4H, H_{20}), 3.75 - 3.61 (m, 20H, H_{19}, H_{24}), 3.58 - 3.44 (m, 12H, H_{23}, H_{18}), 3.40 - 3.19 (m, 4H, H_{17}), 2.64 (t, 2H, H_{16}, $J_{16\text{-}15}$ = 6.5 Hz), 2.27 - 2.06 (m, 2H,H_{3a}, H_{3b}), 2.03 (t, 2H, H_7, $J_{7\text{-}8}$ = 7.5 Hz), 1.90 - 1.80 (m, 2H, H_4), 1.53 – 1.32 (m, 4H, H_8, H_{15}), 1.12 (brd, 12H, H_9, H_{10}, H_{11}, H_{12}, H_{13}, H_{14}).

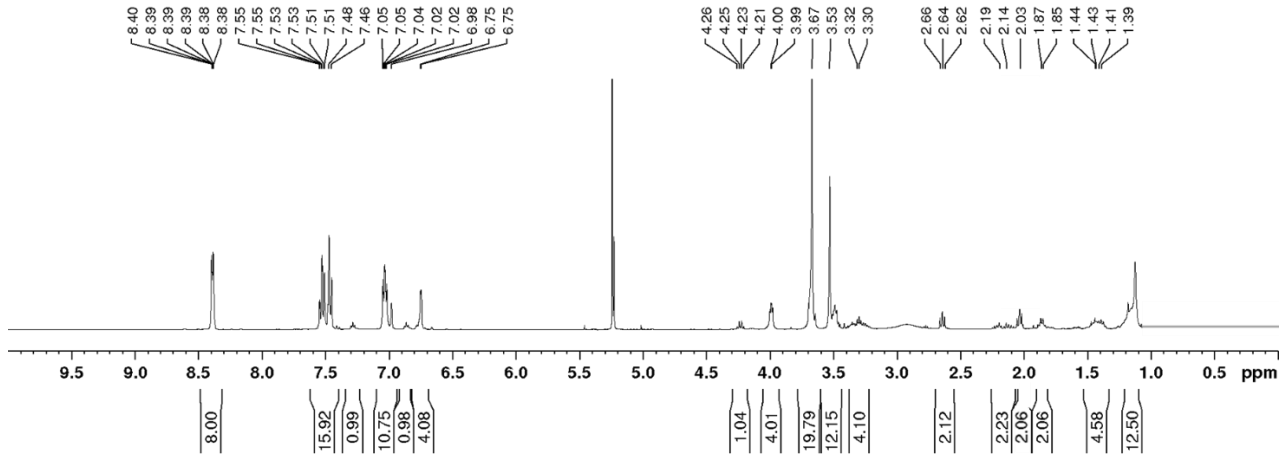

^{13}C-NMR (100MHz, CD_2Cl_2): δ (ppm) = 168.9 (C_5), 168.5 (C_1), 167.5 (C_1), 155.4 (C_{24a}), 154.4 (C_{20a}), 144.5 (C_{28}), 136.3 (C_{21a}), 132.0 (C_{27}), 118.4 (C_{26}), 117.6 (C_{22}, C_{25}), 109.2 (C_{21}), 65.1 (C_{18}), 62.9 (C_{19}), 55.6 (C_{20}), 54.0 (C_{24}), 48.4 (C_{23}), 44.6 (C_2), 36.8 (C_{16}), 34.9 (C_{17}), 34.8 (C_7), 31.9 (C_3), 29.6 - 20.7 (C_3, C_4, C_8, C_9, C_{10}, C_{11}, C_{12}, C_{13}, C_{14}, C_{15}).

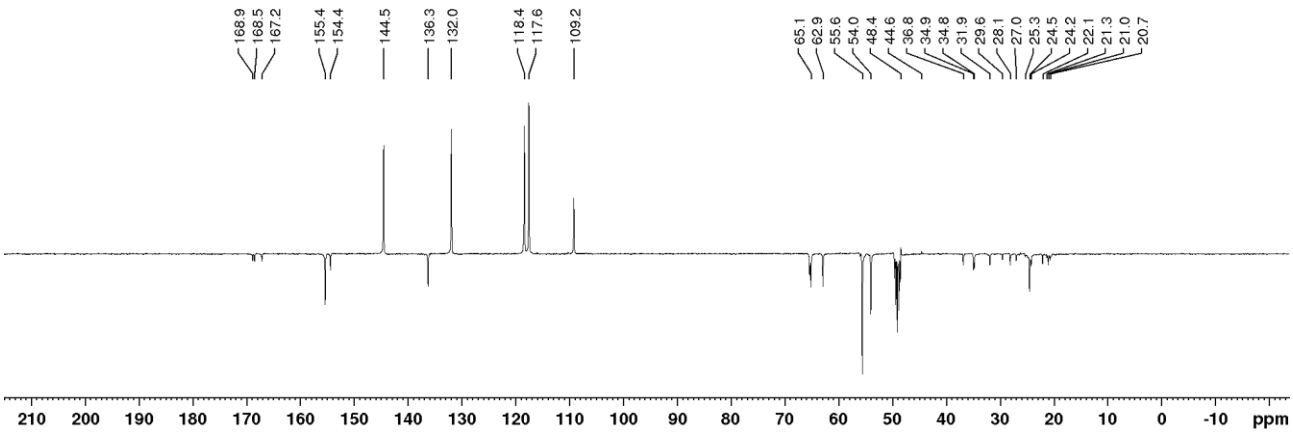

MS (ESI) + m/z: calculated for $[C_{88}H_{108}N_{16}O_7Na]^+$: 1524.86; found: 1525.21.

MPC-4 functionalization (32)

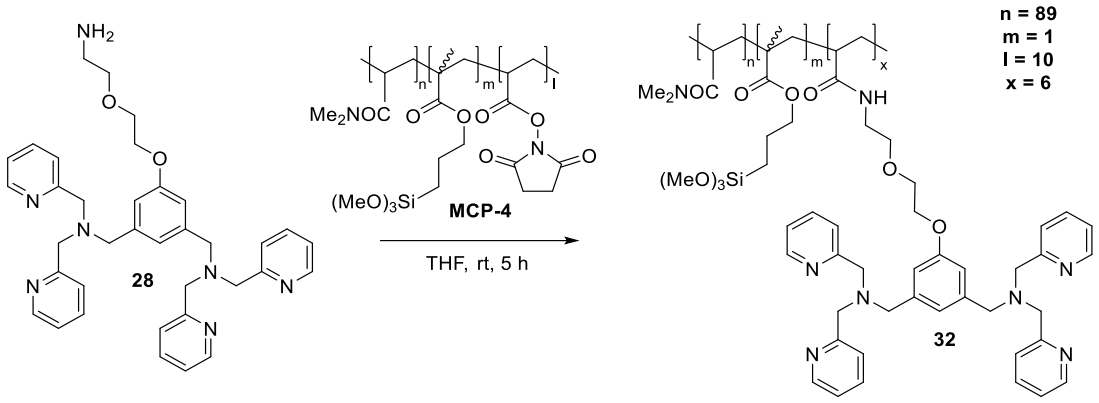

28 (37 mg, 0.061 mmol, 0.6 eq. with respect to NAS groups) was dissolved in 500 µL of dry degassed THF. Separately, **MCP-4** (100 mg, 0.93 mmol containing 10% NAS, 1 eq.) was also dissolved in 500 µL of degassed THF. The two solutions were then combined under Ar atmosphere. The resulting reaction mixture was stirred at RT for 5 h (TLC CH_2Cl_2:MeOH 98:2, R_f (**28**) = 0.15; staining: Ninhydrin). Upon completion, the reaction was diluted 10-fold with Hex to ensure polymer precipitation. Product **32** was recovered as a white powder after filtration on a Büchner funnel and dried overnight *in vacuo.*

Yield: 110 mg, 88%.

Characterization: (see paragraph 2.2).

^{1}H-NMR, DMSO-D6

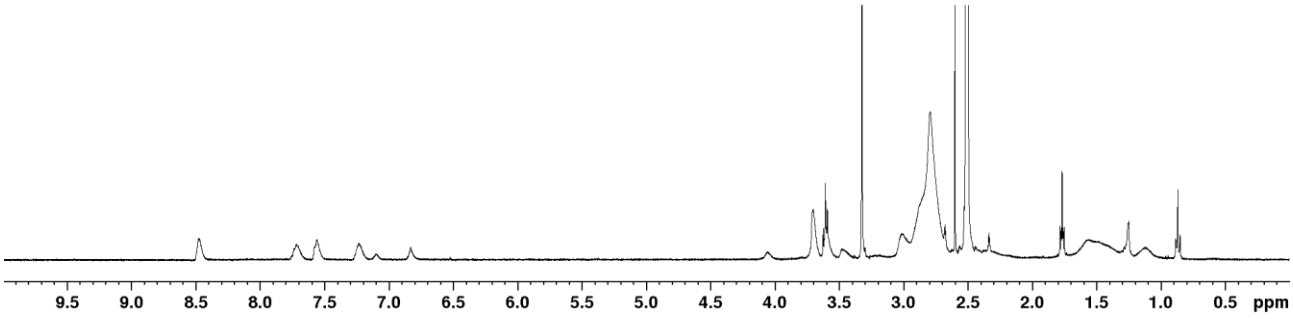

DOSY, DMSO-d6

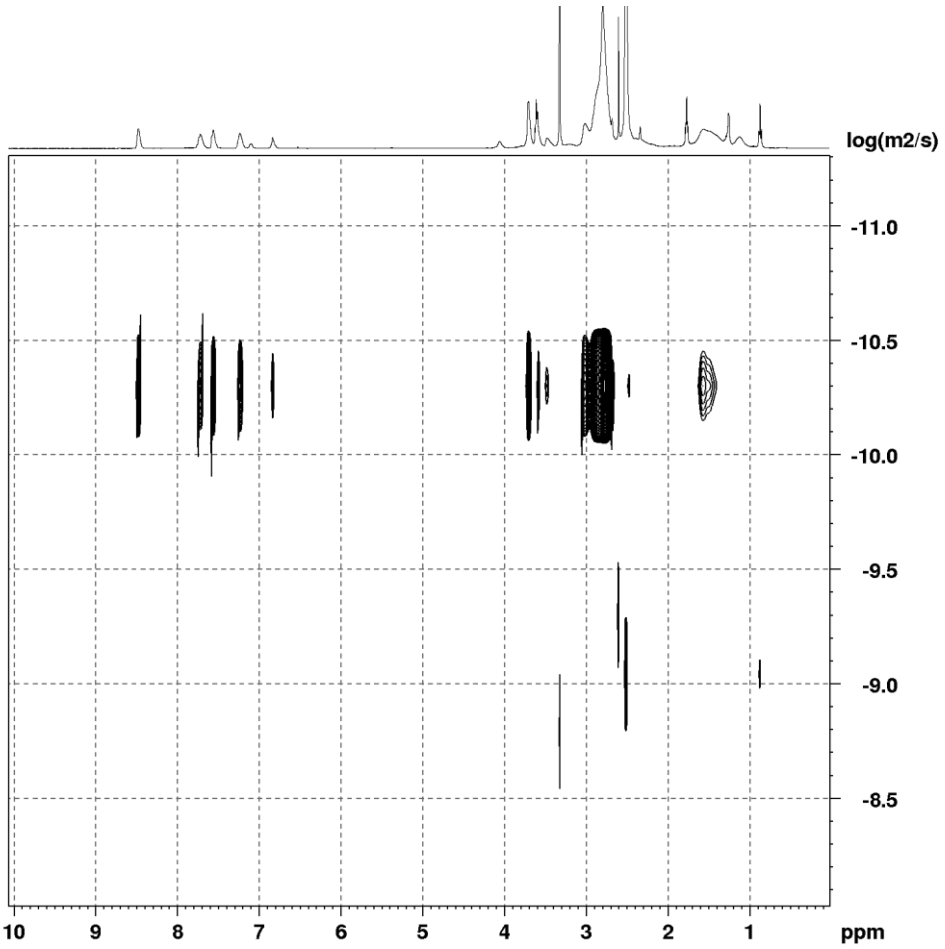

Thermogravimetric analysis (TGA)

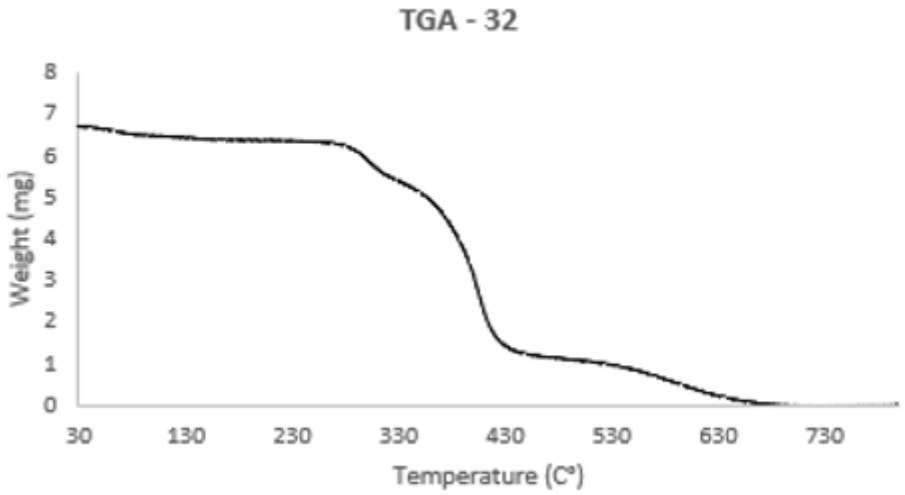

ATR FT-IR

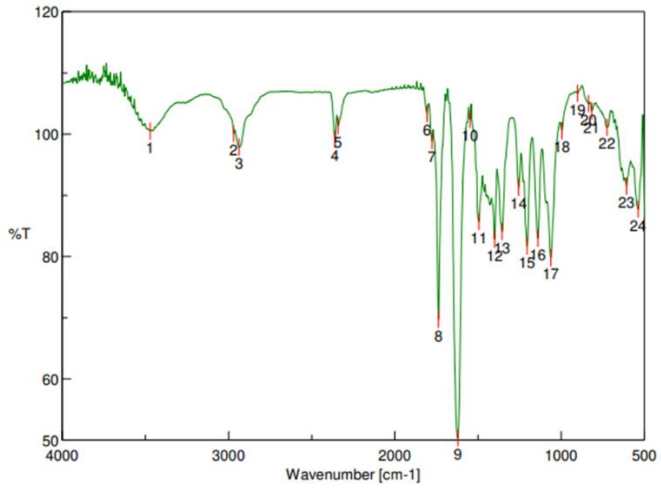

[Result of Peak Picking]

No.	Position	Intensity	No.	Position	Intensity
1	3471.24	100.482	2	2969.84	100.063
3	2936.09	97.8431	4	2360.44	99.1391
5	2341.16	101.314	6	1806.97	103.289
7	1777.08	98.8844	8	1737.55	69.7207
9	1621.84	50.3458	10	1548.56	102.387
11	1494.56	85.7073	12	1401.03	82.8166
13	1355.71	84.0944	14	1256.4	91.2711
15	1205.29	81.7047	16	1140.69	82.9797
17	1062.59	79.7784	18	996.053	100.542
19	901.558	106.635	20	835.99	104.944
21	816.706	103.748	22	725.104	101.076
23	607.467	91.4895	24	537.078	87.7132

MCP-4 Infrared profile

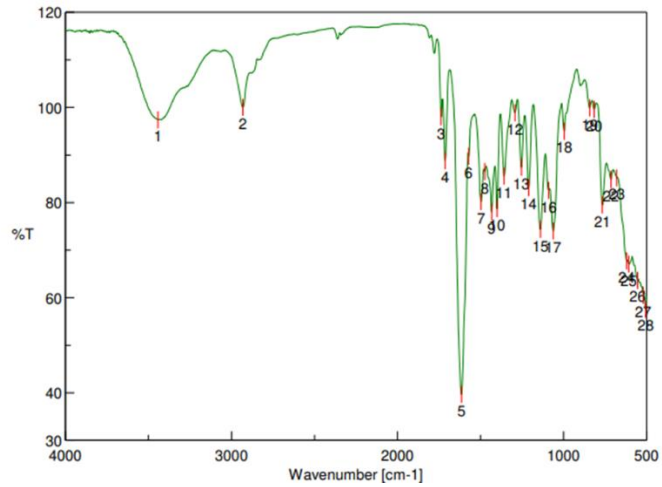

[Result of Peak Picking]

No.	Position	Intensity	No.	Position	Intensity
1	3443.28	97.3703	2	2931.27	100.017
3	1737.55	98.0048	4	1713.44	88.7869
5	1615.09	39.6496	6	1570.74	89.7391
7	1497.45	80.1769	8	1474.31	86.515
9	1432.85	77.994	10	1401.03	78.6855
11	1358.6	85.5403	12	1293.04	98.8563
13	1254.47	87.4084	14	1210.11	83.1171
15	1139.72	74.3333	16	1090.55	82.5257
17	1062.59	74.0103	18	996.053	94.9688
19	842.74	99.8695	20	815.742	99.566
21	766.566	79.4676	22	714.497	84.8619
23	679.785	85.1759	24	620.002	67.6927
25	607.467	67.0472	26	554.434	63.6178
27	520.686	60.5039	28	505.258	57.5599

*Functionalized polymer **32** Infrared profile*

Assessment of the degree of functionalization of polymer 32

UV-Vis spectrophotometry was used to evaluate the degree of functionalization of polymer **32**, considering that its absorbance would only depend on the bis-DPA moiety deriving from compound **28**. Thus, in first place, we determined the molar extinction coefficient (ε) of **28**.

A 10 mM stock solution of **28** in DMF was used to build the calibration curve. Samples from 10 to 80 µM were prepared by dilution of the stock solution in water.

Sample	Conc. (µM)	Abs (λ_{261})
1	80	1.078
2	60	0.817
3	40	0.559
4	20	0.312
5	10	0.166
6	0	0

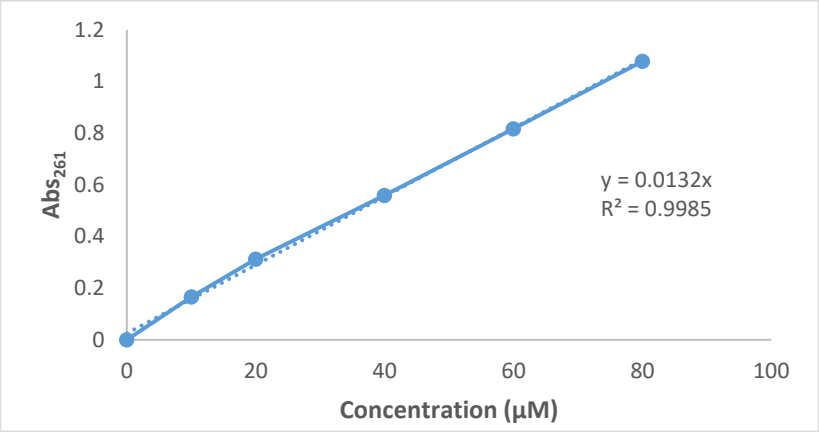

The ε value derived was ε_{261} = 13200 $M^{-1}cm^{-1}$.

Having determined the molar absorptivity of **28**, we could proceed in evaluating the degree of functionalization of polymer **32**. To this aim, in first place, a 0.1 mg/mL aqueous solution of non-functionalized polymer **MCP-4** was prepared as blank.

Subsequently, the absorbance of a 0.1 mg/mL aqueous solution of functionalized polymer **32** was measured at 261 nm: Abs_{261} = 0.643.

The graph below shows the superimposition of absorption spectra of **MCP-4** (used as blank), compound **28** and functionalised polymer **32**.

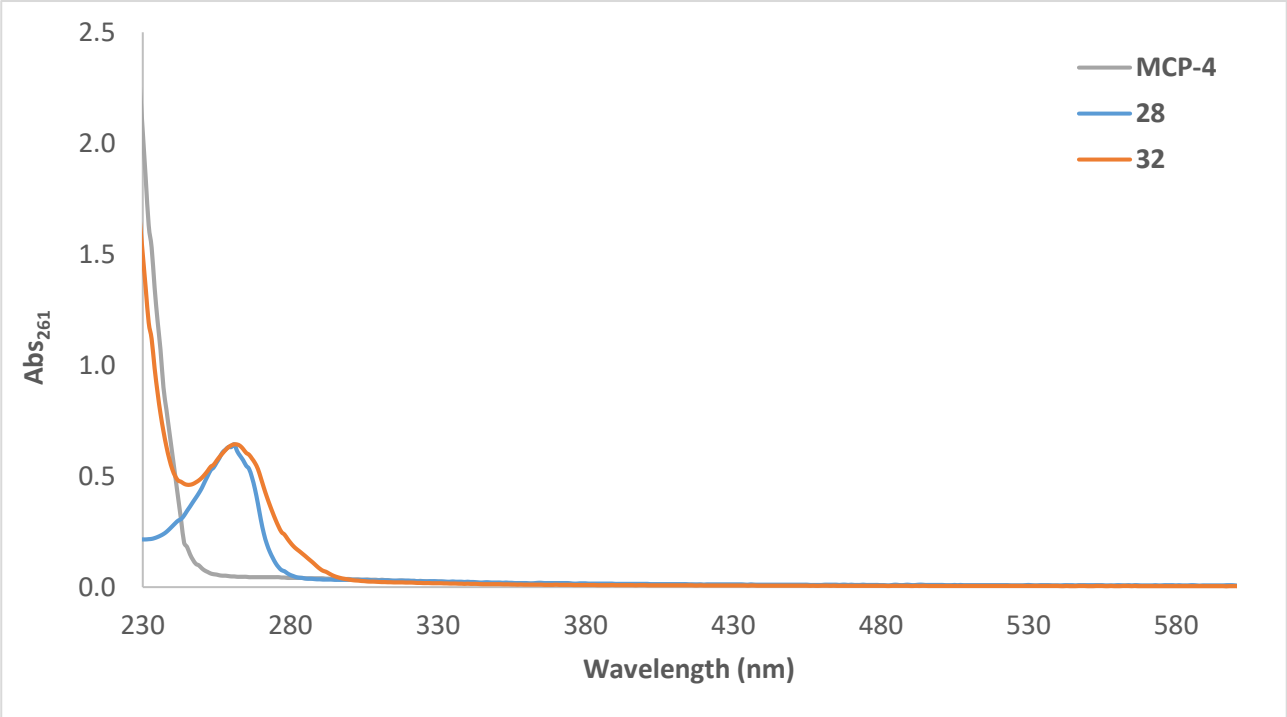

Using the Lambert-Beer equation and the ε_{261} of **28,** we determined its concentration as follows:

$$C = Abs/(\varepsilon \cdot l) = (0.643)/\ (13200\ M^{-1}cm^{-1} \cdot 1\ cm) = \ 0.049\ mM$$

We then calculated the mmol of **28** contained in the analysed sample:

$$n = C \cdot V = 0.049\ mM \cdot 1\ mL = 0.049\ \mu mol$$

Since our sample contained 0.1 mg of functionalised polymer **32**, we could conclude that its degree of functionalization was 0.49 µmol/mg.

Sand surface chemical activation and coating

Sand particles with a diameter of about 300 µm were used for chemical activation and coating with polymer **32**. In first place, with the aim to set up a proper coating procedure, we needed to assess the surface area per gram of sand. Thus, considering that sand grains have a reported density (d) of 1.25 g/cm^3, we could calculate the volume (V) occupied by one gram of sand as follows:

1) $V = \frac{m}{\mathrm{d}} = \frac{1\ g}{1.25\ g/cm^3} = 0.8\ \mathrm{cm}^3 = 800\ \mathrm{mm}^3$

The total surface area was estimated considering the beads as rigid spheres packed with the highest possible density. With these assumptions, we asserted that the volume occupied by the spheres (V_o) is at most $\pi/\sqrt{18}$ of the total volume (about 74%)[87]:

2) $V_O = V\ \frac{\pi}{\sqrt{18}} = 600\ mm^3$

The volume of each sphere (V_S) was calculated considering a radius of 0.15 mm:

3) $V_S = \frac{4}{3}\pi r^3$ = $0.014\ mm^3$

While its surface area (A_S) could be calculated as follows:

4) $A_S = \pi r^2 = 0.07\ mm^2$

From the ratio between the volume occupied by all spheres (V_o) and the volume of one sphere (V_S) we could obtain the number of beads (n) per gram of sand:

5) $n = V_o/V_S = 600\ mm^3/0.014\ mm^3 = 4.2\ \cdot 10^4$

Thus, the total surface area (A_{TOT}) per gram of sand was determined as the product between the number of beads (n) and the area of each sphere (A_S):

6) $A_{TOT}\ = n\ \cdot A_S = 4.2\ \cdot 10^4 \cdot 0.07\ mm^2 = 2.9\ \cdot 10^3\ mm^2$

After having assessed the total surface area per gram of sand, we proceeded with its activation following different strategies.

First method: 2 g of sand were placed in a flask and shaken for 30 minutes in 20 mL 1 M HCl. After filtration on a Büchner funnel, the sand was washed with 10 mL water and placed in a new flask together with 20 mL 1 M NaOH. After 30 min shaking, filtration and washing with water the sand was dried overnight *in vacuo*. For the coating step, an 1%$_{w/w}$ aqueous solution of functionalized polymer **32** was prepared by dissolving 150 mg in 15 mL water. Such solution was stirred with the 'activated sand' for 30 minutes at RT. After filtration and washing with water, the sand was subjected to curing at 80 ° C for 20 minutes.
The resulting coated sand was subjected to TGA analysis. Unfortunately, from the thermogram, we observed no weight loss, indicating that no polymer was anchored on the sand grains surface.

Second method: 2 g of sand were placed in a flask and stirred for 1 hour in 20 mL 2 M HNO_3. After filtration on a Büchner funnel, the sand was washed with 50 mL water. The coating step was performed as in the first method.
The coated sand activated with 2 M HNO_3 was subjected to TGA analysis. Also in this case, no weight loss was observed in the thermogram.

Third method: 2 g of sand were placed in a flask and stirred for 1 h at 70 °C in a solution constituted as follows: 5 parts of water, 1 part of 30%$_{w/v}$ NH_3 and 1 part of 30%$_{w/v}$ H_2O_2. After filtration on a Büchner funnel, the sand was washed with 50 mL water. The coating step was performed as in the first method.
Unfortunately, also with such harsh condition for the chemical activation, we observed no weight loss in the TGA thermogram.

Silica coating

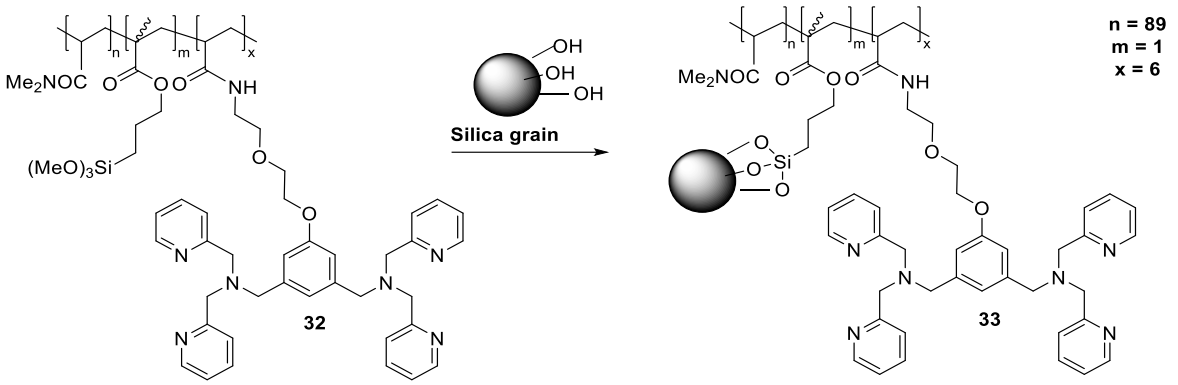

A 1%$_{w/v}$ solution of polymer **32** was prepared by dissolving 50 mg in 5 mL water obtaining a turbid suspension. 750 mg of amorphous silica (average particles size 100 µm, surface area 75 m^2/g) were added and the system was gently shaken for 1 h. The coating process was checked by ^{1}H-NMR (50 µL of the coating solution diluted with 450 µL D_2O). Upon completion, filtration on a Büchner funnel was performed and the solid residue washed with water. The filtrate was analysed by ^{1}H-NMR to assess absence of unreacted polymer **32**.

The solid was then subjected to curing (80°C, 15 minutes) and left under high vacuum for 24 h.

Yield: 800 mg, quantitative.

Thermogravimetric analysis (TGA)

15.70 mg of coated silica 33 were subjected to TGA analysis

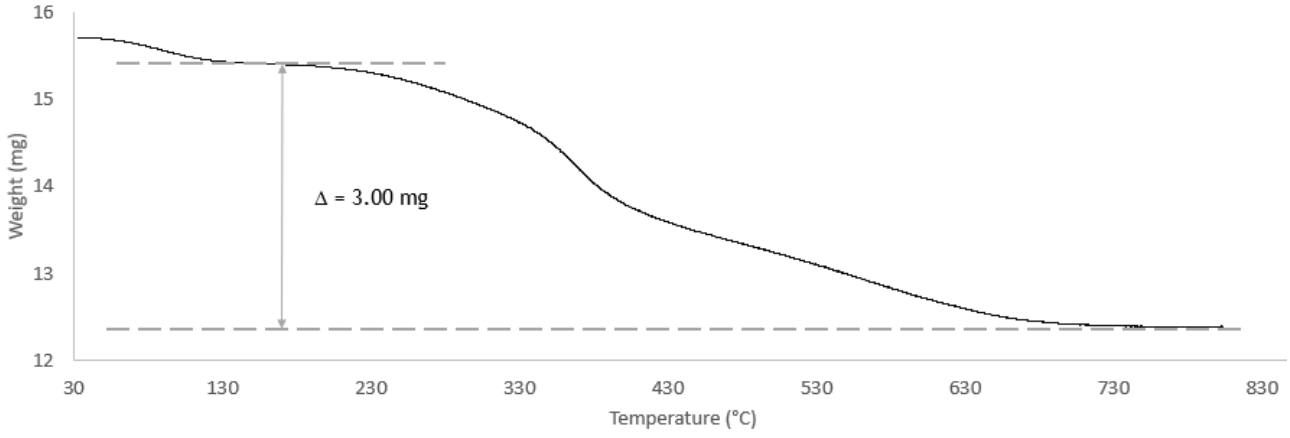

Weight variation (3.00 mg) suggested that one gram of solid **33** can lose up to 200 mg of material. The result is not in line with the amount of polymer **32** used during the coating. As matter of fact we used only 60 mg of functionalized polymer **32** per gram of silica.

Zinc incorporation

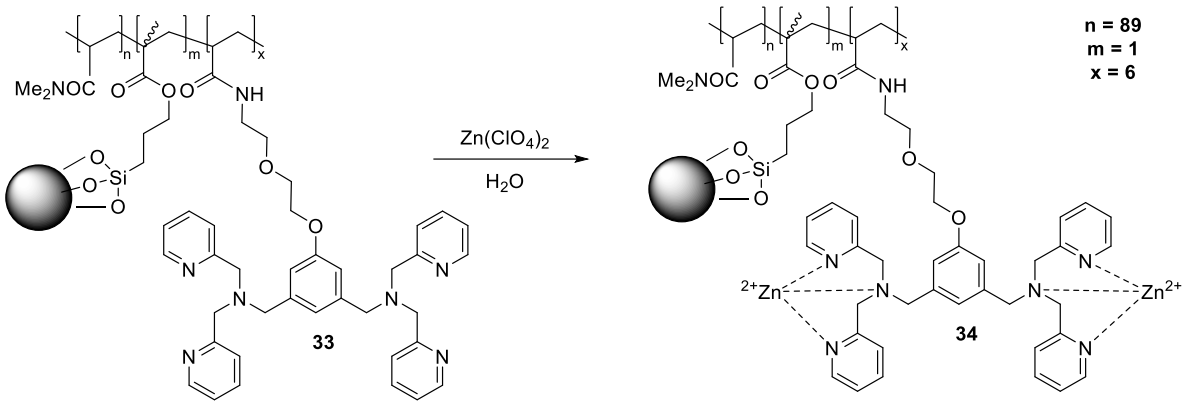

- **Method 1:** 1 mL of 0.21 M $Zn(ClO_4)_2$ water solution was added to 200 mg of coated silica **33**. The system was gently shaken for 30 minutes and the resulting resin **34** was filtered on a Büchner funnel, washed with water and dried overnight *in vacuo*.

- **Method 2:** 200 mg of coated silica **33** were packed in a 1 mL syringe equipped with a frit. 2 mL of a 0.21 M $Zn(ClO_4)_2$ water solution were slowly fluxed through the solid and the resulting resin **34** was washed with 5 mL water.

Zn^{2+} quantification: 100 mg of resin **34**, produced by either of the methods described above, were treated with 20 mL of a 2 M HCl solution for 30 minutes to ensure quantitative Zn^{2+} releasing. The solid was then filtered off and the acid solution subjected to atomic absorption spectroscopy (AAS). By such analysis, a Zn^{2+} concentration of 15.1 mg/mL was determined. From these data, we could calculate that 0.3 mg Zn^{2+} (corresponding to 4.6 µmol) were released from 100 mg of resin **34**, resulting in a Zn^{2+} concentration of 46 µmol/g resin **34**. Since two Zn^{2+} ions are required for nucleotide binding, we could assess that the maximum loading capacity should be 23 µmol nucleotide per g resin **34**.

Assessment of nucleotides retention

General procedure: 200 mg of resin **34** were packed in a column equipped with a frit (Ø = 1 cm, CV = 1 mL) and washed with 5 mL water to ensure proper swelling. 5 mM stock solutions of selected nucleotides (AMP, ADP, ATP, GMP, GDP and ppGpp) were prepared.

For each nucleotide, 200 µL aliquots of a 5 mM stock solution (corresponding to 1 µmol) were loaded on the column, followed by washing with 5 mL of either water or HEPES 10 mM (pH 8.5). 1 mL fractions were collected and analysed by UV-VIS spectrophotometry (λ = 256 nm for guanine-based nucleotides, 260 nm for adenine-based nucleotides) to determine the actual retention capacity of the resin.

Nucleotides release

General procedure: Washing with a releasing solution (0.1 M HCl) was performed to allow nucleotides release from resin **34**. 1 mL fractions were collected and analysed by UV-VIS spectrophotometry (λ = 256 nm for guanine-based nucleotides, 260 nm for adenine-based nucleotides). 6 mL of releasing solution were generally sufficient to ensure complete nucleotide recovery. After additional analyses by PEI-cellulose TLC (eluent: K_2HPO_4 0.75 M) and ^{1}H-NMR (D_2O, 400 MHz), collected fractions were lyophilized. The resulting powder was thus weighted, dissolved in DMSO-d^6 and checked by ^{1}H-NMR.

Resin regeneration

General procedure: After the nucleotide-releasing step, that required the use of an acidic solution, resin **34** was washed with 5 mL HEPES 10 mM (pH 8.5) to restore the optimal pH. Zn-DPA binding moieties were regenerated by slowly fluxing 2 mL of a 0.21 M $Zn(ClO_4)_2$ water solution through the resin. After washing with 5 mL water, the resin was tested again for nucleotide retention but showed a 30% lower capacity with respect to the freshly produced one.

Synthesis and purification of ppGpp

17 mL reaction mixture containing 6 mM **ATP** (57 mg, 0.104 mmol, 2 eq.) and 3 mM GDP (25 mg, 0.052 mmol, 1 eq.) were incubated with 100 mM NaCl, 50 mM HEPES (pH 8), 10 mM $MgCl_2$ and 1 mM DTT at 37°C for 2 h in presence of RelP enzyme (5 µM). The reaction was checked by both ^{1}H-NMR and PEI-cellulose TLC (eluent: 0.75 M K_2HPO_4). Upon completion, the reaction underwent purification as follows.

- **First step –** *Scavenging of unwanted nucleotide*

The pH of the reaction mixture was adjusted to 8.5 by two-fold dilution with $AcONH_4$ 0.25 M, pH 8.8. The resulting solution was fluxed through the previously packed boronic acid resin, equilibrated with the same $AcONH_4$ 0.25 M buffer. The flow-through fraction was checked by PEI-cellulose TLC (eluent: K_2HPO_4 0.75 M) to assess ppGpp presence and purity.

- **Second step –** *ppGpp precipitation*

A 10 M LiCl solution was added to the ppGpp-containing fractions in order to reach a final concentration of 1 M. The latter solution was diluted 4-fold with cold EtOH were added and the resulting suspension was incubated on ice for 20 min. After centrifugation at 4500 rpm (4 °C) for 20 minutes, the resulting white pellet was washed twice with cold EtOH and dried overnight *in vacuo*.

Such procedure allowed the isolation of 25 mg ppGpp as lithium salt (0.042 mmol), that corresponded to an 80% yield (with respect to GDP).

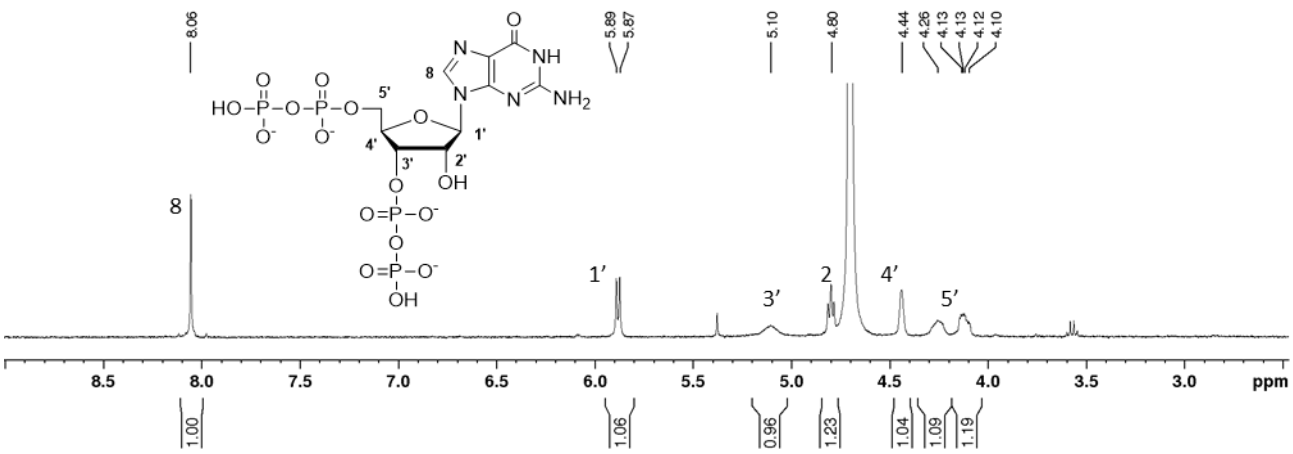

Eventual PPi presence was checked by a commercial PPi spectrophotometric assay (Merck; 2.1.3). The latter kit came as a powder, therefore before use, it was reconstituted by adding 4 mL of water. A blank solution was prepared by mixing, in a 3 mL quartz cuvette, 1 mL of water and 500 µL of reconstituted reactant. The absorbance of the latter solution (BLANK) was recorded at 340 nm over a period of 10 minutes (acquiring every 30 seconds).

In the meantime, a 10 mM ppGpp stock solution was prepared by dissolving 1 mg of ppGpp in 167 µL of water. In another 3 mL quartz cuvette, 975 µL of water, 500 of reactant and 25 µL of the ppGpp stock solution were mixed. The absorbance of the latter cuvette (TEST) was recorded at 340 nm over a period of 10 minutes (acquiring every 30 seconds).

By means of the equation **(1)**, reported in the bulletin of the PPi-assay Kit, it was possible to find out the concentration of PPi present in the stock solution used in the TEST sample.

(1) $(\Delta A_{TEST} - \Delta A_{BLANK}) \times 4.82$

Where ΔA_{TEST} is the variation of the absorbance measured at 340 nm of the TEST sample and ΔA_{BLANK} is the variation of the absorbance measured at 340 nm of the BLANK.

In our case, the value was close to zero, meaning that the ppGpp in hour hands was PPi free.

Annex I: Design of a new Atropine-based organocatalyst

Introduction:

'Organocatalysis is the catalysis with small organic molecules where metal is not part of the active principle'

Benjamin List

In the past 20 years, the field of chemistry known as "Organocatalysis" has experienced an exponential increase driven by a growing environmental interest. Indeed, the main purpose of organo-catalytic chemistry is to eliminate toxic waste since the need for sustainable chemistry is real and urgent.

Organocatalysis dates back to the early 1970s, when **L-Proline** (**62**) was used as chiral catalyst in an industrial process where compound **61** underwent Robinson annulation affording adduct **63** with a 70% of enantiomeric excess (e.e.)[88].

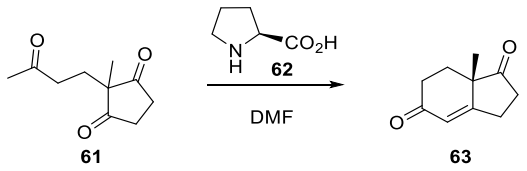

Scheme A: **chiral Robinson annulation driven by L-Proline[88]**

The potential of this result remained unconsidered until the beginning of the 21st century[89], when the use of small organic molecules as asymmetric catalysts began to take place. To date, a number of organocatalysts is available and organocatalysis is one of the pillars of asymmetric catalysis. The catalysis based on small organic molecules has important advantages as they are usually easily available and non-toxic. Furthermore, the absence of transition metals renders this methodology especially appealing for both pharmaceutical and environmental purposes.

Structural modification of proline could be exploited to improve both catalyst ability (e.g. better yields and/or better e.e) and versatility[90], e.g. proline solid-supported[91] or proline-based ligands like *Hayashi-Jørgensen* catalyst[92] (**Cat**). The latter is shown in scheme B, where propionaldehyde **64** and β-nitrostyrene **65** undergo a Michael addition[93].

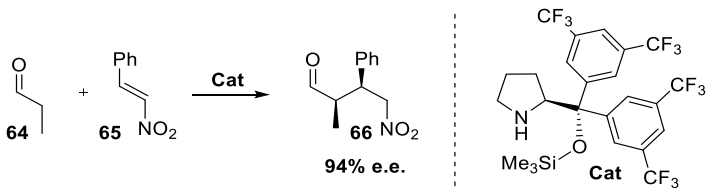

Scheme B: **Structure and an actual application of the Hayashi-Jørgensen[93] (Cat)**

Organocatalysis scope is broad as demonstrated by the numerous applications within several chemical classes. Among these *chiral phase transfer catalysis* (**PTC**)[94] together with accessible methodology for polar *double bonds reduction* (i.e. C=N, C=O)[95] and *carbon-carbon*[96] *bonds formation* are of particular interest for synthetic organic chemists. In the following paragraph, the mechanism of C-C bond formation will be discussed in detail due to its importance and application scope.

C-C bonds formation *via* enamine/iminium ion

The formation of carbon-carbon bonds by means of enamine chemistry (also known as *Schiff bases*) has been known for a long time. Catalytic activity in proline originates from the pyrrolidine moiety which forms an enamine in the presence of carbonyl substrates. In the example shown in scheme C[97], isobutyraldehyde (**67**) undergoes nucleophilic attack by the enamine adduct formed between **L-proline** and **acetone**. Directed by the hydrogen bond, the attack occurs on the *Re-face* of the aldehyde, leading to the formation of intermediate **67a**, which is subsequently hydrolyzed to obtain product **68.**

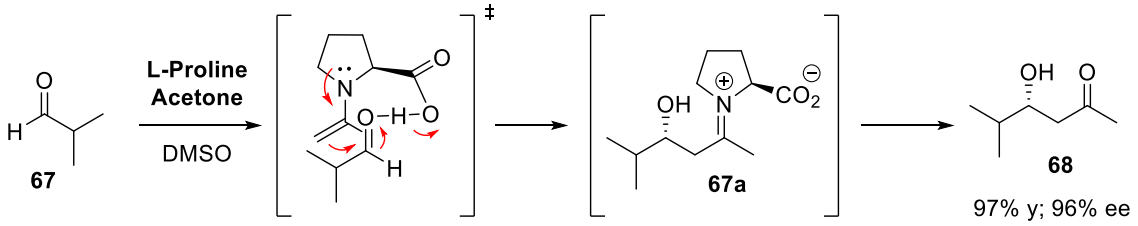

Scheme C: **Mechanism behind proline catalysis**[97]

Proline works very well with sterically non-hindered substrates, while bulkiness is detrimental to its catalytic ability as it prevents enamine formation. To overcome the problem a primary ammine could be employed, though the activation proceeds differently, as shown in Scheme D. A carbonyl compound reacts with either a secondary amine (*left*) or a primary amine (*right*) via enamine/iminium ion depending on carbonyl substrates bulkiness. With sterically non-hindered substrates, enamine formation is favored in the presence of secondary amine (Scheme D, top panel, left) while with a primary amine the iminium ion is preferred (Scheme D, top panel, right). If the substrate is bulky (Scheme D, bottom panel), the situation is the opposite i.e. enamine formation is disfavored with secondary amine and favored with primary amine.

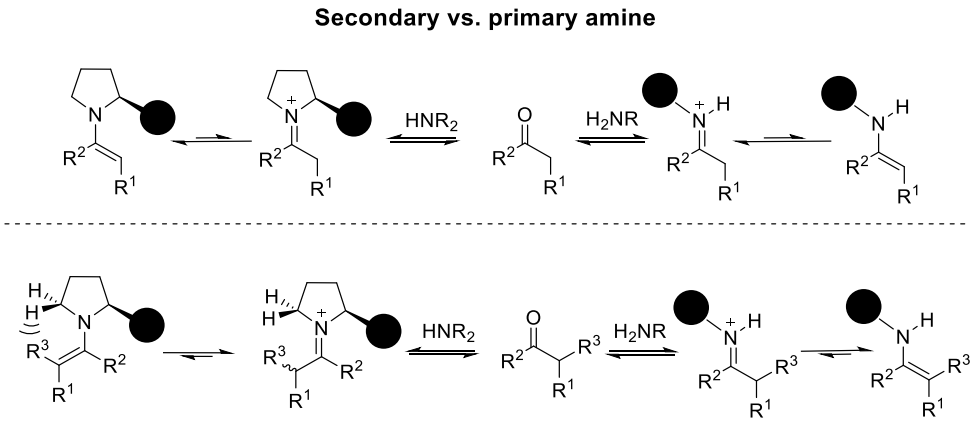

Scheme D: **Enamine/iminium ion competition with a primary (right) and a secondary (left) amine of a non-hindered carbonyl compound and a bulky one**

This mechanism of activation is exploited by amino-quinine shown in scheme E (**catalyst salt**), to efficiently catalyze Michael-type additions *via* iminium ion (Scheme E)[98]. In this case, the catalyst is used as N-Boc-(R)-phenylglycine di-salt to obtain the product in 96% e.e.

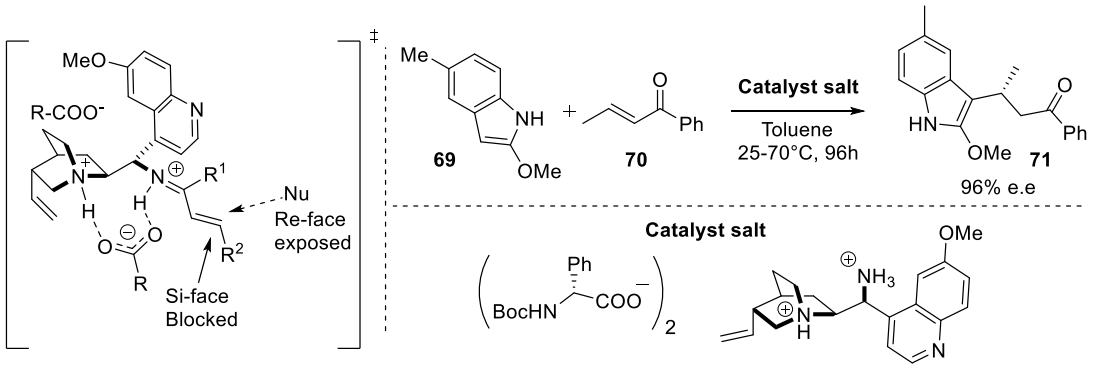

Scheme E: **Application of amino-quinine catalyst in Michael-type addition and the proposed transition state**[98]

The reaction proceeds through formation of the iminium ion between ketone **70** and the primary amino function of the catalyst. The presence of the quinoline ring alone is not sufficient to preferably direct the nucleophilic attack. Enantioselectivity originates indeed from the presence of a *R*-aminoacid residue that efficiently shields the *Si*-face of the iminium ion in the transition state (scheme E).

Aim of the project:

As part of my PhD work, I focused my attention on the synthesis of a new organocatalyst based on **atropine**[99]. Atropine is a natural alkaloid found in many plants, e.g. *Atropa belladonna* (commonly Deadly nightshade). For a long time, atropine has been used for its pharmacologic effects in the treatment of asthma, whooping cough, antiemetic and epilepsy, as it belongs to the muscarinic

receptor antagonist (MRA) family. Atropine is also well known for its remarkably poisonousness, the lowest oral toxic dose (TD_{Lo}) published for human is 33 µg/Kg. Atropine is extracted from plants as a racemic mixture (Figure A). Although the separation of the two enantiomers is possible and well described[100], they are marketed as racemate, since both enantiomers share almost the same pharmacologic effects.

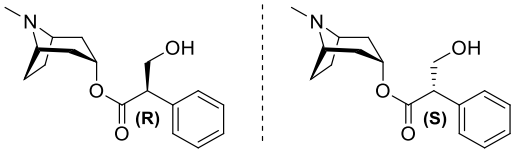

***Figure A*: Atropine enantiomers structure**

In literature there are no evidence of atropine's application as a catalyst. This molecule though shows some of the characteristics that normally belong to organocatalysts. First, it is obtained from natural sources, then, a few simple transformations are in principle sufficient to generate an active catalyst. From a structural point of view, it presents a rigid *tropane moiety* (dashed circle in Figure B). A similar moiety is present in quinine[101] (Figure B), which after appropriate modifications shows catalytic activity[102].

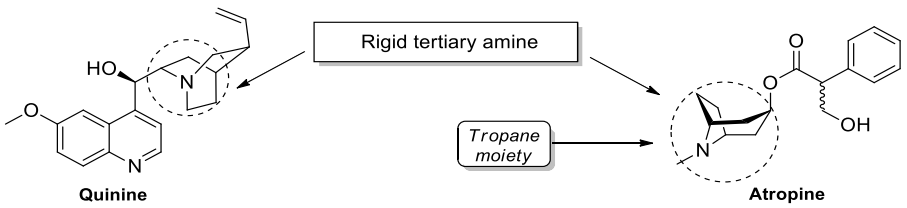

***Figure B:* Quinine vs. Atropine**

The tertiary amine is crucial to confer catalyst ability, as will be discussed later, but modifications on the OH-group are needed. For example, the amino-derivative of quinine (Figure C) was reported to be an efficient catalyst[102,103]. On this basis, I reasoned that an amino-derivative of atropine could act as catalyst as well, in particular **amino-atropine 72** (Figure C) has been designed for the purpose.

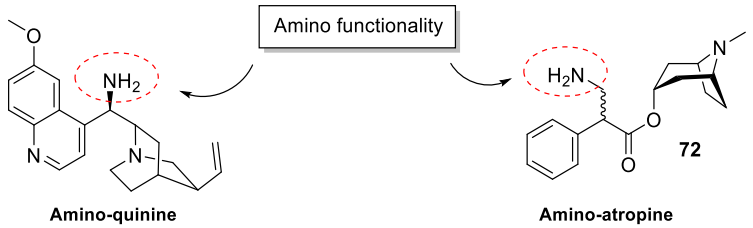

***Figure C:* Comparison between the amino-derived structures of quinine and atropine**

The amino-derivative of atropine (**Cat A**, Scheme F) can be expected to behave similarly to amino-quinine and catalyse Michael-type addition reactions via iminium ion intermediates. The 1,4 addition of a generic nucleophile to crotonaldehyde **73** generates a stereocenter, and the use of an appropriate chiral catalyst, such as **Cat A**, could provide mainly one of the enantiomers.

A model of the transition state for **Cat A** salt, based on the behavior of catalyst salt, is reported in Scheme F. The carboxyl group of the amino-acid residue could interact with the two quaternary nitrogen atoms of the catalyst through hydrogen bonds or electrostatic interactions. The latter interaction confers rigidity to the system allowing exposure of only one of the two iminium ion faces to nucleophilic attack, thus providing enantioselectivity.

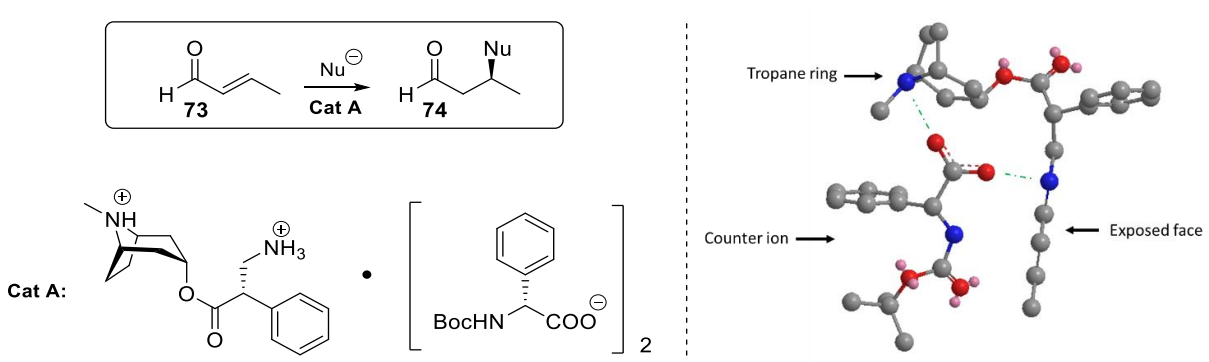

Scheme F: **Example of possible mechanism of an atropine-derived catalyst.**

On this basis, we decided to synthesize the amino-functionalized atropine salt and test its ability as asymmetric catalyst in *Michael-type* addition reactions.

Results and discussion:

To begin, I planned a synthetic pathway to obtain amino-atropine **72** (Figure C). The first step is the tosylation of the atropine hydroxyl group, followed by nucleophilic substitution with NaN_3 and subsequent reduction of the azide to primary amine (Scheme G). However, the first synthetic step led only to the elimination product **77**, rather than the desired compound **75**, mainly due to the high acidity of the α-proton (highlighted in red). Direct addition of ammonia to the conjugated double bond of ester **77** led to the desired product **72**, which was observed by mass analysis of the crude but was not stable under chromatographic purification conditions and could not be isolated. In contrast, addition of methylamine (adduct **78**) or dimethylamine (adduct **79**) led to the desired products in good yield (82% and 74%, respectively). Attempts to obtain the primary amine **72** *via*

the corresponding benzylamine precursors (**80** and **81**, fig. 4) were not successful since the addition reactions proceeded with almost no conversion.

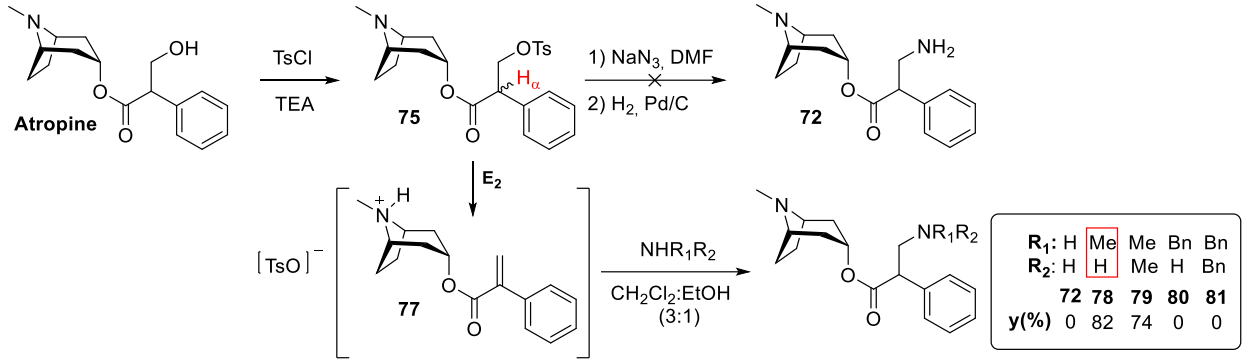

Scheme G: **Synthetic strategy for the synthesis of the amino-derivative of atropine**

As an alternative strategy, we tried to prepare an analogue of amino atropine **72** with one carbon less by reacting N-Boc-phenylglycine **83** with tropine **82** (Scheme H).

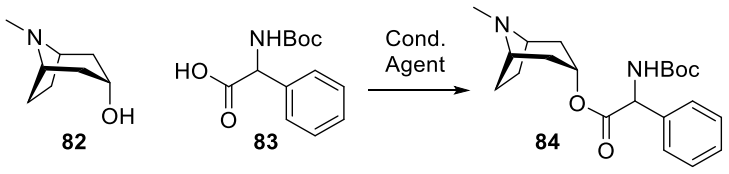

Scheme H: **Synthetic strategy for C-1 homologous synthesis**

TLC, ^{1}H-NMR and mass analysis confirmed that the ester **84** was formed but it did not survive work-up. Different condensing agents (i.e. DCC, EDC·HCl, HATU and CDI) and work-up procedures (i.e. direct chromatography, acidic or basic work-up) were screened, but product degradation was always observed. Despite all the obstacles found during the synthesis of the amino-atropine derivatives, the aminomethylderivative (**78**) could be easily obtained in good yields and we selected to use it for the first catalytic activity test (Scheme I) following the procedures reported for secondary amine catalysts[104,105].

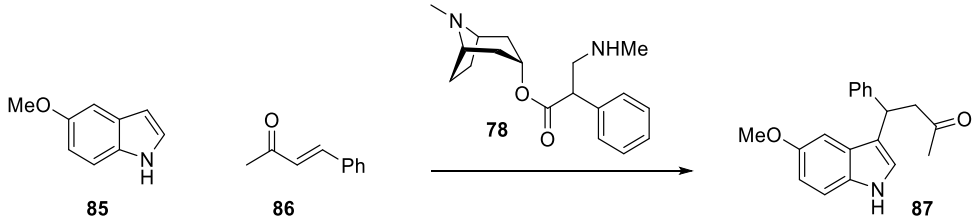

Scheme I: **Attempt of Friedel-Crafts reaction with α,β-unsaturated carbonyl compound.**

Thus molecule **78** was tested as organocatalyst in a Friedel-Crafts type reaction in which an α,β-conjugated carbonyl compound (ketone **86**) underwent Michael addition with 5-methoxyindole (**85**).

This reaction was described by Melchiorre et al.[105] using **85**, **86** and the catalyst **88** or **89** (Figure D) in the presence of TFA in 0.25 M toluene solution, respectively.

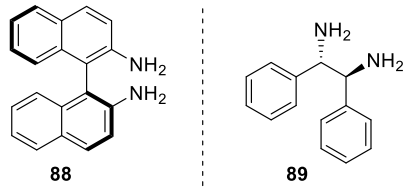

Figure D: **Structure of catalysts 88 and 89.**

To test **78**, the carbonyl compound **86** and the indole **85** were dissolved in toluene (0.25 M), in presence of 0.2 eq. of catalyst **78** and 0.4 eq. of **TFA**, as reported in literature[105]. The formation of a precipitate was immediately observed. This did not happen using either **88** or **89** in the same conditions, which afforded the expect product **87** in 52% and 46% yield, respectively. Most likely, catalyst **78** is not stable under the reaction conditions and indeed it is not recovered upon work-up, where **85** and **86** were recovered intact.

We also tested the catalytic ability of **78** under neutral conditions as described by Hong and coworkers[104]. Therefore, 0.2 eq. of catalyst were mixed with reactants **85** and **86** in MTBE. Also in this case, there is no formation of product **87** was observed as evaluated by ESI-MS analysis of the crude reaction mixture. The same analysis revealed disappearance of the catalyst at (m/z: 289.18) and the appearance of the atropine m/z peak at 290.18, thus hydrolysis of the catalyst amino function is occurring. We inferred that catalyst **78** cannot withstand the reaction conditions. Most likely, this is due to the relatively labile ester function, which needs to be replaced by a more stable moiety in the next generation atropine-derived catalysts.

Conclusion and considerations:

Despite the attractiveness of atropine-based catalysts, i.e. easy synthesis from cheap natural sources, these experiments pointed out some issues related to the feasibility of the catalyst synthesis itself. In particular, amino-atropine **72** in not stable, while methylamino-atropine **78** seems too fragile for standard reaction conditions employed for organocatalytic activation of carbonyl compounds. Due to these reasons, we decided to focus our attention on more promising projects.

Experimental section

Synthesis (1R,3r,5S)-8-methyl-8-azabicyclo[3.2.1]octan-3-yl 2-phenylacrylate (77)

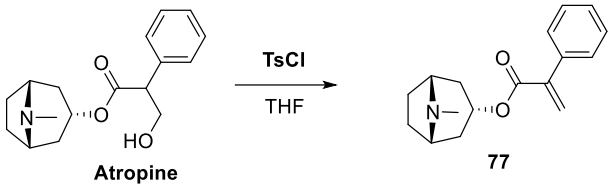

Atropine (1 g, 3.3 mmol, 1 eq.) was dissolved in dry THF (8.5 mL, [**Atropine**] = 0.4 M). **TsCl** (770 mg, 4 mmol, 1.2 eq.) was added to the mixture. The reaction was stirred overnight at rt (TLC CH_2Cl_2:MeOH 8:2 + 0.1% TEA R_f(**77**)= 0.5; Staining: Dragendorff). Upon completion, the reaction mixture was diluted with 10 mL of 3%$_{w/v}$ $NaHCO_3$ and stirred for 15 minutes. The product was extracted with EtOAc (3 x 15 mL). The organic phase was dried over Na_2SO_4 and the solvent evaporated to obtain pure product **77**. The crude was purified *via* automated flash chromatography (Eluent: CH_2Cl_2 with a gradient of MeOH from 0% to 20%).

Yield: 540 mg; 60%.

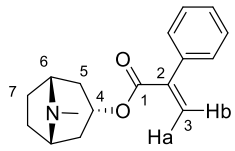

^{1}H-NMR (400MHz, $CDCl_3$): δ (ppm)= 7.48 - 7.32 (m, 5H, Ph), 6.38 (d, 1H, H_{3a}, J_{3a-3b} = 1.2 Hz), 5.91 (d, 1H, H_{3b}), 5.38 (t, 1H, H_4, J_{4-5} = 5.4 Hz), 3.17 (s, 2H, H_6), 2.42 - 2.24 (m, 5H, H_{5a}, NCH_3), 2.05 - 1.90 (m, 2 H, H_{5b}), 1.88 - 1.71 (m, 4H, H_7).

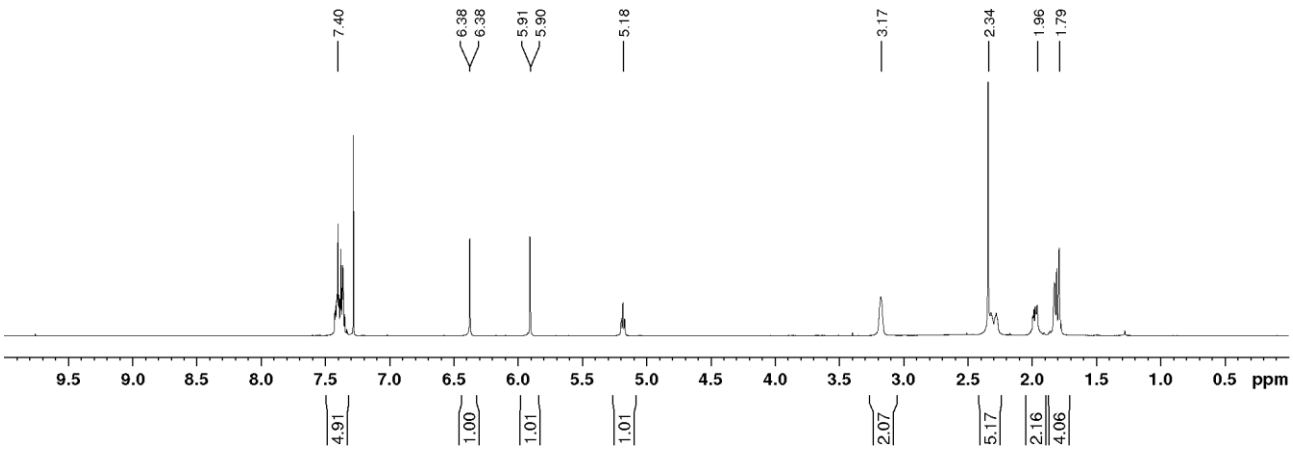

^{13}C-NMR (100MHz, $CDCl_3$): δ(ppm)= 165.4 (C_1), 128.5 - 128.0 (C_{ph}), 127.8 (C_3), 62.1 (C_4), 39.0 ($N\underline{C}H_3$), 35.5 (C_6), 33.9 (C_5), 24.4 (C_7).

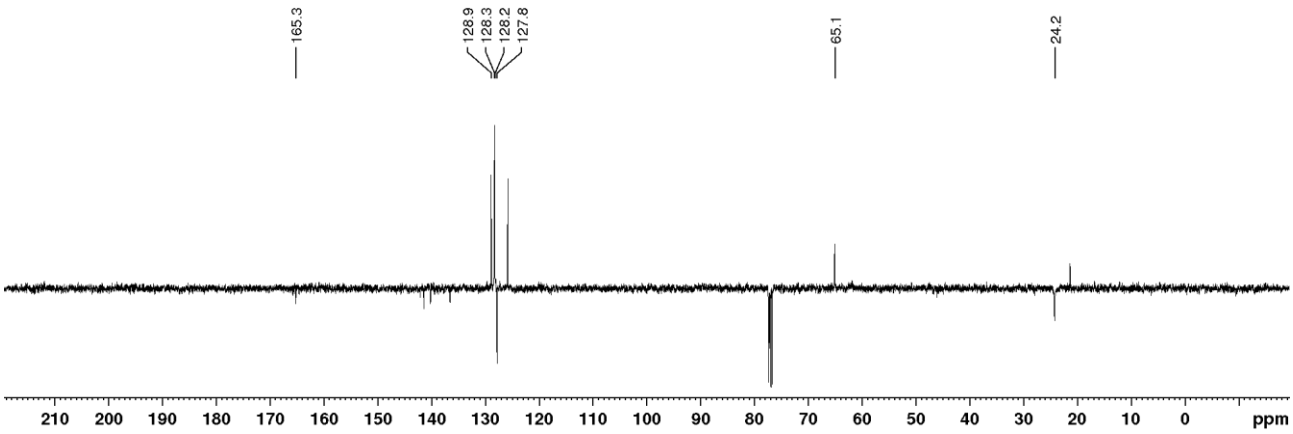

ESI-MS: calculated for $[C_{17}H_{22}NO_2]^+$: 272.16; found: 272.23.

Synthesis (1R,3r,5S)-8-methyl-8-azabicyclo[3.2.1]octan-3-yl 3-(dimethylamino)-2-phenylpropanoate (79)

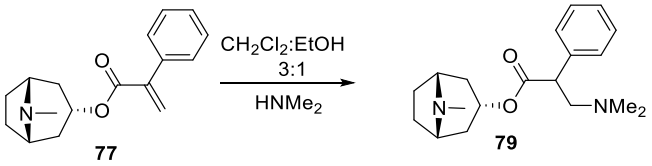

77 79

Compound **77** (64 mg, 0.17 mmol, 1 eq.) was dissolved in 600 µL of dry CH_2Cl_2. 200 µL of a 5 M dimethylamine (1 mmol, 5 eq.) ethanol solution was added. The reaction was stirred at rt for 25 minutes (TLC CH_2Cl_2:MeOH 8:2 + 0.1% TEA R_f(**79**)= 0.5; Staining: Dragendorff). Upon completion, volatiles are removed at reduced pressure. The product is consider sufficiently pure, therefore no other purifications steps are required.

Yield: 40 mg; 70%.

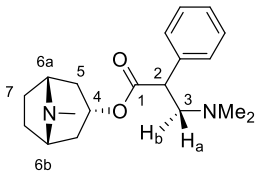

^{1}H-NMR (400MHz, $CDCl_3$): δ (ppm)= 7.40 - 7.21 (m, 5H, Ph), 4.96 (t, 1H, H_4, $J_{4\text{-}5}$ = 5.1 Hz), 3.80 - 3.68 (m, 1H, H_{3a}), 3.14 (t, 1H, H_4, $J_{2\text{-}3}$ = 11 Hz), 3.05 (s, 1H, H_{6a}), 2.96 (s, 1H, H_{6b}), 2.55 – 2.45 (m, 1H, H_{3b}), 2.46 (s, 6H, $H_2CN\underline{Me}_2$), 2.26 (s, 3H, N<u>Me</u>), 2.25 - 1.40 (m, 8H, H_5, H_7).

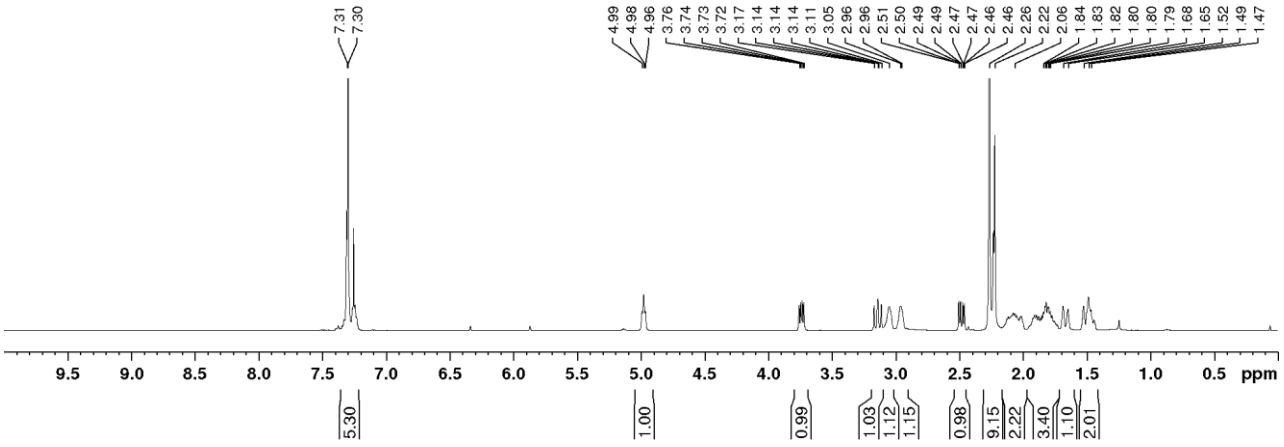

ESI-MS: calculated for $[C_{19}H_{29}N_2O_2]^+$: 317.22; found: 317.89.

Synthesis (1R,3r,5S)-8-methyl-8-azabicyclo[3.2.1]octan-3-yl 3-(methylamino)-2-phenylpropanoate (78)

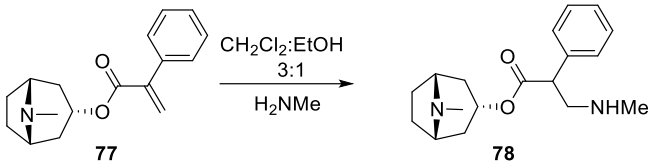

Compound **77** (100 mg, 0.25 mmol, 1 eq.) was dissolved in 940 µL of dry CH_2Cl_2 and 160 µL of EtOH. 220 µL of a 8 M methylamine (1.5 mmol, 7 eq.) ethanol solution was added. The reaction was stirred at rt for 1 h (TLC CH_2Cl_2:MeOH 8:2 + 0.1% TEA R_f(**78**)= 0.15; Staining: Dragendorff). Upon completion, volatiles were removed at reduced pressure. The crude was purified *via* automated chromatography (Eluent: CH_2Cl_2 with a gradient of MeOH from 0% to 10%).

Yield: 63 mg; 82%.

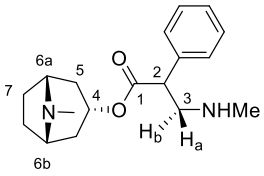

^{1}H-NMR (400MHz, $CDCl_3$): δ (ppm)= 7.40 - 7.20 (m, 5H, Ph), 4.98 (t, 1H, H_4, $J_{4\text{-}5}$ = 5.1 Hz), 3.80 - 3.73 (m, 1H, H_{3a}), 3.30 - 3.20 (m, 1H, H_2), 3.04 (s, 1H, H_{6a}), 2.95 – 2.85 (m, 2H, H_{3b}, H_{6b}), 2.43 (s, 3H, HNMe), 2.21 (s, 3H, NMe), 2.25 - 1.40 (m, 8H, H_5, H_7).

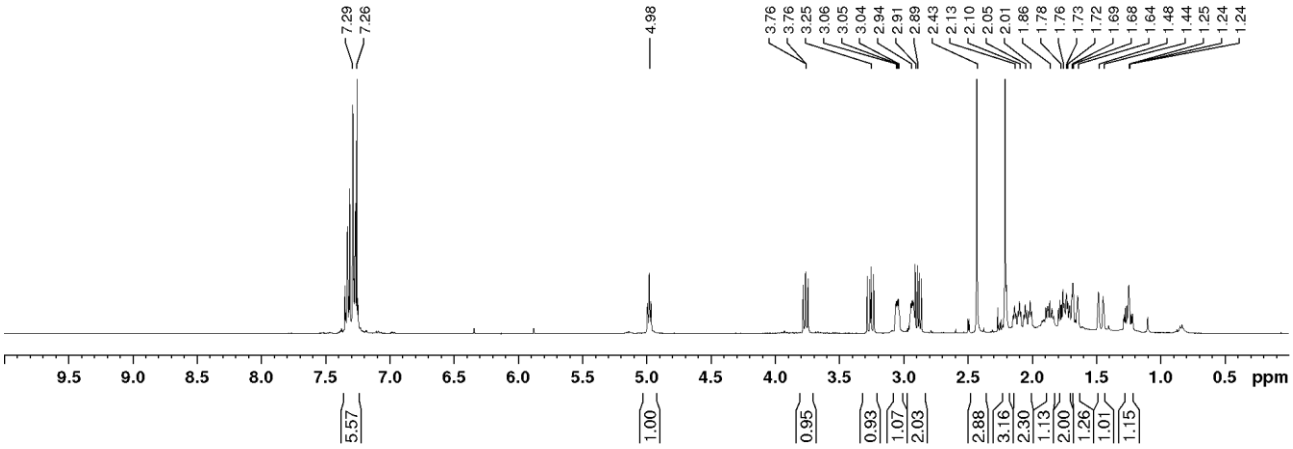

^{13}C-NMR (100MHz, $CDCl_3$): δ(ppm)= 172.2 (C_1), 137.3 (C_q), 129.0 - 127.7 (C_{ph}), 67.8 (C_4), 62.1 (C_6), 59.8 (C_3), 54.2 (C_2), 40.4 ($N\underline{C}H_3$), 36.5 ($HN\underline{C}H_3$), 36.2 (C_5), 25.5 (C_{7a}), 25.1 (C_{7b}).

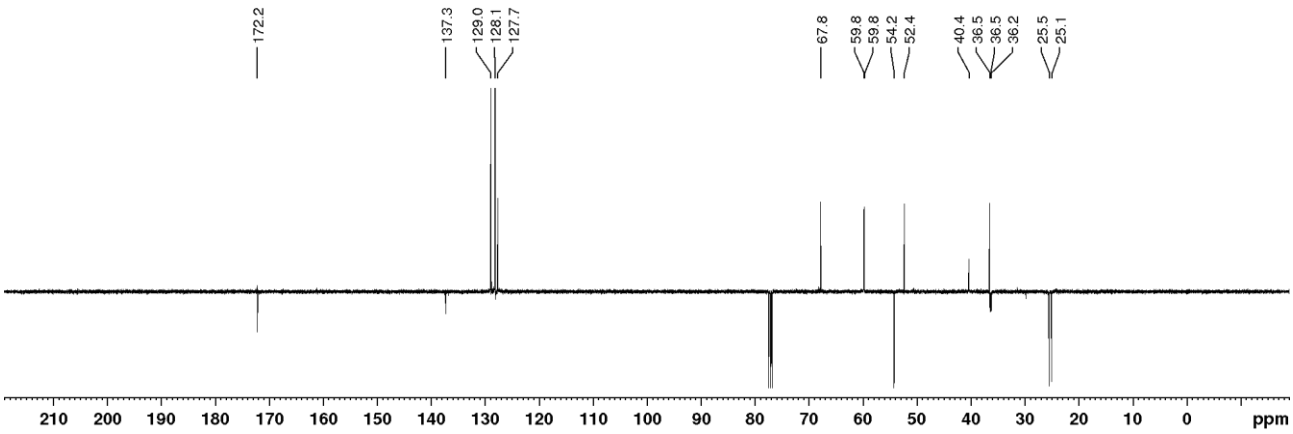

ESI-MS: calculated for $[C_{18}H_{27}N_2O_2]^+$: 303.20; found: 303.36.

Synthesis 4-(5-methoxy-1H-indol-3-yl)-4-phenylbutan-2-one (87)

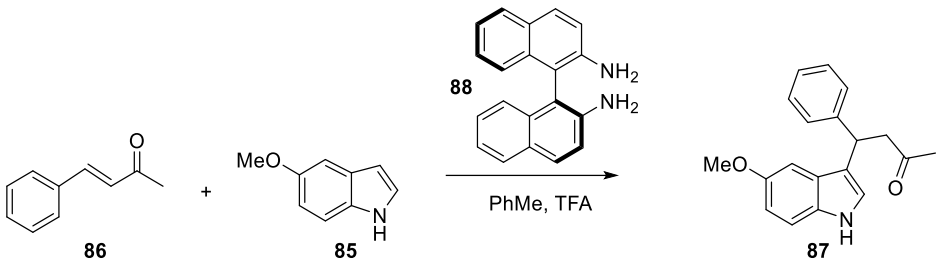

86 + 85 → 87

The catalyst **88** (20 mg, 0.07 mmol, 0.2 eq.) was dissolved in dry toluene (1.7 mL, [**86**] = 0.25 M). TFA (10 µL, 0.14 mmol, 0.4 eq.) was added to the mixture. After 5 minutes of stirring, ketone **86** (50 mg, 0.34 mmol, 1 eq.) was dissolved in the reaction mixture. After 10 minutes, indole **85** (60 mg, 0.4 mmol, 1.2 eq.) was added too. The reaction was stirred at rt 24 h (TLC Hex:EtOAc 8:2 R_f(**87**)= 0.15; Staining: Dragendorff). Upon completion, 4 mL of hexane were added to the reaction mixture. After 5 minutes of stirring, the mixture was filtered over a silica pad using a Hex:Et_2O (1:1) mixture. The solvent was evaporated to obtain pure product **87**. The crude was purified via automated flash chromatography (Eluent: Hex with a gradient of EtOAc from 15% to 60%).

Yield: 52 mg; 52%.

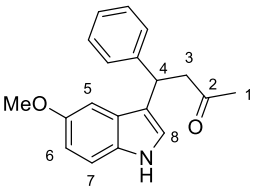

^{1}H-NMR (400MHz, $CDCl_3$): δ (ppm)= 7.96 (brd, 1H, NH), 7.36 - 7.13 (m, 6H, Ph, H_5), 6.96 (s, 1H, H_8), 6.87 - 6.77 (m, 2H, H_6, H_7), 4.78 (t, 1H, H_4, $J_{3\text{-}4}$ = 7.5 Hz), 3.75 (s, 3H, OMe), 3.30 - 3.10 (m, 2H, H_3), 2.08 (s, 3H, H_1).

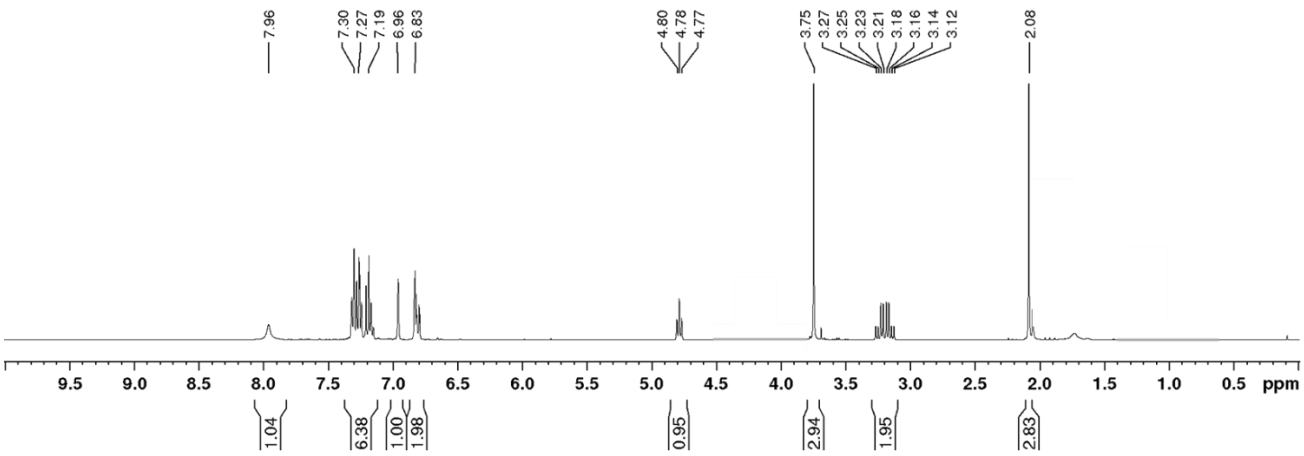

Bibliography

(1) Spellberg, B.; Blaser, M.; Guidos, R. J.; Boucher, H. W.; Bradley, J. S.; Eisenstein, B. I.; Gerding, D.; Lynfield, R.; Reller, L. B.; Rex, J.; Schwartz, D.; Septimus, E.; Tenover, F. C.; Gilbert, D. N. Combating Antimicrobial Resistance: Policy Recommendations to Save Lives. *Clin. Infect. Dis.* **2011**. https://doi.org/10.1093/cid/cir153.

(2) Balaban, N. Q.; Helaine, S.; Lewis, K.; Ackermann, M.; Aldridge, B.; Andersson, D. I.; Brynildsen, M. P.; Bumann, D.; Camilli, A.; Collins, J. J.; Dehio, C.; Fortune, S.; Ghigo, J. M.; Hardt, W. D.; Harms, A.; Heinemann, M.; Hung, D. T.; Jenal, U.; Levin, B. R.; Michiels, J.; Storz, G.; Tan, M. W.; Tenson, T.; Van Melderen, L.; Zinkernagel, A. Definitions and Guidelines for Research on Antibiotic Persistence. *Nat. Rev. Microbiol.* **2019**. https://doi.org/10.1038/s41579-019-0196-3.

(3) Irving, S. E.; Choudhury, N. R.; Corrigan, R. M. The Stringent Response and Physiological Roles of (Pp)PGpp in Bacteria. *Nature Reviews Microbiology*. 2020. https://doi.org/10.1038/s41579-020-00470-y.

(4) Alexander Fleming. On the Antibacterial Action of Cultures of a Penicillium, with Special Reference to Their Use in the Isolation of B. Injluenzae. *Br.]ournal Exp. Pathol.* **1929**.

(5) Abraham, E. P.; Chain, E. An Enzyme from Bacteria Able to Destroy Penicillin [1]. *Nature*. 1940. https://doi.org/10.1038/146837a0.

(6) Akatsu, S.; Noguchi, H. The Drug-Fastness of Spirochetes to Arsenic, Mercurial, and Iodide Compounds in Vitro. *J. Exp. Med.* **1917**. https://doi.org/10.1084/jem.25.3.349.

(7) Seydel, J. K. Sulfonamides, Structure-Activity Relationship, and Mode of Action. *J. Pharm. Sci.* **1968**. https://doi.org/10.1002/jps.2600570902.

(8) Huovinen, P.; Sundstrom, L.; Swedberg, G.; Skold, O. Trimethoprim and Sulfonamide Resistance. *Antimicrobial Agents and Chemotherapy*. 1995. https://doi.org/10.1128/aac.39.2.279.

(9) Benveniste, R.; Davies, J. R-Factor Mediated Gentamicin Resistance: A New Enzyme Which Modifies Aminoglycoside Antibiotics. *FEBS Lett.* **1971**. https://doi.org/10.1016/0014-5793(71)80282-X.

(10) Fauvart, M.; de Groote, V. N.; Michiels, J. Role of Persister Cells in Chronic Infections: Clinical Relevance and Perspectives on Anti-Persister Therapies. *Journal of Medical Microbiology*. 2011. https://doi.org/10.1099/jmm.0.030932-0.

(11) Bigger, J. W. The Bactericidal Action of Penicillin on Staphylococcus Pyogenes. *Ir. J. Med. Sci.* **1944**. https://doi.org/10.1007/BF02948462.

(12) Moyed, H. S.; Bertrand, K. P. HipA, a Newly Recognized Gene of Escherichia Coli K-12 That Affects Frequency of Persistence after Inhibition of Murein Synthesis. *J. Bacteriol.* **1983**. https://doi.org/10.1128/jb.155.2.768-775.1983.

(13) Korch, S. B.; Henderson, T. A.; Hill, T. M. Characterization of the HipA7 Allele of Escherichia Coli and Evidence That High Persistence Is Governed by (p)PpGpp Synthesis. *Mol. Microbiol.* **2003**. https://doi.org/10.1046/j.1365-2958.2003.03779.x.

(14) Balaban, N. Q.; Merrin, J.; Chait, R.; Kowalik, L.; Leibler, S. Bacterial Persistence as a Phenotypic Switch. *Science (80-.).* **2004**. https://doi.org/10.1126/science.1099390.

(15) Gefen, O.; Balaban, N. Q. The Importance of Being Persistent: Heterogeneity of Bacterial Populations under Antibiotic Stress: Review Article. *FEMS Microbiology Reviews*. 2009. https://doi.org/10.1111/j.1574-6976.2008.00156.x.

(16) De Groote, V. N.; Fauvart, M.; Kint, C. I.; Verstraeten, N.; Jans, A.; Cornelis, P.; Michiels, J. Pseudomonas Aeruginosa Fosfomycin Resistance Mechanisms Affect Non-Inherited Fluoroquinolone Tolerance. *J. Med. Microbiol.* **2011**. https://doi.org/10.1099/jmm.0.019703-0.

(17) Silver, L. L. Fosfomycin: Mechanism and Resistance. *Cold Spring Harb. Perspect. Med.* **2017**. https://doi.org/10.1101/cshperspect.a025262.

(18) Bernat, B. A.; Timothy Laughlin, L.; Armstrong, R. N. Fosfomycin Resistance Protein (FosA) Is a Manganese Metalloglutathione Transferase Related to Glyoxalase I and the Extradiol Dioxygenases. *Biochemistry* **1997**. https://doi.org/10.1021/bi963172a.

(19) Castañeda-García, A.; Rodríguez-Rojas, A.; Guelfo, J. R.; Blázquez, J. The Glycerol-3-Phosphate Permease GlpT Is the Only Fosfomycin Transporter in Pseudomonas Aeruginosa. *J. Bacteriol.* **2009**. https://doi.org/10.1128/JB.00748-09.

(20) Riordan, J. R.; Rommens, J. M.; Kerem, B. S.; Alon, N. O. A.; Rozmahel, R.; Grzelczak, Z.; Zielenski, J.; Lok, S. I.; Plavsic, N.; Chou, J. L.; Drumm, M. L.; Iannuzzi, M. C.; Collins, F. S.; Tsui, L. C. Identification of the Cystic Fibrosis Gene: Cloning and Characterization of Complementary DNA. *Science (80-.).* **1989**. https://doi.org/10.1126/science.2475911.

(21) Govan, J. R. W.; Deretic, V. Microbial Pathogenesis in Cystic Fibrosis: Mucoid Pseudomonas Aeruginosa and Burkholderia Cepacia. *Microbiological Reviews*. 1996. https://doi.org/10.1128/mmbr.60.3.539-574.1996.

(22) Mulcahy, L. R.; Burns, J. L.; Lory, S.; Lewis, K. Emergence of Pseudomonas Aeruginosa Strains Producing High Levels of Persister Cells in Patients with Cystic Fibrosis. *J. Bacteriol.* **2010**. https://doi.org/10.1128/JB.01651-09.

(23) Smith, E. E.; Buckley, D. G.; Wu, Z.; Saenphimmachak, C.; Hoffman, L. R.; D'Argenio, D. A.; Miller, S. I.; Ramsey, B. W.; Speert, D. P.; Moskowitz, S. M.; Burns, J. L.; Kaul, R.; Olson, M. V. Genetic Adaptation by Pseudomonas Aeruginosa to the Airways of Cystic Fibrosis Patients. *Proc. Natl. Acad. Sci. U. S. A.* **2006**. https://doi.org/10.1073/pnas.0602138103.

(24) LaFleur, M. D.; Kumamoto, C. A.; Lewis, K. Candida Albicans Biofilms Produce Antifungal-Tolerant Persister Cells. *Antimicrob. Agents Chemother.* **2006**. https://doi.org/10.1128/AAC.00684-06.

(25) WHO. *Global Tuberculosis Report 2018. Geneva: World Health Organization; 2018.*; 2018. https://doi.org/WHO/HTM/TB/2017.23.

(26) Ojha, A. K.; Baughn, A. D.; Sambandan, D.; Hsu, T.; Trivelli, X.; Guerardel, Y.; Alahari, A.; Kremer, L.; Jacobs, W. R.; Hatfull, G. F. Growth of Mycobacterium Tuberculosis Biofilms Containing Free Mycolic Acids and Harbouring Drug-Tolerant Bacteria. *Mol. Microbiol.* **2008**. https://doi.org/10.1111/j.1365-2958.2008.06274.x.

(27) Torrey, H. L.; Keren, I.; Via, L. E.; Lee, J. S.; Lewis, K. High Persister Mutants in Mycobacterium Tuberculosis. *PLoS One* **2016**. https://doi.org/10.1371/journal.pone.0155127.

(28) Wakamoto, Y.; Dhar, N.; Chait, R.; Schneider, K.; Signorino-Gelo, F.; Leibler, S.; McKinney, J. D. Dynamic Persistence of Antibiotic-Stressed Mycobacteria. *Science (80-.).* **2013**. https://doi.org/10.1126/science.1229858.

(29) Wilmaerts, D.; Windels, E. M.; Verstraeten, N.; Michiels, J. General Mechanisms Leading to Persister Formation and Awakening. *Trends in Genetics*. 2019. https://doi.org/10.1016/j.tig.2019.03.007.

(30) Wang, T.; El Meouche, I.; Dunlop, M. J. Bacterial Persistence Induced by Salicylate via Reactive Oxygen Species. *Sci. Rep.* **2017**. https://doi.org/10.1038/srep43839.

(31) Dörr, T.; Vulić, M.; Lewis, K. Ciprofloxacin Causes Persister Formation by Inducing the TisB Toxin in Escherichia Coli. *PLoS Biol.* **2010**. https://doi.org/10.1371/journal.pbio.1000317.

(32) Barraud, N.; Buson, A.; Jarolimek, W.; Rice, S. A. Mannitol Enhances Antibiotic Sensitivity of Persister Bacteria in Pseudomonas Aeruginosa Biofilms. *PLoS One* **2013**. https://doi.org/10.1371/journal.pone.0084220.

(33) Conlon, B. P.; Nakayasu, E. S.; Fleck, L. E.; Lafleur, M. D.; Isabella, V. M.; Coleman, K.; Leonard, S. N.; Smith, R. D.; Adkins, J. N.; Lewis, K. Activated ClpP Kills Persisters and Eradicates a Chronic Biofilm Infection. *Nature* **2013**. https://doi.org/10.1038/nature12790.

(34) Pu, Y.; Li, Y.; Jin, X.; Tian, T.; Ma, Q.; Zhao, Z.; Lin, S. yuan; Chen, Z.; Li, B.; Yao, G.; Leake, M. C.; Lo, C. J.; Bai, F. ATP-Dependent Dynamic Protein Aggregation Regulates Bacterial Dormancy Depth Critical for Antibiotic Tolerance. *Mol. Cell* **2019**. https://doi.org/10.1016/j.molcel.2018.10.022.

(35) Kalia, D.; Merey, G.; Nakayama, S.; Zheng, Y.; Zhou, J.; Luo, Y.; Guo, M.; Roembke, B. T.; Sintim, H. O. Nucleotide, c-Di-GMP, c-Di-AMP, CGMP, CAMP, (p)PpGpp Signaling in Bacteria and Implications in Pathogenesis. *Chemical Society Reviews*. 2013. https://doi.org/10.1039/c2cs35206k.

(36) Germain, E.; Castro-Roa, D.; Zenkin, N.; Gerdes, K. Molecular Mechanism of Bacterial Persistence by HipA. *Mol. Cell* **2013**. https://doi.org/10.1016/j.molcel.2013.08.045.

(37) Takahashi, K.; Kasai, K.; Ochi, K. Identification of the Bacterial Alarmone Guanosine 5'-Diphosphate 3'-Diphosphate (PpGpp) in Plants. *Proc. Natl. Acad. Sci. U. S. A.* **2004**. https://doi.org/10.1073/pnas.0308555101.

(38) Irving, S. E.; Corrigan, R. M. Triggering the Stringent Response: Signals Responsible for Activating (p)PpGpp Synthesis in Bacteria. *Microbiology (United Kingdom)*. 2018. https://doi.org/10.1099/mic.0.000621.

(39) Glass, T. L.; Holmes, W. M.; Hylemon, P. B.; Stellwag, E. J. Synthesis of Guanosine Tetra- and Pentaphosphates by the Obligately Anaerobic Bacterium Bacteroides Thetaiotaomicron in Response to Molecular Oxygen. *J. Bacteriol.* **1979**. https://doi.org/10.1128/jb.137.2.956-962.1979.

(40) Wells, D. H.; Gaynor, E. C. Helicobacter Pylori Initiates the Stringent Response upon Nutrient and PH Downshift. *J. Bacteriol.* **2006**. https://doi.org/10.1128/JB.188.10.3726-3729.2006.

(41) Gallant, J.; Palmer, L.; Pao, C. C. Anomalous Synthesis of PpGpp in Growing Cells. *Cell* **1977**. https://doi.org/10.1016/0092-8674(77)90329-4.

(42) Hood, R. D.; Higgins, S. A.; Flamholz, A.; Nichols, R. J.; Savage, D. F. The Stringent Response Regulates Adaptation to Darkness in the Cyanobacterium Synechococcus Elongatus. *Proc. Natl. Acad. Sci. U. S. A.* **2016**. https://doi.org/10.1073/pnas.1524915113.

(43) Costanzo, A.; Ades, S. E. Growth Phase-Dependent Regulation of the Extracytoplasmic Stress Factor, ΣE, by Guanosine 3',5'-Bispyrophosphate (PpGpp). *J. Bacteriol.* **2006**. https://doi.org/10.1128/JB.01981-05.

(44) Gaca, A. O.; Colomer-Winter, C.; Lemos, J. A. Many Means to a Common End: The Intricacies of (p)PpGpp Metabolism and Its Control of Bacterial Homeostasis. *Journal of Bacteriology*. 2015. https://doi.org/10.1128/JB.02577-14.

(45) Shimada, T.; Yoshida, H.; Ishihama, A. Involvement of Cyclic AMP Receptor Protein in Regulation of the Rmf Gene Encoding the Ribosome Modulation Factor in Escherichia Coli. *J. Bacteriol.* **2013**. https://doi.org/10.1128/JB.02279-12.

(46) Pacios, O.; Blasco, L.; Bleriot, I.; Fernandez-Garcia, L.; Ambroa, A.; López, M.; Bou, G.; Cantón, R.; Garcia-Contreras, R.; Wood, T. K.; Tomás, M. (P)PpGpp and Its Role in Bacterial Persistence: New Challenges. *Antimicrob. Agents Chemother.* **2020**. https://doi.org/10.1128/AAC.01283-20.

(47) Atkinson, G. C.; Tenson, T.; Hauryliuk, V. The RelA/SpoT Homolog (RSH) Superfamily: Distribution and Functional Evolution of Ppgpp Synthetases and Hydrolases across the Tree of Life. *PLoS One*

2011. https://doi.org/10.1371/journal.pone.0023479.

(48) Hogg, T.; Mechold, U.; Malke, H.; Cashel, M.; Hilgenfeld, R. Conformational Antagonism between Opposing Active Sites in a Bifunctional RelA/SpoT Homolog Modulates (p)PpGpp Metabolism during the Stringent Response. *Cell* **2004**. https://doi.org/10.1016/S0092-8674(04)00260-0.

(49) Mechold, U.; Potrykus, K.; Murphy, H.; Murakami, K. S.; Cashel, M. Differential Regulation by PpGpp versus PppGpp in Escherichia Coli. *Nucleic Acids Res.* **2013**. https://doi.org/10.1093/nar/gkt302.

(50) Mechold, U.; Murphy, H.; Brown, L.; Cashel, M. Intramolecular Regulation of the Opposing (p)PpGpp Catalytic Activities of RelSeq, the Rel/Spo Enzyme from Streptococcus Equisimilis. *J. Bacteriol.* **2002**. https://doi.org/10.1128/JB.184.11.2878-2888.2002.

(51) Hogg, T.; Mechold, U.; Malke, H.; Cashel, M.; Hilgenfeld, R. Erratum: Conformational Antagonism between Opposing Active Sites in a Bifunctional RelA/SpoT Homolog Modulates (p)PpGpp Metabolism during the Stringent Response (Cell (April 2, 2004) 117 (57-68)). *Cell*. 2004. https://doi.org/10.1016/S0092-8674(04)00406-4.

(52) Manav, M. C.; Beljantseva, J.; Bojer, M. S.; Tenson, T.; Ingmer, H.; Hauryliuk, V.; Brodersen, D. E. Structural Basis for (p)PpGpp Synthesis by the Staphylococcus Aureus Small Alarmone Synthetase RelP. *J. Biol. Chem.* **2018**. https://doi.org/10.1074/jbc.RA117.001374.

(53) Syal, K.; Joshi, H.; Chatterji, D.; Jain, V. Novel PppGpp Binding Site at the C-Terminal Region of the Rel Enzyme from Mycobacterium Smegmatis. *FEBS J.* **2015**. https://doi.org/10.1111/febs.13373.

(54) Krohn, M.; Wagner, R. Procedure for the Rapid Preparation of Guanosine Tetraphosphate (PpGpp) from Escherichia Coli Ribosomes. *Anal. Biochem.* **1995**. https://doi.org/10.1006/abio.1995.1138.

(55) Cruvinel, G. T.; Neves, H. I.; Spira, B. Glyphosate Induces the Synthesis of PpGpp. *Mol. Genet. Genomics* **2019**, *294* (1), 191–198. https://doi.org/10.1007/s00438-018-1499-1.

(56) Kim, E. E.; Wyckoff, H. W. Reaction Mechanism of Alkaline Phosphatase Based on Crystal Structures. Two-Metal Ion Catalysis. *J. Mol. Biol.* **1991**. https://doi.org/10.1016/0022-2836(91)90724-K.

(57) Sakamoto, T.; Ojida, A.; Hamachi, I. Molecular Recognition, Fluorescence Sensing, and Biological Assay of Phosphate Anion Derivatives Using Artificial Zn(II)-Dpa Complexes. *Chem. Commun.* **2009**. https://doi.org/10.1039/b812374h.

(58) Uddin, M. G.; Zafrul Azam, A. T. M. A Novel Oligo-DNA Probe Carrying Non-Nucleosidic Silylated Pyrene Derivatives: Synthesis and Excimer Forming Ability. *Am. J. Biochem. Mol. Biol.* **2013**. https://doi.org/10.39231ajbmb.2013.175.181.

(59) Nishizawa, S.; Kato, Y.; Teramae, N. Fluorescence Sensing of Anions via Intramolecular Excimer Formation in a Pyrophosphate-Induced Self-Assembly of a Pyrene-Functionalized Guanidinium Receptor [9]. *Journal of the American Chemical Society*. 1999. https://doi.org/10.1021/ja991497j.

(60) Cho, H. K.; Lee, D. H.; Hong, J. I. A Fluorescent Pyrophosphate Sensor via Excimer Formation in Water. *Chem. Commun.* **2005**. https://doi.org/10.1039/b417845a.

(61) Rhee, H. W.; Lee, C. R.; Cho, S. H.; Song, M. R.; Cashel, M.; Choy, H. E.; Seok, Y. J.; Hong, J. I. Selective Fluorescent Chemosensor for the Bacterial Alarmone (p)PpGpp. *J. Am. Chem. Soc.* **2008**. https://doi.org/10.1021/ja0759139.

(62) Nugent, J. W.; Lee, H.; Lee, H. S.; Reibenspies, J. H.; Hancock, R. D. Mechanism of Chelation Enhanced Fluorescence in Complexes of Cadmium(Ii), and a Possible New Type of Anion Sensor. *Chem. Commun.* **2013**. https://doi.org/10.1039/c3cc45829f.

(63) Fontaine, B. M.; Duggal, Y.; Weinert, E. E. Exploring the Links between Nucleotide Signaling and Quorum Sensing Pathways in Regulating Bacterial Virulence. *ACS Infectious Diseases*. 2018.

https://doi.org/10.1021/acsinfecdis.8b00255.

(64) Glaser, C. Untersuchungen Über Einige Derivate Der Zimmtsäure. *Justus Liebigs Ann. Chem.* **1870**. https://doi.org/10.1002/jlac.18701540202.

(65) Addy, P. S.; Saha, B.; Singh, N. D. P.; Das, A. K.; Bush, J. T.; Lejeune, C.; Schofield, C. J.; Basak, A. 1,3,5-Trisubstituted Benzenes as Fluorescent Photoaffinity Probes for Human Carbonic Anhydrase II Capture. *Chem. Commun.* **2013**. https://doi.org/10.1039/c3cc38251f.

(66) Oh, J.; Hong, J. I. Discrimination of Redox-Responsible Biomolecules by a Single Molecular Sensor. *Org. Lett.* **2013**. https://doi.org/10.1021/ol303403x.

(67) Conti, G.; Minneci, M.; Sattin, S. Optimised Synthesis of the Bacterial Magic Spot (P)PpGpp Chemosensor PyDPA. *ChemBioChem* **2019**. https://doi.org/10.1002/cbic.201900013.

(68) Jain, V.; Saleem-Batcha, R.; China, A.; Chatterji, D. Molecular Dissection of the Mycobacterial Stringent Response Protein Rel. *Protein Sci.* **2006**. https://doi.org/10.1110/ps.062117006.

(69) Hara, A.; Sy, J. Guanosine 5'-Triphosphate, 3'-Diphosphate 5'-Phosphohydrolase. Purification and Substrate Specificity. *J. Biol. Chem.* **1983**. https://doi.org/10.1016/S0021-9258(18)33039-4.

(70) Guo, B.; Gurel, P. S.; Shu, R.; Higgs, H. N.; Pellegrini, M.; Mierke, D. F. Monitoring ATP Hydrolysis and ATPase Inhibitor Screening Using 1H NMR. *Chem. Commun.* **2014**. https://doi.org/10.1039/c4cc04399e.

(71) Van Duin, M.; Peters, J. A.; Kieboom, A. P. G.; Van Bekkum, H. Studies on Borate Esters 1. The Ph Dependence of the Stability of Esters of Boric Acid and Borate in Aqueous Medium as Studied by 11B NMR. *Tetrahedron* **1984**. https://doi.org/10.1016/S0040-4020(01)91300-6.

(72) Steinchen, W.; Schuhmacher, J. S.; Altegoer, F.; Fage, C. D.; Srinivasan, V.; Linne, U.; Marahiel, M. A.; Bange, G. Catalytic Mechanism and Allosteric Regulation of an Oligomeric (p)PpGpp Synthetase by an Alarmone. *Proc. Natl. Acad. Sci. U. S. A.* **2015**. https://doi.org/10.1073/pnas.1505271112.

(73) O'Brien, W. E. A Continuous Spectrophotometric Assay for Argininosuccinate Synthetase Based on Pyrophosphate Formation. *Anal. Biochem.* **1976**. https://doi.org/10.1016/0003-2697(76)90337-7.

(74) Merrifield, R. B. Solid Phase Peptide Synthesis. I. The Synthesis of a Tetrapeptide. *J. Am. Chem. Soc.* **1963**. https://doi.org/10.1021/ja00897a025.

(75) Flynn, D. L.; Crich, J. Z.; Devraj, R. V.; Hockerman, S. L.; Parlow, J. J.; South, M. S.; Woodard, S. Chemical Library Purification Strategies Based on Principles of Complementary Molecular Reactivity and Molecular Recognition. *J. Am. Chem. Soc.* **1997**. https://doi.org/10.1021/ja963462e.

(76) Sabatini, V.; Pargoletti, E.; Longoni, M.; Farina, H.; Ortenzi, M. A.; Cappelletti, G. Stearyl Methacrylate Co-Polymers: Towards New Polymer Coatings for Mortars Protection. *Appl. Surf. Sci.* **2019**. https://doi.org/10.1016/j.apsusc.2019.05.097.

(77) Zilio, C.; Sola, L.; Damin, F.; Faggioni, L.; Chiari, M. Erratum to: Universal Hydrophilic Coating of Thermoplastic Polymers Currently Used in Microfluidics (Biomedical Microdevices (2014) 16, (107-114) DOI: 10.1007/S10544-013-9810-8). *Biomedical Microdevices*. 2014. https://doi.org/10.1007/s10544-014-9840-x.

(78) Roncada, P.; Cretich, M.; Fortin, R.; Agosti, S.; De Franceschi, L.; Greppi, G. F.; Turrini, F.; Carta, F.; Turri, S.; Levi, M.; Chiari, M. Acrylamide-Agarose Copolymers: Improved Resolution of High Molecular Mass Proteins in Two-Dimensional Gel Electrophoresis. In *Proteomics*; 2005. https://doi.org/10.1002/pmic.200401272.

(79) M. Costantini; S. Sattin. Manuscript in Preparation.

(80) Angiolini, L.; Benelli, T.; Giorgini, L.; Mauriello, F.; Salatelli, E. New Optically Active Methacrylic

Polymers Bearing Side-Chain Bisazoaromatic Moieties. *Macromol. Chem. Phys.* **2007**. https://doi.org/10.1002/macp.200600497.

(81) Bhattacharya, S.; Datta, A.; Berg, J. M.; Gangopadhyay, S. Studies on Surface Wettability of Poly(Dimethyl) Siloxane (PDMS) and Glass under Oxygen-Plasma Treatment and Correlation with Bond Strength. *J. Microelectromechanical Syst.* **2005**. https://doi.org/10.1109/JMEMS.2005.844746.

(82) Suriano, R.; Levi, M.; Pirri, G.; Damin, F.; Chiari, M.; Turri, S. Surface Behavior and Molecular Recognition in DNA Microarrays from N,N-Dimethylacrylamide Terpolymers with Activated Esters as Linking Groups. *Macromol. Biosci.* **2006**. https://doi.org/10.1002/mabi.200600088.

(83) Schoff, C. K. Thermogravimetric Analysis. *CoatingsTech*. 2009. https://doi.org/10.3139/9781569906446.010.

(84) Beaulieu, N.; Dickinson, R. A.; Deslongchamps, P. Stereoelectronic Control in Acetal Formation. *Can. J. Chem.* **1980**. https://doi.org/10.1139/v80-405.

(85) Viegas, A.; Manso, J.; Nobrega, F. L.; Cabrita, E. J. Saturation-Transfer Difference (STD) NMR: A Simple and Fast Method for Ligand Screening and Characterization of Protein Binding. *J. Chem. Educ.* **2011**. https://doi.org/10.1021/ed101169t.

(86) Vasile, F.; Della Volpe, S.; Ambrosio, F. A.; Costa, G.; Unver, M. Y.; Zucal, C.; Rossi, D.; Martino, E.; Provenzani, A.; Hirsch, A. K. H.; Alcaro, S.; Potenza, D.; Collina, S. Exploration of Ligand Binding Modes towards the Identification of Compounds Targeting HuR: A Combined STD-NMR and Molecular Modelling Approach. *Sci. Rep.* **2018**. https://doi.org/10.1038/s41598-018-32084-z.

(87) Hales, T. C. A Proof of the Kepler Conjecture. *Annals of Mathematics*. 2005. https://doi.org/10.4007/annals.2005.162.1065.

(88) Hajos, Z. G.; Parrish, D. R. Asymmetric Synthesis of Bicyclic Intermediates of Natural Product Chemistry. *J. Org. Chem.* **1974**. https://doi.org/10.1021/jo00925a003.

(89) List, B. Proline-Catalyzed Asymmetric Reactions. *Tetrahedron*. 2002. https://doi.org/10.1016/S0040-4020(02)00516-1.

(90) Wang, J.; Li, H.; Mei, Y.; Lou, B.; Xu, D.; Xie, D.; Guo, H.; Wang, W. Direct, Facile Aldehyde and Ketone α-Selenenylation Reactions Promoted by L-Prolinamide and Pyrrolidine Sulfonamide Organocatalysts. *J. Org. Chem.* **2005**. https://doi.org/10.1021/jo0506940.

(91) Cozzi, F. Immobilization of Organic Catalysts: When, Why, and How. *Advanced Synthesis and Catalysis*. 2006. https://doi.org/10.1002/adsc.200606096.

(92) Franzén, J.; Marigo, M.; Fielenbach, D.; Wabnitz, T. C.; Kjærsgaard, A.; Jørgensen, K. A. A General Organocatalyst for Direct α-Functionalization of Aldehydes: Stereoselective C-C, C-N, C-F, C-Br, and C-S Bond-Forming Reactions. Scope and Mechanistic Insights. *J. Am. Chem. Soc.* **2005**. https://doi.org/10.1021/ja056120u.

(93) Zhang, Y.; Wang, C.; Huang, W.; Haruehanroengra, P.; Peng, C.; Sheng, J.; Han, B.; He, G. Application of Organocatalysis in Bioorganometallic Chemistry: Asymmetric Synthesis of Multifunctionalized Spirocyclic Pyrazolone-Ferrocene Hybrids as Novel RalA Inhibitors. *Org. Chem. Front.* **2018**. https://doi.org/10.1039/c8qo00422f.

(94) Dolling, U. H.; Davis, P.; Grabowski, E. J. J. Efficient Catalytic Asymmetric Alkylations. 1. Enantioselective Synthesis of (+)-Indacrinone via Chiral Phase-Transfer Catalysis. *J. Am. Chem. Soc.* **1984**. https://doi.org/10.1021/ja00314a045.

(95) Rossi, S.; Benaglia, M.; Massolo, E.; Raimondi, L. Organocatalytic Strategies for Enantioselective Metal-Free Reductions. *Catalysis Science and Technology*. 2014. https://doi.org/10.1039/c4cy00033a.

(96) Domínguez De María, P.; Bracco, P.; Castelhano, L. F.; Bargeman, G. Influence of the Organocatalyst in the Aldol/Mannich-Type Product Selectivities in C-C Bond Forming Reactions. *ACS Catal.* **2011**. https://doi.org/10.1021/cs100088m.

(97) List, B.; Lerner, R. A.; Barbas, C. F. Proline-Catalyzed Direct Asymmetric Aldol Reactions [13]. *Journal of the American Chemical Society*. 2000. https://doi.org/10.1021/ja994280y.

(98) Bartoli, G.; Bosco, M.; Carlone, A.; Pesciaioli, F.; Sambri, L.; Melchiorre, P. Organocatalytic Asymmetric Friedel-Crafts Alkylation of Indoles with Simple α,β-Unsaturated Ketones. *Org. Lett.* **2007**. https://doi.org/10.1021/ol070309o.

(99) Fang, L. H.; Wang, J. H.; Du, G. H. Atropine. In *Natural Small Molecule Drugs from Plants*; 2018. https://doi.org/10.1007/978-981-10-8022-7_29.

(100) Breton, D.; Buret, D.; Clair, P.; Lafosse, M. Chiral Separation of Atropine by High-Performance Liquid Chromatography. In *Journal of Chromatography A*; 2005. https://doi.org/10.1016/j.chroma.2005.02.073.

(101) Wen, L.; Yuan, Y. H.; Kong, L. L.; Chen, N. H. Quinine. In *Natural Small Molecule Drugs from Plants*; 2018. https://doi.org/10.1007/978-981-10-8022-7_100.

(102) Porta, R.; Benaglia, M.; Coccia, F.; Cozzi, F.; Puglisi, A. Solid Supported 9-Amino-9-Deoxy-Epi-Quinine as Efficient Organocatalyst for Stereoselective Reactions in Batch and under Continuous Flow Conditions. *Adv. Synth. Catal.* **2015**. https://doi.org/10.1002/adsc.201400821.

(103) Wu, F.; Li, H.; Hong, R.; Deng, L. Construction of Quaternary Stereocenters by Efficient and Practical Conjugate Additions to α,β-Unsaturated Ketones with a Chiral Organic Catalyst. *Angew. Chemie - Int. Ed.* **2006**. https://doi.org/10.1002/anie.200502658.

(104) Hong, L.; Wang, L.; Chen, C.; Zhang, B.; Wang, R. An Efficient Enantioselective Method for Asymmetric Friedel-Crafts Alkylation of Indoles with α,β-Unsaturated Aldehydes. *Adv. Synth. Catal.* **2009**. https://doi.org/10.1002/adsc.200800710.

(105) Bartoli, G.; Bosco, M.; Carlone, A.; Pesciaioli, F.; Sambri, L.; Melchiorre, P. Organocatalytic Asymmetric Friedel-Crafts Alkylation of Indoles with Simple α,β-Unsaturated Ketones. *Org. Lett.* **2007**. https://doi.org/10.1021/ol070309o.